

6. SITE 627: SOUTHERN BLAKE PLATEAU¹

Shipboard Scientific Party²

HOLE 627A

Date occupied: 10 February 1985, 0230 EST (beacon dropped)
Date departed: 10 February 1985, 1415 EST (no mud line, first core)
Time on hole: 11 hr, 45 min
Position: 27°38.1'N, 78°17.65'W
Water depth (sea level; corrected m, echo-sounding): 1030
Water depth (rig floor; corrected m, echo-sounding): 1040
Bottom felt (m, drill pipe): 1025.5
Total depth (m): 1036
Penetration (m): 8.80
Number of cores: 1
Total length of cored section (m): 8.8
Total core recovered (m): 9.5
Core recovery (%): 107
Oldest sediment cored:
 Depth sub-bottom (m): 8.8
 Nature: carbonate ooze
 Age: late Miocene

HOLE 627B

Date occupied: 10 February 1985, 1415 EST
Date departed: 17 February 1985, 2030 EST
Time on hole: 7 days, 6 hr, 15 min
Position: 27°38.1'N, 78°17.65'W
Water depth (sea level; corrected m, echo-sounding): 1025.5
Water depth (rig floor; corrected m, echo-sounding): 1036
Bottom felt (m, drill pipe): 1036
Total depth (m): 1572
Penetration (m): 536
Number of cores: 60
Total length of cored section (m): 536
Total core recovered (m): 350.3
Core recovery (%): 65.4
Oldest sediment cored:
 Depth sub-bottom (m): 536
 Nature: dolomite and gypsum
 Age: Albian
 Measured velocity (km/s): 4–5 (Hamilton Frame); 4.2 (seismic interval velocities)

¹ Austin, J. A., Jr., Schlager, W., Palmer, A. A., et al., 1986. *Proc., Init. Repts. (Pt. A), ODP*, 101.

² James A. Austin Jr. (Co-Chief Scientist), Institute for Geophysics, University of Texas at Austin, Austin, TX 78751; Wolfgang Schlager (Co-Chief Scientist), Rosenstiel School of Marine and Atmospheric Sciences, Miami, FL 33149 (current address: Vrije Universiteit, Instituut v. Aardwetenschappen, Postbus 7161, 1007 MC Amsterdam, Netherlands); Amanda A. Palmer, Staff Scientist, Ocean Drilling Program, Texas A&M University, College Station, TX 77843; Paul A. Comet, The University, Newcastle-Upon-Tyne, Newcastle, United Kingdom (current address: Core Labs Singapore, 24A-Lim Teck Boo Rd., Singapore 1953); André Droxler, Rosenstiel School of Marine and Atmospheric Sciences, Miami, FL 33149 (current address: Department of Geology, University of South Carolina, Columbia, SC 29208); Gregor Eberli, Geologisches Institut, ETH-Zentrum, Zürich, Switzerland (current address: Fisher Island Station, University of Miami, Miami, FL 33139); Eric Fourcade, Laboratoire de Stratigraphie, Université Pierre et Marie Curie, 4 Place Jussieu 75230, Paris Cedex 05, France; Raymond Freeman-Lynde, Department of Geology, University of Georgia, Athens, GA 30602; Craig S. Fulthorpe, Department of Geological Sciences, Northwestern University, Evanston, IL 60201; Gill Harwood, Department of Geology, The University, Newcastle-Upon-Tyne, NE1 7RU United Kingdom; Gerhard Kuhn, Geologisches Institut Göttingen, Federal Republic of Germany (current address: Alfred Wegener Institut für Polarforschung, Columbus Center, D-2850 Bremerhaven, West Germany); Dawn Lavoie, NORDA Code 363, Seafloor Geosciences Division, NSTL, MS 39529; Mark Leckie, Woods Hole Oceanographic Institution, Woods Hole, MA 02543 (current address: Department of Geology and Geography, University of Massachusetts, Amherst, MA 01003); Allan J. Melillo, Department of Geological Sciences, Rutgers University, New Brunswick, NJ 08903 (current address: Chevron U.S.A., New Orleans, LA 70114); Arthur Moore, Marathon Oil Company, P.O. Box 269, Littleton, CO 80160; Henry T. Mullins, Department of Geology, Syracuse University, Syracuse, NY 13210; Christian Ravanne, Institut Français du Pétrole, B.P. 311, 92506 Rueil Malmaison Cedex, France; William W. Sager, Department of Oceanography, Texas A&M University, College Station, TX 77843; Peter Swart, Fisher Island Station, University of Miami, Miami, FL 33139 (current address: Marine Geology and Geophysics, Rosenstiel School of Marine and Atmospheric Sciences, Miami, FL 33149); Joost W. Verbeek, Dutch Geological Survey, P.O. Box 157, 2000 A.D. Haarlem, Netherlands; David K. Watkins, Department of Geology, University of Nebraska, Lincoln, NE 68588; Colin Williams, Borehole Research Group, Lamont-Doherty Geological Observatory, Palisades, NY 10964.

Principal results: Site 627 on the southern Blake Plateau was occupied from 10 to 17 February 1985. Hole 627B, located at 27°38.10'N, 78°17.65'W, in 1036 m water depth, penetrated 536 m of sediment with 65% recovery. The hole was abandoned in dolomite and gypsum of Albian age because of shows of wet gas (methane with traces of ethane through hexane).

Hole 627B recovered the following sequence: (1) 0–181 m sub-bottom; carbonate ooze with turbidites, slumps, and debris flow, Pleistocene to early Miocene in age, representing the toe of the prograding Little Bahama Bank; (2) 181–249 m sub-bottom; condensed sequence of argillaceous carbonate ooze and chalk with some chert, early Miocene to Paleocene in age; (3) 249–325 m sub-bottom; nanofossil chalk without platform input and negligible dissolution effects, Campanian in age; (4) 325–344 m sub-bottom; condensed sequence of ooze, chalk, and chert, Santonian to Coniacian in age; (5) 344–468 m sub-bottom; marly chalk, middle Cenomanian to latest Albian in age, deepens upward from inner neritic to outer neritic environment; and (6) 468–536 m sub-bottom; shallow-water dolomites, limestones, and gypsum, late Albian in age, platform-interior environment.

This sequence reflects the drowning and disintegration of the middle Cretaceous carbonate platform (the "megabank"), its transformation into a terrigenous shelf in the Cenomanian, and later into a marginal plateau of bathyal depth (Campanian to early Miocene). Since the early Miocene, this part of the plateau has been part of the advancing flank of the Bahama carbonate platform.

Other important results include the discovery of immature gas-prone source beds in the Cenomanian marls and traces of hydrocarbon in the Albian carbonates and evaporites. Pore waters show geochemical trends similar to those of classical deep-sea sites on ocean crust. Seismic stratigraphy of the site survey provides good correlation with borehole stratigraphy and physical properties.

BACKGROUND AND OBJECTIVES

Background

Both single-channel seismic-reflection profiles and piston-core samples have previously demonstrated that modern slopes in the Bahamas steepen with both height and time and are characterized by facies belts that generally parallel adjacent bank margins (Mullins and Neumann, 1979; Schlager and Chermak, 1979; Schlager and Ginsburg, 1981; Van Buren and Mullins, 1983; Mullins et al., 1984). Schlager and Ginsburg (1981) suggested an evolutionary pattern of carbonate-slope development that could be broken into three stages (Fig. 1):

1. Accretionary, with slope deposition dominated by slumps, gravity flows, and turbidites resulting in seaward progradation of slope and basinward convergence of time lines.
2. Bypass, where slope sedimentation is characterized by mud and decreasing accretions as turbidity currents bypass the slope and deposit on the basin floor (basinward divergence of time lines).
3. Erosional, where outcrops of older material are exposed by downcutting on the slope, and the slope base is either buried by talus or notched by bottom-current erosion and/or carbonate dissolution. As its angle steepened and turbidite deposition became more frequent, a single slope could evolve from accretionary through bypass to erosional.

While Schlager and Ginsburg (1981) emphasized change in time, Mullins et al. (1984) documented change in space. Mullins

et al. subdivided the northern slope of Little Bahama Bank into three facies belts (Fig. 2):

1. An upper slope characterized by fine-grained periplatform ooze and numerous gullies floored by sand.
2. A middle and lower slope (or proximal apron) characterized by mud-supported debris-flow deposits and thick, coarse-grained turbidites.
3. A lower slope (or distal apron) of grain-supported debris flows and thinner, fine-grained turbidite deposits intercalated with periplatform ooze.

The drilling of Bahamian slope transects was designed to study these trends in both space and time.

Carbonate slopes also appear to show a different response to postulated global cycles of relative sea-level change than do their counterparts in siliciclastic environments (Vail et al., 1977). Lynts et al. (1973), Schlager and Ginsburg (1981), Droxler (1984), and Droxler and Schlager (in press) have shown that, unlike clastic slopes, carbonate slopes shed a minimum of material during lowstands (i.e., glacials, when diagenesis produces rapid surface/near-surface lithification and low productivity yields little sediment available for off-bank erosion by turbidity currents), and more during highstands (i.e., interglacials, when large quantities of sediments are produced on the flooded banks and swept off bank edges by waves and currents). At least in the Quaternary, the frequency of turbidites blanketing Bahamian slopes and the timing of their deposition seem to be the inverse of what would be expected on the terrigenous ocean margins off the northeastern United States or in the Gulf of Mexico.

Like the Straits of Florida, Little Bahama Bank also sits on what may once have been a more extensive carbonate megaplatform. Van Buren and Mullins (1983) document a velocity transition to 4.2 km/s material less than 0.5 s beneath the northern slope of the bank, which they correlate with the top of a drowned shallow-water surface of Late Cretaceous(?) age. Prior to subsidence of the Blake Plateau, this may have been part of a carbonate province extending unbroken from the Canadian portion of the East Coast passive continental margin throughout the Bahamas and the Gulf of Mexico.

Three shallow-penetration HPC sites, BAH-9-A (Site 627), BAH-8-A (Site 628), and BAH-7-A (Site 629/Site 630), were chosen to sample the facies belts previously described, and BAH-9-A was also planned for sampling the deeper transitions to high-velocity material believed to mark the top of shallow-water rocks.

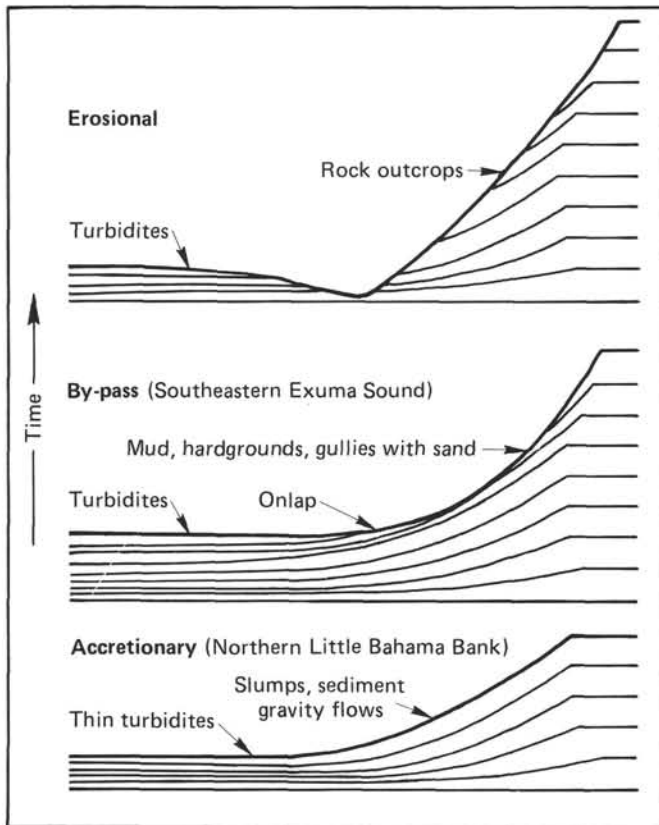


Figure 1. Postulated evolution of modern carbonate slopes (after Schlager and Ginsburg, 1981).

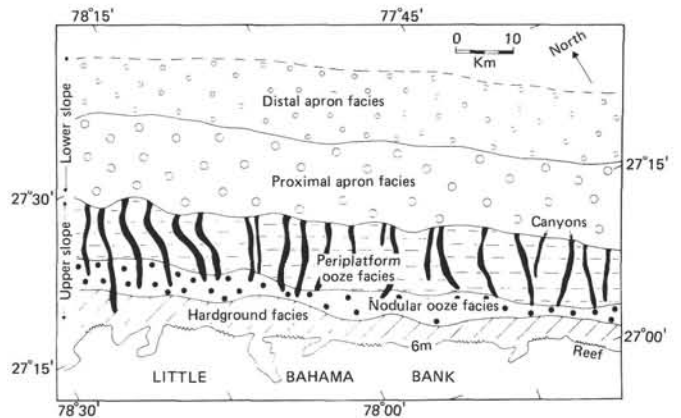


Figure 2. Near-surface sediment facies map for slope north of Little Bahama Bank (after Mullins et al., 1984).

Objectives

The northern Little Bahama Bank transect addresses the following questions:

1. What is the stratigraphic record of a gentle, accreting platform flank, particularly in regard to contributions to the record by pelagic/hemipelagic sedimentation vs. slumps and debris flows? What do the facies patterns look like, both laterally and vertically?
2. How does the slope system respond to paleoceanographic events?
3. How are changes in input from the adjacent carbonate bank related to fluctuations in sea level?
4. How does shallow-burial diagenesis affect periplatform ooze, especially regarding its metastable aragonite and magnesian calcite components?
5. What is the geological significance of the seismic facies change from discontinuous, hummocky reflectors with a compressional wave velocity of 2.78 km/s above 1.85 s on line LBB-18 (BAH-9-A) to high-amplitude, continuous reflectors characterized by a compressional wave velocity of 4.2 km/s below that horizon? If this seismic discontinuity represents the transition to a drowned carbonate platform, why and when did this drowning take place? How can this event be related both to similar phenomena in the Gulf of Mexico and in other parts of the Bahamas (e.g., the Straits of Florida) and to the subsidence of the adjacent Blake Plateau?

OPERATIONS SUMMARY

Introduction

In order to characterize the development of the slope north of Little Bahama Bank in three dimensions prior to Leg 101 drilling, a geophysical site survey of part of that slope was conducted in April 1984. Approximately 225 n. mi of high-resolution multichannel seismic profiles were collected by the University of Texas Institute for Geophysics vessel *Fred H. Moore*. Spacing of the 24-trace, 12-fold water-gun profiles averaged 1–2 n. mi over the upper, gullied part of the slope, and 3 or more n. mi farther seaward (Fig. 3). BAH-9-A, at the intersection of lines LBB-18 and LBB-21, was designed both to sample the stratigraphy of the lower carbonate slope and to penetrate the seismic transition to high-velocity material (shallow-water rocks?). However, examination of structure maps prepared from the site-survey data while en route to Little Bahama Bank suggested that BAH-9-A was on the crest of a structural closure at approximately 500–560 m sub-bottom. Consequently, BAH-9-A was moved upslope along LBB-18 to a new position approximately 1 km southwest. The change in location was approved by the science operator.

Hole 627A

In order to provide a tie between Sites 626 and 627, a 170-n.-mi seismic line was collected continuously from the Straits of Florida site-survey grid to the grid on the northern slope of Little Bahama Bank (Fig. 4). The *JOIDES Resolution* left Site 626 at 0815 hr, 9 February. Both the 3.5- and 12-kHz systems were immediately activated, and the other geophysical gear (a 100-m single-channel streamer with 400 m of leader, two 80-in.³ water guns, and a magnetometer) was deployed from 0900 to 0930 hr. Transit speed between sites was maintained at 8 kt, and the guns were fired every 12 s. The only significant problem during the 17-hr acquisition period was a 40-min gap caused by the loss of compressed air for the guns from the ship's accumulators. Part of the reprocessed digital single-channel line near Site 627 is reproduced as Figure 5.

According to the LORAN C system, the *Resolution* arrived at BAH-9-A at 0230 hr, 10 February. A 15.5-kHz Datasonics beacon was then dropped at the following position: 27°37.46'N, 78°16.8'N. All seismic gear was on board by 0320 hr, and the *Resolution* turned back to range on the beacon. Meanwhile, a bottom-hole assembly (BHA) for hydraulic-piston-core/extended-core-barrel (HPC/XCB) sampling was being made up.

By 1030 hr, ranging on the new beacon was complete. During that time, a discrepancy between the LORAN C and satellite navigation (SATNAV) systems became apparent. The Hole 627A position on the ship's two navigation systems was 27°37.16–24'N, 78°16.57–64'W (LORAN C average), and 27°38.077–105'N, 78°17.636–689'W (SATNAV average), a differential of slightly more than 1 n. mi. Experience during the site surveys had suggested such a systematic offset between LORAN C and SATNAV in this region, and subsequent monitoring of navigation aboard the *Resolution* during Site 627 operations, confirmed that SATNAV north of Little Bahama Bank was more accurate after stationary positioning for several days. The accurate SATNAV Hole 627A position reported above is approximately 1.1 n. mi west-northwest of BAH-9-A.

There was virtually no current at Hole 627A, and the 3.5-kHz returns showed a flat, smooth bottom with little evident penetration. The water depth was 1030 m (corr.), or 1040 m to the rig floor. By 1030 hr, the BHA was completed and pipe was run in the hole (RIH) at Hole 627A. However, a mud-line core at 1415 hr failed to retrieve the sediment surface as a result of a crushed core tube, so the decision was made to offset and try again.

Hole 627B

Hole 627B occupies the same position as Hole 627A. At 1830 hr on 10 February, a mud-line core was successful at a water depth of 1025.5 m (corr.), or 1036 m from the rig floor to the water bottom. Sheared pins in the overshot of Core 627B-2H caused it to stick in the drill pipe 20 m above the bit, but the barrel was retrieved successfully some 5 hr later. Handling problems persisted when the sinker bars on Core 627B-7H were damaged on the rig floor and had to be replaced, costing another 2 hr. Nonetheless, by 1715 hr on 11 February, 16 HPC cores had been taken in a variety of lithologies: stiff oozes, semilithified chinks, and debris flows. Recovery was 97.5% down to the lower/middle Miocene boundary at a sub-bottom depth of 149.7 m, where XCB operations began.

Continuous XCB coring was routine through Core 627B-19X. Drilling and wireline round-trip times averaged slightly over 2 hr/core. Chert fragments began to show up in Core 627B-20X. The presence of nodular chert in Core 627B-20X through Core 627B-26X (181.4 to 248.7 m sub-bottom) caused both excessive wear on the cutting edge of the XCB and slower drilling rates. Chert fragments continued to be found in Core 627B-27X and in Cores 627B-29X through Core 627B-33X.

While setting up for Core 627B-35X, the core barrel became stuck in the drill string 37 m below the rig floor. Approximately 4 hr were lost retrieving this barrel by pulling out the three joints of pipe above it. Poor recovery characterized the interval between Core 627B-36X and Core 627B-42X, but this section is not highlighted by slow drilling rates. Drilling and wireline round-trip times averaged only 1.8 hr/core.

With Core 627B-43X, drilling rates did begin to slow down in Cenomanian green marls, a lithology that dominated the section from Core 627B-38X through Core 627B-47X. Drilling and wireline round-trip times averaged approximately 2.3 hr/core, but recovery was 93.2%.

A combined limestone-dolomite section persisted from Core 627B-51X through Core 627B-54X (506.4 to 514.2 m sub-bottom). Recovery from Cores 627B-47X through 627B-54X aver-

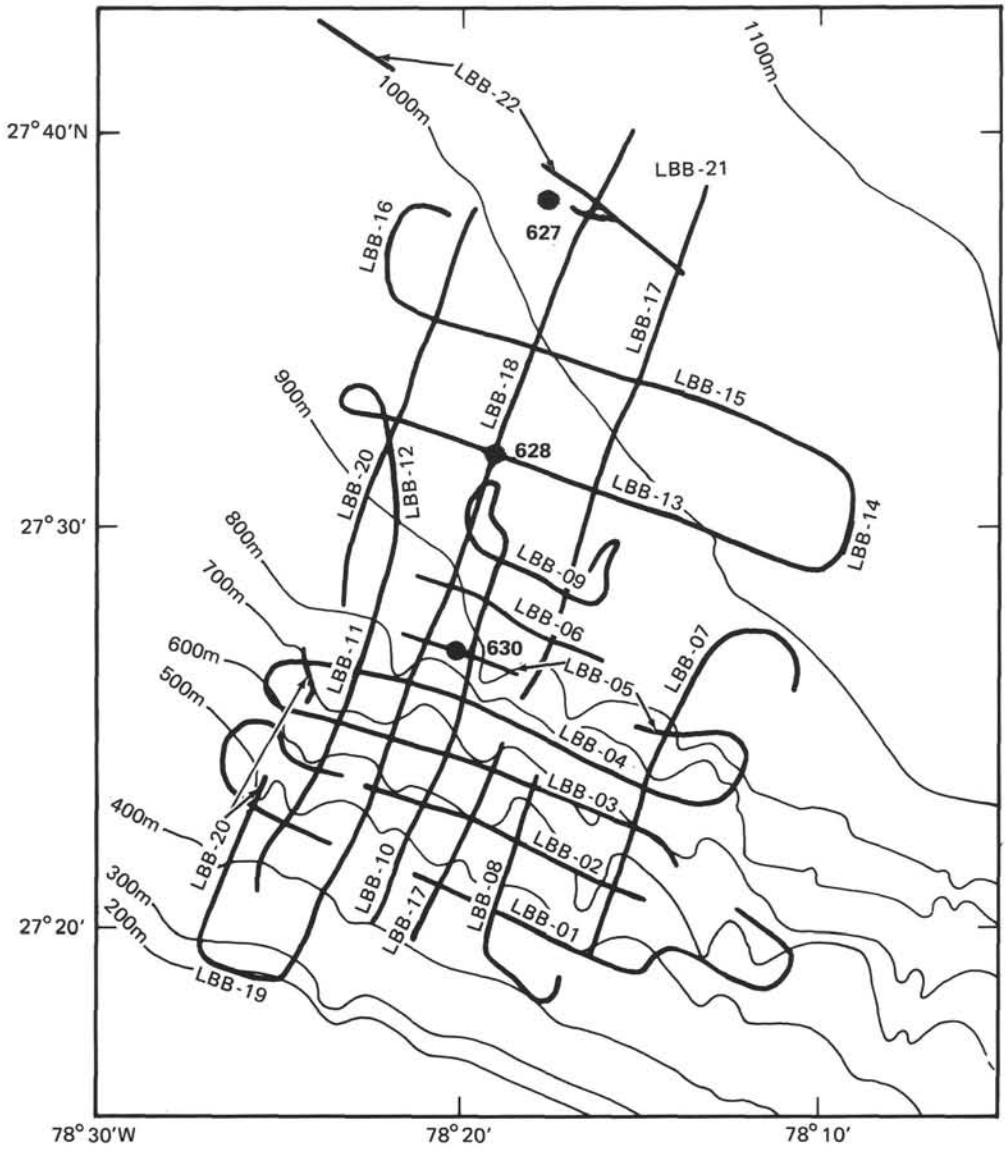


Figure 3. Trackline map for Little Bahama Bank (LBB) region. Locations of the LBB sites drilled are also shown.

aged only 4.4%, but drilling rates improved from Core 627B-50X on, with average round-trip times of less than 2 hr/core. At each connection, the hole was conditioned with 10 bbl of drilling mud.

All drilling stopped for 2 hr while a gray mud in Core 627B-54X, CC, which exuded a petroliferous odor, was analyzed for saturated hydrocarbons. Results suggested that all of the ambient hydrocarbons were the result of local bacterial decomposition and were not thermogenic, so late in the morning of 15 February drilling began again. Recovery from Core 627B-55X through Core 627B-60X, the last core of Hole 627B, averaged 37% in gypsum and dolomitized limestone.

At 0125 hr on 16 February, drilling stopped for good in Hole 627B at 535.8 m sub-bottom, when traces of ethane, propane, and longer chain hydrocarbons showed up along with 90 ppm of methane in Core 627B-60X, CC.

At 0500 hr, 16 February, logging operations began with the drill bit at 100 m sub-bottom. The first run included natural gamma-ray spectroscopy, lithodensity, and neutron logs. During this run, at 0845 hr, 16 February, the logging tool became stuck

at 1508 m below the rig floor (469 m sub-bottom) as a result of an obstruction. Repeated attempts to free the tool failed, so the decision was made late in the morning to attempt to clear the obstruction by RIH without rotation. Unfortunately, while doing this, the pipe encountered another obstruction at 1485 m below the rig floor (446 m sub-bottom) and could not reach the top of the logging tool. Circulation through the drill pipe provided no additional penetration, so the logging cable had to be cut and clamped in order to rotate back into Hole 627B. This operation began at 1915 hr.

The string was RIH from 1475 m below the rig floor in an attempt to get the drill bit over the fishing neck of the logging tool. After every 3 m drilled, the pumps were engaged to clear out the hole. By 2230 hr, the bit had reached a depth of 1486 m below the rig floor. At 2300 hr, the logging-winch operator began to pull in the logging line in an attempt to get the tool back inside the pipe. Unfortunately, this maneuver succeeded only in severing the logging cable.

The decision was then made to attempt to recapture the tool by first lowering the BHA over it, then snagging it with an XCB

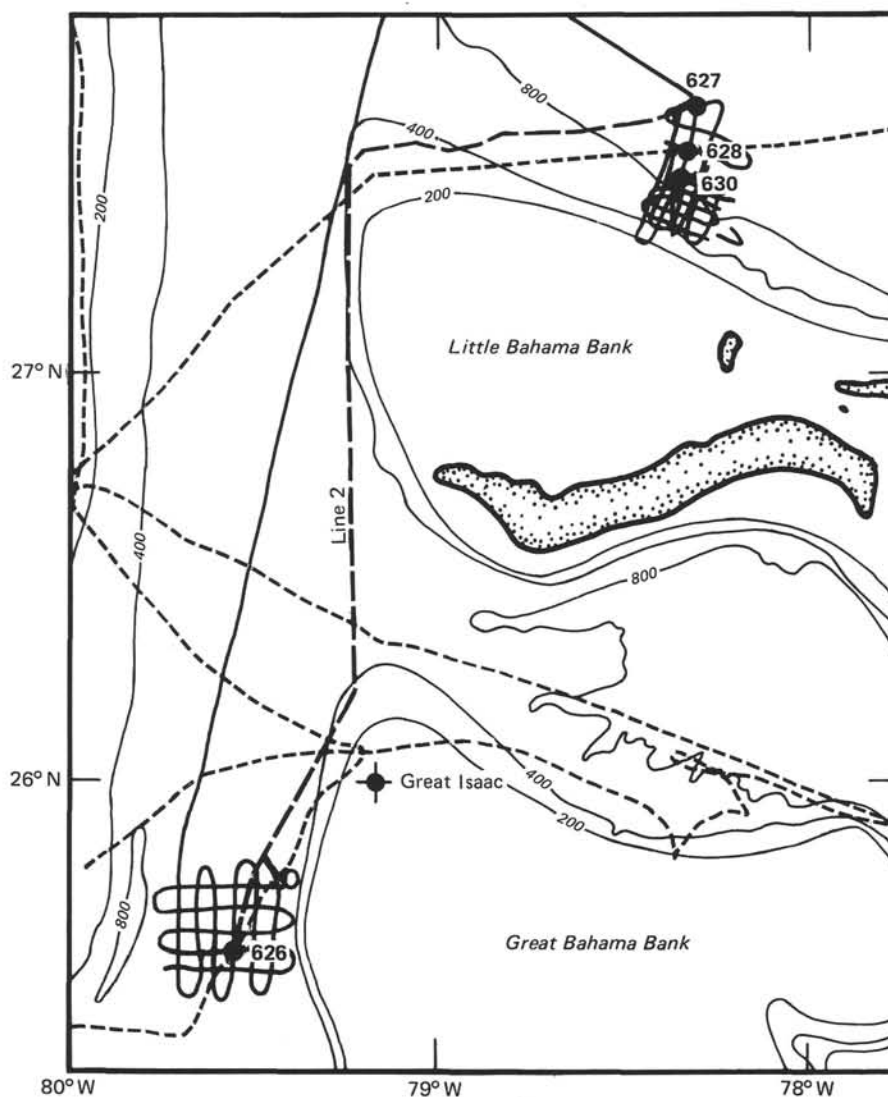


Figure 4. Schematic diagram showing ODP Leg 101, line 2, which ties the Straits of Florida and Little Bahama Bank site-survey grids (see also Fig. 5). Other multichannel seismic-reflection coverage is also shown. Bathymetry shown in meters.

equipped with a slip-type catcher. (As it turned out later, this maneuver was unsuccessful.) The barrel became stuck in the BHA, effectively blocking the base of the pipe and preventing any further out-of-the-pipe logging efforts.

By noon on 17 February, a plug of cement approximately 24 m thick had been slurried into Hole 627B from 536 to 512 m sub-bottom in order to isolate the radioactive source in the logging tool. The cementing process took place with the drill bit at 467 m sub-bottom. Attempts to log in the pipe down to that depth were unsuccessful as a result of further equipment malfunctions, so at 1600 hr the decision was made to abandon Hole 627B completely. The drill bit was pulled to a depth of 63 m sub-bottom by 1700 hr, and 50 bbl of mud was pumped into the hole. All pipe was back on deck by 1930 hr, when it was determined that the logging tool was lost and therefore presumed cemented in the bottom of Hole 627B. The *JOIDES Resolution* was under way for BAH-8-A, approximately 6 n. mi up the slope of Little Bahama Bank along seismic line LBB-18 (Fig. 3), by approximately 2030 hr, 17 February.

The coring summary for Site 627 appears in Table 1.

SEDIMENTOLOGY

Introduction

Two holes were drilled at Site 627. Hole 627A penetrated 8.8 m sub-bottom with 8.8 m (100%) of recovery, although the sediment/water interface was not accurately defined. Hole 627B penetrated 535.8 m and recovered 351 m (65%) of sediment. Recovery with the HPC (97%; Cores 627B-1H through 627B-16H) was significantly greater and less disturbed than with the XCB (53%; Cores 627B-17X through 627B-60X).

Based on lithostratigraphy, six major depositional units were defined at Site 627B.

Unit I (0–181.4 m sub-bottom; Cores 627B-1H through 627B-19X-6, 50 cm)

Unit I contains dominantly carbonate oozes with subordinate unlithified floatstones, grainstones, and packstones. Intervals of ooze with packstones and grainstones occur at 3–43 m, 69–92 m, 110–125 m, 131–144 m, and 179–181 m; intervals of deformed oozes with floatstones and rudstones are found be-

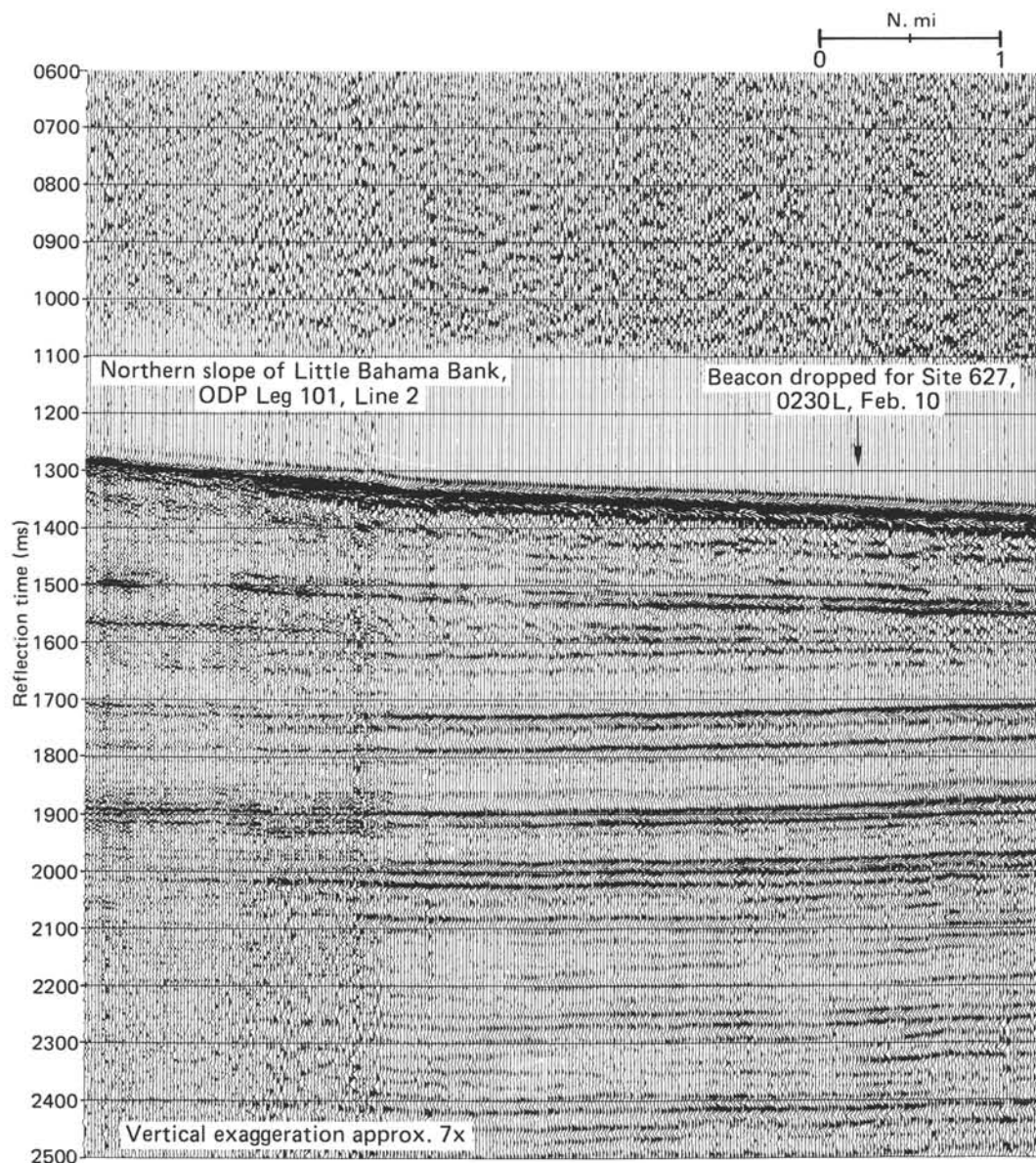


Figure 5. Part of ODP Leg 101, line 2, approaching Site 627. Data sampled at 1 ms. Sound source: two 80-in.³ water guns, rep. rate 12 s. Leader length: 400 m.

tween 43 and 69 m, 92 and 110 m, 125 and 131 m, and 144 and 179 m. Partial lithification of these sediments is visible in Cores 627B-1H to 627B-4H, decreasing downhole, and also in Cores 627B-9H to 627B-11H.

Unit I has been divided into three subunits, based on the varying proportions of sediment types with supportive data from smear slide analyses (Fig. 6) and color changes. These lithologic subunits are as follows:

Subunit IA: (0–108 m sub-bottom, Cores 627B-1H to 627B-12H-5), dominant oozes with thin floatstones, minor packstones, and some deformed laminae in the oozes.

Subunit IB: (108–144 m sub-bottom, Cores 627B-12H to 627B-16H-4), oozes (with lesser proportions of micrite and more nanofossils) with thin packstones.

Subunit IC: (144–181.4 m sub-bottom, Cores 627B-16H-4 to 627B-19X), oozes with packstones and a thick (8-m) floatstone unit.

Subunit IA

The topmost layer of Subunit IA consists of sorted skeletal sand, which may indicate recent winnowing by bottom currents. The carbonate oozes near the top of the sequence contain high percentages of unidentifiable micrite (up to 85%; Fig. 6), which is shown by x-ray-diffraction data to be largely aragonite (and magnesian calcite) (“Inorganic Geochemistry,” this chapter) and is probably derived from the adjacent shallow-water Bahama Platform. As such, these are probably best classified as peri-platform oozes (Schlager and James, 1978). Darker bands within the oozes in Cores 627B-1H and 627B-2H may represent periodic influxes of clays (and organic material?) derived from terrigenous sources. Proportions of foraminifers and nanofossils increase lower in Subunit IA with a decrease in micrite percentage (Fig. 6), indicating possible increased distance from the shal-

Table 1. Coring summary, Site 627.

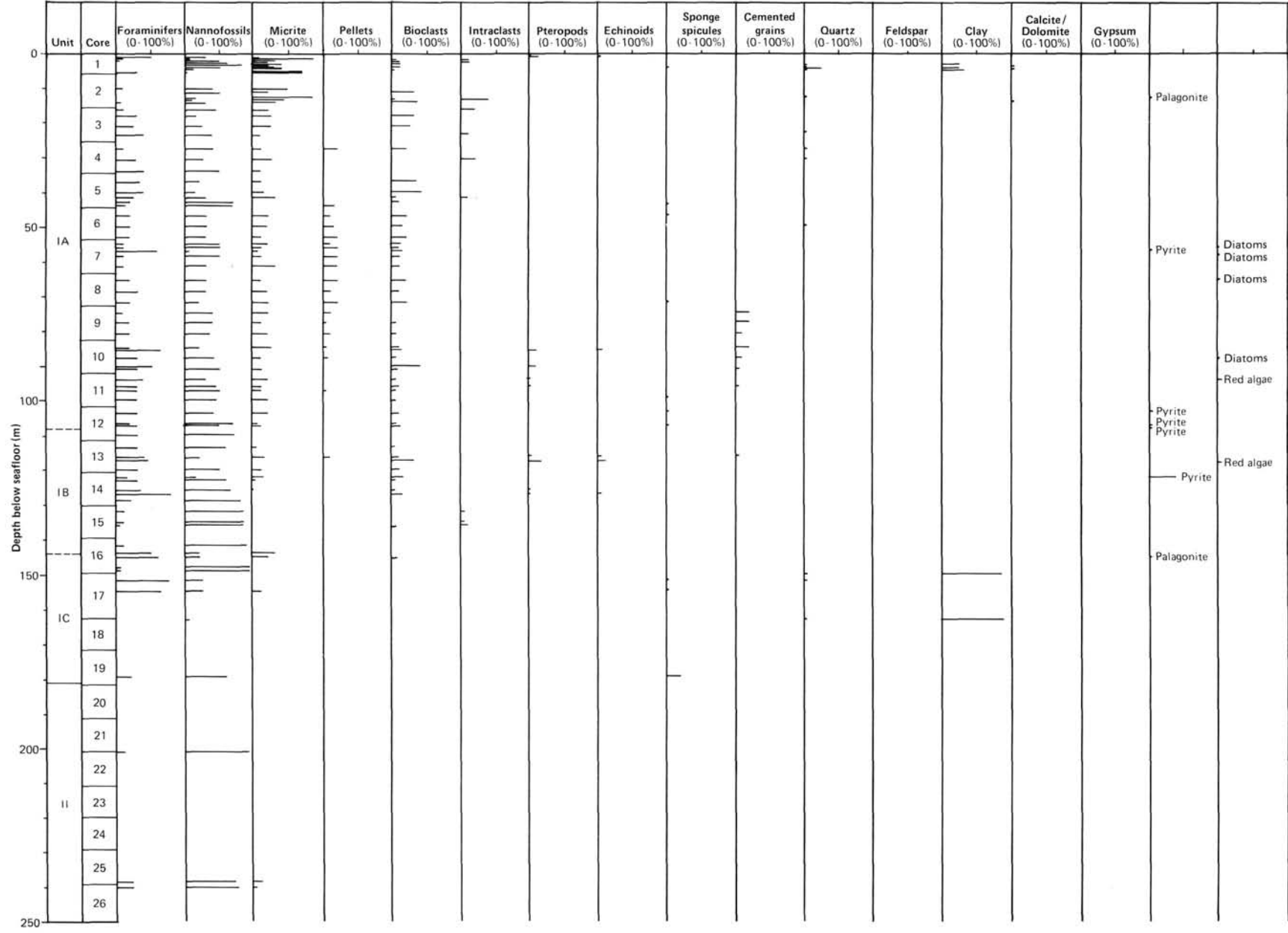
Core no.	Core type ^a	Date (Feb. 1985)	Time	Sub-bottom depths (m)	Length cored (m)	Length recovered (m)	Percentage recovered
Hole 627A							
1	H	10	1600	0-8.8	8.8	9.47	107
Hole 627B							
1	H	10	1800	0-5.8	5.8	5.81	100
2	H	11	0115	5.8-15.5	9.7	6.69	96
3	H	11	0250	15.5-25.2	9.7	9.57	98
4	H	11	0330	25.2-34.7	9.5	9.24	99
5	H	11	0405	34.7-44.2	9.5	9.67	101
6	H	11	0450	44.2-53.8	9.6	9.42	98
7	H	11	0530	53.8-63.3	9.5	9.46	100
8	H	11	0845	63.3-72.9	9.6	8.76	91
9	H	11	0930	72.9-82.5	9.6	9.61	100
10	H	11	1015	82.5-92.0	9.5	10.03	105
11	H	11	1045	92.0-101.5	9.5	9.94	104
12	H	11	1115	101.5-111.3	9.8	9.77	100
13	H	11	1300	111.3-120.8	9.5	8.91	94
14	H	11	1430	120.8-130.3	9.5	9.80	103
15	H	11	1545	130.3-139.9	9.6	6.84	70
16	H	11	1715	139.9-149.7	9.8	9.52	97
17	X	11	2050	149.7-162.2	12.5	5.89	47
18	X	11	2205	162.2-171.8	9.6	2.19	22
19	X	11	2340	171.8-181.4	9.6	9.81	102
20	X	12	0135	181.4-191.0	9.6	0.94	9
21	X	12	0322	191.0-200.7	9.7	8.09	83
22	X	12	0455	200.7-210.2	9.5	0.83	8
23	X	12	0700	210.2-219.9	9.7	7.86	81
24	X	12	0941	219.9-229.4	9.5	0.24	2
25	X	12	1230	229.4-239.1	9.7	0.21	2
26	X	12	1430	239.1-248.7	9.6	2.07	21
27	X	12	1545	248.7-258.2	9.5	9.66	101
28	X	12	1715	258.2-267.5	9.3	7.60	81
29	X	12	1840	267.5-276.6	9.1	9.71	106
30	X	12	2015	276.6-286.3	9.7	5.27	54
31	X	12	2135	286.3-296.0	9.7	5.90	60
32	X	12	2330	296.0-305.6	9.6	9.10	94
33	X	13	0055	305.6-315.0	9.4	2.58	27
34	X	13	0230	315.0-324.7	9.7	9.66	99
35	X	13	0800	324.7-334.3	9.6	5.22	54
36	X	13	0945	334.3-343.9	9.6	0.80	8
37	X	13	1130	343.9-353.5	9.6	1.02	10
38	X	13	1300	353.5-363.1	9.6	9.84	102
39	X	13	1500	363.1-372.7	9.6	9.79	101
40	X	13	1700	372.7-382.4	9.7	9.70	100
41	X	13	1855	382.4-391.9	9.5	9.81	103
42	X	13	2050	391.9-401.5	9.6	9.80	102
43	X	13	2355	401.5-411.1	9.6	9.80	102
44	X	14	0245	411.1-420.7	9.6	8.89	92
45	X	14	0615	420.7-430.0	9.3	1.73	18
46	X	14	0915	430.0-439.7	9.7	9.84	101
47	X	14	1130	439.7-448.7	9.0	9.64	107
48	X	14	1415	448.7-458.3	9.6	0.29	3
49	X	14	1700	458.3-467.8	9.5	0.83	8
50	X	14	1830	467.8-477.5	9.7	0	0
51	X	14	2015	477.5-487.1	9.6	0.39	4
52	X	14	2340	487.1-496.7	9.6	0.28	2
53	X	15	0210	496.7-506.4	9.7	0.57	5
54	X	15	0425	506.4-514.2	7.8	0.52	6
55	X	15	0800	514.2-519.2	5.0	1.89	37
56	X	15	1300	519.2-524.2	5.0	2.06	41
57	X	15	1515	524.2-527.8	3.6	1.10	30
58	X	15	1715	527.8-530.6	2.8	0.87	31
59	X	15	2025	530.6-533.8	3.2	1.06	33
60	X	16	0125	533.8-535.8	2.0	0.86	43

^a H = hydraulic piston; X = extended core barrel.

low-water platform. Darker bands, possibly of terrigenous origin, are, however, also present within the lower half of Subunit 1B (e.g., Cores 627B-10H, 627B-11H, and 627B-12H). Thin (<0.5 m) unlithified packstones and rare grainstones with fine to coarse sands occur, dominated by tests of planktonic foraminifers or aggregates, containing only minor shallow-water debris. These are graded or massive and commonly have sharp

bases and gradational tops. They are interpreted as turbidites. Lithified packstones, present at the tops of some turbidites, have an abrupt dark, pyritic upper contact with overlying unlithified ooze (Fig. 7).

Floatstones with minor clast-supported rudstones, in Cores 627B-6H through 627B-11H, are interpreted as debris flows. Lithified clasts are predominantly planktonic-foraminifer pack-



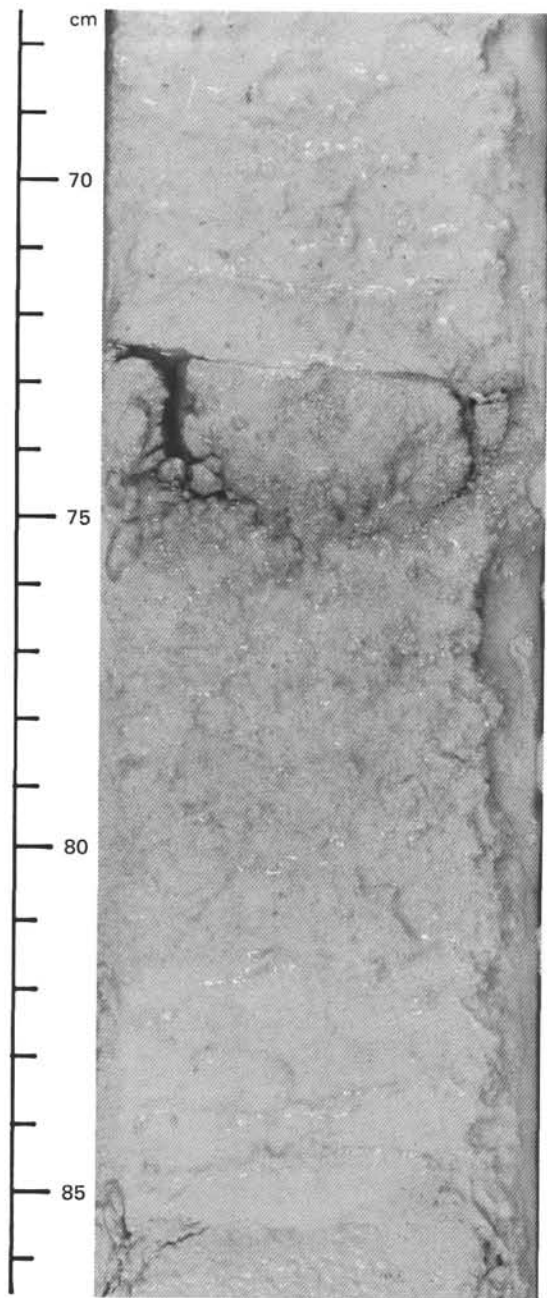


Figure 7. Unlithified to partly lithified packstone, interpreted as a turbidite, with lithification at the top of the turbidite, Section 627B-9H-5.

stones and grainstones and are thus slope-derived. Only minor amounts of coarse-grained shallow-water detritus appear to be present. Downslope sediment movement is also indicated by inclined laminations within the oozes (e.g., Cores 627B-6H, 627B-7H, and 627B-11H) interpreted as slumps (Fig. 8). The base of Subunit IA is defined by an abrupt compositional and color change in Core 627B-12H-5, 108 m sub-bottom (Fig. 9).

Fine-grained sediments in Subunit IA also appear to have a relatively high susceptibility to early submarine diagenesis, particularly near the top of the section. Partly lithified oozes and chalks occur throughout this subunit with minor amounts of well-indurated limestone near the base. Many chalk-ooze couplets appear to occur in cycles, spaced 5–25 cm apart. Also, numerous deep-sea aggregate grains, consisting of cemented plank-

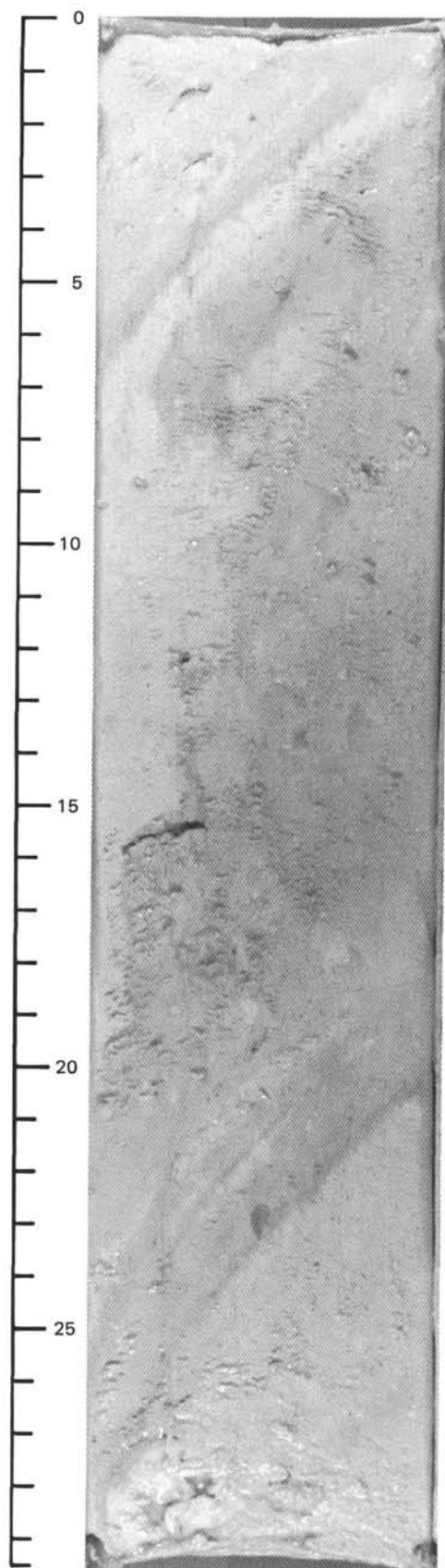


Figure 8. Carbonate oozes with inclined laminations interpreted as slump, Section 627B-6H-7.

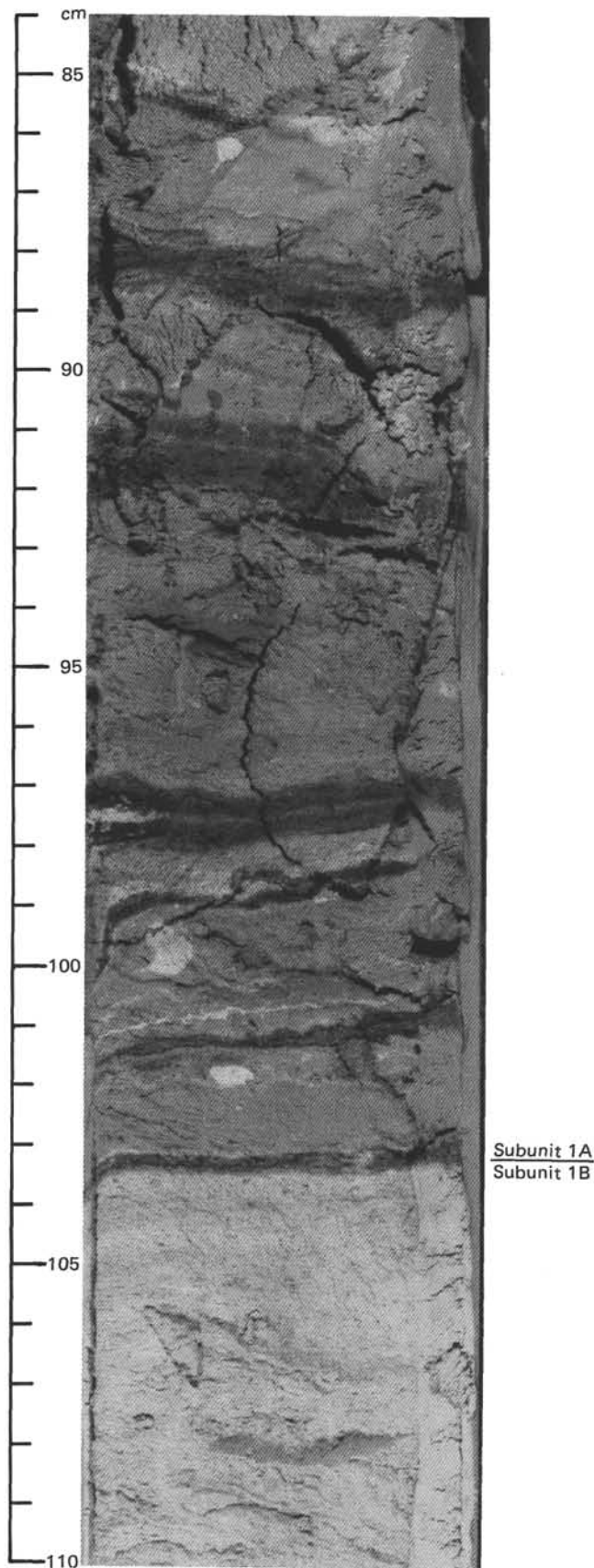


Figure 9. Subunit IA/IB contact with distinct laminations in upper subunit and lighter colored underlying oozes, Section 627B-12H-5.

tonic-foraminifer tests, occur throughout the section, especially near the top of the subunit.

Subunit IB

Although gross sediment types in Subunits IA and IB are similar, significant differences exist. The most common lithology in Subunit IB is burrowed (Fig. 10), unlithified to partly lithified ooze. Unlike Subunit IA, however, the oozes and chalks of Subunit IB have high percentages (up to 90%) of nannofossils and relatively minor amounts of micrite (Fig. 6). Also, the relative degree of diagenetic alteration (i.e., lithification) in Subunit IB is less than that in Subunit IA and perhaps indicates that the original fraction of the metastable bank-derived sediment was smaller. Darker colored greenish oozes are present as layers and in burrows in Cores 627A-14H through 627A-16H and may represent some input of terrigenous clays. Packstones and grainstones are rarer than in Subunit IA and are dominated by pelagic components, principally planktonic foraminifers. However, one thicker packstone (Core 627B-13H-4) contains shallow-water-derived components including red algae. Most packstones in this interval fine upward and are probably turbidites. Gradation can also be noted within some oozes, with cycles of oozes at the base and a progressively upward increase in terrigenous clays (e.g., Core 627B-14H-6). Floatstones are absent from Subunit IB.

Subunit IC

Subunit IC is dominated by packstones and a thick floatstone with minor ooze. The packstones contain high proportions of planktonic foraminifers with nannofossils and rarer sponge spicules (Fig. 6). Graded and nongraded packstones are present. One floatstone (Core 627B-19X), interpreted as a debris flow, contains clasts of claystone, stiff ooze, and chalk in a matrix of foraminifer-nannofossil ooze with some sponge spicules. A dark clay layer is present at the top of Core 627B-17X, which may be the result of alteration of volcanic glass. Recovery in Subunit IC was poorer than in the overlying subunits. Lithification is more advanced in Subunit IC, with many packstones being partly lithified (approximately 30%). It is also more lithified than the underlying unit.

Unit II (181–249 m sub-bottom; Cores 627B-20X through 627B-26X)

Recovery was poor (31%) in these cores, and much of the recovered material consists of downhole contamination of Quaternary material. Lithologies that were recovered are siliceous limestone and chert as well as argillaceous foraminifer-nannofossil ooze containing 70%–90% nannofossils. Silicified planktonic-foraminiferal limestones (Fig. 11) occur in Cores 627B-20X and 627B-22X, and chert fragments were found in Cores 627B-21X and 627-23X. Overall, Unit II appears to be a condensed siliceous-limestone sequence.

Unit III (249–325 m sub-bottom; Cores 627B-27X through 627B-34X)

Most of Unit III consists of discrete alternations of calcareous ooze and well-indurated chalk (Fig. 12). Both the ooze and chalk contain planktonic foraminifers and up to 90% nannofossils. Chalks are highly fractured by drilling but do display some parallel laminations and burrow structures. The spacing of chalk-ooze couplets is variable, but most are on the order of 2–10 cm; many core sections contain subequal proportions of chalk and ooze, although near the base of the unit some sections contain up to 80% chalk. Locally, laminated to burrowed grainstones are present in which most of the sand fraction consists of planktonic-foraminiferal tests, although other skeletal debris and aggregate grains are present as minor constituents.

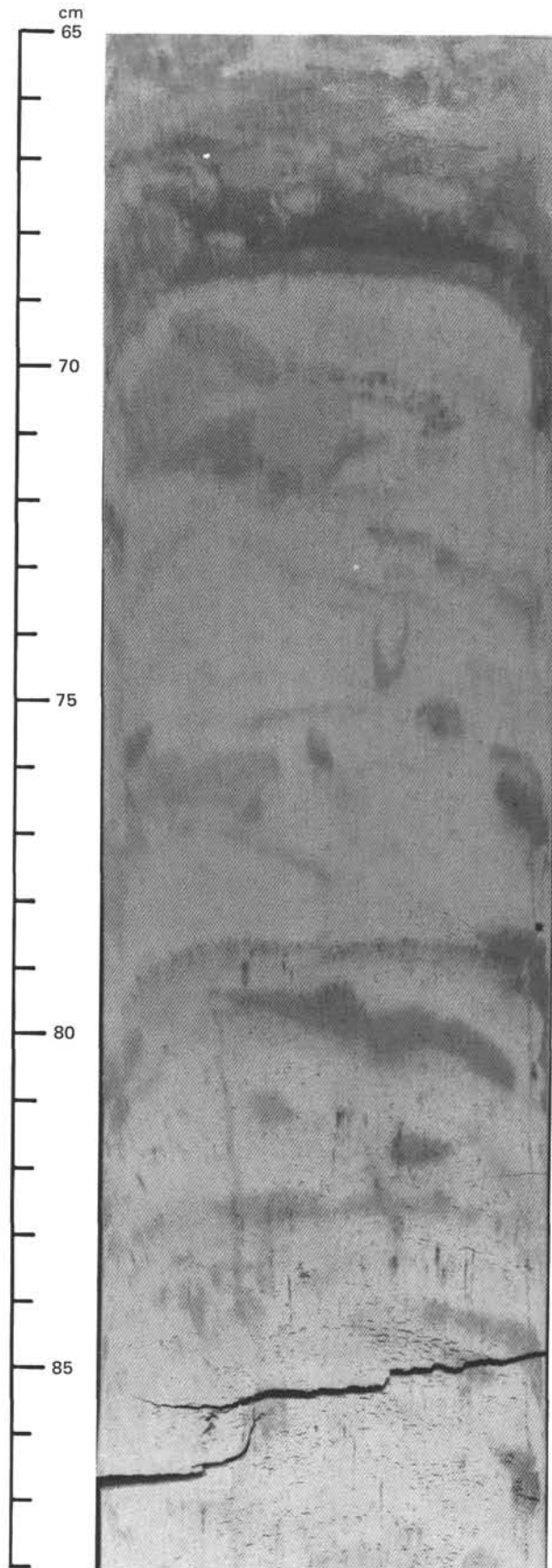


Figure 10. Bioturbated calcareous ooze, Section 627B-15H-4.



Figure 11. Thin-section photomicrograph of silicified limestone in Unit II. Note planktonic foraminifers infilled and partly replaced by chert. Planktonic foraminiferal packstone. Crossed nicols. Long dimension of photomicrograph covers 8 mm.

The top of the unit in Core 627B-27X consists of a 15-cm layer of limestone pebbles some of which are hardgrounds and chert. The matrix is highly disturbed ooze of variable color deformed by drilling. Locally, chinks are glauconitic (>5%), and some display evidence of moldic porosity.

This rather monotonous sequence of soft ooze alternating with lithified chalk (Fig. 12) has the gross appearance of primary cycles. However, core disturbance by the XCB varies from moderate to intense, and chinks are conspicuously fractured. Also, the occurrence of similar rhythms in the underlying unit, combined with the absence of such cycles in HPC cores, strongly suggests that these alternations are products of drilling disturbance.

Unit IV (325–344 m sub-bottom; Cores 627B-35X through 627B-36X)

Unit IV represents a condensed section of porous limestones. Core 627B-35X recovered only downhole-contaminated sediment from younger units. Core recovery in this section was poor, and recovered material contained a number of clasts from overlying units. The limestones contained burrows; in the yellowish limestone (Core 627B-36X), burrows have a light brown (2.5Y 6/4) margin and oxidized pyrite within the burrow fill. One thin section of the yellowish white limestone showed a calcisphere grainstone with cements varying in size from microspar to spar. Most

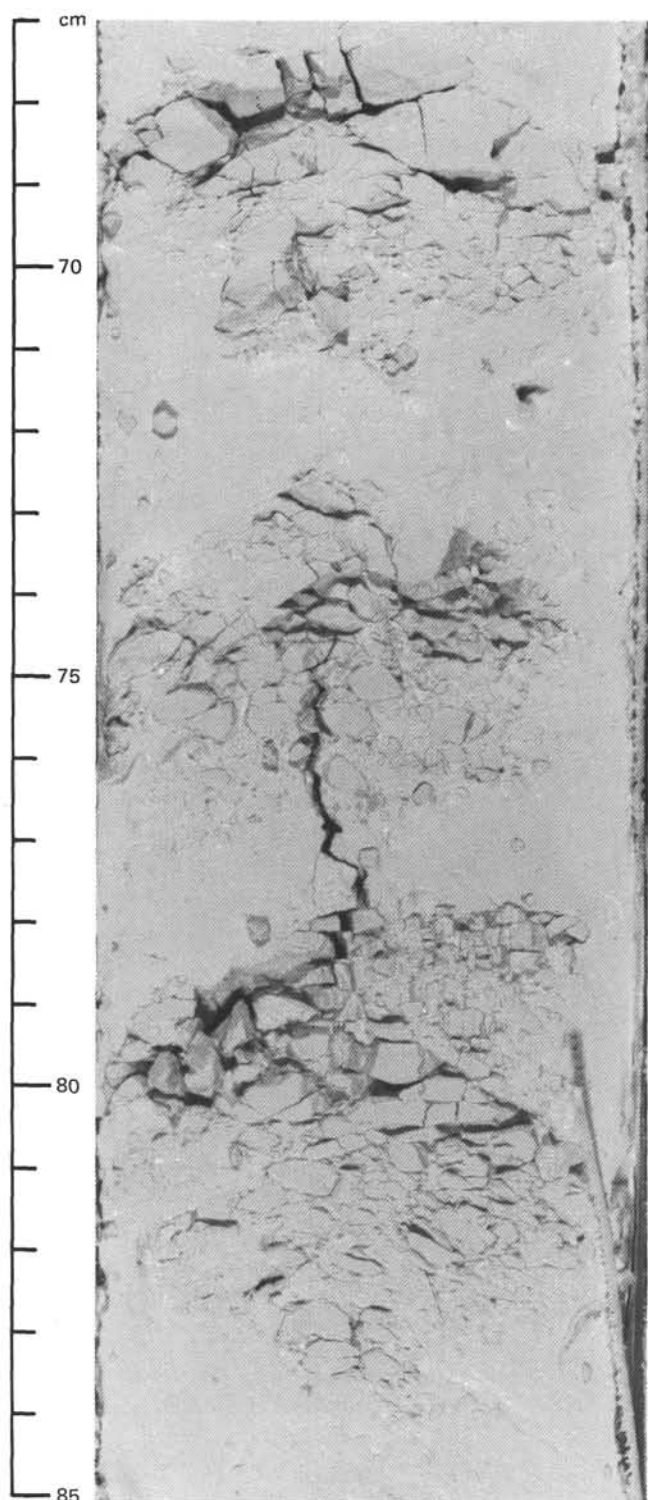


Figure 12. Chalk/ooze sequences in Unit III. Chalk is highly fractured; ooze may be drilling paste. Section 627B-27X-3.

of the porosity was in the form of hollow interiors of calcispheres.

Unit V (344–468 m sub-bottom; Cores 627B-37X through 627B-49X)

Unit V shows a distinct color change to olive gray (5Y 5/2) plus a decrease in total carbonate content. In Core 627B-37X

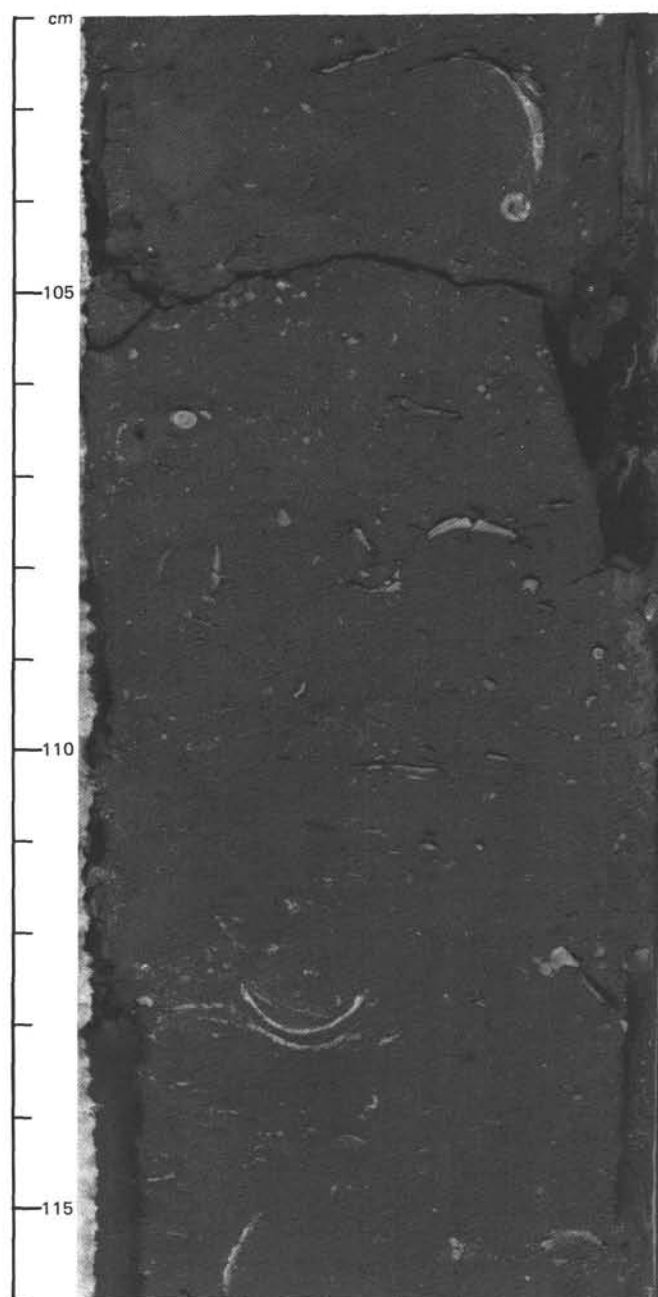


Figure 13. Skeletal olive gray chalk from Unit V, Section 627B-47X-5. Skeletal debris includes oyster valves and echinoid spines.

the gray limestone has marcasite around the burrow rims and contained some clay. Plant fragments were also recorded from Core 627B-37X. Cores 627B-38X to 627B-40X are marly chinks, whereas the underlying cores (Cores 627B-41X to 627B-49X), although still olive gray in color (5Y 5/2 or 5Y 4/2), are chinks and minor limestones. The silt- and clay-sized fraction near the top of the unit contains quartz, feldspar, and relatively low amounts of clay (Fig. 6), but grades downward to clay with minor quartz and feldspar. Traces of dolomite, pyrite, and glauconite are present with planktonic foraminifers and nannofossils (Fig. 6).

Throughout the unit, bioturbation is common to intense. Skeletal debris includes double-valved oysters in the lower part (Fig. 13) and echinoid spines. Some erosion surfaces are recognized within this unit, with truncation of burrows (Fig. 14) by

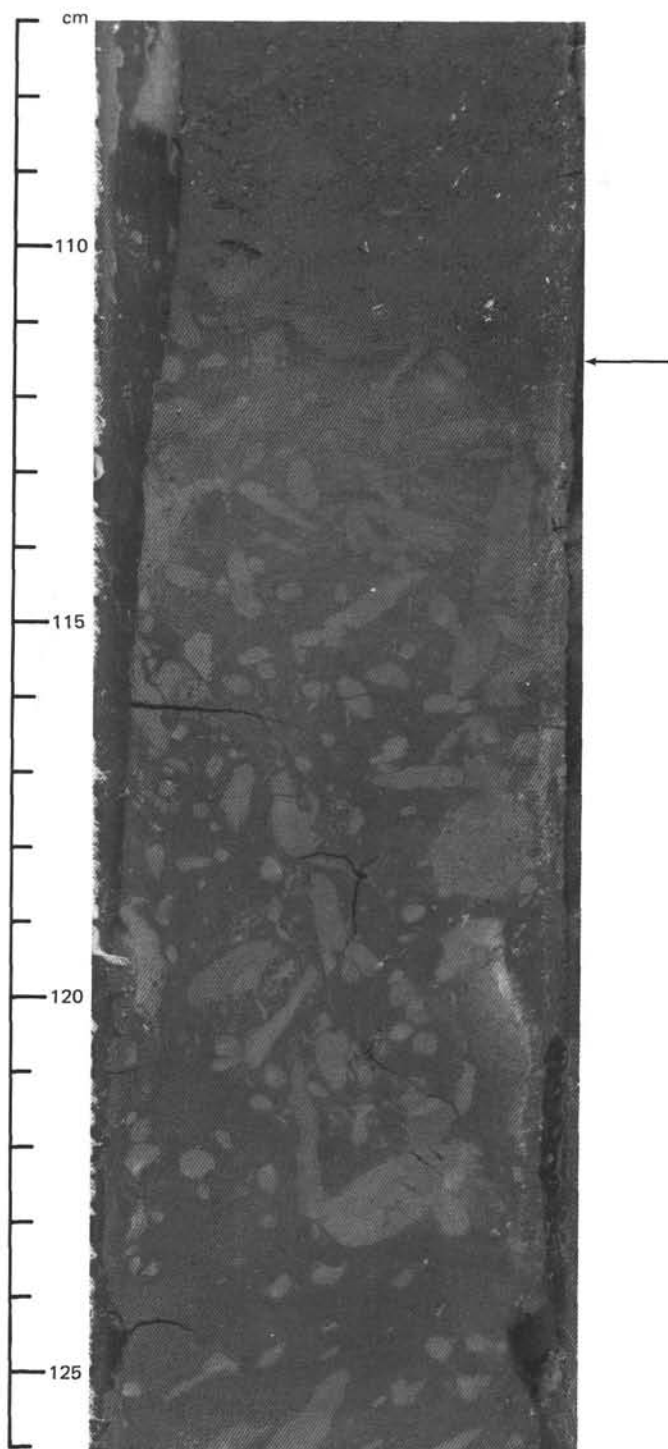


Figure 14. Erosion surface (horizontal arrow) with truncation of burrows. Unit V, Section 627B-39X-2.

coarser skeletal sediments. In many places burrow fills are of lighter colored sediment (with apparent higher carbonate content) not found elsewhere in the unit. Small pyritic or marcasitic concretions are present in some of the coarser skeletal bands some of which fine upward into a homogeneous chalk. The concentration of coarser skeletal debris overlying erosion surfaces indicates winnowing by storm waves; alternatively, these cycles may have been deposited by storm-induced turbidity currents.

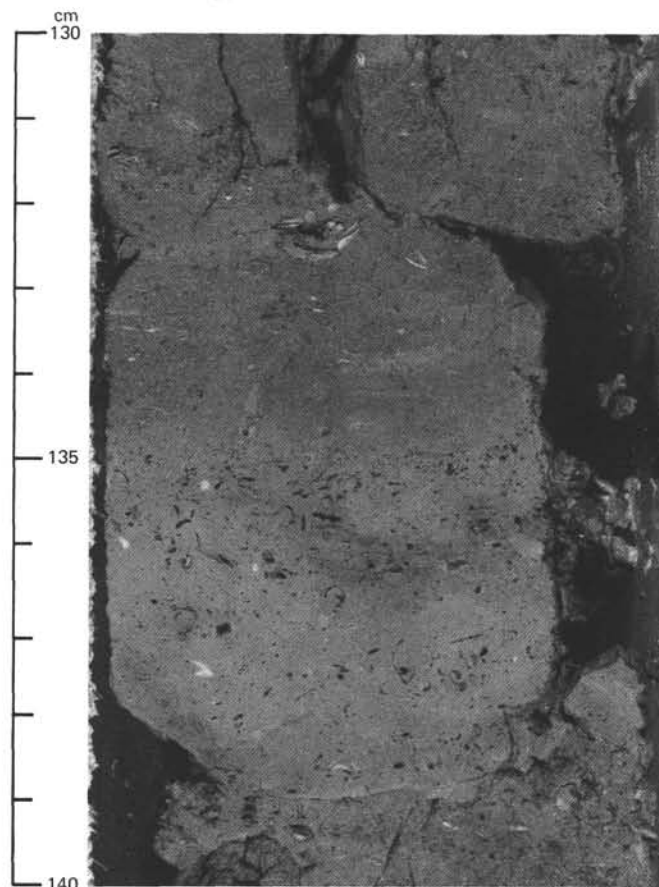


Figure 15. Limestone in Unit V with moldic porosity after dissolution of bivalve fragments, Section 627B-47X-6.

Toward the base of the unit, rare thin limestones with moldic porosity are present (Fig. 15).

Alternations of marly calcareous ooze and marly chalk occur commonly throughout the upper part of this unit and appear to be cyclic; they are also present in the chalks and oozes. The chalks are typically 3–5 cm thick separated by a thin (about 1 cm or less) dark band of marly ooze, best displayed in Core 627B-42X. It is presently unclear whether these alternations are primary depositional/diagenetic features or if they are an artifact of coring with the XCB, although the latter interpretation is preferred. Truncated burrow structures across some ooze/chalk boundaries suggest that these alternations are artifacts.

Unit VI (468–536 m sub-bottom; Cores 627B-50X through 627B-60X)

Unit VI comprises dolostone and gypsum (Fig. 16) with minor amounts of skeletal dolomitic limestone containing miliolid foraminifers (Fig. 17). Some of the dolostones display extensive secondary moldic porosity, whereas others are massive, mottled, finely crystalline dolomite or are laminated (algal mats?). Dolostones also display bioturbated or intraclastic textures with common vugs. The top of Unit VI was put at the base of Core 627B-49X. This assignment is based on the change in drilling rate. Core 627B-50X recovered only downhole contamination.

Massive, organic-rich gypsum was first recovered in Core 627B-55X and continues interbedded with dolostones for the remainder of the cored interval. The gypsum ranges from relatively clear and translucent to dark gray in color, with nodular

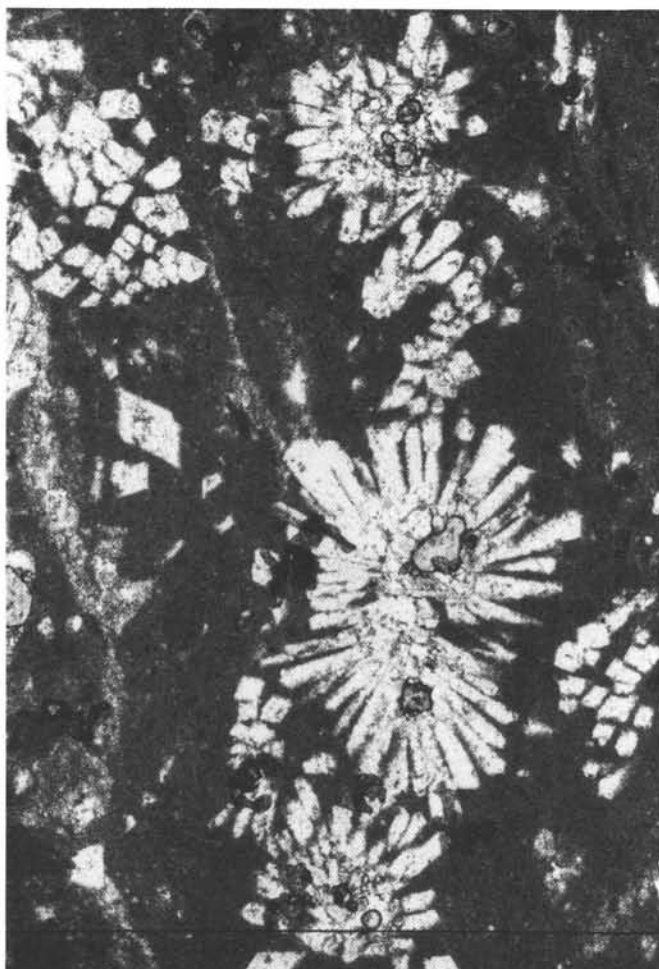


Figure 16. Thin-section photomicrograph of dolostone-gypsum facies of Unit VI. Note finely crystalline dolomite (dark) and replacement by radial crystals of gypsum (light). Small euhedral rhombs of dolomite are also present. Crossed nicols; long dimension of photomicrograph covers 32 mm.

textures and microstructures suggestive of recrystallization and/or remobilization. This unit can be further subdivided into an upper portion (468–514 m, consisting mostly of dolostones and limestones with only minor gypsum, Cores 627B-51X through 627B-54X) and a lower portion (514–536 m, Cores 627B-55X through 627B-60X) of interbedded gypsum and dolostones with minor limestone. Some of the dark-colored gypsum also produced a distinctive petroliferous odor upon cutting. Because of the occurrence of hydrocarbons (“Organic Geochemistry,” this chapter), Hole 627B was terminated at a total subsurface depth of 536 m.

Discussion

The six major lithologic units in Hole 627B (Table 2) form a highly distinctive vertical succession of facies punctuated by unconformities. Unit VI consists of dolostones and gypsum with minor limestones that were deposited on a restricted, shallow-water-carbonate platform during the late Albian. Bioturbated, skeletal dolostones with miliolid foraminifers and moldic porosity indicate deposition in a shallow, subtidal carbonate-lagoon environment, whereas dolostones provide possible evidence of a tidal or supratidal environment. Furthermore, the occurrence of

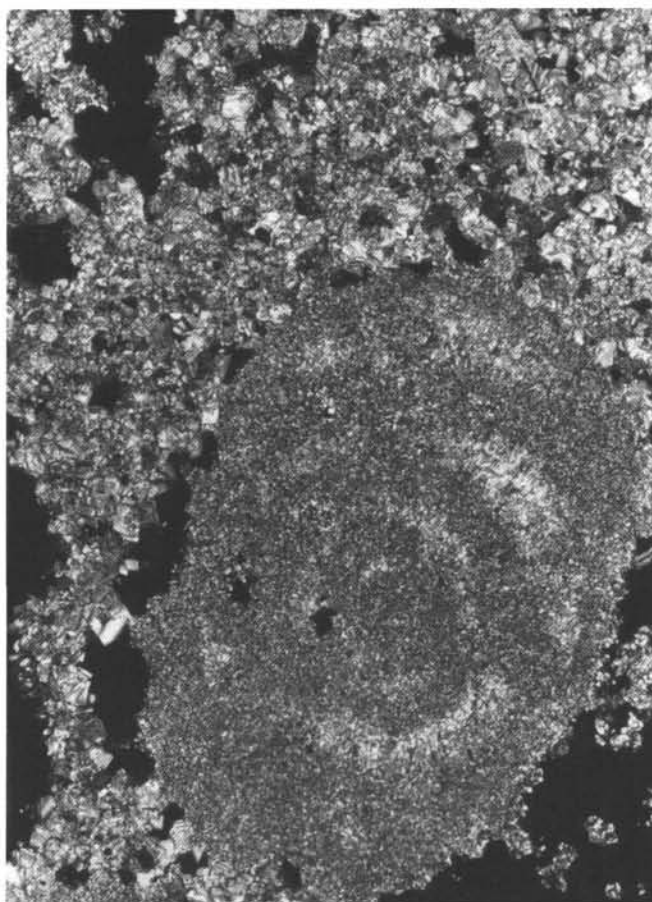


Figure 17. Thin-section photomicrograph of dolomitized miliolid from Unit VI. Larger subhedral dolomite crystals adjoin voids (black). Crossed nicols; long dimension of photomicrograph is 32 mm.

massive gypsum also implies a very shallow, low-energy, evaporative environment, possibly one of supratidal sabkhas.

The transition between dolostones and gypsum of Unit VI and overlying marls of Unit V appears to be abrupt, although lithostratigraphic and biostratigraphic control across this boundary is poor. This facies succession implies a rapid upward change from a shallow-water-carbonate platform to an open shelf. Although the provenance of the terrigenous components in Unit V is uncertain, it is a significant facies that separates underlying shallow-water carbonate/evaporites from overlying deep-water carbonates of Units I through III. In contrast, overlying Unit IV represents a condensed, relatively shallow-water stratigraphic section indicative of nondeposition and/or erosion.

Unit III marks the onset of pelagic carbonate sedimentation in the late Campanian on the southern Blake Plateau. The chalks and oozes of this unit are dominated by planktonic foraminifers and nannofossils and appear to represent an oceanic-plateau depositional environment with water depths of a few hundred to possibly a thousand meters. This chalk sequence also has relatively high rates of sediment accumulation (21–22 m/m.y.), which implies increased biological productivity of surface waters combined with lack of seafloor dissolution.

Unit II represents another punctuated, condensed stratigraphic section of deep-water chalks and oozes between the early Paleocene and early Miocene.

Sediment gravity-flow deposition on the lower slope north of Little Bahama Bank began in the early Miocene. A 35-m-thick

Table 2. Lithostratigraphic summary, Site 627.

Unit	Sub-bottom depths (m)	Age	Accumulation rate (m/m.y.)	Dominant lithology
I	0–181	early Miocene–Quaternary	7–15	Chalk, redeposited limestones
^a II	181–249	early Paleocene–early Miocene	1–3	Silicified limestone, chert
III	249–325	late Campanian	21–22	Chalk
^a IV	325–344	middle Cenomanian–early Santonian	2–3	Calcsphere limestone
V	344–468	late Albian–early Cenomanian	20–55	Marl
VI	468–536	late Albian		Dolostone, gypsum, limestone

^a Contains internal unconformities.

compound gravity-flow facies in Subunit IC appears to be correlative with partially coeval deposits of the Great Abaco Member in the Blake–Bahama Basin (Bliefnick et al., 1983) and those drilled at Site 626 in the northern Straits of Florida. The large areal distribution of these gravity-flow deposits suggests a tectonic and/or eustatic event of at least regional significance (see Site 626 chapter, this volume).

Subunit IB consists mostly of unlithified ooze and partially indurated chalk of middle to late Miocene age, although minor amounts of redeposited carbonates are also present. The oozes and chalks are composed dominantly of nannofossils and planktonic foraminifers with only minor amounts of micrite. These data suggest that Subunit IB represents a deep-water depositional environment relatively far from any carbonate platforms. This is further supported by modest sediment-accumulation rates of 7–10 m/m.y.

Subunit IA appears to mark a significant increase in platform input during the late Miocene at Site 627 north of Little Bahama Bank. This subunit consists mostly of deformed soft-sediment slump folds and debris-flow deposits interbedded with calcareous (periplatform) oozes and turbidites. Such an onset of slope sedimentation supports the carbonate-slope evolutionary scheme of Schlager and Ginsburg (1981). In their model, accretionary slopes dominated by slumps and debris flows evolve into bypass slopes with predominantly turbidites at the toe-of-slope, which in turn evolve into erosional slopes.

The late Pliocene to Quaternary section of Subunit IA records “contemporary” deposition along the distal lower slope north of Little Bahama Bank. This section consists of a mix of debris-flow deposits and periplatform oozes that are punctuated by numerous thin, fine-grained carbonate turbidites. Most of the clasts in these redeposited carbonates are slope-derived with little input of coarse-grained, shallow-water detritus. This composition could reflect the open-ocean, windward setting of this margin (Mullins and Neumann, 1979) and/or distance (about 50 km) from the Bahama Banks. In addition, the degree of early submarine diagenesis (represented by lithified layers) appears to increase upward in Unit I, which may reflect increasing input of metastable, bank-derived aragonite and magnesian calcite as this carbonate slope prograded seaward.

Conclusions

Overall, the lithostratigraphy of Site 627B appears to represent a sequence deepening upward, punctuated by unconformities and capped by a carbonate-slope facies prograding seaward. Very shallow-water dolostones and evaporites of Unit VI are followed abruptly by outer-shelf marls of Unit V, which in turn pass through a condensed section in Unit IV into oceanic-plateau chalks of Unit III, which pass through a second condensed sequence of Unit II and finally into “contemporary” carbonate-slope facies of Unit I.

BIOSTRATIGRAPHY

Introduction

Site 627 was drilled in order to aid in correlation of the regional seismic-stratigraphic framework with the Gulf of Mexico and the eastern coast of North America, to date the drowning of the southern Blake Plateau, and to examine the causes of platform drowning. Drilling at this site penetrated to a sub-bottom depth of 535.8 m and recovered Cenozoic and Cretaceous sediments.

All depths referred to are sub-bottom depths, and samples are from the core catcher unless otherwise specified.

Calcareous Nannofossils

Hole 627A

Drilling at Hole 627A recovered one core taken with the HPC. The upper 160 cm contains sediment in which *Emiliania huxleyi* is common to abundant. This indicates the younger part of Zone NN21 (late Pleistocene). The interval from Core 627A-1H (161 cm) through Core 627A-1H, CC contains an assemblage that lacks *E. huxleyi* and includes *Pseudoemiliania lacunosa*, indicating an NN19 age (early Pleistocene to latest Pliocene). No Neogene nannofossils were observed. Thus, lower and upper Pleistocene sediments are present in this core with a distinct hiatus separating them. This hiatus includes all of Zone NN20 and the older portion of Zone NN21.

Hole 627B

The first core of this hole contains essentially the same sediments as in Core 627A-1H (see above). The early Pleistocene (NN19) fauna recognized at the base of Core 627B-1H continues through Core 627B-2H. *Discoaster brouweri* and *Discoaster pentaradiatus* appear in the poorly to moderately preserved assemblage from Core 627B-3H, indicating Zone NN17, which is correlated with the late Pliocene. These two discoasters are joined by *Discoaster surculus* in Core 627B-4H, indicating Zone NN16 (late Pliocene). A poorly to moderately preserved assemblage from Core 627B-5H contains *Reticulofenestra pseudumbilica* and *Discoaster asymmetricus*. The rarity of ceratoliths in this assemblage makes it difficult to assign a zone precisely, so it has been designated as Zone NN14/15 (early Pliocene). The underlying Core 627B-6H, however, contains *Ceratolithus tricoroniculatus* occurring with *D. asymmetricus*. This indicates NN14 (early Pliocene). *Ceratolithus rugosus* is found in Core 627B-7H, indicating Zone NN12, which correlates with the early Pliocene to late Miocene.

The interval from Cores 627B-8H to 627B-14H contains nannofossil assemblages that are strongly overgrown. In Cores 627B-8H to 627B-9H, *Discoaster quinqueramus* is present. This is characteristic of Zone NN11, indicating the late Miocene. In

Cores 627B-10H through 627B-13H, most zonal marker species are either missing or unrecognizable, so that zonal assignments can be made only tentatively. The only discoasters that are present in this interval are strongly overgrown six-rayed forms. *Discoaster aulakos* occurs in Cores 627B-12H and 627B-13H, and *Discoaster* sp. cf. *D. exilis* occurs in Core 627B-13H, suggesting a range of zones from NN6 to NN10 (correlating with the late middle Miocene to late Miocene). This generalized zonal assignment agrees with the more definitive planktonic-foraminiferal assignment for this interval.

In Core 627B-14H *D. aulakos* was not observed. The absence of this form, in conjunction with the presence of *Discoaster brouweri* (early forms), *Discoaster variabilis*, and the sporadic occurrence of *Sphenolithus heteromorphus*, suggests Zone NN5 (middle Miocene). *Sphenolithus heteromorphus* is first consistently encountered in Core 627B-15H, indicating Zone NN5. This zone has been correlated with the middle Miocene. A similar assemblage of Zone NN5 occurs throughout Core 627B-16H. The co-occurrence of *S. heteromorphus*, *D. variabilis*, and *Helicopontosphaera ampliaperta* at the base of Core 627B-17X indicates Zone NN4, which straddles the early/middle Miocene boundary. *Sphenolithus belemnos* occurs with *S. heteromorphus* in Core 627B-18X, indicating the top part of Zone NN3 (early Miocene). *Sphenolithus heteromorphus* is absent from Core 627B-19X. In this core, *Sphenolithus belemnos* occurs with *Triquetrorhabdulus carinatus* and a large number of specimens of *Cyclicargolithus abisecta*, suggesting the lower part of Zone NN1-2. The NN1 assignment (earliest Miocene) is more in accordance with those of the planktonic foraminifers and radiolarians.

Recovery from Cores 627B-20X through 627B-23X was poor, with much of the material coming from downhole contamination (Pleistocene and Neogene). Chert fragments are common in this interval, as are isolated layers of foraminifer-nannofossil ooze. Nannofossil assemblages from these ooze fragments contain a latest Oligocene (NP25) assemblage that includes *Sphenolithus ciperoensis*, *Reticulofenestra bisecta*, *Zygrhabdolithus bijugatus*, and common *Cyclicargolithus abisecta*. Despite the nannofossil age obtained from the calcareous ooze, the siliceous sediments appear to be part of the early-middle Eocene cherts that are widespread in this part of the ocean (Bermuda Rise Formation). Thin sections of the chert fragments within this interval contain middle to early Eocene planktonic foraminifers. In fact, Eocene taxa such as *Discoaster lodoensis* and *Discoaster barbadensis* occur in samples from Core 627B-22X. In Core 627B-23X, these and other Eocene forms such as *Tribrachiatulus orthostylus* and *Discoaster lodoensis* are common enough to assign this interval to NP12/13 (early Eocene). It is most probable, therefore, that part of the interval from Core 627B-20X to Core 627B-23X is early to middle Eocene and that most of the calcareous-ooze fragments are downhole contaminants.

Recovery from Core 627B-24X consisted of 0.2 m of sediment containing abundant, well to moderately preserved assemblages from the late Paleocene. Characteristic forms include *Fasciculithus tympaniformis*, *Chiasmolithus bidens*, and *Heliolithus riedeli*, suggesting nannofossil Zone NP8. This age assignment is tentative, however, as the discoasters generally present in this zone were not found. The absence of discoasters in this sample may indicate a somewhat stressed environment, possibly related to cooler surface waters. In Core 627B-25X, *Heliolithus kleinpellii* occurs without discoasters or *H. riedeli*, indicating that this assemblage belongs to Zone NP6. This zone is also correlated with the late Paleocene. The only sedimentary record of the early Paleocene occurs near the base of Core 627B-26X. Assemblages from the base of this core can be assigned to nannofossil Zone NP2 based on the absence of *F. tympaniformis* and *Chiasmolithus danicus*. *Braarudosphaera bigelowi* is abundant,

which may indicate a shallow-water deposit. This lower Paleocene material is separated from the underlying Cretaceous by 20 cm of severely disturbed ooze, chert, and limestone pebbles with hardground surfaces in Core 627B-27X, 0-17 cm.

No Maestrichtian sediment was recovered, as the sediment just below the pebble layer is of late Campanian age. The condition of preservation of the nannofossils, although generally good, prevented positive identification of *Reinhardtites anthophorus* in samples from core catchers in Cores 627B-27X through 627B-32X. These nannofossil assemblages belong to either the *Tranolithus phacelosus* Zone or the *Quadrum trifidum* Zone (middle to late Campanian). Characteristic forms present include *Quadrum trifidum*, *Quadrum nitidum*, *Eiffellithus parallelus*, and *Reinhardtites levis*. *Lithastrinus grilli* joins this assemblage in Cores 627B-33X and 627B-34X, whereas *Quadrum trifidum* disappears from them. This indicates the *Quadrum nitidum* Zone (middle Campanian). Samples from Cores 627B-35X and 627B-36X were too poorly preserved and mixed with obvious downhole contaminants to yield a reliable age determination.

Samples from the green marly chalks in Cores 627B-37X and 627B-38X contain assemblages that include *Eiffellithus turriseiffeli*, *Lithraphidites acutum*, and *Corollithion kennedyi* (? = *C. completum*), indicating the *Lithraphidites acutum* Zone. This zone correlates with the middle to late Cenomanian. The presence of *Reinhardtites fenestratus* and *Rhagodiscus asper* in these assemblages suggests the middle Cenomanian portion of the zone. In the sequence from Cores 627B-39X through 627B-49X, *L. acutum* has not been observed. These assemblages include *E. turriseiffeli*, *Vekshinella angusta*, *Cruciellipsis chiastia*, and *Pre-discosphaera columnata*, indicating the *E. turriseiffeli* Zone (late Albian to middle Cenomanian). The *E. turriseiffeli* Zone can be divided into two subzones based on the extinction of *Hayesites albiensis* in the latest Albian. This taxon has not been observed in any samples within this interval, indicating the younger *Pre-discosphaera spinosa* subzone. This subzone is correlated with the very latest Albian to middle Cenomanian. The primitive nature of the eiffellithids and prediscosphaerids in the basal part of the core sequence, as well as the absence of *C. kennedyi* from Cores 627B-45X through 627B-49X, suggests that this interval is not younger than the earliest Cenomanian. The presence of *Braarudosphaera africana* in Core 627B-49X, in addition to the criteria cited immediately above, suggests that this core is earliest Cenomanian or possibly latest Albian.

No nannofossils were observed in the underlying sequence of shallow-water dolostones and evaporites.

Planktonic Foraminifers

Hole 627B

Sediments of early Pleistocene age are present in Cores 627B-1H and 627B-2H (5.8 m, 15.5 m). Species that indicate the lower *Globorotalia truncatulinoides* Zone (N22) include *Globorotalia truncatulinoides* and *G. tosaensis*. The benthic-foraminiferal fauna in Core 627B-1H is composed of deep-sea forms, whereas that of Core 627B-2H contains deep-sea and neritic forms.

Uppermost Pliocene (*Globorotalia tosaensis* Zone, N21/N22) sediments are present in Core 627B-3H (25.20 m). Diagnostic species include *Globorotalia tosaensis* and *G. miocenica*. Deep-water benthic foraminifers are present in this sample. A probable late Pliocene age (*Globorotalia miocenica* Zone, N19 part) is assigned to Core 627B-4H (34.7 m), based on the absence of *Globorotalia truncatulinoides*, *G. tosaensis*, *G. margaritae*, and the presence of *Globorotalia* sp. cf. *G. miocenica*. Deep-water and neritic benthic foraminifers are present in this sample. Cores 627B-5H, 627B-6H, and 627B-7H (44.2 m, 53.80 m, 63.3 m) represent the lower Pliocene *Globorotalia margaritae* Zone (N18/N19 part), based on the presence of *Globorotalia margaritae*.

Other important species include *Globoquadrina altispira altispira*, *Globorotalia plesiotumida*, and *Globigerina nepenthes*. The benthic foraminifers in these samples are predominantly deep-water forms.

Upper Miocene sediments are present in Cores 627B-8H, 627B-9H, and 627B-10H (72.9 m, 82.5 m, 92.0 m). Species that indicate the *Neogloboquadrina acostaensis* Zone (N16/N17 part) include *Neogloboquadrina acostaensis*, *Globoquadrina dehiscentes*, *Globorotalia plesiotumida*, and *G. linguaensis*. Deep-sea forms dominate the benthic assemblage in these samples.

Core 627B-11H and most of Core 627B-12H appear to be part of a slump deposit that has been emplaced onto younger sediments in the lower part of Core 627B-12H. Species indicative of the middle Miocene *Globorotalia fohsi lobata/robusta* Zone (N11 part through N13 part) are present in Section 627B-11-3 (95.25 m) and Core 627B-11H, CC (101.5 m). Neritic and deep-sea benthic foraminifers are present in these samples. Core 627B-12H, CC (111.3 m) contains planktonic species indicative of the late middle Miocene *Globorotalia mayeri* Zone (N13 part/N14). Thus, it appears that sediments of the latest middle Miocene *Globorotalia menardii* Zone (N15) are missing.

Core 627B-13H (120.8 m) is contained within the middle Miocene *Globorotalia fohsi lobata/robusta* Zone (N11 part through N13 part). Species present include *Globorotalia fohsi lobata*, *G. fohsi fohsi*, *G. fohsi praefohsi*, and *G. fohsi peripheroacuta*. Large specimens of *Globoquadrina altispira altispira* are abundant. The benthic-foraminiferal fauna is composed entirely of deep-water species. An assemblage that includes *Globorotalia fohsi* sp. cf. *G. lobata*, *G. fohsi fohsi*, and *G. fohsi peripheroacuta* is present in Core 627B-14H (130.3 m), indicating a middle Miocene age (*Globorotalia fohsi fohsi* Zone, N10/N11 part). Specimens of *Globoquadrina altispira altispira* are large and abundant. All benthic foraminifers are deep-water species. Core 627B-15H (139.9 m) is assigned to the early middle Miocene *Globorotalia fohsi peripheroronda* Zone (N9). Diagnostic species include *Globorotalia fohsi peripheroronda*, *Orbulina suturalis*, and *Praeorbulina glomerosa* (s.l.). Specimens of *Globoquadrina altispira altispira* are reduced in both number and size. The benthic-foraminiferal fauna is dominated by deep-water species, with some neritic species present. The presence of *Praeorbulina glomerosa* (s.l.) and *Globigerinoides sicanus* without *Orbulina* in Core 627B-16H (149.7 m) suggests that these sediments are contained within the early middle Miocene *Praeorbulina glomerosa* Zone (N8 part). All benthic foraminifers are deep-water species.

Cores 627B-17X, 627B-18X, and the upper part of 627B-19X (162.2 m, 171.8 m, 172.4 m) are assigned to the *Globigerinatella insueta* Zone (N7/N8 part; early Miocene/early middle Miocene), as suggested by the absence of *Praeorbulina* and *Catapsydrax*. The presence of *Globigerinoides sicanus* suggests that these sediments are from the upper part of this zone (Stainforth et al., 1975). As at Site 626, *Globigerinatella insueta* is a rare species and, in fact, was not observed in the samples examined from this site. Only benthic foraminifers indicative of deep water are present in Cores 627B-17X and 627B-18X. The debris-flow deposits of Core 627B-19X contain a mixture of deep-water and neritic benthic foraminifers.

The lower part of Core 627B-19X (181.4 m) as well as part of Core 627B-20X (191.0 m) is contained within the early Miocene *Globorotalia kugleri* Zone (N4), based on the presence of *G. kugleri*, *G. pseudokugleri*, *G. opima nana*, *Globigerina angulicentralis*, and *Globigerina* sp. cf. *G. ciperoensis*. Thus, it appears that the *Catapsydrax stainforthi* and *Catapsydrax dissimilis* Zones are missing. This hiatus almost certainly corresponds to a lithologic break in Section 627B-19X-6. Also present in Core 627B-20X (191.0 m) is a single specimen of *Morozovella*, which may be derived from *in-situ* Eocene deposits in the interval from 181.4 to 191.0 m sub-bottom. Therefore, a second

unconformity, separating lowermost Miocene–uppermost Oligocene sediments from chert-bearing Eocene strata, probably occurs within the interval of Core 627B-20X.

Chert was first encountered in Core 627B-20X. Recovery of *in-situ* strata was negligible from Core 627B-20X through 627B-23X (181.4–219.9 m sub-bottom), presumably owing to the difficulty in coring chert-bearing intervals. Nearly all sediment recovered in this interval is downhole contamination consisting of Neogene debris and an abundance of Pleistocene material (including well-preserved pteropods). Planktonic foraminifers indicating a latest Oligocene–earliest Miocene age (N4) also constitute a significant fraction of the caved material. Eocene planktonic foraminifers are sparse in the mixed debris but are abundant in the chert nodules. Thin clay-rich layers from Cores 627B-21X and 627B-22X contain a higher concentration of Eocene taxa, although the dominant component is the earliest Miocene–latest Oligocene fauna. The occurrence of *Globorotalia pomeroli* in a chert nodule from Core 627B-20X, CC indicates a late middle Eocene to late Eocene age (mid-P12 to P16). A middle Eocene age (P11/P12) in Core 627B-21X, CC is indicated by the presence of *Hantkenina dumblei*, *Acarinina bullbrookii*, and *Morozovella* sp. cf. *M. spinulosa*. A poorly constrained early middle to late early Eocene age is suggested for Core 627B-22X, CC. Core 627B-23X, CC contains an early Eocene (P7/P8) assemblage that includes *Morozovella formosa formosa*, *M. aragonensis*, *M. subbotinae*, *Acarinina quarta*, and *A. wilcoxensis*.

A stratigraphic break separates the lower Eocene from Paleocene strata in Cores 627B-24X through 627B-26X (219.9 to 248.7 m sub-bottom). Planktonic foraminifers of the late Paleocene *Planorotalites pseudomenardii* Zone (P4) are present in Core 627B-24X, CC. Diagnostic taxa include *Planorotalites pseudomenardii*, *P. pusilla* s.l., *Morozovella velascoensis*, *M. conicotruncana/angulata*, and *M. aequa*. Core 627B-25X, CC is late early Paleocene in age (P2/P3a), as indicated by the presence of *Subbotina pseudobulloides*, *S. triloculinoides*, *Planorotalites compressus*, *Subbotina praecursoria*, and *Morozovella conicotruncana/angulata*. Core 627B-26X, CC contains an abundance of *Subbotina pseudobulloides* and *S. triloculinoides*, indicative of the early Paleocene *Subbotina pseudobulloides* Zone (P1b).

The lower Paleocene section is unconformably underlain by Campanian chalks and oozes (Core 627B-27X-1, 20 cm, through Core 627B-34X; 248.9 to 324.7 m sub-bottom). Two zones are recognized, the *Globotruncana calcarata* Zone of latest Campanian age in Cores 627B-27X to 627B-31X and the *Globotruncana ventricosa* Zone of middle to late Campanian age in Cores 627B-32X to 627B-34X. The occurrence of *G. calcarata* serves to distinguish the two zones. *Globotruncana subspinoso*, the ancestor of *G. calcarata*, occurs in Cores 627B-31X and 627B-32X. Other characteristic taxa of the late Campanian include *Globotruncana linneiana*, *G. rosetta*, *G. fornicata* s.l., *G. orientalis*, *G. stuartiformis*, *G. arca*, *G. atlantica*, and *Pseudotextularia elegans*. A diverse benthic-foraminiferal fauna indicative of outer neritic to bathyal depths occurs throughout the upper Campanian interval. Common forms include *Bolivinoidea*, *Neoflabellina*, *Stensioina*, *Eouvigerina*, bolivinids, buliminids, and nodosariids.

Problems with core-barrel retrieval in the interval from 324.7 to 334.3 m sub-bottom (Core 627B-35X) resulted in the recovery of caved material. Core 627B-36X yields a Coniacian–early Santonian age, as suggested by the occurrence of *Globotruncana sigali*, *G. coronata*, *G. lapparenti*, *G. angusticarinata*, *G. tarfayaensis*, and *G. undulata*. Abundant calcispheres and common pellets of phosphatic material and glauconite are also noted. Benthic foraminifers include *Gavelinella*, *Lenticulina*, *Eouvigerina*, a questionable cibicid, and bolivinids.

Another major hiatus separates the Coniacian deposits from a thick sequence of latest Albian–earliest Cenomanian to middle Cenomanian marly chalks in Cores 627B-37X through 627B-

49X (343.9 to 467.8 m sub-bottom). The *Rotalipora reicheli* Zone of middle Cenomanian age occurs in Core 627B-37X. Diagnostic planktonic taxa include *Rotalipora reicheli*, *R. cushmani*, and *R. greenhornensis*. Abundant specimens of *Pithonella* and/or calcispheres occur in Core 627B-37X. According to Tappan (1980), these supposed free-floating calcareous algal spores or cysts occur in outer-shelf environments. High concentrations of *Pithonella* have been attributed to blooms, perhaps related to nutrient availability near the shelf-slope break. Most planktonic specimens are juvenile forms of *Hedbergella* and *Globigerinelloides*. *Heterohelix moremani* is also present in significant numbers. Keeled taxa (*Rotalipora* and *Praeglobotruncana*) are rare. The paucity of keeled forms and the abundance of juveniles suggest a neritic environment. Also present in Core 627B-37X, CC are ostracodes and a fairly diverse benthic-foraminiferal fauna including species of *Lingulogavelinella*, *Gavelinella*, *Lenticulina*, *Fronducularia*, and *Tritaxia*.

Core 627B-43X, CC is late early Cenomanian to middle Cenomanian in age, based on *Rotalipora* aff. *cushmani*, *R. greenhornensis*, and *R. gandolfii* (upper *R. gandolfii* or *R. reicheli* Zone). A latest Albian to early Cenomanian age is suggested for Cores 627B-45X to 627B-47X based on the co-occurrence of *Rotalipora gandolfii* and *R. appenninica*. The absence of *Planomalina buxtoni* suggests an early Cenomanian age, although environmental exclusion from a neritic environment may be a viable explanation. The presence of *R. gandolfii*, *Hedbergella washitensis*, and *H. libyca* in Core 627B-49X suggests a latest Albian-earliest Cenomanian age for the base of this depositional unit.

The proportion of planktonics to benthics decreases from Core 627B-37X to Core 627B-49X. The number of keeled specimens (deepest dwelling forms) also decreases through this interval, whereas the proportion of shallow-dwelling taxa (*Gubkinella graysonensis*, *Guembelitra cenomana*, *Heterohelix moremani*, *Hedbergella libyca*, and *H. washitensis*) to intermediate-depth forms (other hedbergellids and *Globigerinelloides* spp.) increases downsection (see Leckie, 1984). Stratigraphically, these trends suggest that the depositional setting gradually changed from an inner neritic (Core 627B-49X) to an outer neritic environment (Core 627B-37X).

Carbonate-platform deposits are present from Cores 627B-50X through 627B-60X. These strata are barren of planktonic foraminifers.

Radiolarians

Twenty samples were selected for radiolarian study from clay-rich intervals of Hole 627B. Half of these came from Cores 627B-18X and 627B-19X, and contained few to common radiolarians, along with abundant siliceous sponge spicules. The other samples proved to be barren of radiolarians except for Sample 627B-12-5, 62–64 cm, which contained several nondiagnostic taxa. A few radiolarians were also observed in thin sections of chert pebbles from Core 627B-21X. The occurrence of *Phorocorytis* sp. suggests an early to middle Eocene age.

Sample 627B-18X-1, 60–62 cm, from unlithified foraminiferal packstone, contains sparse, moderately preserved radiolarians. Diagnostic species are rare and include *Stichocorys wolffii*, *Stichocorys delmontensis*, and *Didymocorytis mammifera*. These species indicate the upper *Calocycletta costata* to lower *Dorcadospyrus alata* Zones, of latest early to earliest middle Miocene age, respectively.

Nine samples were taken from the lithologically heterogeneous Core 627B-19X. The upper six are from green clay intraclasts from the unlithified floatstone in the upper part of the core, above Sample 627B-19X-6, 50 cm. The lower three samples are from the firm nannofossil ooze in the lower part of the core. Radiolarians and siliceous sponge spicules are much more abundant in the ooze than in the floatstone clasts.

The six samples from Sections 627B-19X-1 through 627B-19X-5 are from mud clasts in the floatstone, and age assignments obtained from the clasts do not necessarily apply to the matrix. The appearance of *Stichocorys delmontensis* in Sample 627B-19X-5, 20–22 cm, suggests the *Stichocorys delmontensis* Zone. This is supported by the occurrence of *D. atechus*, which has its last appearance near the top of the *S. delmontensis* Zone. However, *Liriospyris stauropora* also occurs, and this species first appears near the base of the overlying *Stichocorys wolffii* Zone. *Stichocorys wolffii* occurs in Sample 627B-19X-2, 46–48 cm. This suggests that clasts in Sections 1 and 2 represent the lower *S. wolffii* Zone, whereas those in Sections 3 through 5 of Core 627B-19X may represent the upper *S. delmontensis* Zone. Other species that occur in the mud-clast samples and indicate these zones are *Cyrtocapsella cornuta*, *Cyrtocapsella japonica*, *Cyrtocapsella tetrapera*, *Theocorys spongoconum*, *Carpocanopsis cingulata*, *Eucyrtidium diaphanes*, *Didymocorytis prismatica*, *Carpocanopsis favosa*, and *Carpocanopsis bramlettei*.

The floatstones in Core 627B-19X and overlying cores are tentatively identified as representing debris flows of the Great Abaco Member of the Blake Ridge Member first recovered at Site 391 (see "Summary and Conclusions" section, this chapter). The radiolarian results here agree with those obtained by Weaver and Dinkelman (1978) from Site 391 (Blake-Bahama Basin), with slumped material representing the *S. wolffii* and *S. delmontensis* Zones occurring within *C. costata* Zone material. Likewise, Jansa et al. (1979) indicate that the Great Abaco Member may occur in the lower through upper Miocene section in the Blake-Bahama region.

Samples 627B-19X, CC, 627B-19X-7, 20–22 cm, and 627B-19X-6, 60–62 cm (from the firm ooze), are assigned to the *Cyrtocapsella tetrapera* Zone of early Miocene age, based on the presence of *C. tetrapera* (the first occurrence of which marks the base of the zone) and the absence of *Stichocorys delmontensis* and *Carpocanopsis bramlettei* (the first occurrence of which marks the base of the overlying *Stichocorys delmontensis* Zone). *Calocycletta serrata*, a species restricted to the lower part of the *C. tetrapera* Zone, occurs in these samples and suggests that they represent only the lower part of the zone. Other species that support this age assignment are *Didymocorytis prismatica*, *Cyclampterium pegetrum*, *Lychnocanoma elongata*, *Calocycletta virginis*, *Calocycletta robusta*, *Tepka perforata*, *Cyrtocapsella cornuta*, *Dorcadospyrus atechus*, *Eucyrtidium diaphanes*, *Theocorys spongoconum*, *Dorcadospyrus simplex*, and *Carpocanopsis favosa*.

Larger Benthic Foraminifers

Hole 627A

Sample 627A-01H-01, 50–52 cm, recovered from Pleistocene sediments, contains *Archaias angulatus*.

Hole 627B

Much of the Neogene sediment recovered from Hole 627B was pelagic in nature and did not contain larger foraminifers, but Core 627B-01H yields *Archaias angulatus*. Samples from 627B-12H-4 and 627B-13X-4 (middle Miocene with planktonic foraminifers) contain *Nummulites cojimarensis* and *Amphistegina*. These forms are considered to be redeposited from the Little Bahama Bank platform. Sample 627B-14H-5, 80–82 cm (dated as Zones N10/N11 with planktonic foraminifers), yields *Nummulites* sp., *Miogypsina* sp. and *Lepidocyclina* (*L.*) *yurnagunensis* (which disappears in Zone N7), which are reworked. Core 627B-17X-1 (early-middle Miocene Zones N7/8) also contains *Miogypsina* sp. and *Lepidocyclina* (*L.*) *yurnagunensis*. Much of the material recovered in the interval from Cores 627B-21X through 627B-23X was Quaternary sediment emplaced as down-hole contamination. Assemblages from these cores contain *Ar-*

chias angulatus, *Nummulites cojimarensis*, *Amphistegina* sp., *Sphaerogypsina* sp., and *Gypsina vesicularis*. The stratigraphic range of *A. angulatus* spans the Oligocene to Holocene. *Nummulites cojimarensis* ranges from planktonic-foraminiferal Zones N7 to N20 (middle Miocene to late Pleistocene). In addition, some specimens of *Lepidocyclina* sp. were recovered. This taxon disappears in the middle Miocene. All of these larger foraminifers are considered to be reworked or redeposited into the Quaternary sediment at Site 627 from the Little Bahama Bank platform.

No larger foraminifers were found from the pelagic and hemipelagic sediments in Cores 627B-24X to 627B-49X. Core 627B-52X, CC contains generalized textularids, miliolids, *Nezzazata* sp., *Nummoloculina* sp. aff. *N. heimi*, *Cuneolina pavonia parva*, and *Paracoskinolina sunnilandensis*. The latter species has been described from the Albian of Texas and is known only from the Albian in the western hemisphere. The many citations of *P. sunnilandensis* from the Barremian and early Aptian of the Old World are considered to be in error. This European form must be considered to be a new species. The assemblages with *P. sunnilandensis* and *Nummoloculina* suggest a late Albian age. In addition, *Cuneolina pavonia parva* is known to occur only in the upper part (Albian to Cenomanian) of the Cat Island section of Great Bahama Bank (Freeman-Lynde et al., 1981). These tropical foraminifers are typical of shallow-water, back-reef environments. Core 627B-57X contains *Nummoloculina* sp. aff. *N. heimi* and the same generalized miliolids as in Core 627B-52X, suggesting a similar age.

These larger foraminifers indicate that the top of the shallow-water platform drilled at Site 627 must be attributed to the Albian and most probably is late Albian in age.

Summary

Drilling at Site 627 recovered Albian through Quaternary sediments. A short section of upper Pleistocene (160 cm in Core 627A-1H) is separated from the lower Pleistocene by an unconformity. The underlying section suggests relatively continuous sedimentation from late Miocene through early Pleistocene time. A possible hiatus separates this section from the underlying uppermost lower Miocene to middle Miocene. A substantial unconformity separates Neogene sediments from siliceous sediments deposited during the early to middle Eocene. Below this lies a short section of Paleocene. The range of ages and the thinness of the section suggest that sedimentation during this time may have been either punctuated or condensed. The Cenozoic section is separated from the Mesozoic by a substantial hiatus that includes the earliest Paleocene and all of the Maestrichtian. The underlying upper Campanian section consists of purely pelagic sediment with open-ocean microfaunas and microfloras. This relatively thick Campanian section is underlain by a sequence of lower to middle Cenomanian hemipelagic marls. The microfaunas indicate that the top of this Cenomanian section represents an outer-shelf (outer-neritic) environment, whereas the base is inner shelf (?middle neritic). The underlying sequence of shallow-water-platform dolostones and evaporites is Albian and most probably late Albian in age. These stratigraphic relationships in the mid-Cretaceous suggest that little time elapsed between deposition of the shallow-water-platform sediments and subsequent deposition of the hemipelagic sequence.

SEDIMENT-ACCUMULATION RATES

About 185 m of Quaternary and Neogene strata is present at Hole 627B. The uppermost Miocene to Holocene sediments accumulated at an average rate of 14–15 m/m.y. (Fig. 18), whereas the upper lower Miocene through middle Miocene sequence accumulated at a slightly reduced rate of about 7–10 m/m.y. Redeposition characterizes much of the Neogene section. Shore-

based studies are needed to delineate more precisely the hiatuses and slumped or displaced units within this sequence. The base of a debris flow in Sample 627B-19X-6, 50 cm, marks a stratigraphic break of about 4 m.y. separating late early Miocene sediments from those of the earliest Miocene. A section of uppermost Oligocene–lowermost Miocene nannofossil ooze and foraminifer packstone of unknown thickness overlies silicified limestone-bearing strata of Eocene age first encountered in Core 627B-20X. Most if not all of the Oligocene is missing. The Eocene section in Cores 627B-20X through 627B-23X accumulated at a very slow average rate, 1–3 m/m.y. A hiatus of up to 3–4 m.y. may separate the Paleocene from Eocene nannofossil-foraminifer ooze and chalk recovered in Cores 627B-24X through 627B-26X. The Paleocene sequence accumulated at a rate of less than 5 m/m.y.

Maestrichtian and lowermost Paleocene sediments are missing at Hole 627B. A stratigraphic break of 4–5 m.y. spans the Cretaceous/Tertiary boundary. Upper Campanian nannofossil ooze and chalk are present in Sample 627B-27X-1, 20 cm, through Core 627B-34X. This sequence accumulated at a rate of about 15–36 m/m.y. Two additional hiatuses in the Upper Cretaceous section separate Campanian from Coniacian–lower Santonian sediments in Core 627B-36X and uppermost Albian–middle Cenomanian marly chinks in Cores 627B-37X through 627B-49X. This latter unit accumulated at a rate in the range of 24–37 m/m.y. Insufficient biostratigraphic control in the underlying sequence of dolostones and gypsum (Cores 627B-50X through 627B-60X) precludes the estimation of sediment-accumulation rates in this section.

INORGANIC GEOCHEMISTRY

Interstitial Water

Interstitial-water samples were taken from Core 627A-1H and the first five cores of Hole 627B. Thereafter, every third core was sampled, recovery permitting. The results (see Figs. 19 and 20 and Tables 3 and 4) indicate considerable variation in the Ca and Mg concentrations with increasing depth, with several pronounced deviations from the trends typical of previous DSDP sites (see Gieskes, 1981). These deviations from the otherwise constant downhole increases in Ca and decreases in Mg can be ascribed to contamination by normal seawater, a scenario confirmed by corresponding changes in the pH and alkalinity as well as the presence of recent sediment in sub-bottom cores (See "Sedimentology" section, this chapter). Sulfate concentrations show a wide range of values (see Fig. 20; between 24 and 34 mmol) but are essentially not depleted from their seawater concentrations. This is similar to results obtained at Site 626.

As at Site 626, explanations must be sought for the trends in Ca and Mg. Whereas at Site 626, no source of igneous or terrigenous materials was detected that might provide sufficient Ca, at Site 627 a section containing considerable amounts of feldspar and clay minerals was penetrated between 354 and 468 m sub-bottom (Cores 627B-38X to 627B-49X). Whether the amounts of igneous minerals in this unit are sufficient to produce the observed calcium and magnesium gradients remains to be determined.

Underlying this section, gypsum was encountered. This mineral may possibly act as a source of SO_4^{2-} and may account for the absence of gradients in this parameter.

X-Ray Studies

A number of samples from Holes 627A and 627B were x-rayed in order to determine (1) approximate percentages of aragonite, calcite, dolomite, and quartz; (2) the amount of mol% MgCO_3 in the calcite and dolomite; and (3) the presence of other minerals; the data are shown in Tables 5 and 6 and in Figures 21, 22,

and 23. The results from these studies complement interpretations made regarding the sedimentology. For example, the upper Miocene portion of Hole 627B, extending to a sub-bottom depth of 110 m, is characterized by abundant but highly variable amounts of aragonite (see Fig. 22). Such an abundance supports the notion of a slope facies for this unit, the varying amounts of aragonite reflecting differing rates of input from the bank. Generally, variations in aragonite are accompanied by antipathetic changes in calcite. However, there are also significant amounts of dolomite, quartz, and feldspar, particularly in the upper 10 m. One sample from 4.4 m sub-bottom (Core 627B-1H) was taken and demineralized using acetic acid. This process revealed a complex suite of minerals (albite, pyrite, marcasite, corundum, and pyrope). These minerals would seem to indicate erosion from a felsic terrane or possibly aerosol input.

Below 110 m sub-bottom, in the middle Miocene, aragonite was detected in only four samples two of which (198.4 and 216.1 m sub-bottom) were almost certainly downhole contaminants. This conclusion was based on the normal seawater Ca and Mg concentrations present in the interstitial waters and confirmed by the biostratigraphy (see "Biostratigraphy" section, this chapter). The interval between 110 and 258 m sub-bottom is also characterized by the ubiquitous presence of quartz in quantities between 1% and 2% (see Table 5). This interval has been interpreted as being a more open-ocean facies than the aragonite-rich distal-slope facies. The gradual disappearance of aragonite with depth can be considered to be a result of (1) increased alteration to low-Mg calcite and/or (2) a change in facies from distal-slope to open-ocean sediments.

The quartz component disappears in the Campanian chalk sequence, which is composed of 100% low-Mg calcite and extends to 335 m (Fig. 23).

In the Cenomanian part of the section, calcite concentrations are reduced to between 50% and 60% of the rock, principally as a result of an increase in the quartz, feldspar, and clay-mineral content. Based on the percentage weight reduction during demineralization and a comparison of peak intensities with laboratory standards, it is estimated that clay concentrations in the bulk samples are less than 10%. These clays are believed to be mixed-layer illite-montmorillonites with scattered palygorskite. In addition, small amounts of diagenetic sulfides, pyrite, and marcasite were detected. Several heavy minerals, including rutile and spinel, were also present. Indications are that the non-carbonate mineral portions were derived from a felsic igneous-metamorphic terrane similar in nature to that responsible for the assemblage found in Sample 627C-1H-5, 140–150 cm.

In the Albian interval, a facies change from clastics to evaporites and shallow-water limestone and dolomite occurred. Dolomite and gypsum were the principal mineral components detected in this zone.

Carbonate-bomb analyses (see Table 7 and Fig. 24) show a gradual decline in the percentage of carbonate with increasing depth, which reaches a value of 78% at 150 m sub-bottom. This decrease coincides with an increase in percentage of quartz. Below this carbonate decrease, the carbonate increased to a maximum of 95% in the middle Campanian chinks. The transition from chinks to marly chinks was marked by an abrupt decrease in carbonate content. X-ray analyses reveal this decrease to be a result of increases in quartz, feldspar, and other igneous minerals.

ORGANIC GEOCHEMISTRY

Ninety rock samples were taken from Site 627B for analysis using the Rock-Eval method. Some gas data also were obtained from just above terminal depth. The Rock-Eval data are given in Figures 25 through 28, and the gas data in Table 8.

Rock-Eval Data

Certain technical problems were encountered in obtaining the pyrolysis data. First, an aragonite standard appeared to decompose partially on heating to give CO₂ (S₃ peak), and the Neogene section contained aragonite. Second, the Total Organic Carbon module on the Rock-Eval failed to function. However, certain limited estimates could still be made as to the kerogen type and maturity at Site 627.

The lithology at Hole 627B is subdivided into six major lithologic units (see "Sedimentology" section, this chapter). These are a carbonate-sand sequence containing turbidites (Subunits IA, IB, and IC), a Paleogene carbonate condensed sequence containing chert (Unit II), a Campanian chalk sequence (Unit III), a Coniacian limestone (Unit IV), an Albian-Cenomanian green marl (Unit V), and finally a sequence of dolomite, limestone, and gypsum of Albian age (Unit VI).

The kerogen in Units I, II, and III consisted of low amounts of type IV kerogen (Fig. 28)—i.e., detrital, reworked, highly oxidized, terrestrial organic matter. These zones have no source potential at all, but some localized clay-rich zones a few centimeters thick were much richer in pyrolyzable hydrocarbons (S₂) and had some gas potential. Much of the kerogen in Unit I was apparently approaching maturity (T_{max} of about 435°; see Fig. 26). This material was then deposited under oxidizing conditions in sediments sufficiently immature to contain aragonite.

The Cenomanian-Albian chalk and green marly chalk also contained terrigenous organic material, but the S₂ content was considerably higher. This material appeared to be less oxidized. It probably corresponds to type III kerogen and as such would be capable of generating gas if it had been more deeply buried. However, the kerogen remained immature (T_{max} < 435°; see Figs. 26 and 27).

Cenomanian kerogen for the western North Atlantic has been shown to be deposited under oxic conditions (Tissot et al., 1980). The data presented would corroborate this view, particularly as no planktonic component was noted (S₂/S₃ < 2.5; see Fig. 28). Moreover, the S₂ content of the marls gradually diminished during the upper part of the Cenomanian section (see Fig. 27), implying that sedimentary oxidizing conditions were more prominent during the upper Cenomanian as compared with the lower Cenomanian, when conditions were more reducing.

It is interesting to compare the S₂ content of the Neogene clay-rich zones with that of the Cenomanian green marly chinks and chinks (see Fig. 27). They are similar and much higher in S₂ content than associated carbonate zones. It appears that the clay facies here is much more conducive to the preservation of organic matter than the carbonate facies. This may reflect the lower porosity and permeability of clay facies in excluding oxidizing solutions during diagenesis and maintaining a reducing micro-environment. Alternatively, the high sedimentation rates during the Cenomanian may have given insufficient time for complete benthic reworking of the organic matter.

The most interesting lithologies geochemically were in Unit VI. This was a shallow-water-carbonate platform containing dolomites, limestones, and gypsum. The kerogen appeared to be essentially algal in origin (though sampling was limited)—i.e., a type I kerogen (see Fig. 27). Samples of bituminous marl and gypsum were found to contain a large S₂ component, implying their richness in lipid material. The source potential for this kind of organic matter is high. The S₁ (or free hydrocarbon) component was also high in these samples. This may reflect either the onset of organic maturation and hydrocarbon formation at an anomalously low burial depth in an unusual matrix or the presence of migrated hydrocarbons. It is not possible to clearly prove or disprove which hypothesis is correct without a

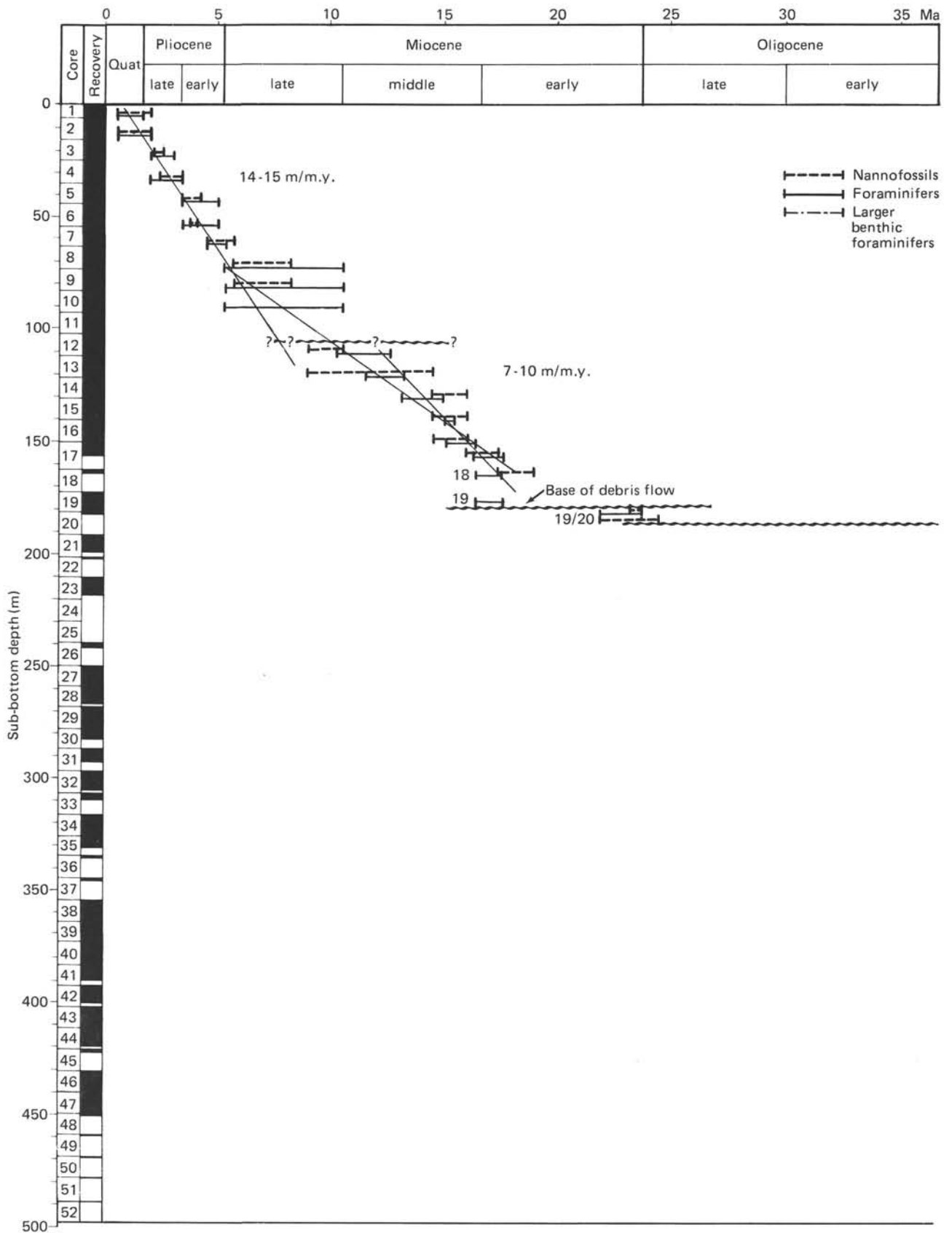


Figure 18. Sediment-accumulation rates, Site 627.

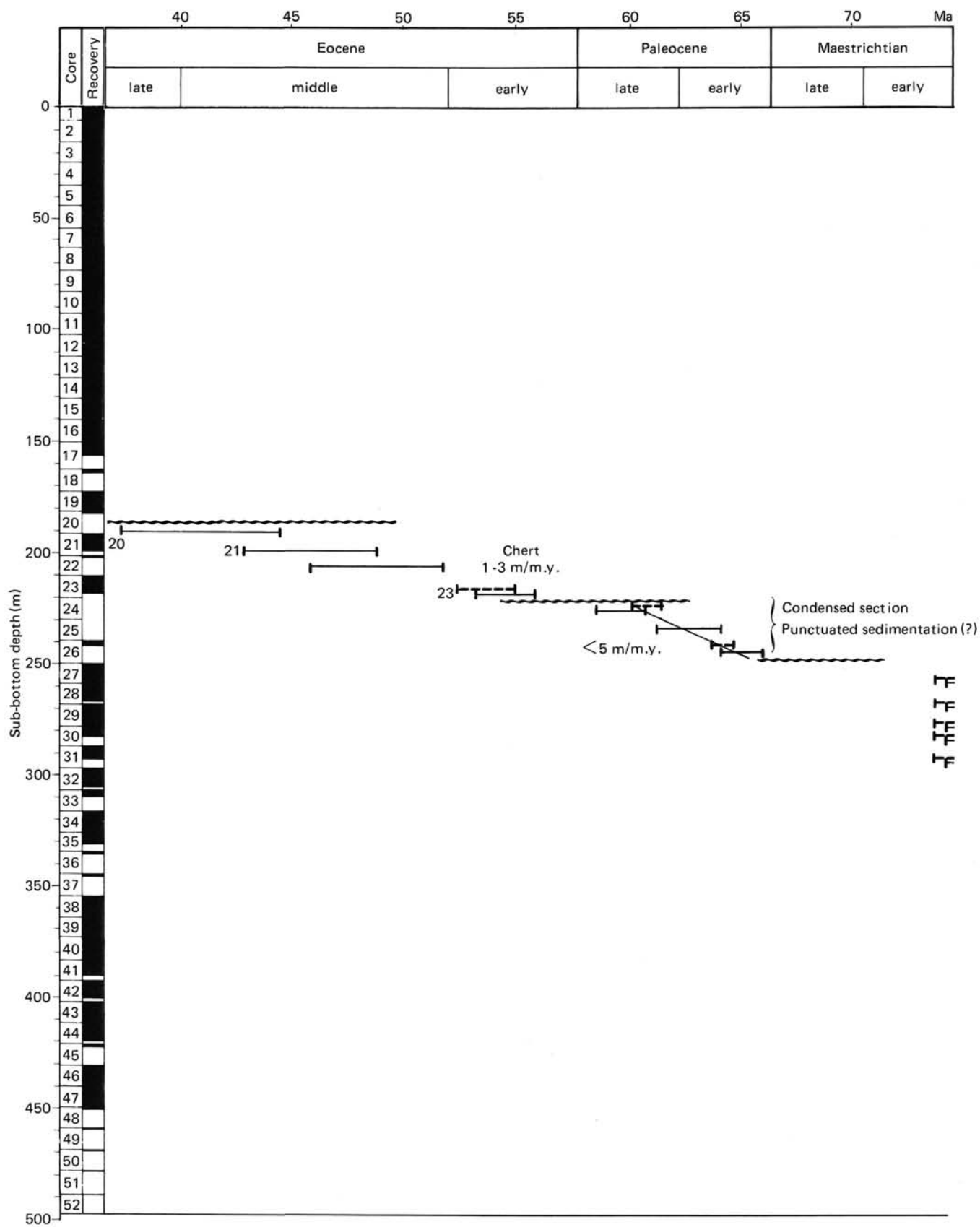


Figure 18 (continued).

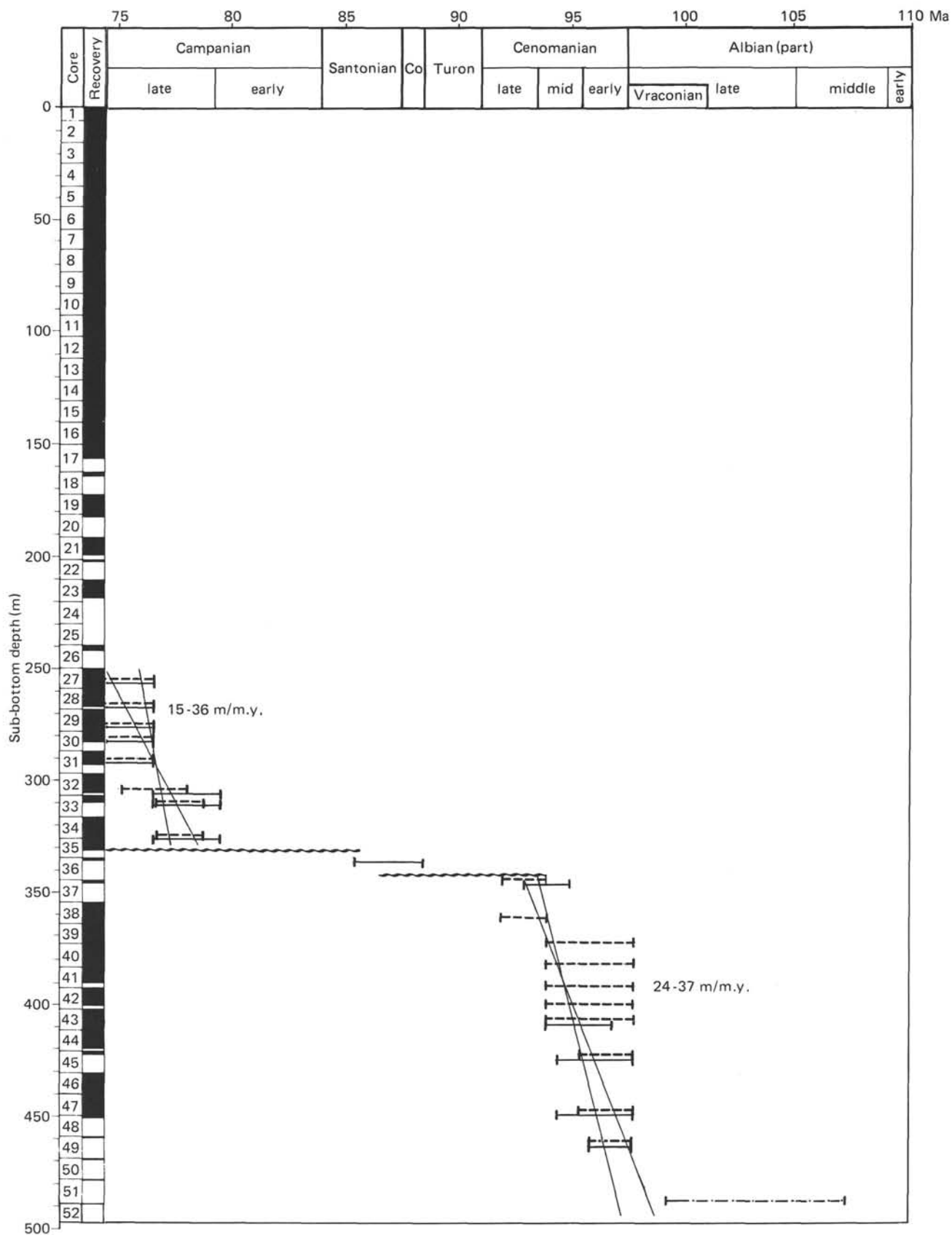


Figure 18 (continued).

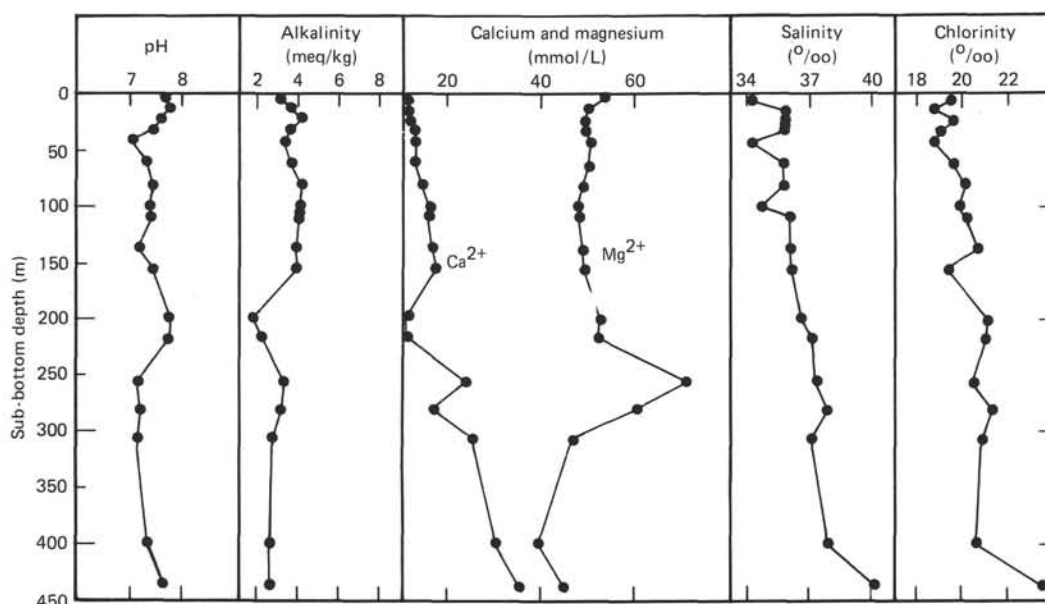


Figure 19. Summary of interstitial-water analyses, Hole 627B.

more extensive Rock-Eval data set for this zone as well as a comprehensive gas-chromatography-mass-spectrometry study of the soluble extracts. A shore-based study of these samples is planned.

Hydrocarbon Monitoring and Gas Analyses

The hydrocarbon gases from Unit VI were analyzed by gas chromatography. Two samples were taken from Core 627B-59X, CC (530.7 m sub-bottom), and another sample from Sample 627B-59X-1, 10 cm (533.7 m sub-bottom). The analysis of the gas from Core 627B-59X, CC, which was taken immediately from the core, showed methane at about 500 parts per million (ppm) and little or no ethane or higher homologs. The two samples from Sample 627B-59X-1, 10 cm, were taken after an equilibrium time of a half hour. The first sample contained 120 ppm methane and vestigial amounts of other hydrocarbons up to C_6 (see Table 8).

The second gas sample from Sample 627B-59X-1, 10 cm, contained methane at about 5000 ppm and small amounts of other hydrocarbons (see Table 8). During the drilling of Core 627B-59X, considerable gas pressures were also noted within the core barrel. The combined presence of increasing hydrocarbon gas content, pressure within the core barrel, and oil-stained sediments signified the possibility of encountering a large hydrocarbon accumulation nearby. Drilling was therefore terminated.

PALEOMAGNETISM

Natural Remanent Magnetization

Two hundred forty oriented paleomagnetic samples were obtained from Neogene, Paleogene, and Cretaceous cores from Hole 627B. The Neogene and Paleogene samples were taken from soft calcareous oozes and clays by pressing a 7-cm³ plastic box into the sediment on the split face of the core. Because the Cretaceous core material was generally more indurated, the samples in that section were mostly 12-cm³ cylindrical minicores drilled perpendicular to the split face. Plastic boxes were also used, however, when the softness of the recovered material permitted.

Most of the paleomagnetic samples, as expected, have natural remanent magnetizations (NRMs) too weak to be accurately measured by the shipboard Molspin spinner magnetometer (on the order of 2×10^{-8} emu to 1×10^{-6} emu). However, the Paleocene chalks of Core 627B-26X and the Campanian chalks,

recovered in Cores 627B-27X through 627B-34X, were an exception. Their NRMs range from as low as 3.1×10^{-6} emu to as high as 1.3×10^{-4} emu. From 33 of these samples a mean NRM inclination of 51.2° and a standard deviation of 12.7° were calculated. This value is indistinguishable from the geocentric axial dipole inclination for Site 627 of 46.1° . It is likewise to be expected, considering the observation that the North American Plate has moved primarily east-west with respect to the hot-spots and spin axis since the Cretaceous (Morgan, 1981).

All of the inclinations measured in Cores 627B-26X through 627B-34X were positive, indicating a normal polarity. As several geomagnetic polarity reversals occurred during the period of time that these sediments were deposited, the uniformity of the polarity of these samples is somewhat surprising. An initial biostratigraphic examination of the Campanian cores has suggested an age of approximately 70–76 Ma (see "Biostratigraphy" section, this chapter). Although various geomagnetic time scales differ by a few million years in the exact timing of polarity chrons of this age, it seems likely that the samples in question record chron 33N, a long interval of normal polarity that lasted from about 78.8 to 72.5 Ma (Harland et al., 1982). This hypothesis will be tested later by a denser sampling of these cores.

Magnetic Susceptibility

Susceptibility measurements were made of the cored material from Hole 627B using the same methods explained in the summary for Hole 626C. In this manner approximately 3000 datum points were generated. The raw susceptibility data are plotted versus sub-bottom depth in Figure 29A and B. Although most of the data plot between about -1×10^{-6} G/Oe and 5×10^{-6} G/Oe, the most notable feature is the occurrence of many large-amplitude spikes. These spikes are almost certainly the result of metallic contamination from the drilling apparatus. Even though it has been impossible to search the core material for metal fragments at the occurrence of each spike, approximately two dozen such investigations have been carried out on Leg 101. In virtually every case in which the rise in susceptibility has been more than an order of magnitude greater than the mean susceptibility value for a given core section, the rise can be attributed to bits of metal from the drilling and coring apparatus or rust from the drill string. In no instance on Leg 101 has it been possible to attribute such a large change in susceptibility to a specific sedi-

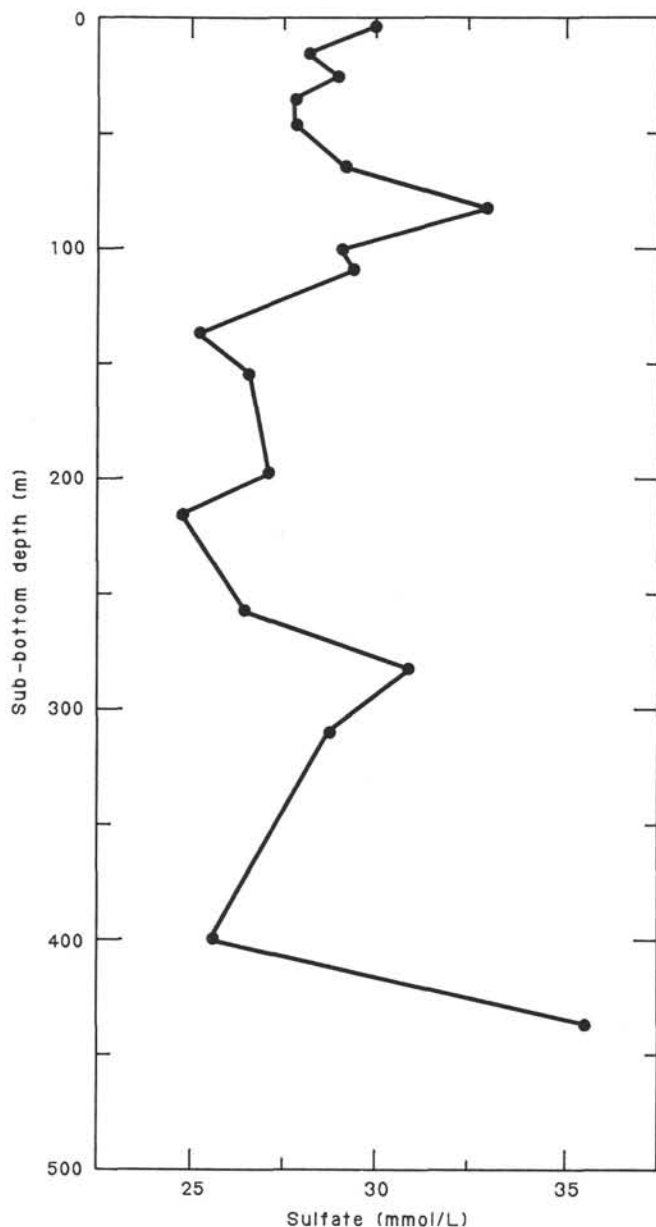


Figure 20. Inorganic sulfate concentrations of interstitial water vs. depth, Site 627.

mentary layer or to a change in the lithology within a core. Presumably, some of the smaller spikes have the same origin.

It appears that the magnetic-susceptibility signature of metallic contamination takes on several somewhat different forms. In the most common manifestation of the phenomenon, large susceptibility values are obtained within the top meter or so of each core (e.g., in Section 1). Usually the contamination appears to affect only the upper few tens of centimeters of that

section, although it extends farther down some cores. As indicated by decreasing susceptibility values downcore, the intensity of the contamination decreases with distance from the top. If the cored material was recovered *in situ*, a possible explanation of this phenomenon is that the core barrel, descending through the pipe toward the bottom assembly, scrapes minute rust flakes off the inside of the drill pipe. On the other hand, if the cored material is out of place, then the rust may be scraped from the outside of the drill pipe (see "Paleomagnetism" section, Site 626 chapter, this volume). In either case, these flakes fall ahead of the core to the top of the sediment, where they are incorporated within the first section of core. The susceptibility spikes that appear to be in this category are labeled *DA* in Figure 29A.

Sometimes an entire core will appear to be contaminated. This occurrence can be recognized by an abrupt rise in magnetic susceptibility at the top of the core, erratic but higher than average values throughout the core, and followed by an abrupt return to lower susceptibility readings in the succeeding core. Some of the more spectacular susceptibility anomalies of this type appear to be associated with unconsolidated sands that have fallen into the hole and been cored. In Hole 627B, this occurred at sub-bottom depths of 191–201 m (Core 627B-21X), 210–216 m (Core 627B-23X), and 325–329 m (Core 627B-35X). In each of these cores, labeled *CO* in Figure 29A, large rust flakes were seen to be disseminated throughout all of the core sections. It seems unlikely that such large flakes would be formed inside the drill pipe because of the scraping action of the core traveling up and down the drill string. Instead, this rust probably forms on the outside of the drill pipe. The rotary motion of the pipe causes the surrounding material to abrade away the rust, disseminating it throughout the sand.

Similar, but usually smaller, susceptibility anomalies occur in cores whose liners were broken during coring. Core 627B-13H, at sub-bottom depths of 111 to 121 m, is an example. Its liner was found at recovery to be broken in several places. In Figure 29A, susceptibility values measured from this core (labeled *BL*) are slightly higher and show more variation than those of the cores directly above and below it. As the cause of the liner breakage is unclear, it is difficult to explain the apparent metallic contamination of the core in such a case. It has been suggested that the core liner sometimes shatters during an HPC because of the vacuum created on the inside by the pull of the retreating piston (D. Huey, pers. comm., 1985). If this is indeed the cause of the breakage, then the same vacuum may cause a rapid injection of water into the core at the time of the break, bringing with it a slight amount of rust from the core barrel.

Despite the short-wavelength-high-amplitude susceptibility fluctuations, the data display some interesting long-wavelength trends. Figure 29B shows a plot of the average susceptibility of each core section versus sub-bottom depth. In order to generate this plot, the mean for each 1.5-m core section was calculated, and values not falling within two standard deviations of the mean were excised. Furthermore, all the data that appear to be associated with downhole contamination were also removed. Although some spikes still remain, the longer variations show up more clearly.

The overall trend of the susceptibility is an increase with depth. Averages near the top of the hole are commonly near

Table 3. Analyses of interstitial waters from Hole 627A.

Sub-bottom depth (m)	pH	Alkalinity (meq/kg)	Salinity (‰)	Chlorinity (‰)	Ca (mmol/L)	Mg (mmol/L)	SO ₄ (mmol/L)
Surface seawater	8.26	2.21	—	20.54	10.42	54.68	28.77
4.4	7.67	3.26	34.6	19.80	11.49	51.38	24.85

Table 4. Analyses of interstitial waters from Hole 627B.

Sub-bottom depth (m)	pH	Alkalinity (meq/kg)	Salinity (‰)	Chlorinity (‰)	Ca (mmol/L)	Mg (mmol/L)	SO ₄ (mmol/L)
4.4	7.64	3.08	33.9	19.37	11.12	52.31	29.96
13.2	7.72	3.51	35.6	18.67	11.28	49.81	27.61
22.9	7.57	4.08	35.6	19.52	11.74	49.81	29.01
32.6	7.41	3.51	35.5	18.95	12.62	48.58	27.14
42.1	7.03	3.23	34.0	18.67	12.89	50.09	27.04
61.2	7.32	3.53	35.5	21.25	12.68	49.75	28.45
80.3	7.43	4.06	35.6	20.05	14.31	48.56	33.58
99.4	7.36	4.00	34.5	19.76	15.86	47.29	28.49
108.9	7.42	3.97	35.9	20.07	15.52	47.52	28.95
136.2	7.15	3.80	35.9	20.61	16.44	48.44	24.99
154.1	7.43	3.91	36.0	19.27	17.49	48.72	26.76
198.4	7.77	1.71	36.5	21.04	10.74	52.13	27.22
216.1	7.74	2.16	37.0	20.93	11.12	51.75	24.37
256.1	7.16	3.30	37.2	20.37	23.78	70.94	26.16
281.0	7.22	3.13	37.8	21.25	16.69	60.09	30.32
307.0	7.15	2.69	37.8	20.79	25.32	46.46	28.58
362.0				No recovery of water			
399.3	7.36	2.58	37.8	20.56	30.30	39.25	25.51
437.4	7.66	2.61	40.2	23.45	35.39	44.83	35.29

-0.4×10^{-6} G/Oe, and those near the bottom are about 3×10^{-6} G/Oe. Shorter wavelength variations are also apparent. A decrease in susceptibility from about 5×10^{-6} G/Oe to -0.4×10^{-6} G/Oe is observed within the first 10 m below the ocean bottom and may be related to dissolution of magnetic minerals during diagenesis near the seafloor. Between 40 and 100 m sub-bottom the susceptibility is usually less than zero, suggesting that the sediment is made up of calcium carbonate and water nearly devoid of any ferrous minerals. Below 100 m the susceptibility and its variation increase slightly with depth. The large spike at 170 m is from large susceptibility values measured in Cores 627B-18H and 627B-19H, Sections 1 and 2. These readings may well result from metallic contamination; however, they were retained for this plot because they did not exactly fit the criteria discussed above.

From 240 to 320 m sub-bottom, the measurements correspond to Paleocene (Core 627B-26X) and Campanian (Cores 627B-27X through 627B-34X) chalk. The susceptibility decreases at first to a minimum at about 250 m depth. This decrease is followed in depth by a maximum of susceptibility at approximately 270 m and another minimum at 300 to 320 m. It appears that the susceptibility records some sort of cyclic variation in the magnetic properties of these sediments. This variation is evident in the paleomagnetic measurements made of samples from this section of the hole. The samples from Cores 627B-27X to 627B-29X, located at the susceptibility maximum, all have strong magnetic moments, whereas only about half the samples from Cores 627B-31X, 627B-33X, and 627B-34X have magnetic moments strong enough to be above the noise level of the Molspin spinner magnetometer.

The susceptibility means from 350 to 460 m sub-bottom were measured from the Cenomanian green marly chinks. Although the measurements show quite a bit of fluctuation, it appears as if long-wavelength variations in susceptibility characterize these cores as well. Probable peaks occur at depths of approximately 370, 400, and 455 m.

It is not clear exactly what kinds of changes were recorded by the susceptibility values. Because magnetic minerals are usually microcrystalline and present only in minute amounts, identification of the responsible mineral is usually difficult. Most studies of magnetic minerals in marine sediments conclude that these minerals are primarily allochthonous grains of magnetite and titanomagnetite (Kobayashi and Nomura, 1974). However, authigenic magnetic minerals may be significant in slowly accumulating pelagic clays (Bloemendal, 1980).

PHYSICAL PROPERTIES

Physical-property measurements have been made on cores from Site 627 as described in the "Introduction and Explanatory Notes" (this volume). Physical-property data from Site 627 are listed in Table 9 and are graphically represented in Figure 30.

Hole 627A

Only one core was recovered from Hole 627A. The data are listed in Table 9 and are not discussed here.

Hole 627B

Considering general trends first, all parameters change markedly three times within the profile: once at 245 m sub-bottom, a second time at 349 m sub-bottom, and a third at 450 m sub-bottom (Fig. 30). In addition to these three abrupt changes, all parameters show considerable variability.

Compressional Wave Velocity

From the water/sediment interface down, velocities increase slightly in the first 130 m from 1572 to nearly 2000 m/s. From 130 m sub-bottom to 270 m sub-bottom, sediment velocities decrease again from 2000 to 1748 m/s. This decrease in velocity correlates with a sequence of debris flows and turbidites ("Sedimentology" section, this chapter). No data exist for the interval between 201 and 240 m sub-bottom, because recovery was poor. Below this data gap the velocities shift to about 1800 m/s. Indurated chalk layers within this profile show velocities between 2200 and 2500 m/s. Between 322 and 353.5 m sub-bottom, there is another period of poor recovery. Below 353.5 m sub-bottom, velocities increase significantly to an average value of 2000 m/s with extremes reaching 3000 m/s. An abrupt break in lithology occurs at 478 m sub-bottom, and velocity measurements were made only on uncut pieces of dolostones and gypsum below this point. Compressional wave velocities range between 3000 and 5000 m/s for these rocks. The lowest values are from porous dolostones at the top of the lithified region. Velocities from clear gypsum reach 5000 m/s and higher.

Water Content, Porosity, and Wet-Bulk Density

Water content, porosity, and wet-bulk density were determined using gravimetric and volumetric techniques. Since these techniques are destructive, data could be collected only above 450 m sub-bottom. As a whole, water content and porosity decrease with increasing depth, and density increases with increasing

Table 5. X-ray analyses of samples from Hole 627B.

Sub-bottom depth (m)	Calcite ^a (%)	Aragonite (%)	Dolomite ^b (%)	Quartz (%)	Comments
4.4	53	0	31	7	Feldspar present
6.7	75	25	0	0	
13.2	51	44	1	4	
22.9	64	32	3	0	
32.6	79	18	2	0	
42.1	93	0	7	0	
46.4	89	6	5	0	
47.4	83	7	10	0	
54.1	93	0	4	3	
56.9	95	0	2	3	Green color
60.5	100	0	0	0	Unlithified
60.5	100	0	0	0	Lithified
61.2	77	16	7	0	
64.0	62	35	3	0	
78.5	100	0	0	0	Unlithified
78.5	100	0	0	0	Lithified
79.6	100	0	0	0	Turbidite top
79.7	88	12	0	0	Turbidite bottom
80.3	98	0	0	2	
90.7	59	41	0	0	
90.8	66	31	0	3	Turbidite top
90.9	65	32	0	3	Turbidite base
99.4	53	47	0	0	
109.0	98	0	0	2	
117.0	100	0	0	0	
119.5	99	0	0	1	
123.0	99	0	0	1	
123.6	96	0	0	4	
130.6	86	14	0	0	
136.2	98	0	0	2	
145.1	79	21	0	0	
154.1	98	0	0	2	
162.9	98	0	0	2	
177.0	99	0	1	0	
182.3	100	0	0	0	
198.4	82	16	2	0	
200.9	99	0	0	1	
216.1	85	16	2	0	
239.8	98	0	0	2	
256.1	98	0	0	2	
258.2	98	0	0	2	
260.4	100	0	0	0	
281.0	100	0	0	0	
282.7	100	0	0	0	
290.0	100	0	0	0	
298.2	100	0	0	0	
306.3	100	0	0	0	
317.2	100	0	0	0	
334.0	100	0	0	0	
345.0	100	0	0	0	
362.0	65	0	2	33	
363.1	88	0	0	12	
366.4	59	0	0	41	
380.9	70	0	2	28	
384.6	76	0	2	22	
399.3	73	0	4	23	
403.7	90	0	2	8	
416.1	93	0	1	6	
421.5	91	0	1	8	Feldspar present
437.4	88	0	2	10	
487.1	0	0	100	0	
519.2	100	0	0	0	
524.2	0	0	0	0	Gypsum present
527.8	0	0	0	0	Gypsum present

^a All measured calcite was low in magnesium.

^b Dolomite composition varied between 52 and 58 mol% MgCO₃.

depth. However, the water content, porosity, and density profiles (Fig. 30) display considerable variability.

Between the water/sediment interface and 201 m sub-bottom, the profiles, especially for water content and porosity, are characterized by great variability. Within the first 50 m of sediment, trends of increasing density and decreasing water content

Table 6. X-ray analyses of samples from Hole 627A.

Sub-bottom depth (m)	Calcite (%)	Aragonite (%)	Dolomite (%)	Quartz (%)	Comments
2.00	88	11	2	0	
2.11	89	0	11	0	
2.42	76	24	0	0	Unlithified
2.42	98	0	0	2	Lithified
4.35	73	27	0	0	
5.94	78	22	0	0	Lithified
5.99	100	0	0	0	Unlithified
7.10	74	26	0	0	
7.13	76	24	0	0	
8.80	47	53	0	0	Lithified

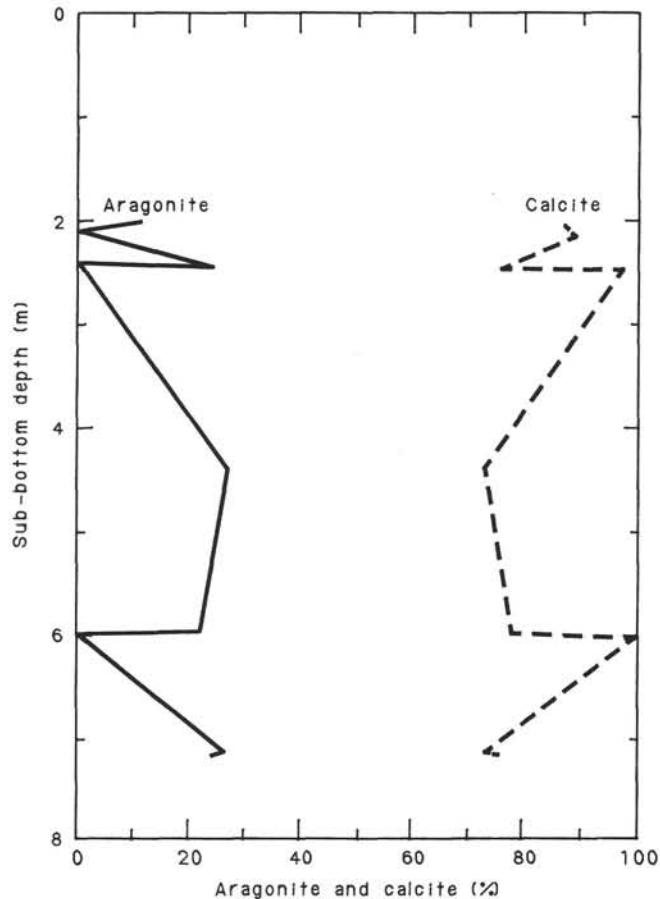


Figure 21. Percentage variations in the calcite and aragonite content, Hole 627A.

and porosity are recognizable. Noteworthy is the low water content (55.55% at 5.2 m sub-bottom) in the upper few meters.

The water content and porosity increase sharply at 50 m sub-bottom. Between 50 and 106.7 m sub-bottom, values for water content range between 37% and 54%, for porosity between 54% and 61%, and for density between 1.75 and 1.90 g/cm³. At 106.7 m sub-bottom, water content drops to 33.68% but increases from this low point downhole until it reaches values around 70% at 161-177 m sub-bottom. This represents a 15% increase in water content from the top few meters. Porosity follows the same trend, until a maximum value of 66.3% is reached, also at 177 m sub-bottom. The high water content and porosity in this part of Hole 627B (108 to 177 m) correspond to

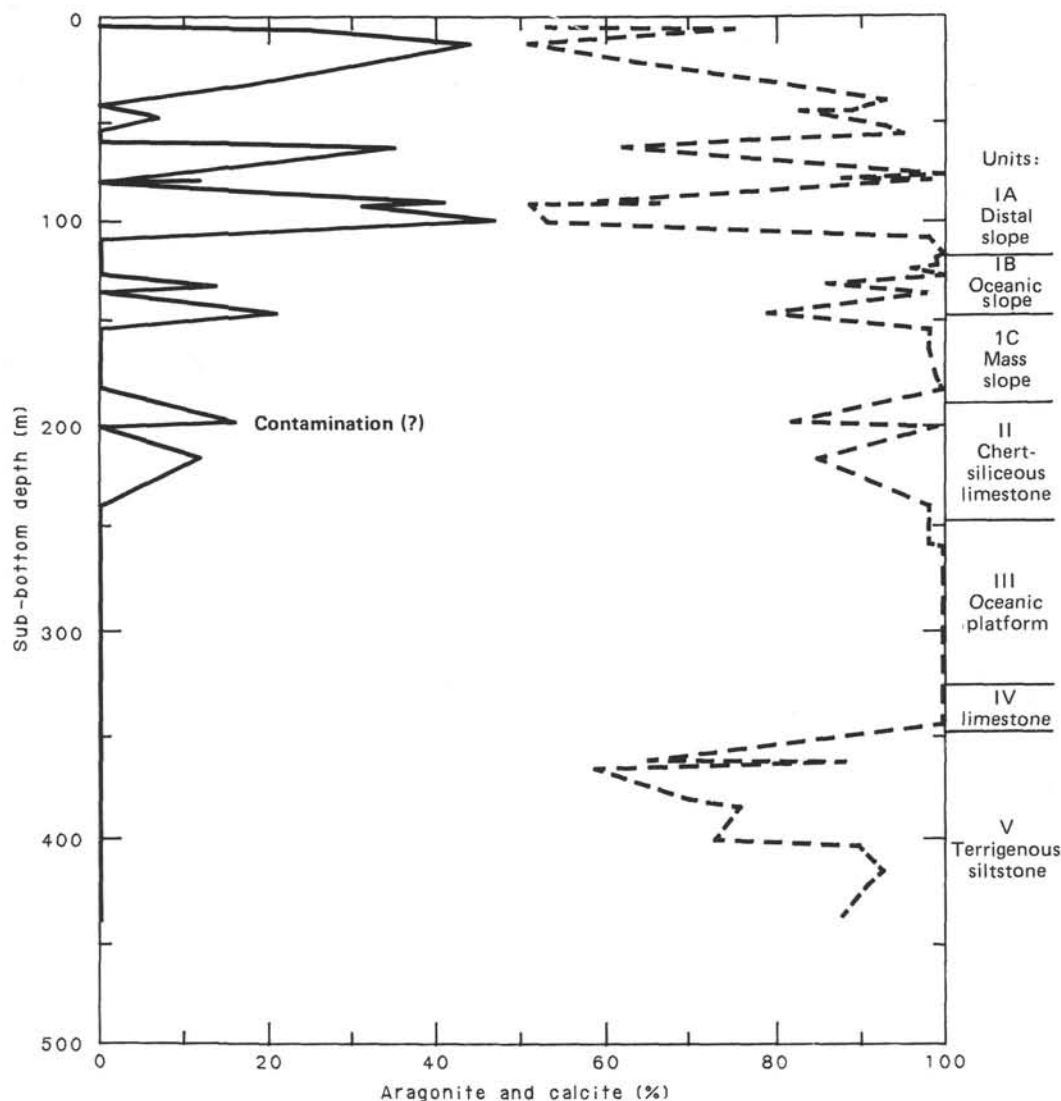


Figure 22. Percentage variations in the calcite and aragonite content of Hole 627B.

the zone of debris flows and turbidites ("Sedimentology" section, this chapter).

Between 250 and 324 m sub-bottom, high density values and correspondingly low water content and porosity values characterize the recovered sediments. This interval shows a reverse trend, with increasing water content and porosity and decreasing density downhole (Fig. 31). Lithologically, this section is composed of a uniform alternation of ooze and partially lithified chalks ("Sedimentology" section, this chapter). At 334.5 m sub-bottom, a significant shift to higher density (2.10 g/cm^3) and lower water content (20%) and porosity (30%–40%) values occurs. At 403.7 m sub-bottom, density values drop to 1.58 g/cm^3 and then increase steadily downhole to a maximum value of 2.35 g/cm^3 . Water content and porosity do not display any obvious trend in this part of the hole.

Thermal Conductivity

Thermal conductivity was measured for all cores soft enough for the temperature probes to be inserted. Below Core 627B-47X, indurated sediments and rock were recovered. From these cores, samples were taken for shore-based laboratory temperature studies. Thermal-conductivity values show considerable variability, but overall they increase downhole.

Within the first 201 m sub-bottom, three changes can be recognized. Between 0 and 50 m sub-bottom, conductivity remains constant at $2.5 \times 10^{-3} \text{ cal} \times \text{°C}^{-1} \times \text{cm}^{-1} \times \text{s}^{-1}$. At 50 m sub-bottom, conductivity increases to $3.11 \times 10^{-3} \text{ cal} \times \text{°C}^{-1} \times \text{cm}^{-1} \times \text{s}^{-1}$. At 100.2 m sub-bottom, conductivity values increase sharply and then steadily decrease downhole. This reversed trend of decreasing conductivity correlates with water content, which increases in the same part of the hole.

Between 355.7 and 448.7 m sub-bottom the mean conductivity value is higher ($3.54 \times 10^{-3} \text{ cal} \times \text{°C}^{-1} \times \text{cm}^{-1} \times \text{s}^{-1}$) than above. Between 400 and 420 m sub-bottom, slightly lower values correlate with lower density values in the same interval.

Shear Strength

Shear strength could be determined only to 340 m sub-bottom. Below this depth, sediments were too well consolidated for application of the miniature vane shear. Within the first 50 m, shear strength is low, 0 to 3 kPa. Shear strength increases from 5.21 kPa at 65.5 m to 20.9 kPa at 162.9 m sub-bottom. Between 250.4 and 323.3 m sub-bottom, shear strength decreases, which correlates well with increased water content and porosity and with decreasing density.

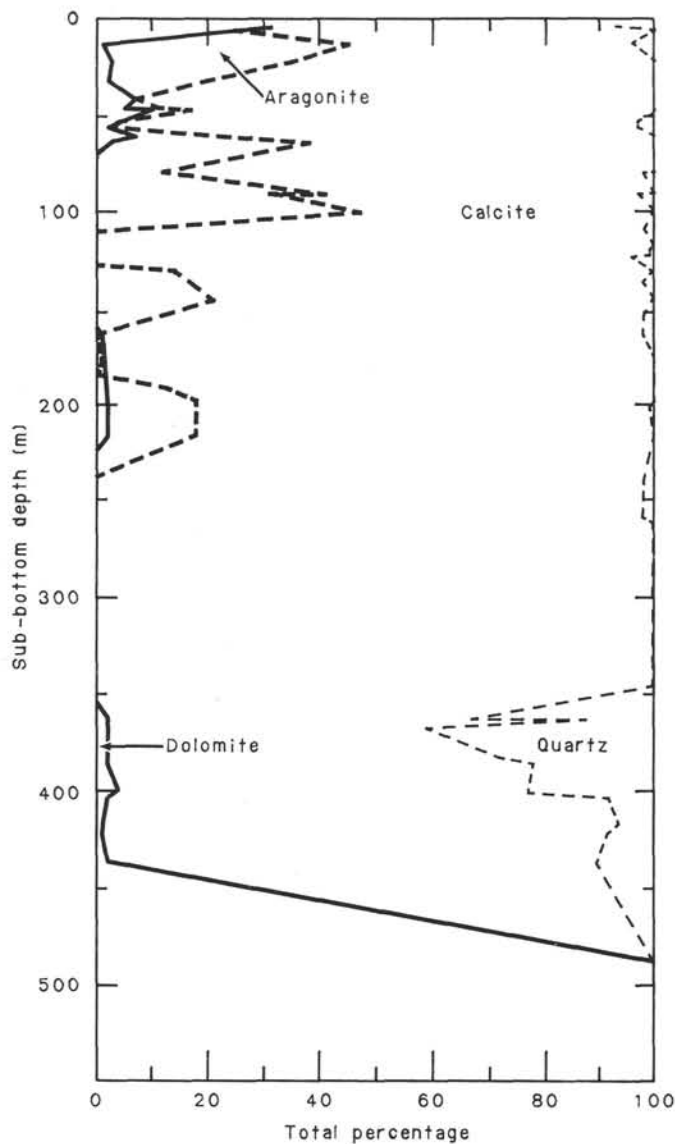


Figure 23. X-ray data, Site 627.

Discussion and Interpretation

Three significant shifts occur in the downhole distribution curve. For porosity an idealized downhole distribution curve in sediments with a high carbonate content is constructed after Bryant et al. (1981) in order to evaluate the direction and magnitude of the shifts. Above the data gap at 201 m sub-bottom, measured porosity values are higher than the constructed curve. This interval correlates well with the interval of debris flows (see "Sedimentology" section, this chapter) and shows a trend in the opposite direction to that of the idealized curve. The shift at 247 m seems to be a shift back to predicted values.

The second shift in the data curve below the data gap between 334 and 353.5 m sub-bottom is away from the values predicted by the constructed curve, i.e., lower porosity values. This shift in values indicates that sediments below 353 m sub-bottom are more compacted than expected, requiring additional overburden pressure. Thus, this shift in measured values suggests that an erosional event has occurred.

This interpretation is supported by the lithostratigraphy. Sediments of the first zone with poor recovery (219–246 m sub-bottom) are Paleocene in age. Sediments of Core 627B-26X, the

Table 7. Carbonate-bomb data, Site 627.

Sub-bottom depth (m)	CaCO ₃ content (%)
5.17	63
5.2	92
6.7	95
8.2	98
9.5	92
12.5	88
16.8	91
17.7	93
20.7	91
23.7	86
27.4	92
30.4	90
33.4	97
36.9	97
39.9	87
42.9	86
46.4	88
49.4	93
52.4	94
56.0	94
59.0	89
62.0	95
65.5	92
68.5	94
71.5	95
75.1	87
78.1	97
81.1	91
84.7	94
87.7	84
90.7	85
94.2	92
97.2	83
100.2	89
103.7	90
106.7	91
109.7	85
118.0	90
129.0	78
132.5	87
148.1	89
154.9	79
162.9	83
177.0	82
181.8	89
194.7	89
200.8	88
210.2	77
239.8	82
256.9	87
263.4	86
269.7	89
278.8	95
290.0	88
297.2	91
306.3	93
323.2	94
334.4	92
344.3	96
344.7	88
361.7	35
362.4	38
369.7	51
380.9	51
384.6	51
387.6	48
390.6	56
394.1	48
397.1	64
400.1	68
403.7	60
406.7	49
409.6	67
413.3	58
416.3	67
418.8	68
419.3	69
421.5	63
432.2	60
435.2	72
438.2	72

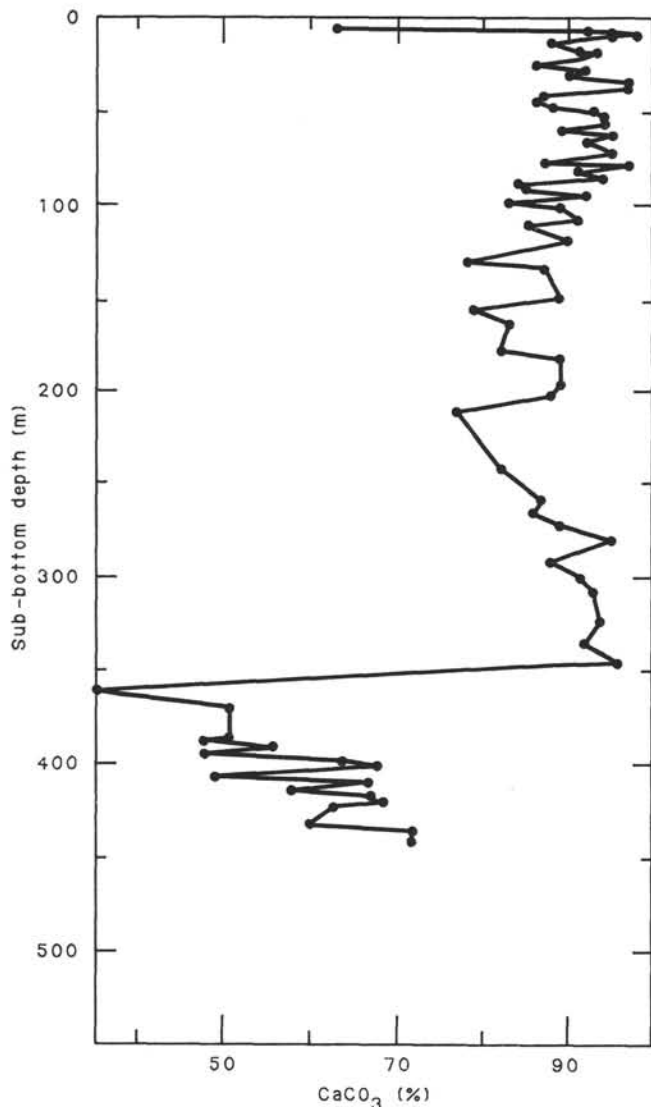


Figure 24. Carbonate-bomb data, Site 627.

first core with better recovery at 239 m, are still of Paleocene age. Their physical-property values are the same as values measured from underlying Campanian ooze-chalk alternations. This suggests that the missing Maestrichtian sediments were not eroded but rather that they were never deposited at Site 627.

Sediments from the second zone of poor recovery (Core 627B-36X) are Coniacian and Santonian in age, while green marly chalks and chalks of Core 627B-37X are already of Cenomanian age. This means that this second shift in physical-property data, which is interpreted as a product of an erosional event, coincides with a stratigraphic unconformity.

The third unconformity in the physical-property curve reflects the transition between the green marly chalks and chalks of late Albian-Cenomanian age and the highly lithified dolostones and gypsum of late Albian age.

Also noteworthy is the fact that the physical-property data display trends reverse to those illustrated by the general curve, once between 106.7 and 177 m sub-bottom and again between 201 and 324 m sub-bottom. The first interval correlates with the identified sequence of debris flows and turbidites, both having unlithified matrix sediment. The second interval correlates with the Campanian ooze-chalk alternations (see "Sedimentology" section, this chapter). This uniform sequence contains no ap-

parent redeposited layers to cause higher water content and lower velocity values, and the composition of the ooze changes little downhole. Nannofossils are abundant in the whole sequence. The planktonic foraminifers are more abundant in the upper part of the sequence, whereas the larger benthic foraminifers are more abundant in the lower part. Where the larger benthic foraminifers are numerous enough, they may have caused the sediment to have a higher porosity, which in turn would have affected the other physical-property parameters.

DOWNHOLE MEASUREMENTS

As a consequence of the poor hole conditions that trapped a set of logging tools and eventually led to their loss, the only section of Hole 627B that was successfully logged covered the bottom 67 m of the borehole (469 to 536 m sub-bottom). A combination of three Schlumberger tools, the Natural Gamma Spectrometry Tool (NGT), the Litho-Density Tool (LDT), and the Compensated Neutron Tool (CNTG), made up this logging run. The NGT is similar to a standard gamma-ray tool in that it provides a measurement of the formation background gamma radiation, but the NGT also analyzes the spectra of that radiation, enabling it to identify the amounts of uranium, thorium, and potassium present in the formation. The LDT yields two quantities, bulk density (R_{hob}) and photoelectric-absorption index (P_e), by bombarding the formation with gamma rays and quantifying the effects of Compton scattering and photoelectric absorption. The borehole lithologies can then be identified by consulting tabulated values of P_e and R_{hob} for various minerals. The CNTG is described in the "Downhole Measurements" section of the Site 626 chapter, this volume.

Log Characterization

Figure 32 displays the resulting curves from the three tools. Total natural gamma radiation (SGR) and natural gamma radiation minus that radiation from uranium (CGR) are shown in the first column of the figure. Both curves are fairly uniform throughout the logging interval, a result that reflects the consistent nature of the lithology in this section of the hole.

Those gamma-ray variations that do occur are more easily seen in the second column of the figure, which reproduces the NGT results in terms of the concentrations of potassium, uranium, and thorium present in the formation. Rises in the amount of potassium that are combined with falls in the amount of thorium are the most prominent features of the curves and appear in a number of intervals (471-475, 480-483, 486-488, 491-497, 501-508, and 510-520 m sub-bottom). Overall, the averages of the curves are potassium concentration equal to 0.5%, uranium concentration equal to 2 ppm, and thorium concentration equal to 3 ppm. The uranium curve is by far the smoothest, exhibiting little variation over the interval covered by the logging run.

The third column of Figure 32 presents the two quantities directly measured by the LDT, P_e , and R_{hob} . The value of bulk density stays at 2.25 g/cm^3 throughout the entire logging interval, while the value of P_e is 4.1 ± 0.4 . There does not appear to be any correlation between the variations in radioactive-mineral concentrations and variations in the P_e curve. Two porosity measurements appear in the fourth column of the figure, thermal porosity (ϕ_{Th}) from the CNTG and a porosity (ϕ_{D}) estimated from the bulk density by assuming a pure limestone matrix. The neutron porosity curve stays at a relatively constant value of $32\% \pm 4\%$ for the entire interval. The density porosity curve also remains fairly constant, although at a lower value of $27\% \pm 2\%$.

Interpretation

The interval covered by this logging run corresponds to the section designated as Unit IV on the basis of the lithostrati-

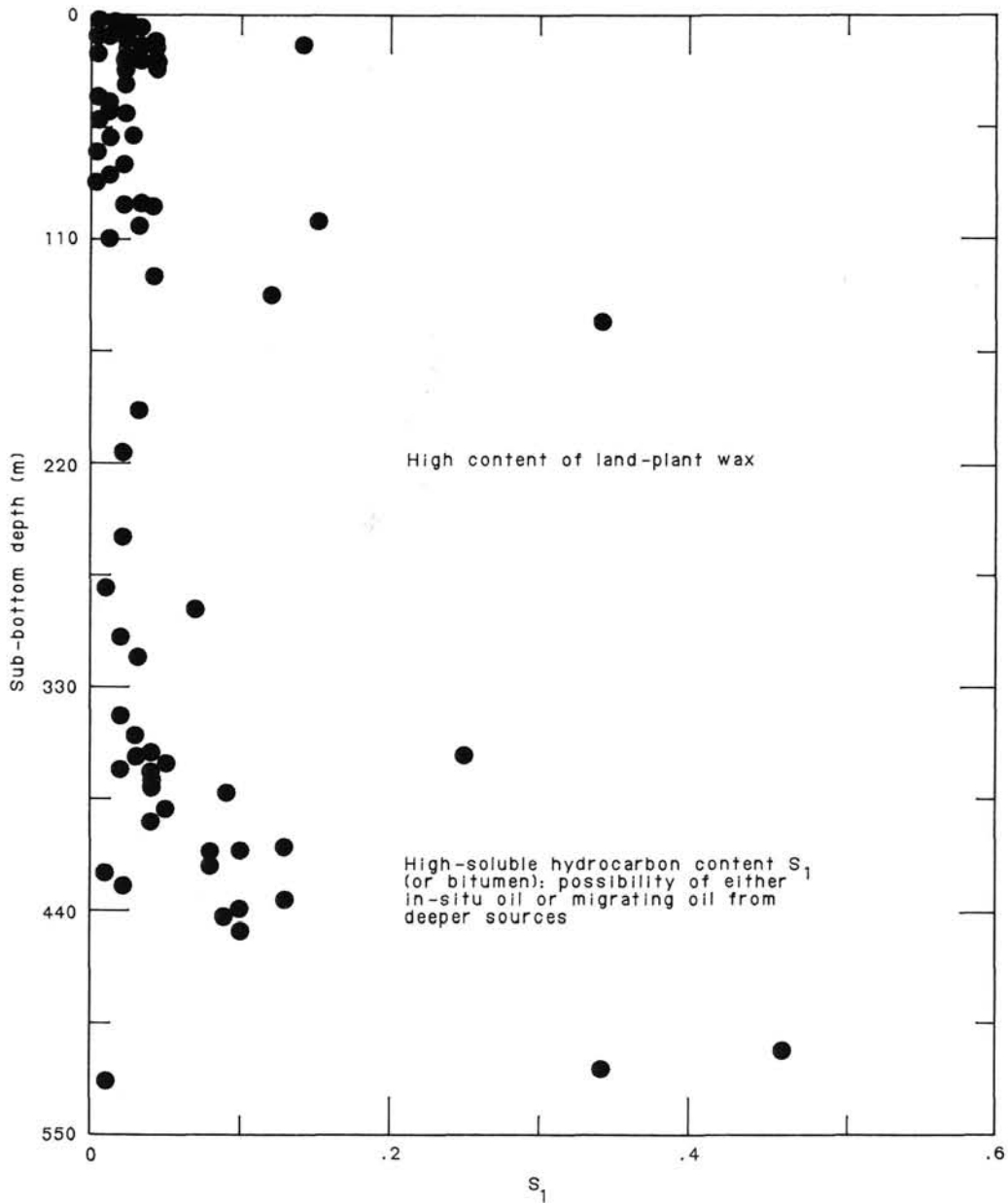


Figure 25. Downhole variation in bitumen content (soluble organics), Hole 627B.

graphic studies. This unit covers a transition from interbedded dolomite and limestone with significant moldic porosity to a layer of gypsum and dolomite that begins somewhere between 515 and 519 m sub-bottom. Gypsum also occurs in some of the dolomite pores above 515 m sub-bottom (see "Sedimentology" section, this chapter). Table 10 shows some of the material properties of these minerals, including those that are measured by the tool combination which was run in Hole 627B. The change in lithologies of Unit VI suggests that these properties should be reflected in the logs at the depths corresponding to the presence of each of the three minerals. For the section of the logs corresponding to the layer of gypsum (515 to 536 m sub-bottom), the measured values of Pe (4.1) and Rhob (2.25 g/cm³) come close to the expected values given in Table 10. The absence of potassium, uranium, and thorium is also consistent with the presence of gypsum, and the thermal porosity of 32%, which reflects the percentage of water by volume in the formation, matches al-

most exactly the 31.1% water content of gypsum. Thus, these logs clearly confirm the occurrence of gypsum in this section.

The presence of the interbedded dolomite and limestone is much more difficult to determine. All of the curves are relatively smooth throughout the logging interval, a fact that without the correcting influence of the cores would lead to the incorrect conclusion that gypsum is the sole lithologic component of Unit VI. A careful examination of the data actually shows a correlation of the logs with both lithologies. Consider the NGT curves. While most of the peaks in potassium concentration occur above the appearance of massive gypsum at 515 m sub-bottom (consistent with a possible higher percentage of potassium in dolomite and limestone), a clear change in the average concentration does not appear. The Pe curve is not of much use in this case, because interbedding of limestone and dolomite in equal quantities yields an average Pe nearly the same as that for gypsum (4.11 compared to 4.0). Finally, limestone and dolomite

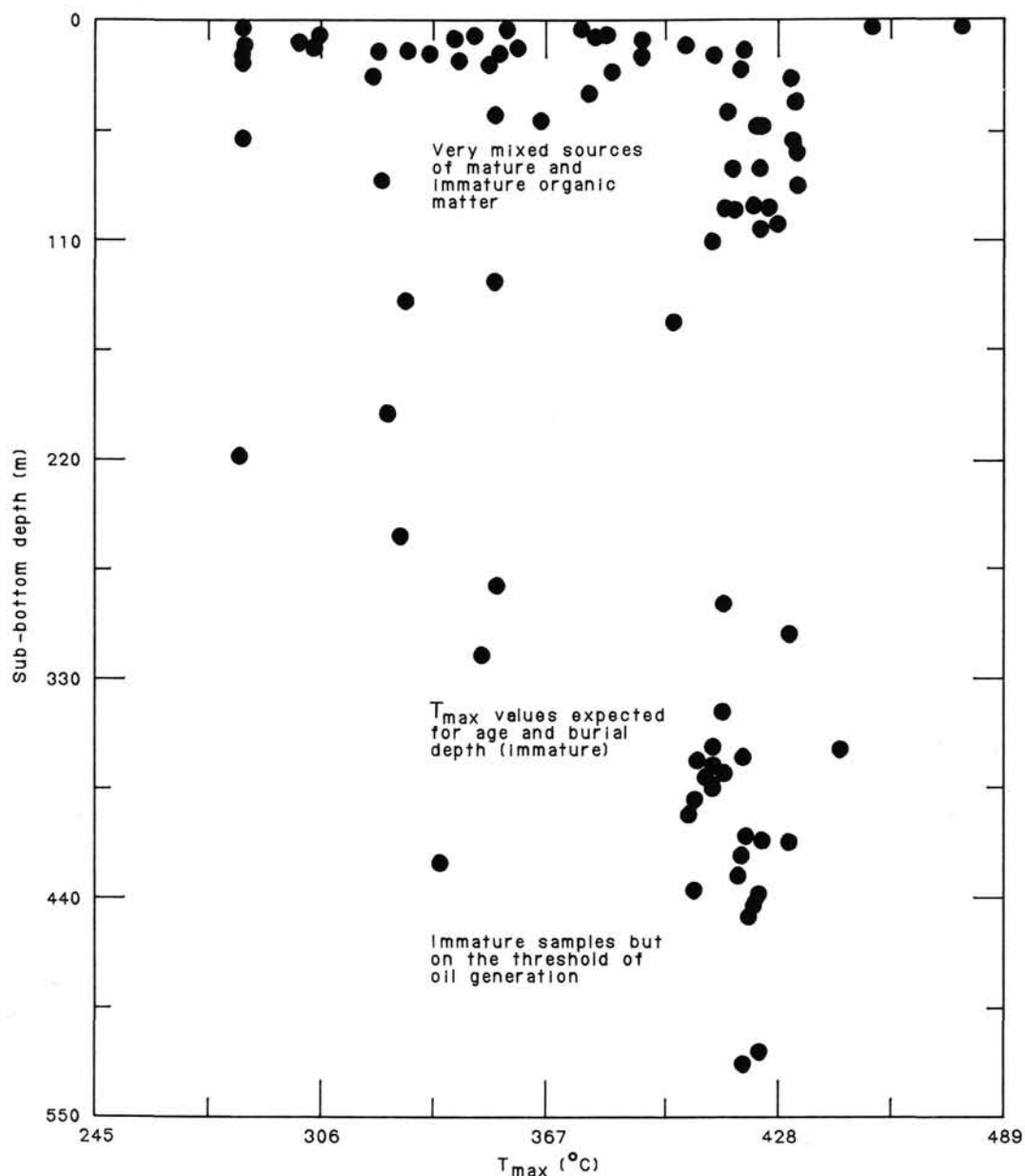


Figure 26. Downhole variation in T_{max} , Hole 627B.

with porosities on the order of 20%–30% will produce log density readings in a range from 2.2 to 2.5 g/cm³, and these readings are not significantly different from the 2.25 g/cm³ measured by the logs (Serra, 1984).

Therefore, the lack in the logs of a clear lithologic boundary indicating the point of change from gypsum to dolomite and limestone does not mean that the logs are giving incorrect values or that the boundary is not there. Instead, correlation of the logs with core analyses shows that the set of logs run in this hole reacts in the same way to gypsum as it does to porous interbedded dolomite and limestone.

SEISMIC STRATIGRAPHY

Introduction

Hole 627B sampled the seven uppermost seismic sequences identified on site-survey profile LBB-18 (Fig. 33). Depths to the sequence boundaries were calculated from the time section us-

ing both velocity–time curves available: a sonobuoy collected during the site surveys and a semblance calculation from LBB-18 itself. A comparison of the two calculations is given in Table 11. All of these sequence boundaries correlate either with lithologic breaks or hiatuses in Hole 627B. These correlations are detailed below.

Seismic Correlations

Sequence A/Sequence B

This boundary (47–48 m sub-bottom) corresponds closely in depth to a lithologic break in Core 627B-5H-5 at approximately 41 m sub-bottom between un lithified foraminifer ooze–chalk (above) and slumps (below) of early Pliocene age.

Sequence B/Sequence C

The base of sequence B (109–119 m sub-bottom) is interpreted here to mark the base of the slump sequence the top of which is

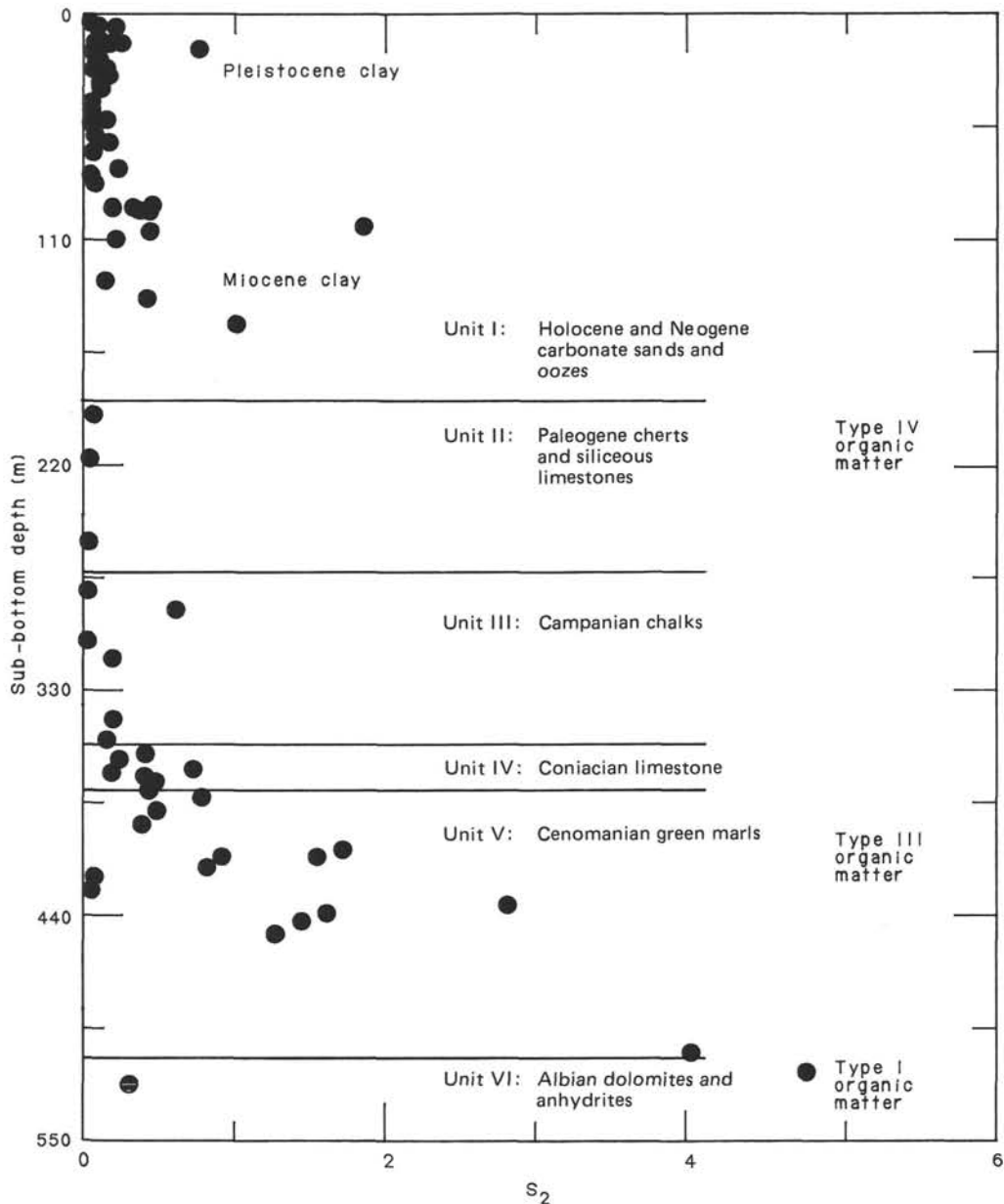


Figure 27. Downhole variation in kerogen type, Hole 627B. Note that assigning of kerogen type is here based on (1) the S_2 peak height and (2) the S_2/S_3 ratio. TOC values were not available for calculating the position of the various samples analyzed on the Van Krevelen diagram. The kerogen typing thus is approximate but gives an indication of source potential.

in Section 627B-5H-5. At this contact, in Sample 627B-12H-5, 103 cm (approximately 108.7 m sub-bottom), upper middle-upper Miocene slumps (Subunit IA, see "Sedimentology" section, this chapter) overlie stiff oozes of the same age (lithologic Subunit IB).

Sequence C/Sequence D

This boundary (146–164 m sub-bottom) is the highest amplitude horizon in the entire section except for the target horizon (top of sequence G; Fig. 33). A strict depth correlation places the C/D boundary within uppermost lower Miocene debris flows, but a more likely correlation is with the base of these flows in Sample 627B-19X-6, 50 cm (approximately 179.8 m sub-bottom), which is also the limit of an early Miocene hiatus in Hole 627B. Preliminary shipboard calculations of acoustic impedance based on Hamilton Frame velocities and GRAPE densities sup-

port this correlation. The discrepancy between depth in hole and depth on the seismic profile may be explained in part by local relief on the C/D surface (approximately 0.01 s on LBB-18, or approximately 10 m; Fig. 33) and in part by the fact that Hole 627B was drilled in an area outside the available seismic control (see "Operations Summary," this chapter, and the Site 626 chapter for extended discussions).

Sequence D/Sequence E

The top of sequence E (208–227 m sub-bottom) correlates in depth with an early Eocene–late Paleocene hiatus between between Core 627B-23X (210.2–219.9 m sub-bottom) and Core 627B-24X (219.9–229.4 m sub-bottom). Sequence E appears to be generally equivalent to the chalks of middle–late Campanian age recovered from Core 627B-27X to Core 627B-34X (248.7–324.7 m sub-bottom).

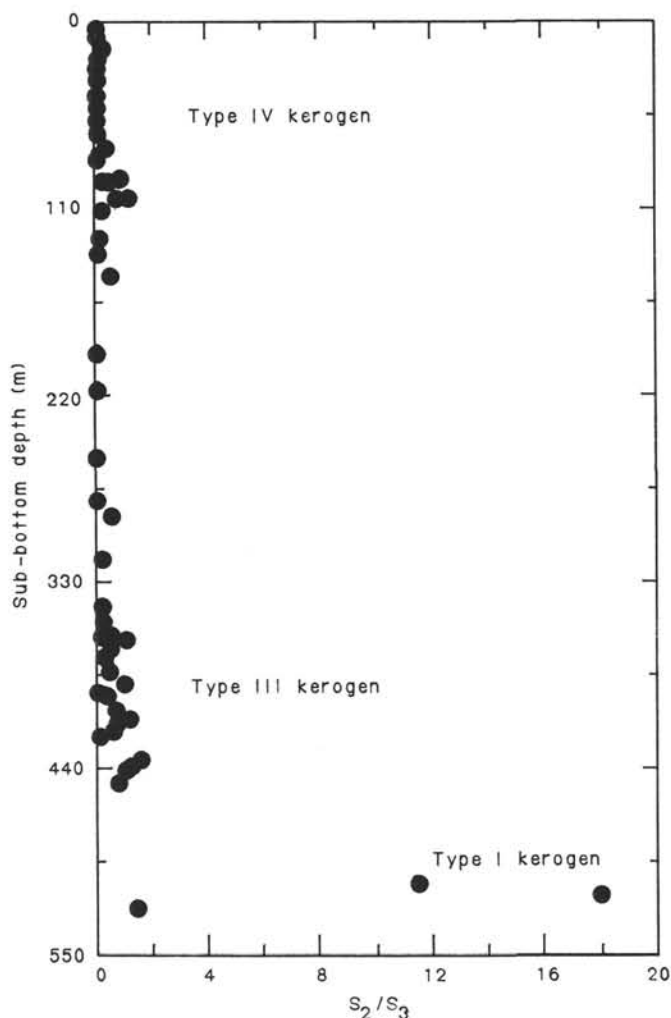


Figure 28. Kerogen-type variation, Hole 627B. See explanation in Figure 27 caption.

Table 8. Gas analyses, Hole 627B.

Sample	C ₁ Methane (ppm)	C ₂ Ethane (ppm)	C ₃ Propane (ppm)	C ₄ Butane ^a (ppm)	C ₅ Butane (ppm)	C ₆ + Hexane (ppm)
627B-59X, CC	511.0	1.6	3.3	42.7	—	1.2
627B-59X-10A	115.4	6.8	16.3	138.9	13.7	3.6
627B-59X-10B	4820.0	4.5	3.6	42.3	—	1.0

^a Acetone gives a contaminant peak with one of the butane peaks.

Sequence E/Sequence F

This boundary (336–363 m sub-bottom) ties most closely to the lowermost Coniacian–uppermost middle Cenomanian hiatus between Core 627B-36X (334.3–343.9 m sub-bottom) and Core 627B-38X (343.9–353.5 m sub-bottom). The significance of this boundary is discussed below.

Sequence F/Sequence G

As predicted, the top of sequence G (474–531 m sub-bottom) was found to mark the transition to a drowned carbonate bank of mid-Cretaceous age. That prediction was based on indications of the presence of 4.2-km/s material from both the avail-

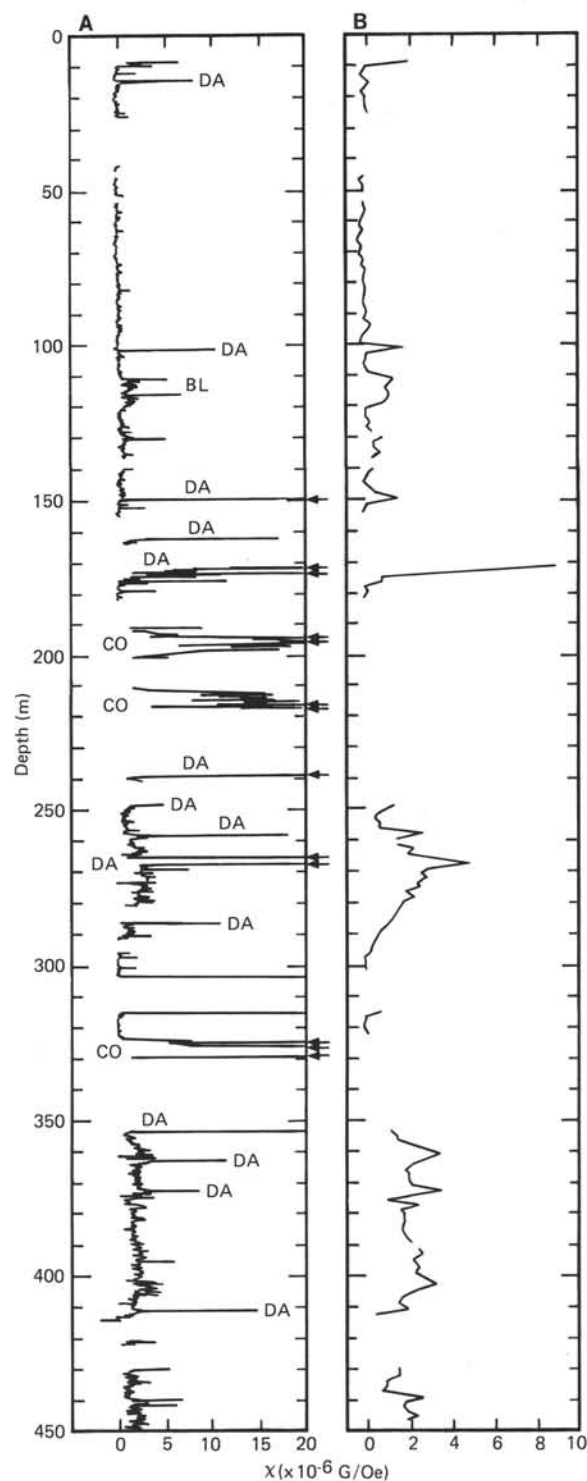


Figure 29. Magnetic-susceptibility values ($\times 10^{-6}$ G/Oe) plotted vs. depth for Hole 627B. A. Raw susceptibility values plotted vs. depth. Several types of susceptibility anomalies are labeled. CO refers to susceptibility anomalies caused by the inclusion of rust flakes in coarse sands that fell down the hole and were cored. Large susceptibility spikes (arrows), greater than an order of magnitude larger than the average value for a core and occurring at the top of the core, are common and appear to be caused in some manner by drilling. Anomalies fitting this description are labeled DA. BL denotes the occurrence of higher susceptibility values in a core with a broken liner. B. Mean values for each core section plotted vs. depth, with peaks caused by downhole contamination removed.

Table 9. Physical properties of sediments, Site 627.

Sample (level in cm)	Sub-bottom depth (m)	Velocity ^a (m/s)	Wet-bulk density ^b (g/cm ³)	Impedance (10 ³ × g/cm ² × s)	Porosity ^b (%)	Dry water content ^b (%)	Shear strength (kPa)	Thermal conductivity (10 ⁻³ × cal × °C ⁻¹ × cm ⁻¹ × s ⁻¹)
Hole 627A								
1-2, 70			1.67		63.48	61.01		
1-4, 67		2216 (a)	1.97	4.36	48.72	33.02		
1-6, 70		1572 (a)	1.79	2.81	57.84	47.68		
Hole 627B								
1-2, 70	2.2						2.378	2.368
1-4, 70	5.2	1540 (a)	1.66	2.56	59.65	55.55		2.445
2-3, 30	9.2	1792 (c)						
2-3, 70	9.6	1538 (a)	1.79	2.75	57.63	47.71	2.605	2.956
2-3, 90	9.8	1563 (c)						
2-5, 42	12.3	1537 (c)						
2-5, 75	12.6	3506 (c)	1.65	5.78	65.50	65.66	0.793	2.606
2-5, 90	12.8							
2-7, 12	15.0		1.86				0.906	2.629
3-2, 70	17.2	1548 (a)	1.74	2.69	57.83	49.72	1.359	2.706
3-4, 68	20.2	1549 (a)	1.89	2.90	54.06	40.85		2.867
3-6, 70	23.2	1564 (a)	1.79	2.80	57.40	47.14		2.841
4-2, 70	27.2	1556 (a)	1.76	2.74	58.49	49.70	0.680	2.571
4-4, 68	30.2	1585 (a)	1.74	2.76	59.80	52.32	0.566	2.715
4-6, 70	33.2	1502 (a)	1.70	2.55	62.47	57.87	0.340	2.528
5-2, 70	36.7		1.75		58.36	50.06	0.906	2.592
5-4, 70	39.7		1.74		60.28	52.84	1.133	2.749
5-6, 70	42.7		1.80		56.77	46.2	3.058	2.422
6-2, 70	46.4		1.84		56.28	44.06	2.944	3.113
6-4, 70	49.4	1972 (a)	1.93	3.81	49.62	34.79	2.378	3.069
6-6, 70	52.4	1837 (a)	1.76	3.23	56.93	47.95	1.296	2.995
7-2, 70	56.0	1835 (a)	1.81	3.32	55.31	44.17		2.987
7-4, 70	59.0	1621 (a)	1.73	2.80	59.60	52.47		1.205
7-6, 70	62.0	1868 (a)	1.80	3.36	56.31	45.49		2.944
8-2, 70	63.4	1592 (a)	1.86	2.96	54.79	41.94	5.21	
8-4, 68	66.4	1581 (a)	1.79	2.83	57.96	47.98	7.36	
8-6, 68	69.4	1559 (a)	1.76	2.74	58.11	49.37	4.87	
9-2, 70	75.3	1926 (a)	1.79	3.45	55.16	44.63	5.08	2.985
9-4, 70	78.3	2104 (a)	1.79	3.77	56.72	46.18	7.03	2.841
9-6, 70	81.3	1720 (a)	1.77	3.04	58.05	48.49	5.78	2.833
10-2, 35	84.5	1435 (c)						
10-2, 70	84.9		1.75		58.87	50.29	2.51	2.672
10-2, 75	84.9	1586 (a)						
10-4, 40	87.6	1540 (c)						
10-4, 75	87.9	1714 (c)	1.78	3.05	58.58	48.94	13.33	2.514
10-4, 120	88.4	1602 (c)						
10-6, 20								
10-6, 68	90.8	1653 (c)						
10-6, 70	90.8	1815 (a)	1.75	3.18	61.91	54.35	13.30	2.572
10-6, 104	91.2	1635 (c)						
11-2, 18	93.9	1780 (c)	1.90	3.38	51.38	37.27	8.25	
11-2, 70	94.4	1693 (c)						2.642
11-2, 70	94.4	1634 (a)						
11-2, 113	94.8	1707 (c)						
12-2, 4	102.2	1883 (c)						
12-2, 70	102.9	1781 (a)	1.79	3.19	53.09	42.35	6.98	2.917
12-2, 70	102.9	1792 (c)						
12-2, 125	103.4	1631 (a)						
12-4, 70	105.9	2055 (c)						2.829
12-4, 70	105.9	1925 (a)	1.95	3.75	48.74	33.68	41.258	
12-4, 123	106.4	1849 (c)						
12-6, 34	108.5	1886						
12-6, 70	108.9	1880 (c)	1.71	3.21	58.25	51.61	11.425	3.046
12-6, 70	108.9	1771 (a)						
12-6, 113	109.3	1861 (c)						
13-2, 135	113.5	1945 (c)						
13-2, 58	114.1	2014 (c)	1.75	3.52	59.07	50.83	22.216	
13-2, 69	114.2	1776 (a)						2.897
13-5, 30	118.2	1957 (c)						2.860
13-5, 70	118.6	1782 (a)	1.77	3.15	57.49	48.21	8.860	
13-5, 120	119.2	1917 (c)						
14-2, 23	122.5	2041 (c)						
14-2, 70	123.0	2076 (c)						2.650
14-2, 70	123.0	1891 (a)	1.84	3.48	52.65	40.40	12.695	
14-2, 130	123.6	1921 (c)						
14-4, 23	125.5	1974 (c)						
14-4, 70	126.0	1669 (c)	1.76	2.94	59.77	51.41	17.138	3.059
14-4, 70	126.0	1545 (a)						
14-4, 100	126.3	2035 (c)						

Table 9 (continued).

Sample (level in cm)	Sub-bottom depth (m)	Velocity ^a (m/s)	Wet-bulk density ^b (g/cm ³)	Impedance (10 ⁵ × g/cm ² × s)	Porosity ^b (%)	Dry water content ^b (%)	Shear strength (kPa)	Thermal conductivity (10 ⁻³ × cal × °C ⁻¹ × cm ⁻¹ × s ⁻¹)
Hole 627B (cont.)								
14-6, 23	127.5	1966 (c)						2.210
14-6, 70	128.0	2006 (c)	1.84	3.69	56.84	45.02	27.294	
16-2, 70	142.4	1895 (c)						
16-2, 70	142.4	1812 (a)	1.84	3.33	49.50	37.02	57.13	2.820
16-2, 110	144.8	1806 (c)						
16-4, 20	144.9	1862 (c)						
16-4, 70	145.4	1850 (c)						2.870
16-4, 70	145.4	1919 (a)	1.87	3.46	52.66	39.40	6.35	
16-6, 10	148.3	1831 (c)						
16-6, 70	148.4	1876 (c)						2.770
16-6, 70	148.5	1569 (a)	1.82	3.41	56.37	45.15	102.83	
17-2, 20	158.2	1960 (c)						
17-2, 66	158.5	1907 (c)						2.230
17-2, 70	158.5	1496 (a)	1.57	2.35	69.68	79.11	15.87	
17-2, 110	159.0	2022 (c)						
17-4, 40	159.7	1874 (c)						
17-4, 70	160.0	1500 (c)						2.510
17-4, 70	160.0	1804 (a)	1.63	2.94	66.66	68.49		2.565
18-1, 70	170.3	1804 (c)						
18-1, 70	170.3	1844 (a)	1.61	5.36	65.45	67.93	20.95	
18-1, 110	170.8	1679 (c)						
19-2, 70	174.0	1571 (c)	1.48	2.33	73.42	96.17		2.470
19-4, 70	177.0	1523 (c)	1.60	2.44	66.34	69.83		2.763
19-4, 100	177.3	1805 (c)						
19-6, 30	179.6	1481 (c)						
19-6, 70	180.0	1762 (c)						2.929
19-6, 70	180.0	1749 (a)	1.76	3.08	58.84	50.89	2.83	
19-6, 100	180.6	1734 (c)						
20-1, 3	190.1	3660 (chert)	1.74	6.37				
20-1, 40	190.5	1897 (c)	1.83	3.47	50.84	38.71		2.926
21-1, 30	209.7	3587 (clast)						2.843
21-3, 70	196.3		1.74		59.31	51.69		2.717
21-4, 70	197.8		1.77		56.67	47.17		2.717
21-6, 70	200.8		1.74		59.56	51.85		
22-1, 15	209.5		1.78		57.24	47.58		
26-1, 53	247.0	1774 (c)						
26-1, 70	247.8	1696 (c)						
26-1, 70	247.3	1782 (a)	1.94	3.29	47.41	32.59		3.502
27-2, 20	248.9	1817 (c)						
27-2, 70	249.4	1604 (c)	1.92	3.08	50.11	35.7	5.69	2.537
27-2, 105	250.1	1738 (c)						
27-4, 25	252.2	2140 (c)						
27-4, 70	252.7	2017 (c)	1.90	3.83	49.98	36.07	15.04	
27-4, 95	252.8	1890 (c)						
27-4, 130	253.2	1639 (a)						
27-6, 25	255.0	1860 (c)						
27-6, 70	255.4	2104 (c)						3.490
27-6, 70	255.4	1722 (a)	1.88	3.96	50.02	36.41	13.41	
27-6, 120	256.0	1760 (c)						
28-2, 15	260.0	1989 (c)						
28-2, 70	260.6	2123 (c)						1.910
28-2, 70	260.6	1844 (a)	1.92	4.08	51.50	38.08	4.88	
28-4, 20	264.7	1671 (c)						
28-4, 28	264.8	2303 (clast)						
28-4, 70	265.1	2048 (c)	1.88	3.85			22.22	1.880
28-4, 130	265.9	1846 (c)						
29-2, 2	267.5	1935						
29-2, 60	268.1	2100						
29-2, 70	268.2	2673 (a)	1.92	5.113	54.15	39.61	10.79	3.480
29-2, 114	268.7	1731 (c)						
29-4, 15	270.6	1511 (c)						
29-4, 20	270.7	1661 (c)						
29-4, 70	271.2	2134 (c)						3.380
29-4, 70	271.2	1913 (a)	1.88	3.60	50.88	37.23	8.89	
29-4, 80	271.3	1762 (c)						
29-6, 10	273.6	1822 (c)						
29-6, 70	274.2	1999 (a)	1.96	3.92	50.24	34.72	15.87	3.190
29-6, 110	274.6	1816 (c)						
30-2, 10	282.6	1669 (c)						
30-2, 70	283.2	1903 (a)	1.86	3.54	51.14	38.22	4.44	2.330
30-4, 10	285.6	1941 (c)						3.540
30-6, 30	288.8	2278 (c)						
31-2, 20	291.8	1600 (c)						
31-2, 70	292.3	1812 (c)						2.730

Table 9 (continued).

Sample (level in cm)	Sub-bottom depth (m)	Velocity ^a (m/s)	Wet-bulk density ^b (g/cm ³)	Impedance (10 ⁵ × g/cm ² × s)	Porosity ^b (%)	Dry water content ^b (%)	Shear strength (kPa)	Thermal conductivity (10 ⁻³ × cal × °C ⁻¹ × cm ⁻¹ × s ⁻¹)
Hole 627B (cont.)								
31-2, 70	292.3	1604 (a)	1.83	2.94	55.81	44.06		
31-3, 20	293.3	1653 (c)						
31-3, 70	293.8	1807 (c)						2.790
31-3, 70	293.8	1525 (a)	1.94	2.96	49.72	34.73		
31-3, 150	294.6	4202 (chert)						
32-2, 20	298.2	1725 (c)						
32-2, 70	298.7	1771 (c)						3.090
32-2, 70	298.7	1902 (a)	1.82	3.46	56.14	44.68	9.52	
32-2, 100	299.0	1620 (c)						
32-4, 75	302.4	1824 (c)	1.82	3.32	55.95	44.67		
32-6, 20	304.2	1751 (c)						
32-6, 70	304.7	1641 (a)	1.83	3.00	54.78	42.79	16.50	3.360
32-6, 95	305.0	1719 (c)						
33-1, 70	313.1	1703 (c)	1.77	3.01	57.41	48.26	1.62	3.300
34-2, 70	317.2	1743 (a)	1.76	3.07	51.56	41.63	4.06	3.340
34-4, 70	318.7	1695 (a)	1.84	3.12	52.34	40.05	4.88	3.120
34-6, 60	321.6	1602 (c)	1.81	2.90	55.33	44.21	12.19	
34-6, 80	321.8	2213 (c)						3.140
36-1, 15	349.2	3960 (clast)	2.38	9.42	23.59	11.22		
37-1, 40	352.0	2140 (c)	1.85	3.96	53.72	40.98		
38-2, 10	355.1	2349 (c)						
38-2, 70	355.7	2791 (a)	2.22	6.20	31.02	16.50		3.530
38-2, 70	355.7	2143 (c)						
38-4, 25	358.2	2751 (c)						
38-4, 70	358.7	2062 (a)	2.19	4.52	33.61	18.40		3.060
38-4, 80	358.8	2779 (c)						
38-4, 110	359.1	2188 (c)						
38-6, 20	361.2	2354 (c)						
38-6, 70	361.7	2027 (a)	2.08	4.22	40.98	24.90		5.565
38-6, 75	361.8	2239 (c)						
39-1, 20	363.3	1877 (c)						
39-1, 60	363.7	1976 (c)	2.10	4.15	41.82	25.20		
39-1, 60	363.7	1714 (a)						
39-1, 110	364.2	2006 (c)						
39-3, 20	366.3	2004 (c)						
39-3, 70	366.8	2278 (c)						
39-3, 70	366.8	1826 (a)	2.16	3.94	41.06	23.80		
39-3, 110	367.2	2072 (c)						
39-5, 20	369.3	2044 (c)						
39-5, 60	369.7	1828 (a)	2.11	3.86	41.84	25.10		
39-5, 70	369.8	2039 (c)						
39-5, 110	370.2	2069 (c)						
40-2, 28	374.4	1766 (c)						3.610
40-2, 60	374.8	2437 (c)						
40-2, 70	374.9	2216 (a)	2.23	4.94	30.86	16.30		
40-2, 108	375.3	2884 (c)						
40-4, 20	377.4	2432 (c)						
40-4, 68	377.9	3160 (c)						
40-4, 70	377.9	2025 (a)	2.13	4.31	39.33	23.00		3.050
40-4, 100	378.2	3279 (c)						
40-6, 20	380.4	1945 (c)						
40-6, 64	380.8	3309 (c)						
40-6, 70	380.9	2166 (a)	2.16	4.68	36.63	20.70		3.610
40-6, 100	381.2	2878 (a)						
41-2, 20	384.1	1970 (c)						
41-2, 70	384.6	1907 (c)						
41-2, 70	384.6	2133 (a)	2.17	4.63	36.82	21.02		2.964
41-4, 20	387.1	1899 (c)						
41-4, 70	387.6	2205 (c)						
41-4, 70	387.6	2047 (a)	2.17	4.44	31.79	16.88		3.640
41-4, 100	387.9	1834 (c)						
41-6, 20	390.1	1814 (c)						
41-6, 70	390.6	1925 (c)						
41-6, 70	390.6	1877 (a)	2.15	4.04	29.93	15.62		3.660
31-6, 100	390.9	2205 (c)						
42-2, 20	393.6	1899 (c)						
42-2, 70	394.1	1780 (c)						
42-2, 70	394.1	1844 (c)	2.04	3.76	41.26	25.62		3.680
42-2, 100	394.4	1754						
42-4, 20	396.6	1827 (c)						
42-4, 70	397.1	1845 (c)						
42-4, 70	397.1	1962 (a)	2.15	4.22	41.26	18.84		
42-4, 100	397.4	1878 (c)						
42-6, 20	399.6	1887 (c)						

Table 9 (continued).

Sample (level in cm)	Sub-bottom depth (m)	Velocity ^a (m/s)	Wet-bulk density ^b (g/cm ³)	Impedance (10 ⁵ × g/cm ² × s)	Porosity ^b (%)	Dry water content ^b (%)	Shear strength (kPa)	Thermal conductivity (10 ⁻³ × cal × °C ⁻¹ × cm ⁻¹ × s ⁻¹)
Hole 627B (cont.)								
42-6, 70	400.1	1957 (c)						
42-6, 70	400.1	1986 (a)	2.12	4.21	33.65	19.48		
43-2, 20	402.8	2093 (c)						
43-2, 67	403.7	2058 (c)						
43-2, 66	403.7	1842 (a)	1.58	2.91	38.28	32.39		3.210
43-2, 100	404.0	2025 (c)						
43-4, 30	405.9	2052 (c)						
43-4, 73	406.3	1790 (c)						
43-4, 73	406.3	2001 (a)	1.80	3.60	41.47	30.24		
43-4, 100	406.6	2142 (c)						
43-6, 20	408.8	1887 (c)						
43-6, 57	409.5	1995 (a)	1.82	3.63	32.60	22.17		3.630
43-6, 100	409.6	2142 (c)						
44-2, 70	412.6	1971	2.08	4.10	39.02	23.70		2.600
44-4, 70		1947	1.99	3.87	38.62	21.74		
44-6, 70	415.6	2032	1.95	3.96	41.50	23.80		
45-1, 27	428.8	1919 (c)						
45-1, 79	429.3	2121 (c)	2.07	4.39				
46-2, 20	431.7	1872 (c)						
46-2, 75	432.2	1960 (c)	2.09	4.00				3.071
46-2, 110	432.6	1849 (c)						
46-4, 75	435.2	2000 (c)						
46-4, 72	435.2	1942 (a)	2.19	4.25				3.250
46-4, 120	435.7	1923 (c)						
46-6, 20	434.7	1943 (c)						
46-6, 70	435.2	2181 (c)	2.18	4.73				
46-6, 70	435.2	2169 (a)						
46-6, 120	435.7	2559 (c)						
47-1, 20	439.9	2248 (c)						
47-1, 70	440.4	2046 (c)	2.07	4.24	46.93	29.52		
47-1, 75	440.4	2135 (a)						
47-1, 135	441.1	2081 (c)						
47-3, 20	442.9	2440 (c)						
47-3, 75	443.4	2720 (a)	2.31	6.28	32.50	16.68		
47-3, 120	443.9	2322 (c)						
47-6, 75	447.5	2809 (c)						
47-6, 75	447.5	2914 (a)	2.16	6.29	39.55	22.68		3.473
47-6, 120	448.0	2237						
51, CC	486.5	3780 (dolostone)						
		3723 (dolostone)						
52, CC		3084 (limestone?)						
		3249 (limestone?)						
53, CC		4393, 4387						
55-1, 73		5068 (c)						
		5780 (b)						
55-1, 41		3624 (c)						
56, CC		5431						
57-1, 150		4183						
59-1, 5		4949 (gypsum)						

^a The letter *a* in parentheses indicates an axis of measurement along the length of the core, usually perpendicular to bedding; *b* indicates an axis across the core, parallel to the plane of the split core face, usually parallel to bedding; *c* indicates an axis across the core, perpendicular to the plane of the split core face, usually parallel to bedding.

^b Determined by gravimetric and volumetric techniques.

able sonobuoy profile and profile LBB-18 (Table 11). However, note that the velocity transition occurs higher/shallower in the sonobuoy results (1.787 s/474 m sub-bottom) than on the site-survey reflection profile (1.848 s/531 m sub-bottom). This discrepancy has two possible explanations. First, the reflection velocities could simply be more accurate because they involve spatial averaging over less than 1 km, whereas the sonobuoy measurement averages over 18 km or more. However, the sonobuoy velocities are refractions, and the refracted wave would propagate over the highest velocity path available to it. Therefore, the differential between these results may have a physical basis. This possibility is substantiated by results from Hole 627B, where the first unequivocal evidence for (high-velocity) shallow-water platform deposits occurs in Core 627B-51X at 477.5–487.1 m sub-bottom, thereby correlating with the sonobuoy re-

sult, whereas the evaporites that are interpreted to constitute the top of *G* on the site-survey profile do not occur until Core 627B-55X at 514.2–519.2 m sub-bottom, a reasonable tie to the reflection velocity transition.

Hole 627B: Correlations with Global Cycles of Relative Sea-Level Change

Results from Hole 627B suggest a mixed response of this distal-carbonate-slope environment to postulated eustatic sea-level changes (Fig. 34). The most pronounced hiatus in Hole 627B separates the latest Oligocene from the latest Eocene (25.5–37.5 Ma) in Core 627B-20X (181.4–191 m sub-bottom). It could be correlated with either the C/D boundary (depth mismatch of approximately 30 m) or the D/E boundary (depth mismatch of the same amount), but it may be represented by neither one. In-

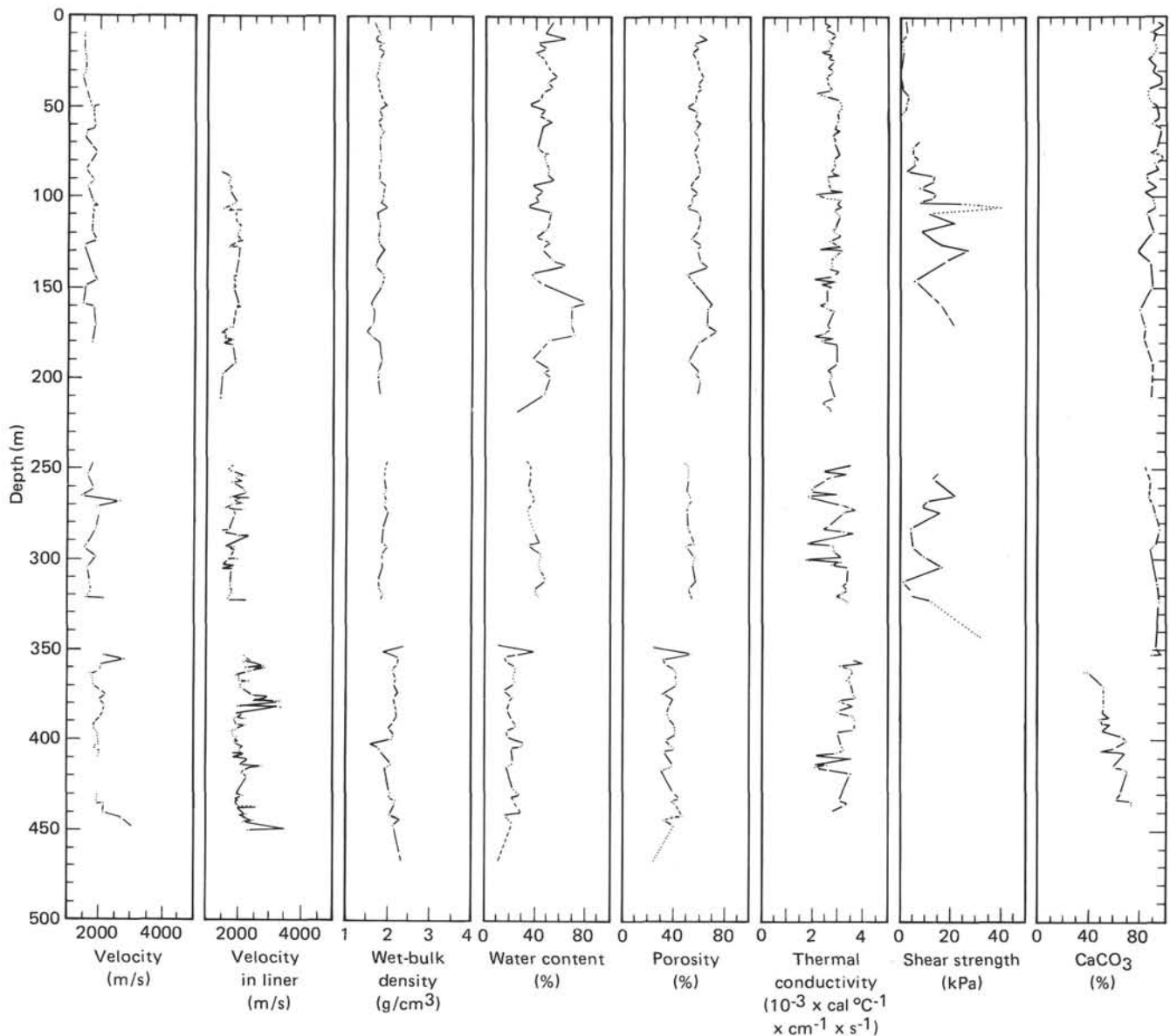


Figure 30. Graphic summary of physical properties, Hole 627B. Density, water content, and porosity values were determined by gravimetric and volumetric techniques.

stead, the hiatus could tie with another, unrecognized sequence boundary within sequence D, which is beyond the resolution of the available geophysical results. (Sequence D at Hole 627B is only 0.055 s thick; see Fig. 33.) Between Hole 627B and Site 628 (BAH-8-A), such a sequence boundary is discernible on LBB-18 (see "Seismic Stratigraphy," Site 628 chapter).

Other significant hiatuses in Hole 627B span the early Paleocene-early Maestrichtian (66–69.5 Ma) between Core 627B-26X (239.1–248.7 m sub-bottom) and Core 627B-27X (248.7–258.2 m sub-bottom) and the early Eocene-late Paleocene (56–59 Ma) between Core 627B-23X (210.2–219.9 m sub-bottom) and Core 627B-24X (219.9–229.4 m sub-bottom). However, only the latter correlates in depth with both a sequence boundary, D/E, and a postulated sea-level lowstand (the TP1/TP2.1 sea-level fall, approximately 59 Ma; Vail and Hardenbol, 1979).

Perhaps the most significant potential correlation with Vail et al. (1977) in Hole 627B occurs between the E/F boundary and the postulated mid-Cenomanian sea-level fall at 97 Ma. At Site 627, the E/F boundary is interpreted as the earliest Conia-

cian-latest middle Cenomanian hiatus, approximately 86–95 Ma, between Core 627B-36X (334.3–343.9 m sub-bottom) and Core 627B-37X (343.9–353.5 m sub-bottom). This is a minimum mismatch of 2 m.y., which is a significant discrepancy if the assumption that a lowstand causes erosion is correct. Furthermore, if a Cenomanian lowstand terminated the input of carbonate detritus to Site 627 by exposing an ancestral Little Bahama Bank to rapid subaerial lithification, then there should be some evidence of this change in depositional regime within the older Cenomanian marls in Hole 627B. There is no such evidence.

However, two other factors must be taken into account. First, the Cretaceous sea-level cycles have never been published in detail, and a Coniacian lowstand may in fact exist to account for the Hole 627B hiatus in question. Second, the originally published age of the Vail et al. (1977) mid-Cretaceous sea-level drop may be younger, given approximately 8 years of subsequent documentation.

Another possible tie to the E/F boundary may be with the early Campanian-early Santonian hiatus (approximately 75–81

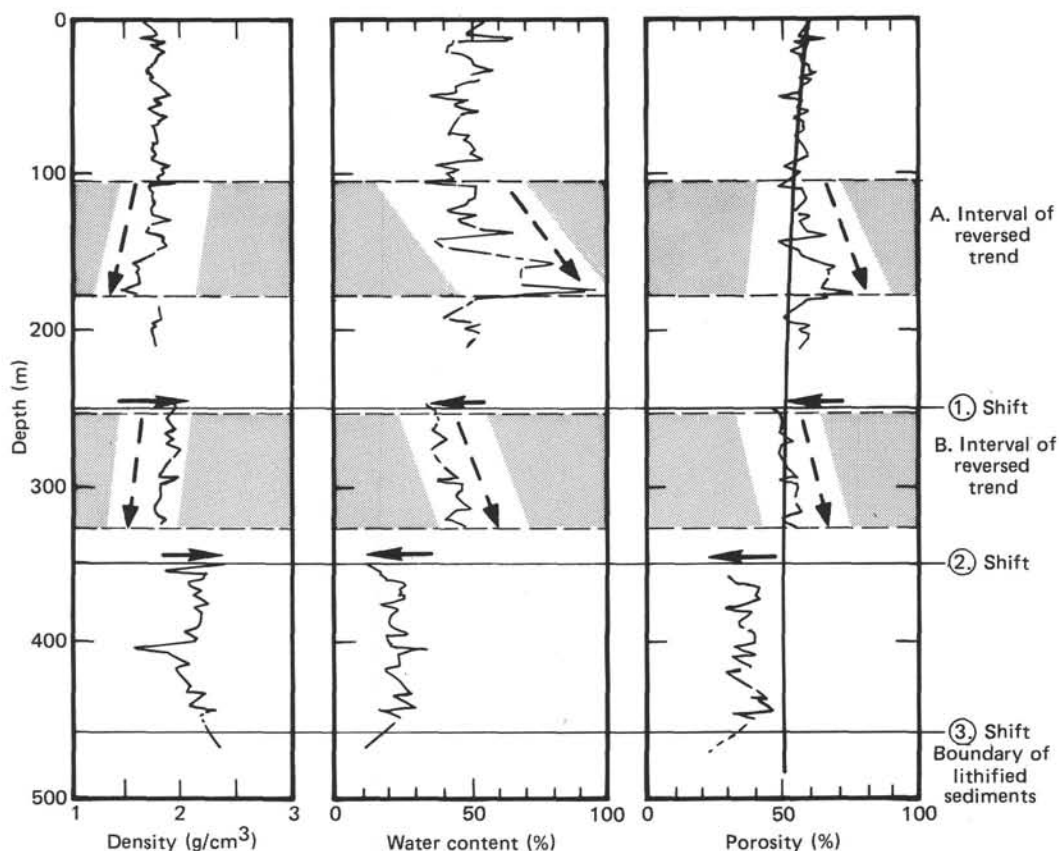


Figure 31. Physical-properties downhole distribution curve of sediments overlying the lithified shallow platform sediments show two main features: A. Shifts in the data curve. The shift at 345 m sub-bottom away from the idealized curve for porosity indicates additional overburden pressure and is evidence for an erosional event. B. Two intervals of reverse trends are caused by lithologic features. Interval A is correlated with a sequence of debris flows and turbidites. Interval B is correlated with a change in composition of the ooze. Thick line (in porosity plot) is a constructed downhole distribution curve. After Bryant et al. (1981).

Ma), which occurs between Core 627B-34X (315.0–324.7 m sub-bottom) and Core 627B-36X (334.3–343.9 m sub-bottom). Because of close association in depth with the mid-Cenomanian event, the two hiatuses probably cannot be distinguished seismically. Interestingly, the Campanian–Santonian depositional break occurs within Vail et al.'s (1977) Cretaceous supercycle Kb, the long highstand characterizing the Late Cretaceous. Such a prolonged erosional episode lends credence to the notion that carbonate slopes respond quite differently from clastic slopes to fluctuating sea levels through time.

In summary, the correlations between the hiatuses documented in Hole 627B and the Vail et al. (1977) sea-level curve are somewhat ambiguous at present. One of the problems may be that this entire region remained sediment-starved for more than 70 m.y. (see "Summary and Conclusions" section, this chapter). During this interval, local as well as global causes for erosion could have complicated a eustatic sea-level signal.

SUMMARY AND CONCLUSIONS

Site 627 was drilled with a dual purpose in mind: it represents the distal end of the slope transect off Little Bahama Bank and provides an opportunity to penetrate the top of the mid-Cretaceous "megabank" not reached at Site 626 in the Straits of Florida. Both tasks were accomplished. Site 626 penetrated 536 m of Cenozoic and Mesozoic sediments, consisting of the following units (Fig. 35 and "Sedimentology" and "Biostratigraphy" sections, this chapter): (1) Unit I, periplatform ooze with

turbidites, slumps, and debris flows, representing the toe of the prograding flank of Little Bahama Bank and including at the base debris flow(s) coeval with the Abaco Member of the Blake Ridge Formation, early Miocene–Pleistocene, 181 m; (2) Unit II, a condensed section of argillaceous carbonate ooze and chalk with some chert and siliceous limestone, Paleocene–early Miocene, 68 m; (3) Unit III, a nannofossil ooze and chalk without platform input and negligible dissolution effects, Campanian, 76 m; (4) Unit IV, a condensed section of carbonate ooze, chalk, and chert with limestone hardgrounds, middle Cenomanian–Santonian, 19 m; (5) Unit V, marly chalk with nannoplankton, planktonic foraminifers, and neritic benthos, deepening upward from inner-neritic (euphotic) to outer-neritic environments, latest(?) Albian–early Cenomanian, 124 m; and (6) Unit VI, shallow-water dolomites, limestones, and gypsum with algal mats and other neritic biota, late(?) Albian, 68 m.

This succession reflects the drowning and disintegration of the mid-Cretaceous carbonate platform, the "megabank," its transformation into a predominantly terrigenous shelf in the Cenomanian, and later into a marginal plateau of bathyal depth (Campanian–early Miocene). Since the early Miocene, this part of the plateau has become part of the prograding flank of Little Bahama Bank.

Sedimentation rates are particularly interesting at this site ("Sediment-Accumulation Rates," this chapter). They reveal periods of steady sedimentation alternating with intervals of slow deposition or nondeposition. Between the termination of the

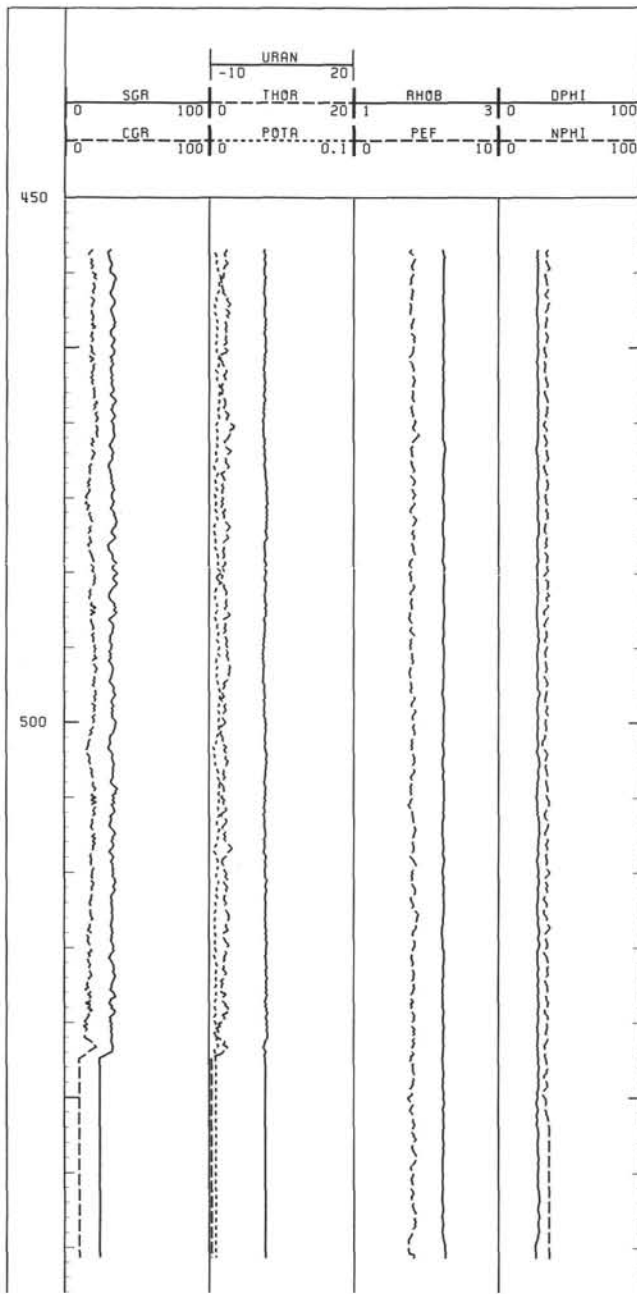


Figure 32. Log curves from Hole 627B, showing natural gamma radiation (SGR and CGR); concentrations of potassium, uranium, and thorium; bulk density (RHOB); photoelectric absorption coefficient (PEF); neutron porosity (NPFI); and density porosity (DPFI). The CGR curve represents the total gamma radiation minus that from uranium. The top of the gypsum layer is indicated by the log response.

terrigenous shelf in the Cenomanian and the arrival of the prograding Bahama Platform in the Miocene, we see a period of 72 m.y. of starved sedimentation, interrupted by a pulse of planktonic carbonate sedimentation in the Campanian. A similar trend exists in the Blake Basin (Sheridan, Gradstein, et al., 1983; Fig. 36) with the exception of the Campanian pulse, which is not recorded in the Blake Basin presumably because it lay below the CCD at the time.

The mid-Cretaceous drowning of carbonate platforms, in conjunction with low-relief hinterland and little terrigenous input, may be the reasons for this unusually long-lasting starvation of the southwestern North Atlantic. Episodic scouring by the Gulf Stream probably accounts for the intermittent character of sedimentation in the oceanic-plateau stage in the late Cretaceous and Paleogene (Pinet and Popenoe, 1985a).

The Cretaceous terrigenous shelf and the underlying carbonate platform are interesting with regard to organic matter ("Organic Geochemistry" section, this chapter). The Cenomanian marls contain immature gas-prone source rocks. The carbonate-evaporite sequence below contains immature oil-prone source beds. A 5-cm section of oil-stained dolomite suggests upward migration of hydrocarbons from deeper in the section.

With regard to sediment mineralogy, several points merit mention ("Inorganic Geochemistry," this chapter): (1) Clay-sized aragonite, interpreted as the bank-derived component of peri-platform ooze, decreases down the hole from 30% to 50% in the Plio-Pleistocene to below x-ray-detection levels in the lower Miocene; this trend may reflect the dissolution of aragonite during burial diagenesis as well as the progradation of the toe-of-slope with concomitant increase of platform input during the Neogene; (2) in the Cenomanian marly chinks the noncarbonate fraction consists mainly of quartz and feldspar and surprisingly little clay; and (3) the carbonate-evaporite sequence of the Albian resembles coeval deposits in south Florida and the Bahamas (Tator and Hatfield, 1975; G. Mackenzie and W. Schlager, unpubl. site-survey report). The dominant evaporite mineral at Site 627, however, is gypsum, not anhydrite. The transformation with burial of gypsum to anhydrite occurs from approximately 300 to 3000 m of burial (Blatt et al., 1980). The reverse reaction, anhydrite to gypsum, takes place very near the surface during the weathering of anhydritic rocks. As the depth of burial at Site 627 is only 500 m, it is almost certain that the gypsum in the Albian platform deposits is a pristine Cretaceous mineral rather than the product of a double conversion, gypsum to anhydrite to gypsum.

Interstitial-water geochemical data revealed strong positive Ca and Mg gradients. These are believed to be governed by diffusion from the underlying Cenomanian marls, which are rich in igneous minerals. The magnitude of these gradients influences the rate and type of diagenetic reactions occurring in the sediments.

Borehole stratigraphy can be tied rather accurately to the seismic stratigraphy of the site surveys, particularly the Cretaceous part of the section (Fig. 35 and "Seismic Stratigraphy" section, this chapter). Both the top of the Albian platform carbonates

Table 10. Material properties of limestone, dolomite, and gypsum, Hole 627B.

Dominant lithology	Density (g/cm ³)	H ₂ O content (vol.%)	Photoelectric absorption index	Th (ppm)	K (wt.%)	U (ppm)
Limestone	2.71	0	5.08	—	0-7 (0.3 avg.)	—
Dolomite	2.87	0	3.14	—	0-7 (0.3 avg.)	>0
Gypsum	2.32	31.1	4.0	—	—	—

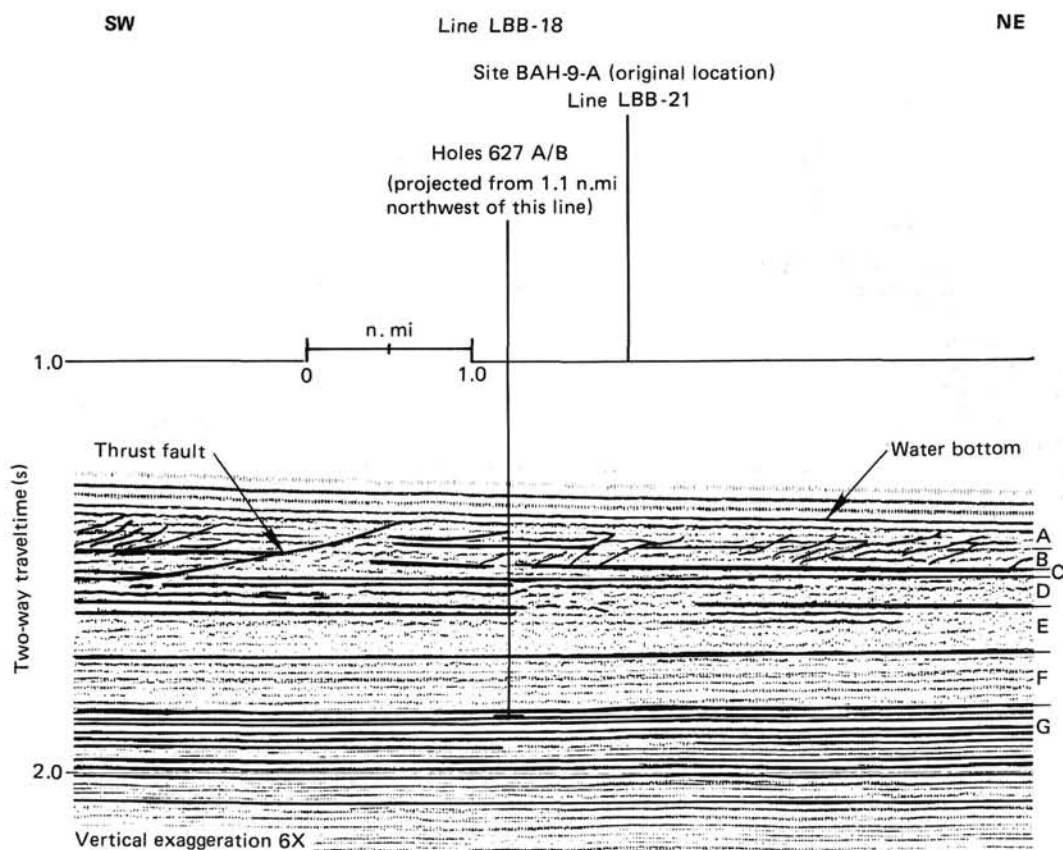


Figure 33. Part of line LBB-18, illustrating the seismic stratigraphy of Site 627. Sequences A through G are discussed in the text. The vertical line denotes depth of penetration of Holes 627A and 627B. Note the thrust faults displacing the section, particularly the large one landward (southwest) of Site 627.

Table 11. Seismic stratigraphy and velocity structure from site-survey profile LBB-18 and sonobuoy 12.

Sequence	s	Thickness		Sub-bottom depth		Sequence boundary	Traveltime (s)	Interval velocity	
		Sonobuoy 12 (m)	Line LBB-18 (m)	Sonobuoy 12 (m)	Line LBB-18 (m)			Sonobuoy 12 (km/s)	Line LBB-18 (km/s)
A	0.055	47	48	47	48	A/B	1.373-1.428	1.70	1.75
B	0.070	72	61	119	109	B/C	1.428-1.485	1.70	1.75
C	0.042	45	37	164	146	C/D	1.498-1.540	2.15	1.75
D	0.055	63	62	227	208	D/E	1.540-1.545	2.15	2.26
E	0.11	136	128	363	336	E/F	1.545-1.595	2.21	2.26
							1.595-1.657	2.21	2.26
F	0.14	111	195	474	531	F/G	1.657-1.708	2.65	2.26
							1.708-1.747	2.65	2.78
G	0.125	285	262				1.747-1.787	2.95	2.78
							1.787-1.848	4.20	2.78
							1.848-1.917	4.20	4.20

Water depth = 1.373 s or 1030 m uncorrected (1040 m corrected).

and the top of the Cenomanian marls correlate with seismic-sequence boundaries and with changes in interval velocities. Furthermore, the results agree well with the seismic stratigraphy of Pinet and Popenoe (1985b). The correlations are less satisfactory in the Neogene section, probably because reflectors show more local relief, so that the 1-n.-mi offset between the borehole and the nearest seismic line becomes significant.

REFERENCES

- Blatt, H., Middleton, G., and Murray, R., 1980. *Origin of Sedimentary Rocks* (2nd ed.): Englewood Cliffs, NJ (Prentice Hall).
- Briefnick, D. M., Robertson, A. H. F., and Sheridan, R. E., 1983. Deposition and provenance of Miocene intraclastic chinks, Blake-Bahama Basin, western North Atlantic. In Sheridan, R. E., Gradstein, F. M., et al., *Init. Repts. DSDP, 76*: Washington (U.S. Govt. Printing Office), 727-748.
- Bloemendal, J., 1980. Paleoenvironmental implications of the magnetic characteristics of sediments from Deep Sea Drilling Project Site 514, southeast Argentine Basin. In Ludwig, W. J., Krashennnikov, V. A., et al., *Init. Repts. DSDP, 71*: Washington (U.S. Govt. Printing Office), 1097-1108.
- Bryant, W. R., Bennett, R. H., and Hatherman, C. E., 1981. Shear strength consolidation, porosity and permeability of oceanic sedi-

ments. In Emiliani, C. (Ed.), *The Sea* (Vol. 7): New York (Wiley), 1555-1616.

Droxler, A. W., 1984. Late Quaternary glacial cycles in the Bahamian deep basins and in the adjacent Atlantic Ocean [Ph.D. dissert.]. Univ. Miami.

Droxler, A. W., and Schlager, W., in press. Glacial/interglacial sedimentation rates and turbidite frequency in the Bahamas. *Geology*.

Freeman-Lynde, R., Cita, M. B., Jadoul, F., Miller, E. L., and Ryan, W. B. F., 1981. Marine geology of the Bahama Escarpment. *Mar. Geol.*, 44:119-156.

Friend, J. K., and Riedel, W. R., 1967. Cenozoic orosphaerid radiolarians from tropical Pacific sediments. *Micropaleontology*, 13:217-232.

Gieskes, J. M., 1981. Deep-sea drilling interstitial water studies: Implications for chemical alteration of the oceanic crust, Layers 1 and 2. *SEPM Spec. Publ.*, 32:149-167.

Harland, W. B., Cox, A. V., Llewellyn, P. G., Pickton, C. A. G., Smith, A. G., and Walters, R., 1982. *A Geologic Time Scale*: Cambridge (Cambridge Univ. Press).

Jansa, L. F., Enos, P., Tucholke, B. E., Gradstein, F. M., and Sheridan, R. E., 1979. Mesozoic-Cenozoic sedimentary formations of the North American Basin; western North Atlantic. In Talwani, M., Hay, W., and Ryan, W. B. F. (Eds.), *Deep Drilling Results in the Atlantic Ocean: Continental Margins and Paleoenvironment*: Washington (Am. Geophys. Union), 1-57.

Kobayashi, K., and Nomura, M., 1974. Ferromagnetic minerals in the sediment cores from the Pacific basin. *J. Geophys.*, 40:501-512.

Leckie, R. M., 1984. Composition of mid-Cretaceous planktonic foraminiferal assemblages: open ocean versus epicontinental sea. *GSA Abstracts with Programs*, 16(6). (Abstract)

Lynts, G. W., Judd, J. B., and Stehman, C. F., 1973. Late Pleistocene history of Tongue of the Ocean, Bahamas. *Geol. Soc. Am. Bull.*, 84: 2665-2684.

Morgan, W. J., 1981. Hotspot tracks and the opening of the Atlantic and Indian Oceans. In Emiliani, C. E. (Ed.), *The Sea*, (Vol. 7): New York (Wiley), 443-487.

Mullins, H. T., Heath, K. C., Van Buren, H. M., and Newton, C. R., 1984. Anatomy of a modern open-ocean carbonate slope: northern Little Bahama Bank. *Sedimentology*, 31:141-168.

Mullins, H. T., and Neumann, A. C., 1979. Deep carbonate bank margin structure and sedimentation in the northern Bahamas. *SEPM Spec. Publ.*, 27:165-192.

Pinet, P. R., and Popenoe, P., 1985a. A scenario of Mesozoic-Cenozoic ocean circulation over the Blake Plateau and its environs. *Geol. Soc. Am. Bull.*, 96:618-626.

_____, 1985b. Shallow seismic stratigraphy and post-Albian geologic history of the northern and central Blake Plateau. *Geol. Soc. Amer. Bull.*, 96:627-638.

Schlager, W., and Chermak, A., 1979. Sediment facies of platform to basin transition, Tongue of the Ocean, Bahamas. *SEPM Spec. Publ.*, 27:193-208.

Schlager, W., and Ginsburg, R. N., 1981. Bahama carbonate platforms—the deep and the past. *Mar. Geol.*, 44:1-24.

Schlager, W., and James, N. P., 1978. Low-magnesian calcite limestones forming at the deep-sea floor, Tongue of the Ocean, Bahamas. *Sedimentology*, 25:675-702.

Serra, O., 1984. *Fundamentals of Well-Log Interpretation*: Amsterdam (Elsevier).

Sheridan, R. E., Gradstein, F. M., et al., 1983. *Init. Repts. DSDP, 76*: Washington (U.S. Govt. Printing Office).

Stainforth, R. M., Lamb, J. L., Luterbacher, H., Beard, J. H., and Jeffords, R. M., 1975. *Cenozoic Planktonic Foraminiferal Zonation and Characteristic Index Forms*: Univ. Kansas Paleontol. Contrib., Art. 62.

Tappan, H. N., 1980. *The Paleobiology of Plant Protists*: San Francisco (Freeman).

Tator, B. A., and Hatfield, L. E. 1975. Bahamas present complex geology. *Oil Gas J.*, 73(43):172-176; 73(44):120-122.

Tissot, B., Demaison, G., Masson, P., Delteil, J. R., and Combax, A., 1980. Paleoenvironment and petroleum potential of middle Cretaceous black shales in Atlantic basins. *AAPG Bull.*, 64:2051-2063.

Vail, P. R., and Hardenbol, J., 1979. Sea-level changes during the Tertiary. *Oceanus*, 22:71-80.

Vail, P. R., Mitchum, R. M., Jr., and Thompson, S., III, 1977. Seismic stratigraphy and global changes of sea level, Part 4: Global cycles of

relative changes of sea level. In Payton, C. E. (Ed.), *Seismic Stratigraphy—Applications to Hydrocarbon Exploration*: AAPG Mem., 26:83-97.

Van Buren, H. M., and Mullins, H. T., 1983. Seismic stratigraphy and geologic development of an open-ocean carbonate slope: The northern margin of Little Bahama Bank. In Sheridan, R. E., Gradstein, F. M., et al., *Init. Repts. DSDP, 76*: Washington (U.S. Govt. Printing Office), 749-762.

Weaver, F. M., and Dinkelman, M. G., 1978. Cenozoic radiolarians from the Blake Plateau and the Blake-Bahama Basin, DSDP Leg 44. In Benson, W. E., Sheridan, R. E., et al., *Init. Repts. DSDP, 44*: Washington (U.S. Govt. Printing Office), 865-886.

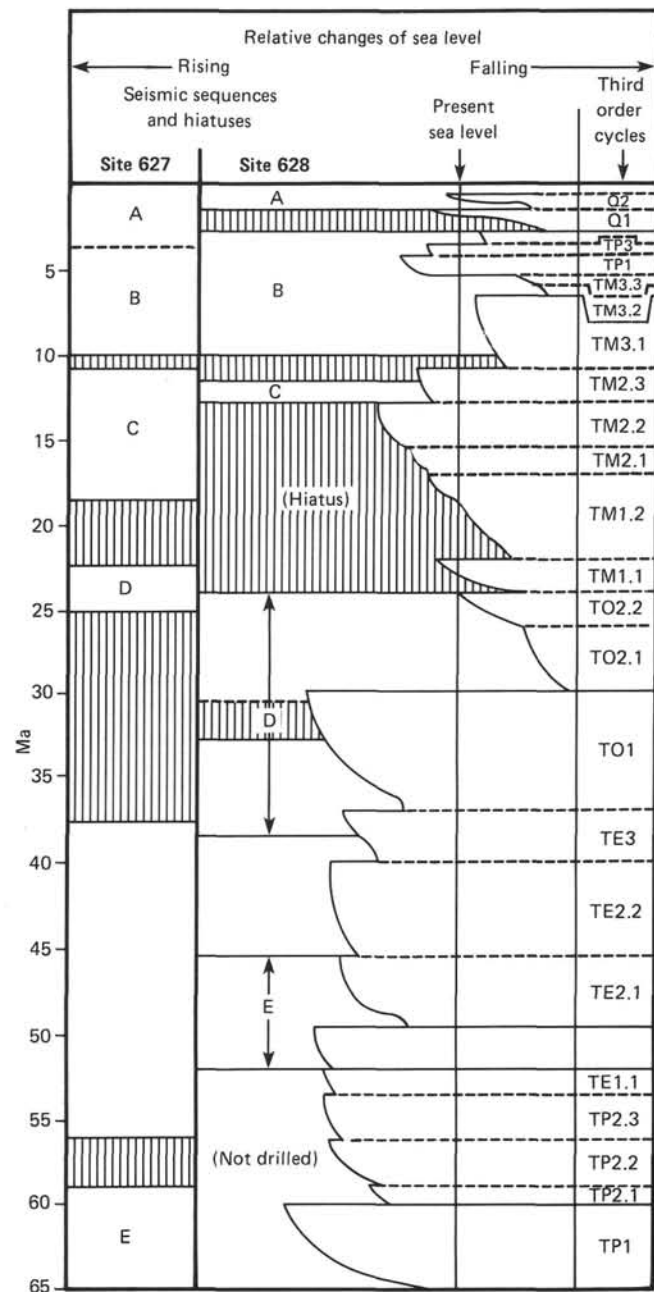
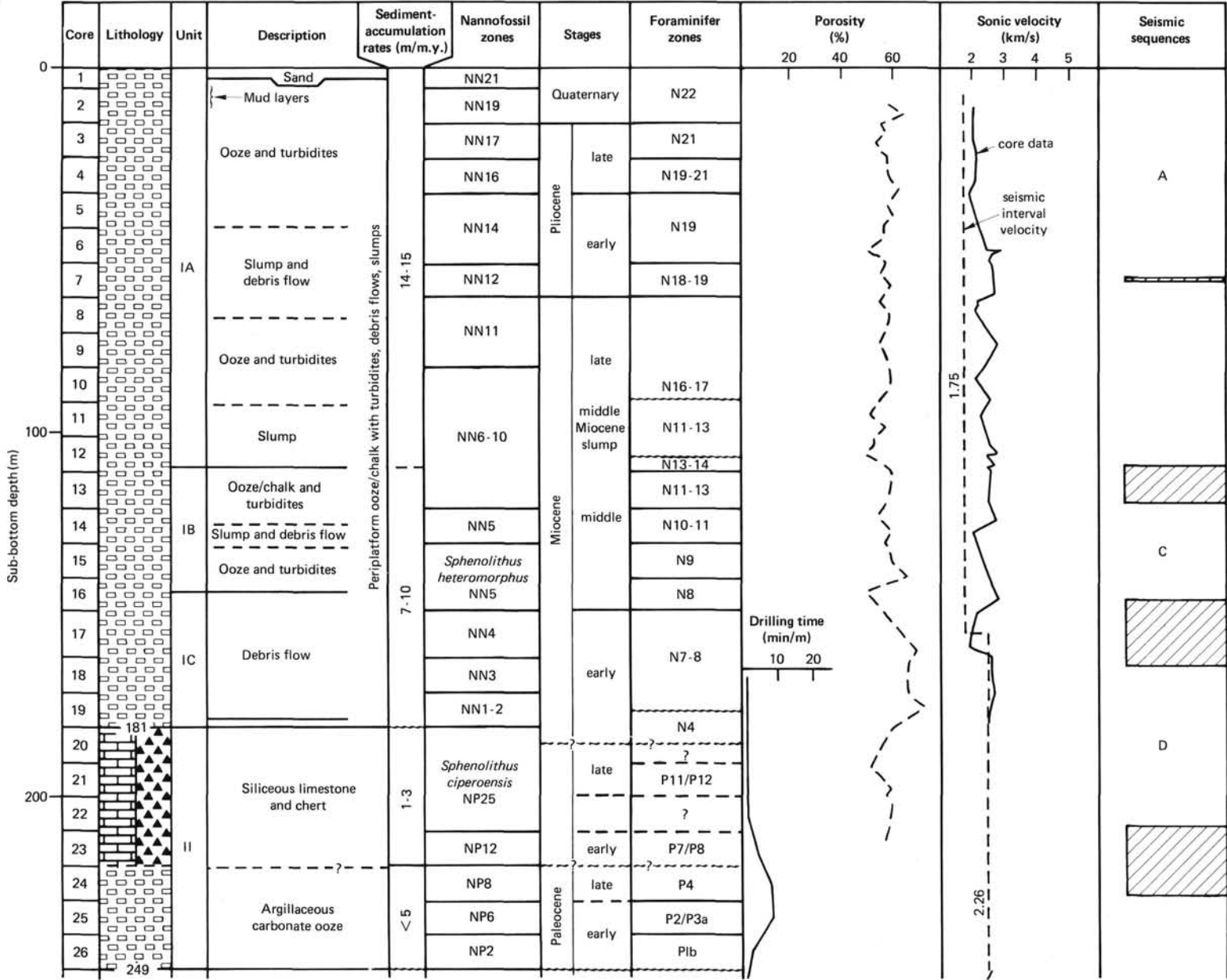


Figure 34. Hiatuses and boundaries of seismic stratigraphic sequences at Sites 627 and 628, correlated with third-order cycles of sea-level curve (Vail et al., 1977).

THIS PAGE INTENTIONALLY BLANK



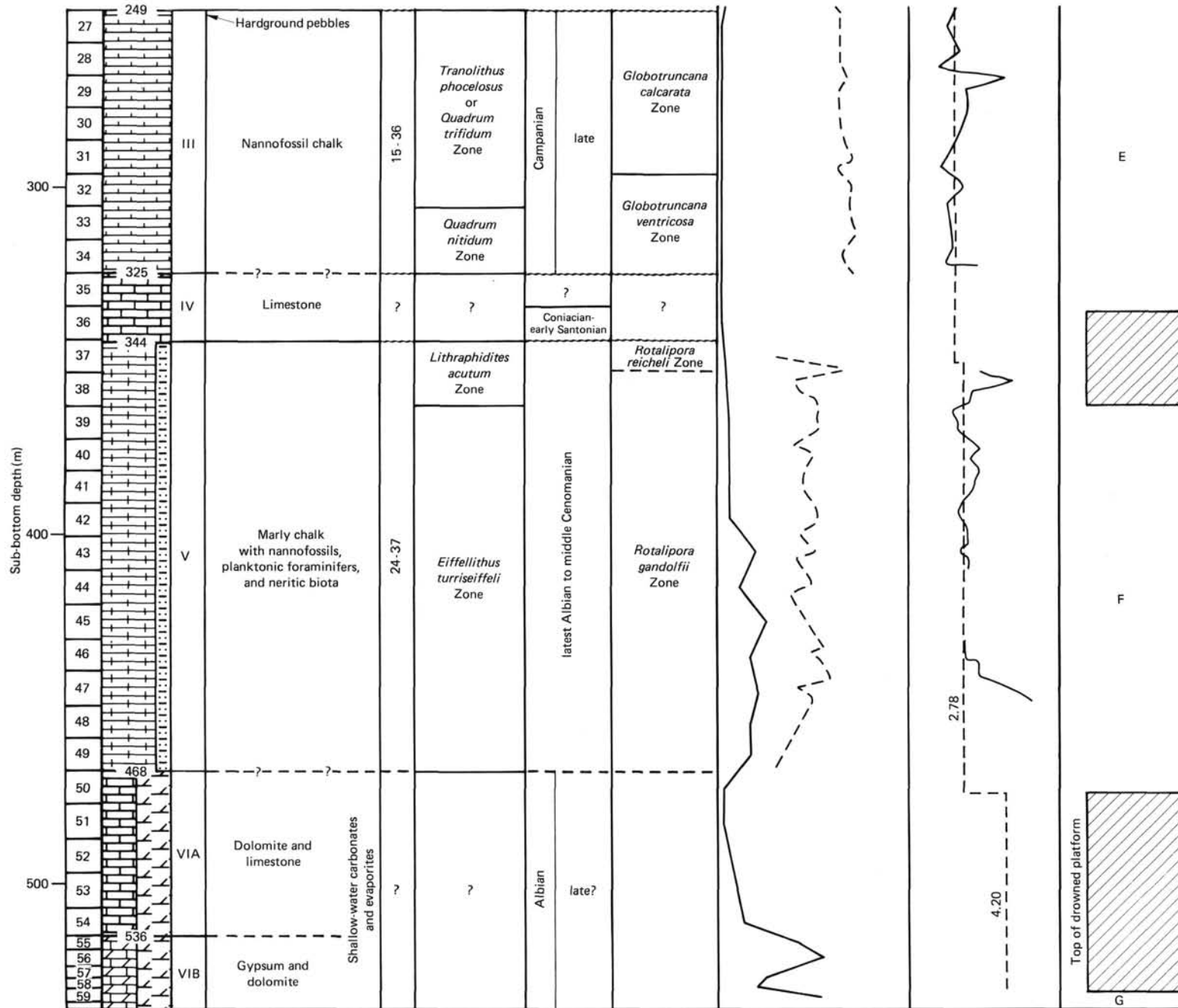


Figure 35. Summary of data for Site 627.

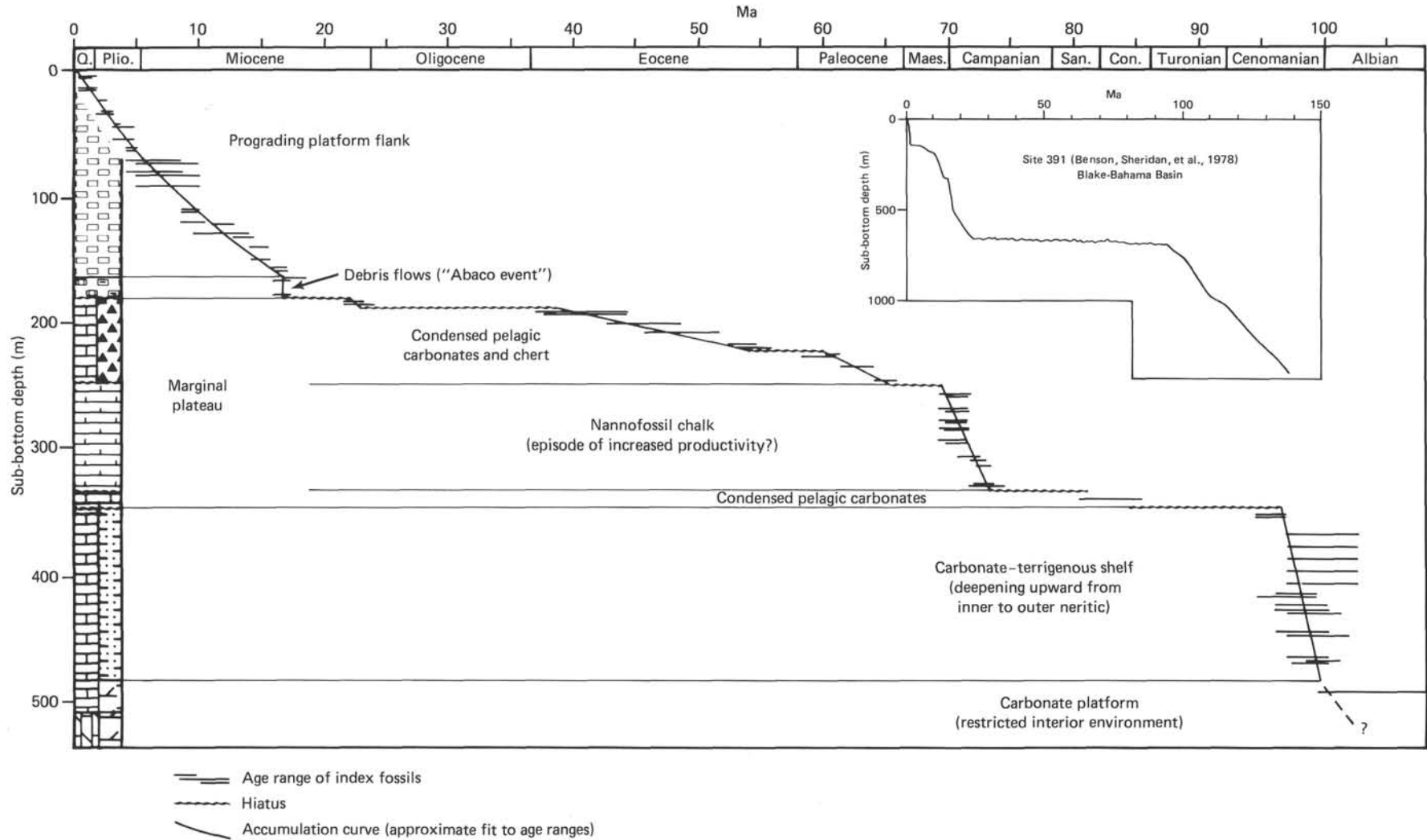
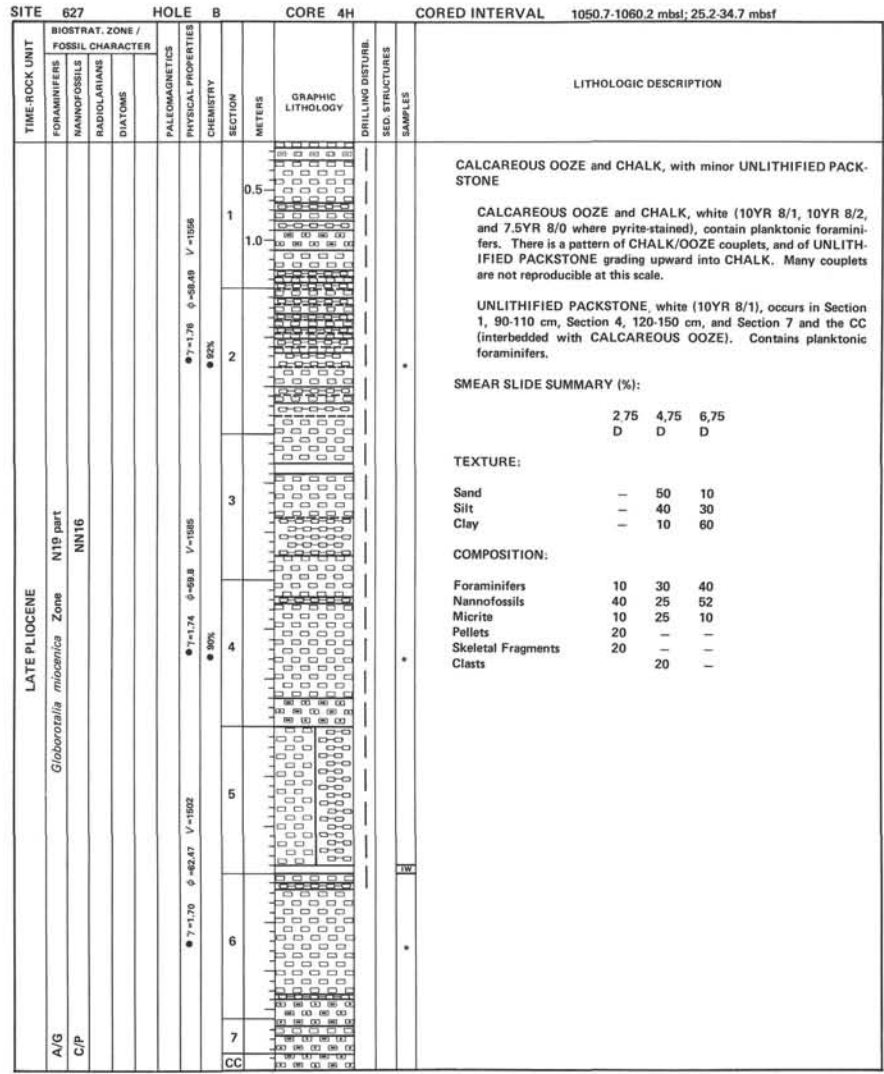
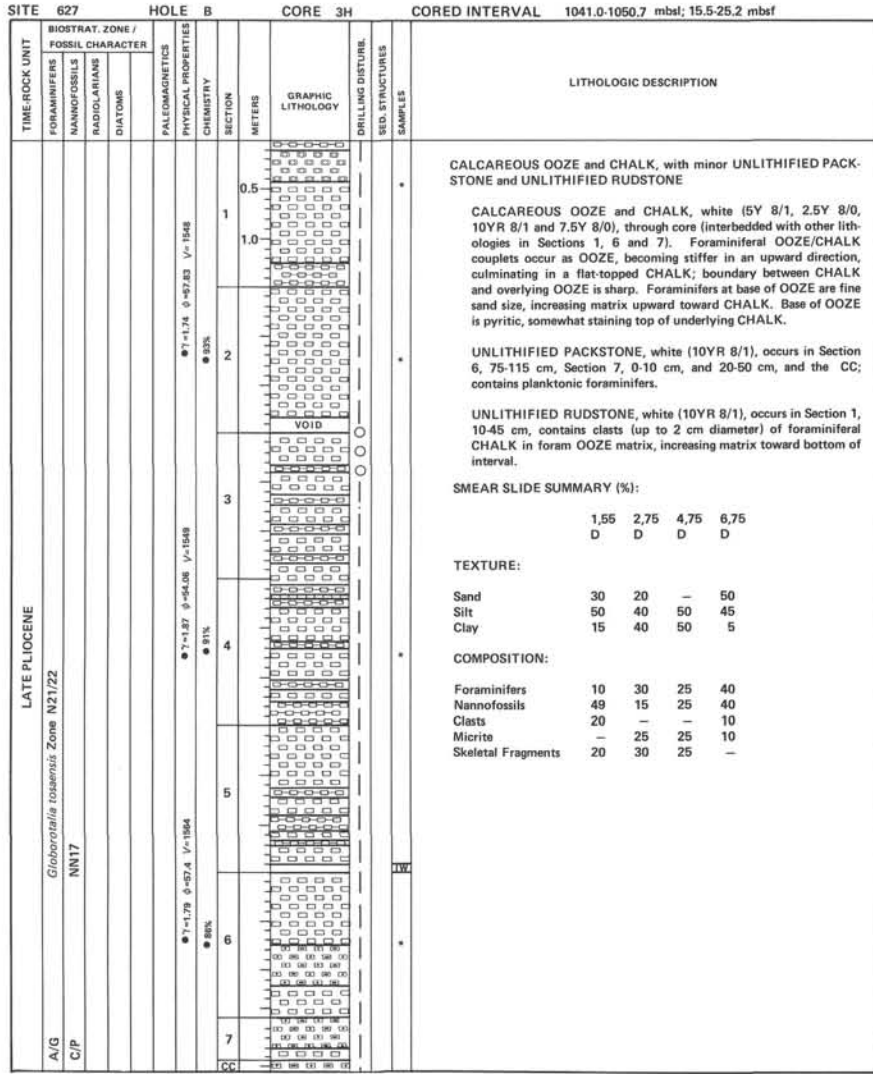
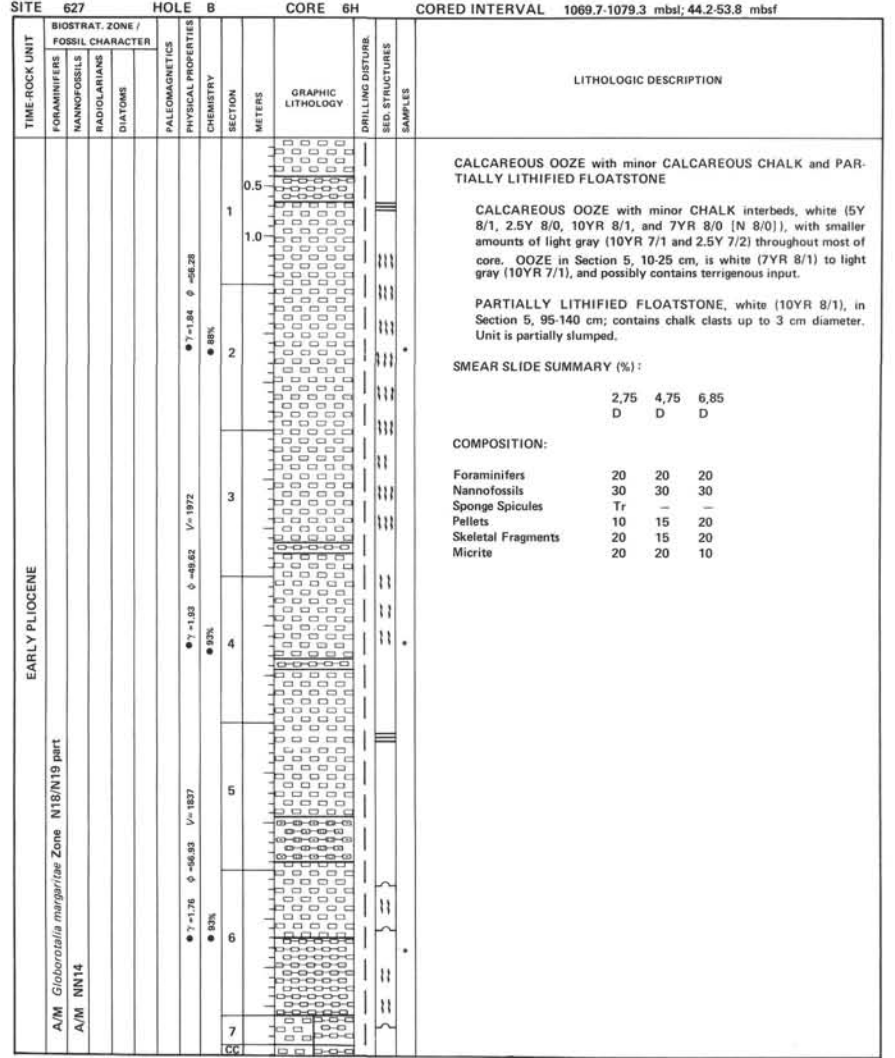
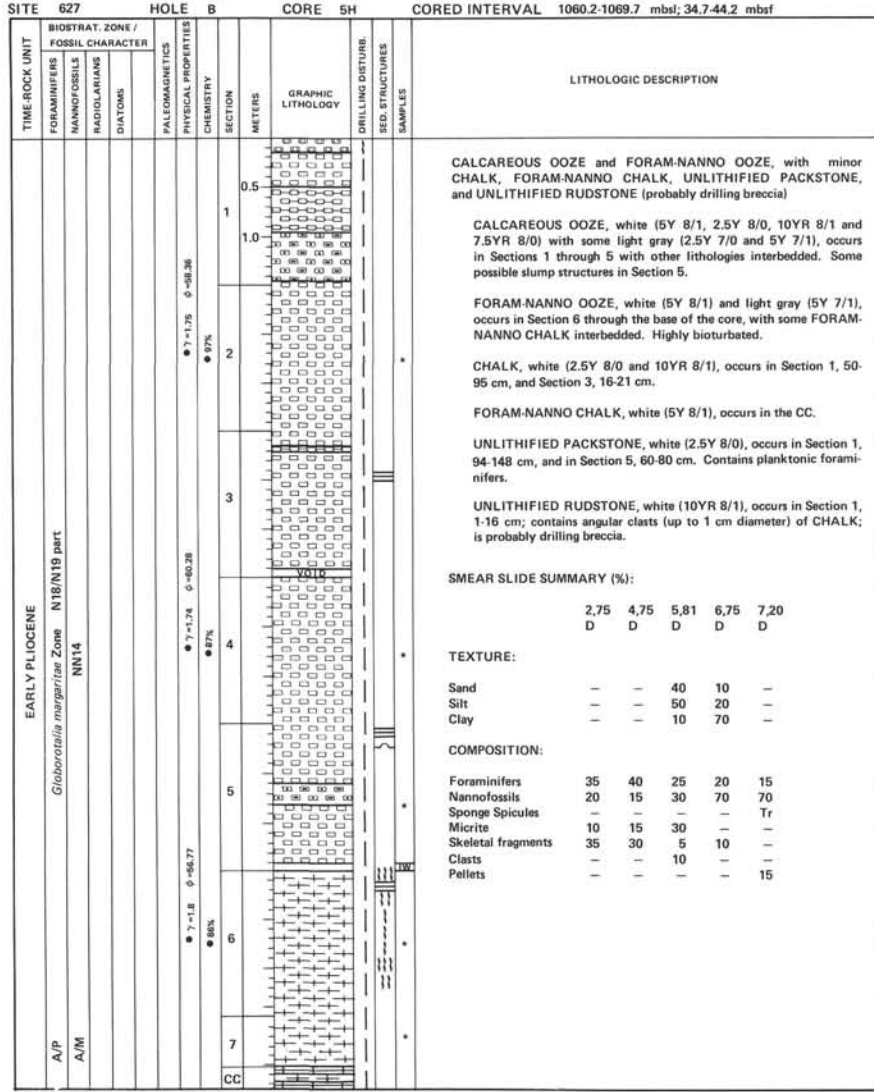
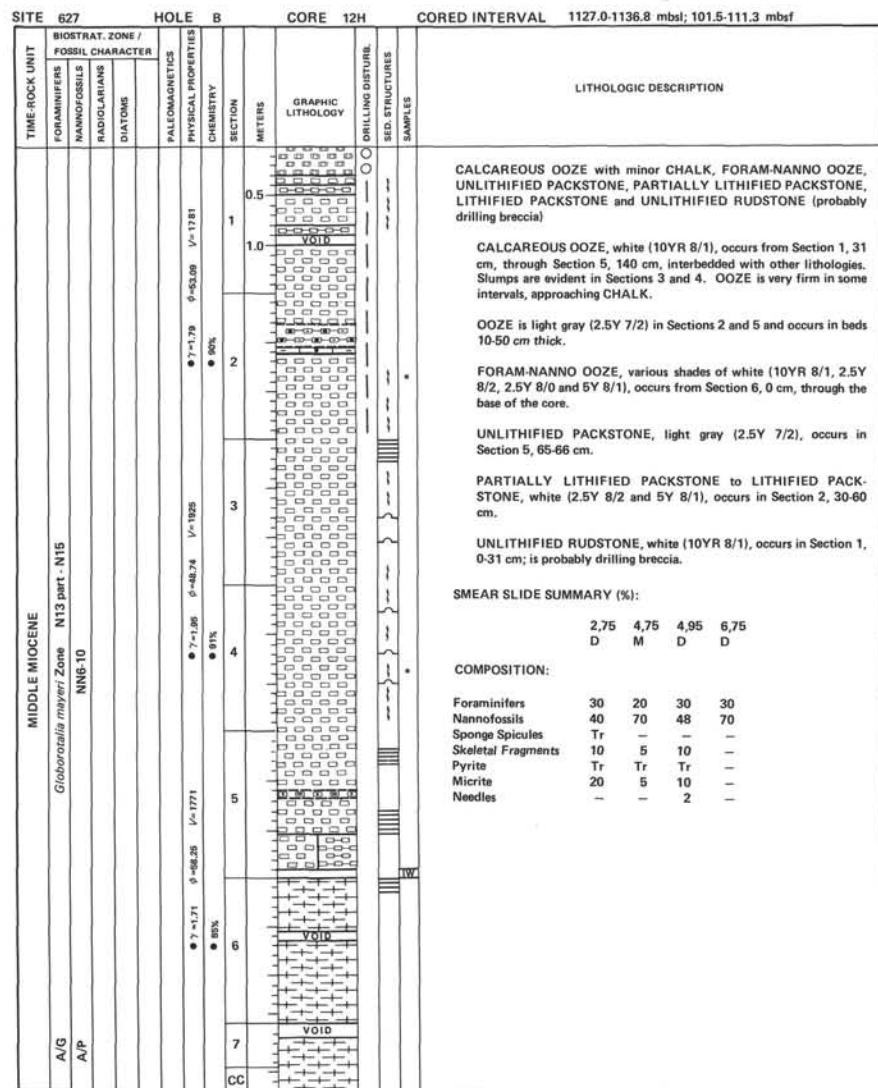
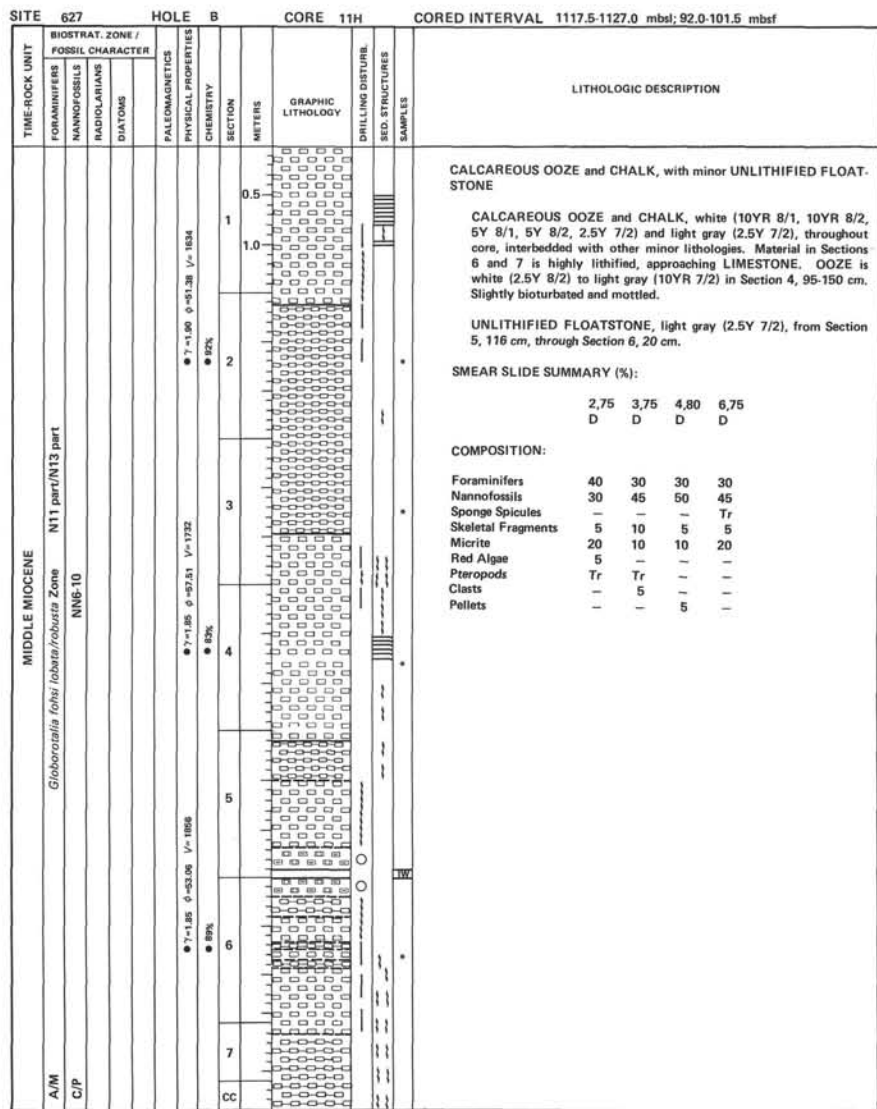


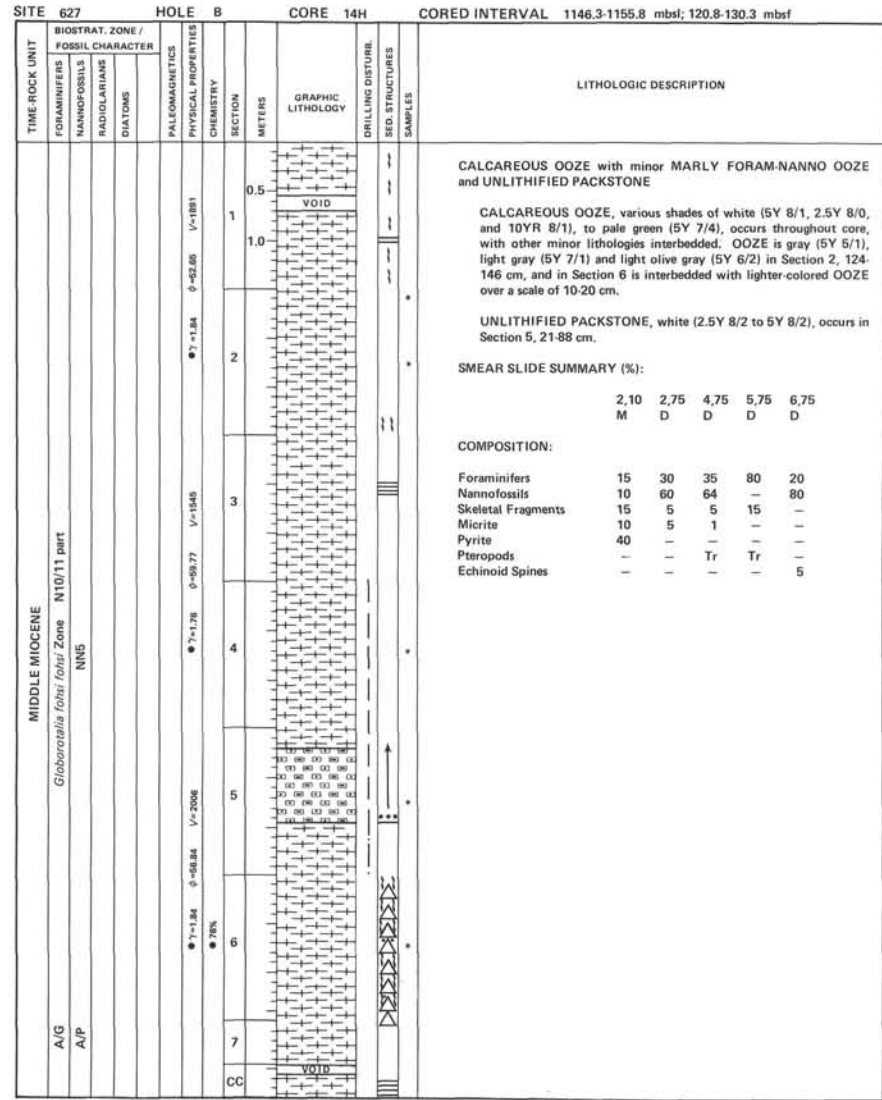
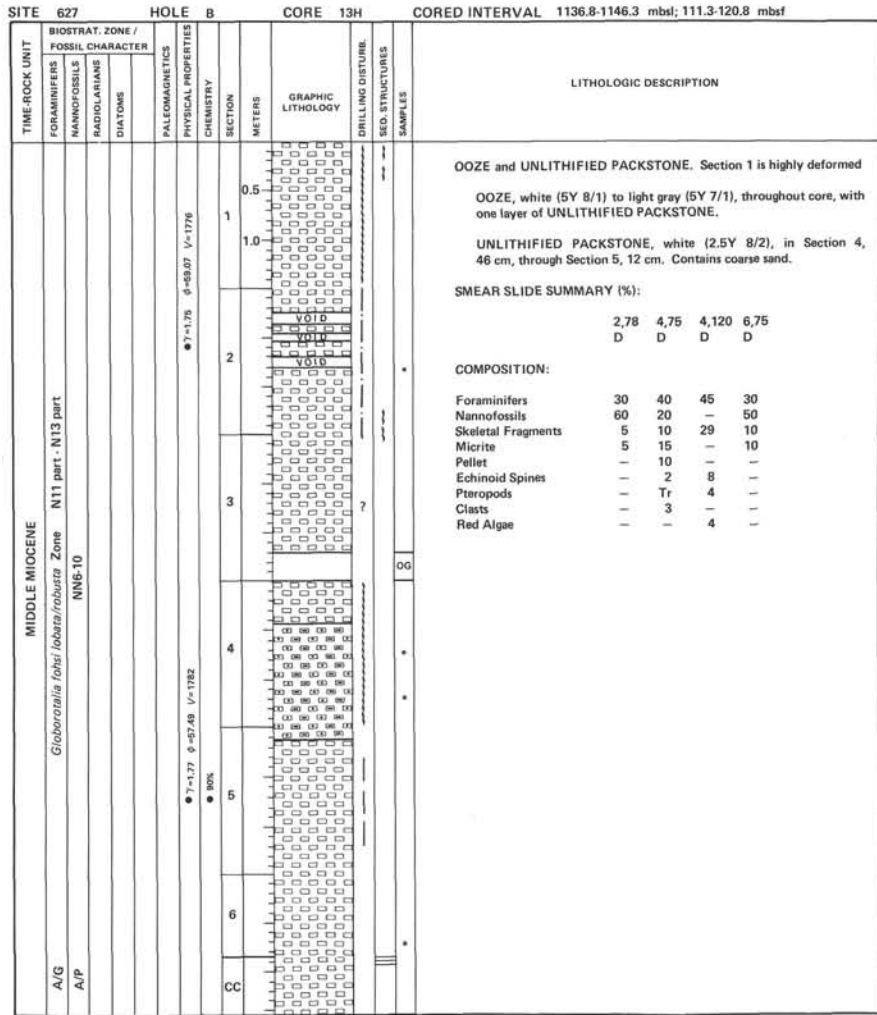
Figure 36. Age-depth curve and geologic history of Site 627, southern Blake Plateau. Note similarity to accumulation curve at Site 391 shown in inset.

TIME-ROCK UNIT	BIOSTRAT. ZONE / FOSSIL CHARACTER			PALEOMAGNETICS	PHYSICAL PROPERTIES	CHEMISTRY	SECTION	METERS	GRAPHIC LITHOLOGY	DRILLING DISTURB.	LITHOLOGIC DESCRIPTION
	FORAMINIFERS	NANNOFOSSILS	RADIOLIARIANS								
PLEISTOCENE	NN21										
	NN19										
	NN22/NN23										
	NN19										
	NN21										
	NN19										
	NN21										
	NN19										
	NN21										
	NN19										
	NN21										
	NN19										
	NN21										
	NN19										
	NN21										
	NN19										
	NN21										
	NN19										
	NN21										
	NN19										
	NN21										
	NN19										
	NN21										
	NN19										
	NN21										
	NN19										
	NN21										
	NN19										
	NN21										
	NN19										
	NN21										
	NN19										
	NN21										
	NN19										
	NN21										
	NN19										
	NN21										
	NN19										
	NN21										
	NN19										
	NN21										
	NN19										
	NN21										
	NN19										
	NN21										
	NN19										
	NN21										
	NN19										
	NN21										
	NN19										
	NN21										
	NN19										
	NN21										
	NN19										
	NN21										
	NN19										
	NN21										
	NN19										
	NN21										
	NN19										
	NN21										
	NN19										
	NN21										
	NN19										
	NN21										
	NN19										
	NN21										
	NN19										
	NN21										
	NN19										
	NN21										
	NN19										
	NN21										
	NN19										
	NN21										
	NN19										
	NN21										
	NN19										
	NN21										
	NN19										
	NN21										
	NN19										
	NN21										
	NN19										
	NN21										
	NN19										
	NN21										
	NN19										
	NN21										
	NN19										
	NN21										
	NN19										
	NN21										
	NN19										
	NN21										
	NN19										
	NN21										
	NN19										
	NN21										
	NN19										
	NN21										
	NN19										
	NN21										
	NN19										
	NN21										
	NN19										
	NN21										
	NN19										
	NN21										
	NN19										
	NN21										
	NN19										
	NN21										
	NN19										
	NN21										
	NN19										
	NN21										
	NN19										
	NN21										
	NN19										
	NN21										
	NN19										
	NN21										
	NN19										
	NN21										
	NN19										
	NN21										
	NN19										
	NN21										
	NN19										
	NN21										
	NN19										
	NN21										
	NN19										
	NN21										
	NN19										
	NN21										
	NN19										
	NN21										
	NN19										
	NN21										
	NN19										
	NN21										
	NN19										
	NN21										
	NN19										
	NN21										
	NN19										
	NN21										
	NN19										
	NN21										
	NN19										
	NN21										
	NN19										
	NN21										
	NN19										
	NN21										
	NN19										
	NN21										
	NN19										
	NN21										
	NN19										
	NN21										
	NN19										
	NN21										
	NN19										
	NN21										
	NN19										
	NN21										
	NN19										
	NN21										
	NN19										
	NN21										
	NN19										
	NN21										
	NN19										
	NN21										
	NN19										
	NN21										
	NN19										
	NN21										
	NN19										
	NN21										
	NN19										
	NN21										
	NN19										
	NN21										
	NN19										
	NN21										

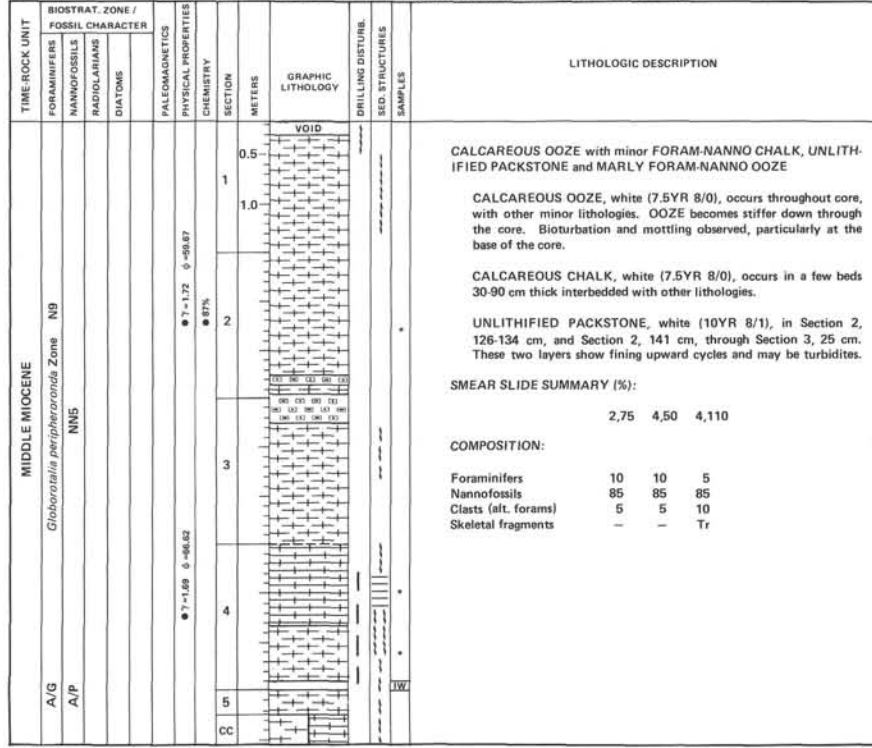




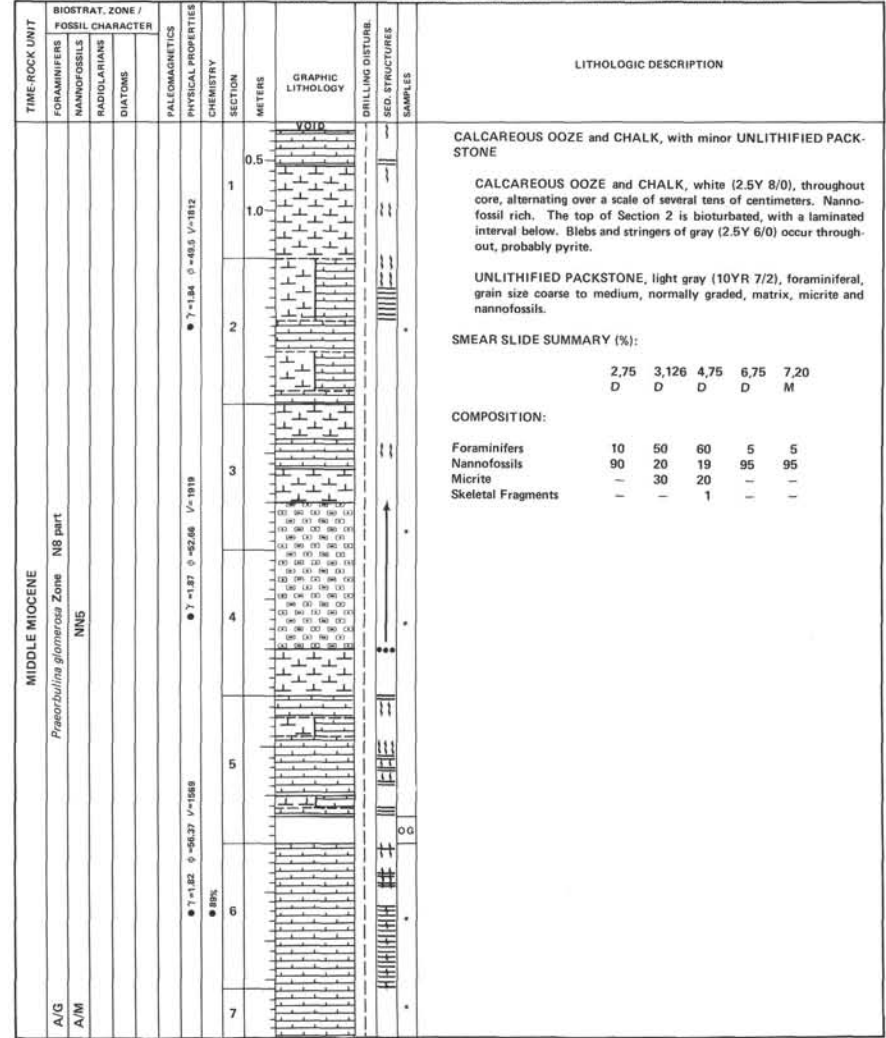




SITE 627 HOLE B CORE 15H CORED INTERVAL 1155.8-1165.4 mbsl; 130.3-139.9 mbsf



SITE 627 HOLE B CORE 16H CORED INTERVAL 1165.4-1175.2 mbsl; 139.9-149.7 mbsf



SITE 627		HOLE B		CORE 20X		CORED INTERVAL 1206.9-1216.5 mbsl; 181.4-191.0 mbsf	
TIME-ROCK UNIT	BIOSTRAT. ZONE / FOSSIL CHARACTER	PALEOMAGNETICS	PHYSICAL PROPERTIES	CHEMISTRY	SECTION	METERS	GRAPHIC LITHOLOGY
LATE EOCENE	R/M A/M ?		V=1827 $\delta = -50.84$ $\gamma = 1.83$	● 89%	1	0.5	
LITHOLOGIC DESCRIPTION							
UNLITHIFIED to LITHIFIED PACKSTONE with minor UNLITHIFIED FLOATSTONE and LIMESTONE. No CC.							
UNLITHIFIED to PARTIALLY LITHIFIED PACKSTONE, white (5Y 8/1), alternating with UNLITHIFIED FLOATSTONE from Section 1, 10-94 cm.							
LIMESTONE, white (5Y 8/1), occurs in Section 1, 0-10 cm; fine-grained, silicified, contains planktonic foraminifers.							

SITE 627		HOLE B		CORE 22X		CORED INTERVAL 1226.2-1235.7 mbsl; 200.7-210.2 mbsf	
TIME-ROCK UNIT	BIOSTRAT. ZONE / FOSSIL CHARACTER	PALEOMAGNETICS	PHYSICAL PROPERTIES	CHEMISTRY	SECTION	METERS	GRAPHIC LITHOLOGY
EARLY MIDDLE EOCENE	? A/M A/M C		V=3587 $\delta = -47.24$ $\gamma = 1.78$		1	0.5	
LITHOLOGIC DESCRIPTION							
UNLITHIFIED PACKSTONE with minor NANNOFOSSIL OOZE throughout core							
UNLITHIFIED PACKSTONE, white (10YR 8/1), in Section 1, 0-30 cm, and the CC, 10-30 cm. Coarse to very coarse grained, contains planktonic foraminifers, pteropods, clasts, and CHERT (to 0.2 cm diameter). In Section 1, 30-43 cm, a clast of SILICIFIED LIMESTONE, light gray (5Y 7/2) is present; possibly downhole contamination.							
NANNOFOSSIL OOZE, white (2.5Y 8/0), occurs as a clast in Section 1, 44-53 cm, and as a thin layer in the CC.							
SMEAR SLIDE SUMMARY (%):							
1.47 M							
COMPOSITION:							
Foraminifers 10 Nannofossils 90							

SITE 627		HOLE B		CORE 21X		CORED INTERVAL 1216.5-1226.2 mbsl; 191.0-200.7 mbsf	
TIME-ROCK UNIT	BIOSTRAT. ZONE / FOSSIL CHARACTER	PALEOMAGNETICS	PHYSICAL PROPERTIES	CHEMISTRY	SECTION	METERS	GRAPHIC LITHOLOGY
MIDDLE EOCENE	P11/12 A/M-G A/M ? C		V=1468 $\delta = -50.31$ $\gamma = 1.68$	● 7=1.74 $\delta = -50.67$ $\gamma = 1.68$	1	0.5	
LITHOLOGIC DESCRIPTION							
UNLITHIFIED PACKSTONE, CALCAREOUS OOZE, and LIMESTONE (probably drilling breccia)							
Entire core contains UNLITHIFIED PACKSTONE, white (10YR 8/1), homogenized; contains pteropods, planktonic foraminifers and some skeletal fragments. Grain size coarse to very coarse. Contains some clasts of CHALK (up to 1 cm diameter) and gray CLAY (up to 0.2 cm diameter) is present in Section 3, and larger clasts in Sections 4 and 5. Probably downhole contamination.							
CALCAREOUS OOZE, white (5Y 8/1), occurs in the CC, 14-22 cm, overlying clasts of CHERT, CHALK, and LIMESTONE; probably drilling breccia.							

SITE 627 HOLE B CORE 29X CORED INTERVAL 1293.0-1302.1 mbsl; 267.5-276.6 mbsf

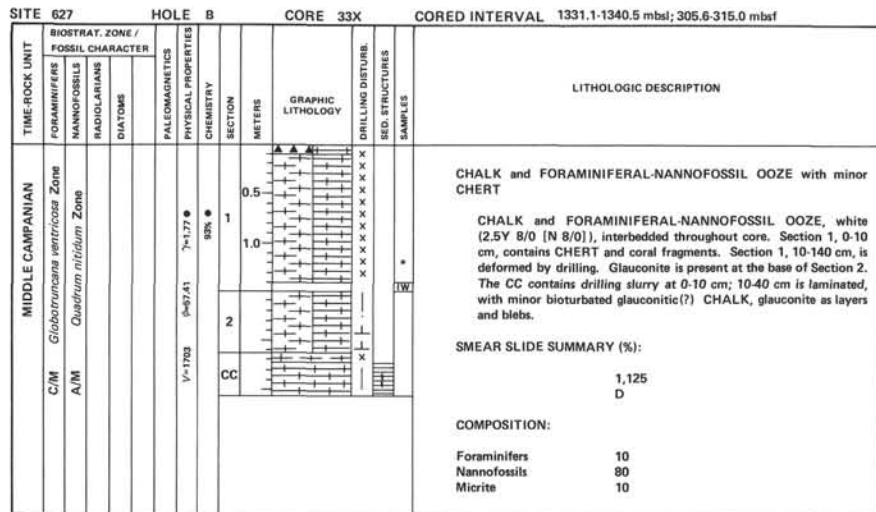
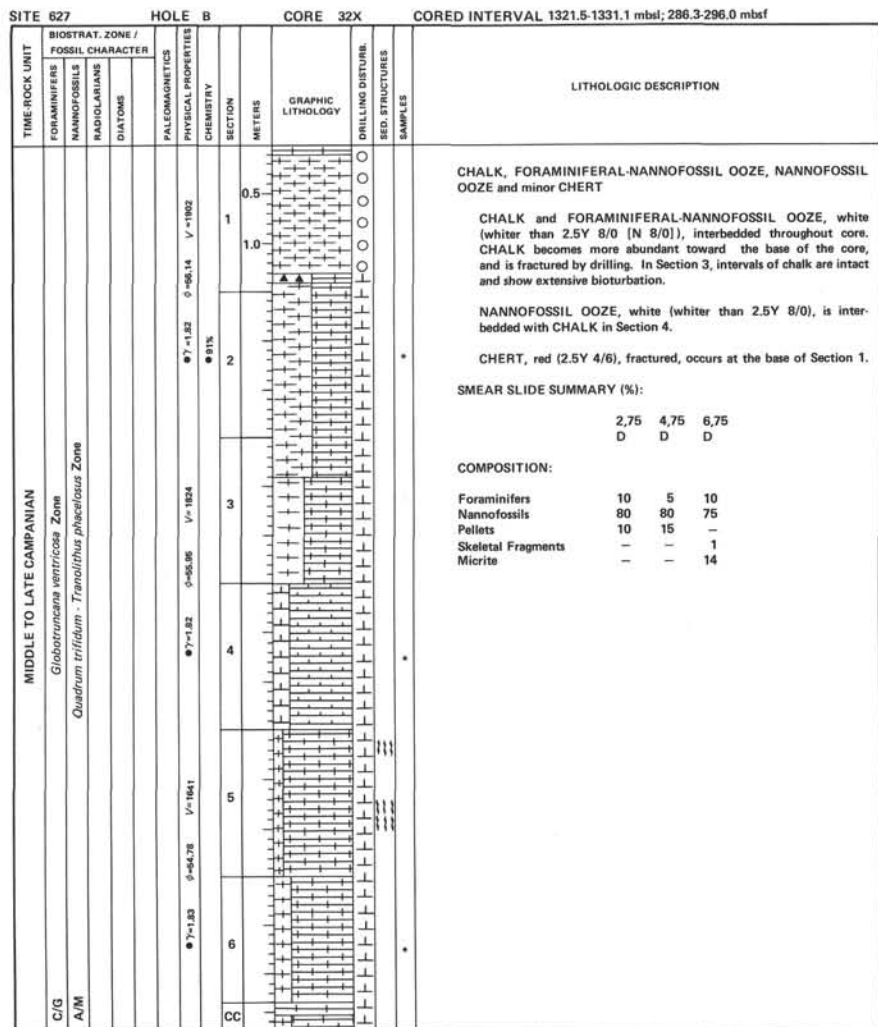
TIME ROCK UNIT	BIOSTRAT. ZONE / FOSSIL CHARACTER	PALEOMAGNETICS	PHYSICAL PROPERTIES	CHEMISTRY	SECTION	METERS	GRAPHIC LITHOLOGY	DRILLING DISTURB.	SED. STRUCTURES	SAMPLES	LITHOLOGIC DESCRIPTION																								
LATE CAMPANIAN	<i>Globotruncana calcarata</i> Zone <i>Quadrum trifidum</i> - <i>Tranolithus phaceloides</i> Zone					0.5 1.0 2 3 4 5 6 7 CC					<p>FORAM-NANNO CHALK and FORAM-NANNO OOZE</p> <p>FORAM-NANNO CHALK alternating with FORAM-NANNO OOZE, white (7.5YR 8/0) throughout core. Section 1, 13 cm, through Section 2, 150 cm, contains 75% CHALK, 25% OOZE. Color is darker where chalk is bioturbated. Section 3, 0 cm, through Section 4, 150 cm, is 50% CHALK, 50% OOZE. Section 5, 0 cm through base of core, is 66% CHALK, 33% OOZE.</p> <p>A drilling lag of CHALK and CHERT, dark reddish brown (2.5YR 3/4) is present, with chert fragments up to 5 cm diameter.</p> <p>SMEAR SLIDE SUMMARY (%):</p> <table border="1"> <tr> <td></td> <td>2,75</td> <td>4,75</td> <td>6,70</td> </tr> <tr> <td>D</td> <td>D</td> <td>D</td> <td>D</td> </tr> </table> <p>COMPOSITION:</p> <table border="1"> <tr> <td>Foraminifers</td> <td>10</td> <td>20</td> <td>10</td> </tr> <tr> <td>Nannofossils</td> <td>80</td> <td>75</td> <td>90</td> </tr> <tr> <td>Pellets</td> <td>10</td> <td>-</td> <td>-</td> </tr> <tr> <td>Micrite</td> <td>-</td> <td>5</td> <td>-</td> </tr> </table>		2,75	4,75	6,70	D	D	D	D	Foraminifers	10	20	10	Nannofossils	80	75	90	Pellets	10	-	-	Micrite	-	5	-
	2,75	4,75	6,70																																
D	D	D	D																																
Foraminifers	10	20	10																																
Nannofossils	80	75	90																																
Pellets	10	-	-																																
Micrite	-	5	-																																

SITE 627 HOLE B CORE 30X CORED INTERVAL 1302.1-1311.8 mbsl; 276.6-286.3 mbsf

TIME ROCK UNIT	BIOSTRAT. ZONE / FOSSIL CHARACTER	PALEOMAGNETICS	PHYSICAL PROPERTIES	CHEMISTRY	SECTION	METERS	GRAPHIC LITHOLOGY	DRILLING DISTURB.	SED. STRUCTURES	SAMPLES	LITHOLOGIC DESCRIPTION								
LATE CAMPANIAN	<i>Globotruncana calcarata</i> Zone <i>Quadrum trifidum</i> - <i>Tranolithus phaceloides</i> Zone					0.5 1 2 3 4 CC					<p>FORAM-NANNO CHALK and FORAM-NANNO OOZE with very minor LIMESTONE (probably downhole contamination)</p> <p>FORAM-NANNO CHALK and FORAM-NANNO OOZE, white (7.5YR 8/0) although chalky part may be darker, occur throughout core in alternating couplets approximately 5 cm thick. CHALK may be "drilling biscuits" with a "drilling paste" of OOZE in between. Top of CHALK is sharp, lower contact gradational with OOZE. In Section 3, 60 cm through the base of the core, broken fragments of CHALK are surrounded by OOZE.</p> <p>LIMESTONE, very pale brown (10YR 5/3), occurs as a single rounded pebble in Section 1, 0-2 cm; partially silicified. Probably is downhole contamination.</p> <p>SMEAR SLIDE SUMMARY (%):</p> <table border="1"> <tr> <td></td> <td>2,76</td> </tr> <tr> <td>D</td> <td>D</td> </tr> </table> <p>COMPOSITION:</p> <table border="1"> <tr> <td>Foraminifers</td> <td>10</td> </tr> <tr> <td>Nannofossils</td> <td>90</td> </tr> </table>		2,76	D	D	Foraminifers	10	Nannofossils	90
	2,76																		
D	D																		
Foraminifers	10																		
Nannofossils	90																		

SITE 627 HOLE B CORE 31X CORED INTERVAL 1311.8-1321.5 mbsl; 276.6-286.3 mbsf

TIME ROCK UNIT	BIOSTRAT. ZONE / FOSSIL CHARACTER	PALEOMAGNETICS	PHYSICAL PROPERTIES	CHEMISTRY	SECTION	METERS	GRAPHIC LITHOLOGY	DRILLING DISTURB.	SED. STRUCTURES	SAMPLES	LITHOLOGIC DESCRIPTION												
LATE CAMPANIAN	<i>Globotruncana calcarata</i> Zone <i>Quadrum trifidum</i> - <i>Tranolithus phaceloides</i> Zone					0.5 1 2 3 4 CC					<p>CHALK and FORAMINIFERAL-NANNOFOSSIL OOZE</p> <p>CHALK and FORAMINIFERAL-NANNOFOSSIL OOZE, white (2.5Y 8/0 [N 8/0]), alternating throughout core. CHALK becomes more prevalent toward base of core, and is fractured by drilling. In the few undisturbed intervals there is extensive bioturbation. Some fractured CHERT was recovered at the base of Section 3.</p> <p>SMEAR SLIDE SUMMARY (%):</p> <table border="1"> <tr> <td></td> <td>2,75</td> <td>4,75</td> </tr> <tr> <td>D</td> <td>D</td> <td>D</td> </tr> </table> <p>COMPOSITION:</p> <table border="1"> <tr> <td>Foraminifers</td> <td>10</td> <td>10</td> </tr> <tr> <td>Nannofossils</td> <td>90</td> <td>90</td> </tr> </table>		2,75	4,75	D	D	D	Foraminifers	10	10	Nannofossils	90	90
	2,75	4,75																					
D	D	D																					
Foraminifers	10	10																					
Nannofossils	90	90																					



SITE 627		HOLE B		CORE 37X		CORED INTERVAL 1369.4-1379.0 mbsl; 343.9-353.5 mbsf	
TIME-ROCK UNIT	BIOSTRAT. ZONE / FOSSIL CHARACTER	SECTION	METERS	GRAPHIC LITHOLOGY	DRILLING DISTURB.	SED. STRUCTURES	SAMPLES
MIDDLE CENOMANIAN		1	0.5				
FORAMINIFERS							
NANNOFOSSILS							
RADIOLARIANS							
DIATOMS							
PALEOMAGNETICS							
PHYSICAL PROPERTIES							
CHEMISTRY							
R/I/M							
C/M							

LITHOLOGIC DESCRIPTION

CHALK with minor CLAY

CHALK, light gray (5Y 7/1), occurs throughout core. Contains downhole contamination including fragments of hardground, foraminiferal PACKSTONE and CHERT, and loose burrow fillings of marcasite, pyrite, crystalline, 0.3-0.6 cm diameter. A plant fragment occurs in Section 1, 37 cm. CHALK is light gray (5Y 7/1) in the CC, 20-35 cm, possibly reflecting higher clay content.

SMEAR SLIDE SUMMARY (%):

Clay	15
Calcite/Dolomite	35
Foraminifers	10
Nannofossils	20
Micrite	10
Clasts	10
Pyrite	Tr

COMPOSITION:

Clay	15
Calcite/Dolomite	35
Foraminifers	10
Nannofossils	20
Micrite	10
Clasts	10
Pyrite	Tr

SITE 627		HOLE B		CORE 38X		CORED INTERVAL 1379.0-1388.6 mbsl; 353.5-363.1 mbsf	
TIME-ROCK UNIT	BIOSTRAT. ZONE / FOSSIL CHARACTER	SECTION	METERS	GRAPHIC LITHOLOGY	DRILLING DISTURB.	SED. STRUCTURES	SAMPLES
MIDDLE CENOMANIAN		1	0.5				
FORAMINIFERS							
NANNOFOSSILS							
RADIOLARIANS							
DIATOMS							
PALEOMAGNETICS							
PHYSICAL PROPERTIES							
CHEMISTRY							
R/I/P							
C/M							

LITHOLOGIC DESCRIPTION

CHALK and MARLY CHALK with minor MUDDY CALCAREOUS SILTSTONE and intraformational CONGLOMERATE, moderately brecciated by drilling

CHALK and MARLY CHALK, dominant colors mottled olive gray (5Y 5/2 and 5Y 4/2) throughout core. Alternating un lithified and lithified layers occur in Section 1, 0-85 cm; flaser bedding and numerous burrows are present. Oyster and bivalve shells and shell fragments present. Pyritized burrow in Section 4, 140 cm, truncated under-surface. Increased MUD content from top of Section 5 through Section 6, 70 cm, and in the CC; becomes MARLY CHALK at the top of Section 5.

CALCAREOUS SILTSTONE, olive gray (5Y 5/2), in Section 5, 78-97 cm.

Intraformational CONGLOMERATE, olive gray (5Y 5/2), mud-supported, in Section 6, 62 cm.

SMEAR SLIDE SUMMARY (%):

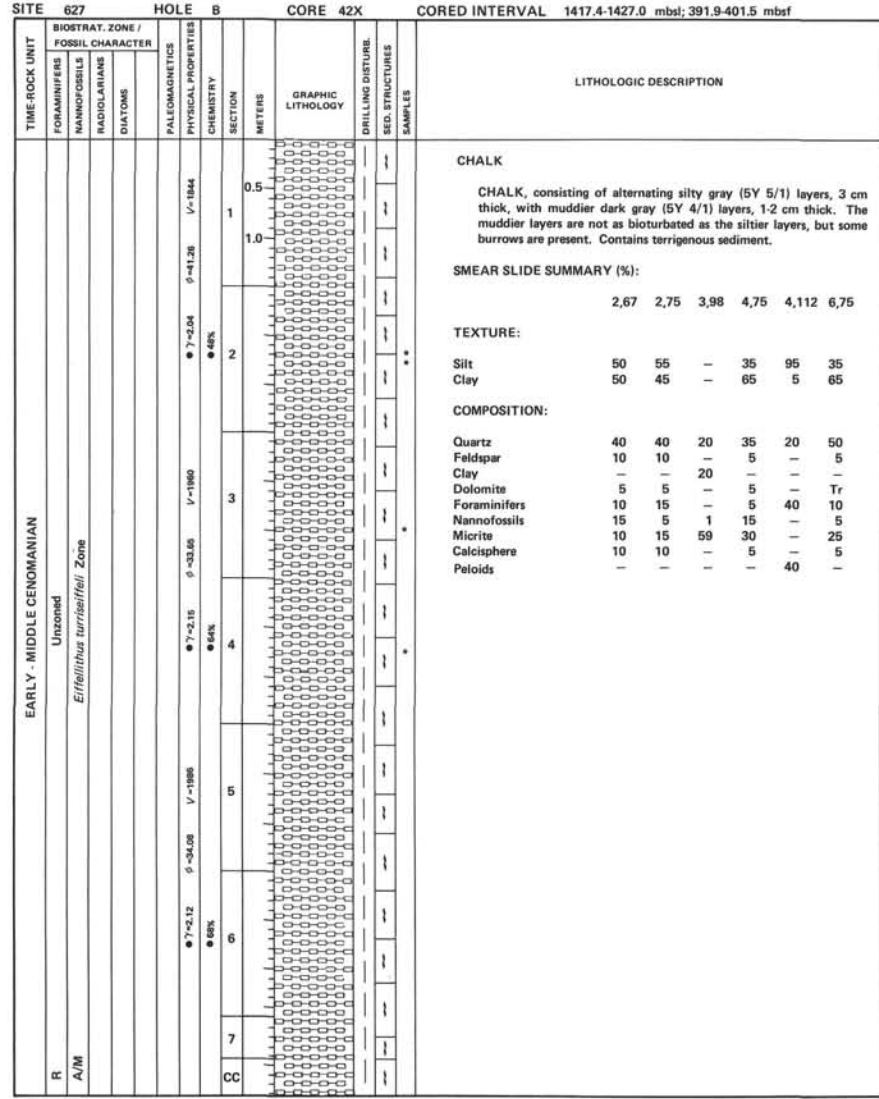
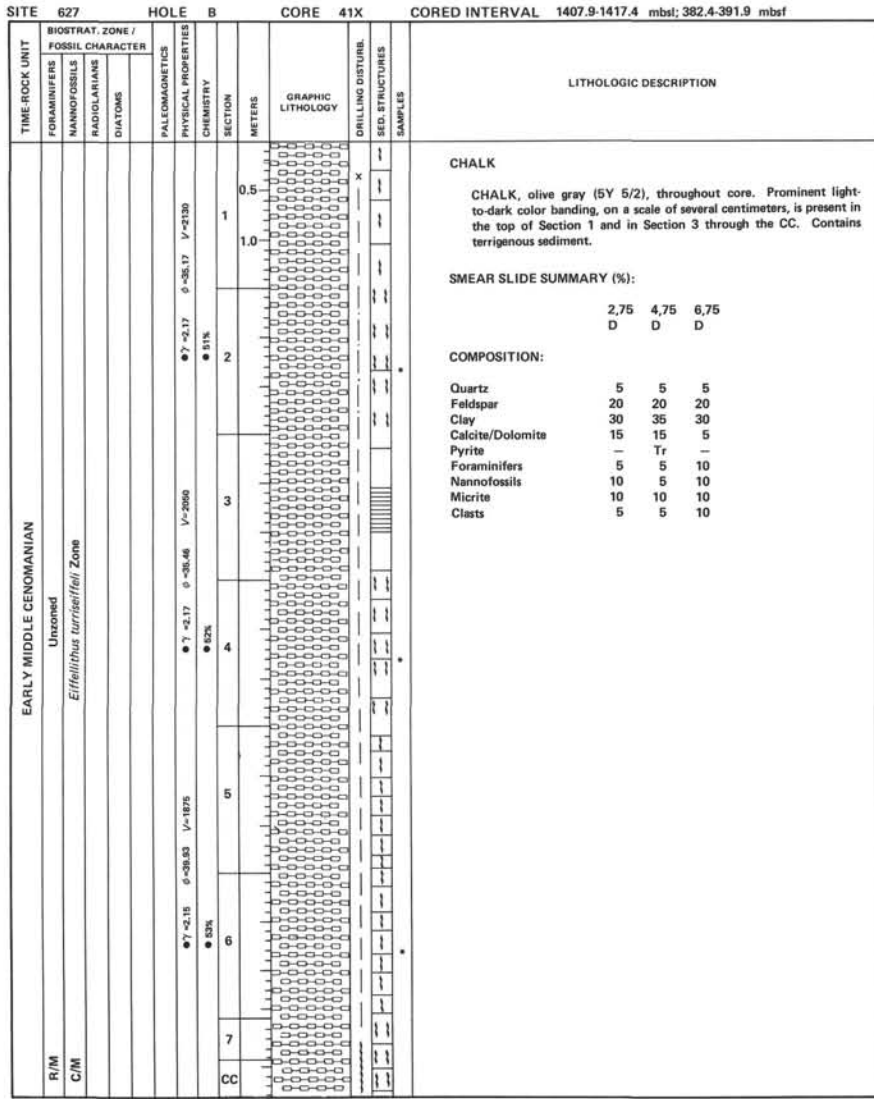
Clay	2.75	4.75	6.75
D	D	D	D

TEXTURE:

Sand	20	10	-
Silt	60	70	-
Clay	20	20	-

COMPOSITION:

Quartz	40	30	20
Feldspar	-	-	10
Clay	20	20	29
Calcite/Dolomite	-	-	1
Accessory Minerals:			
Biotite	-	-	Tr
Pyrite	-	-	Tr
Foraminifers	10	10	10
Nannofossils	10	15	10
Micrite	10	10	10
Clasts	10	15	10



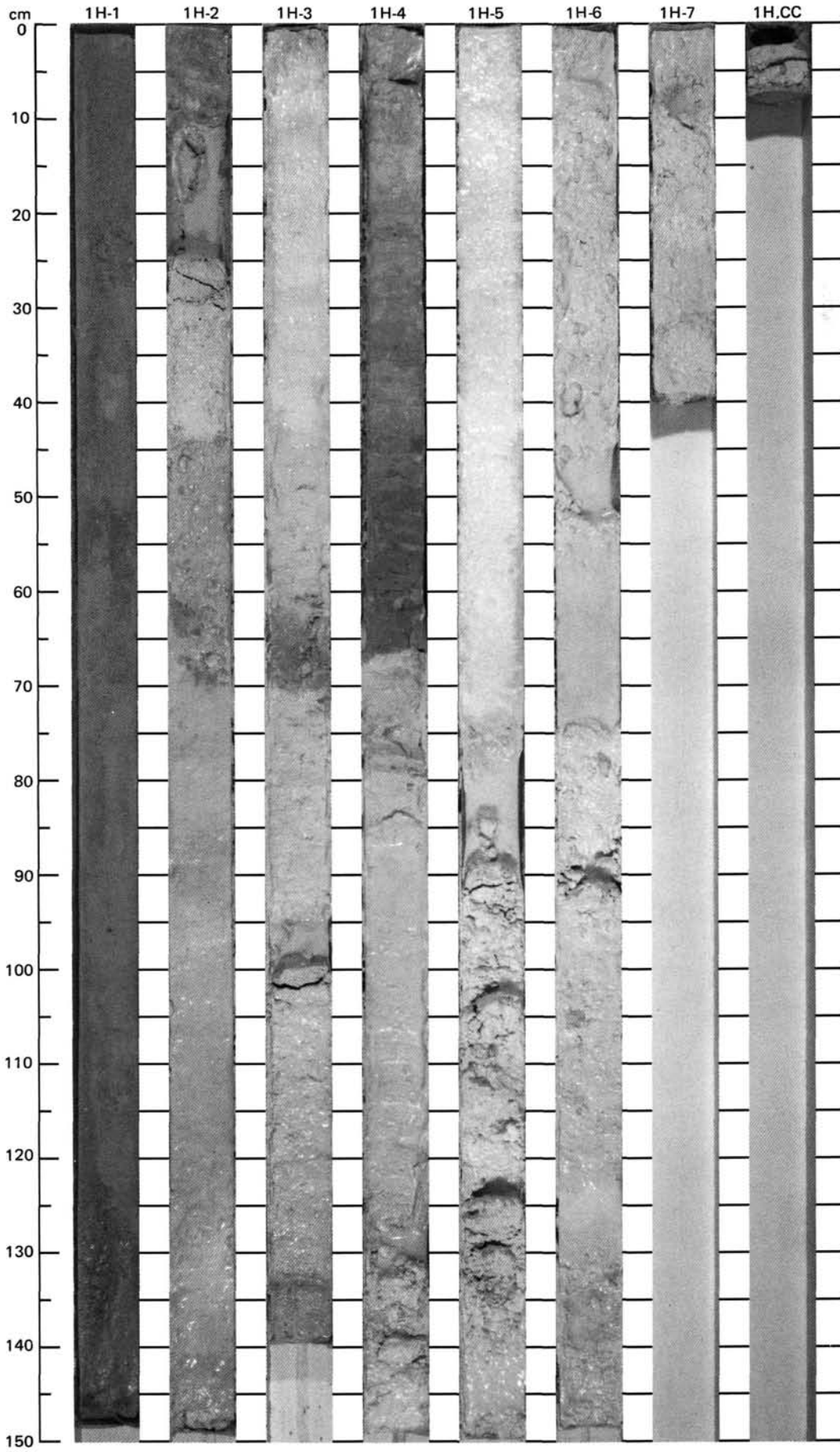
SITE 627		HOLE B		CORE 56X		CORED INTERVAL 1544.7-1549.7 mbsl; 519.2-524.2 mbsf	
TIME-ROCK UNIT	BIOSTRAT. ZONE / FOSSIL CHARACTER	PALEOMAGNETICS	PHYSICAL PROPERTIES	SECTION	METERS	GRAPHIC LITHOLOGY	DRILLING DISTURB. / SED. STRUCTURES / SAMPLES
	FORAMINIFERS MAMMOFOSILS RADIOLARIANS DIATOMS						
	BARREN		V-5400	1 CC	0.5		
<p>LITHOLOGIC DESCRIPTION</p> <p>GYPSUM and DOLOSTONE</p> <p>GYPSUM, very dark grayish brown (10YR 3/2) to translucent, in Section 1, 16-42 cm. Traces of organic matter define secondary nodule margins in Section 1, 16-26 cm. In Section 1, 26-42 cm, a mixture of early phase gypsum (small nodules, 1-2 cm diameter, organic inclusion-rich) and second phase gypsum (larger nodules, up to 6 cm diameter, inclusion-free, replacive margins). Mosaic ("chicken wire") fabric occurs in the CC, 0-21 cm.</p> <p>DOLOSTONE, light grayish-brown (2.5Y 6/2), occurs in Section 1, 0-11 cm, as a breccia of clasts (up to 5 cm diameter), possibly down-hole contamination. DOLOSTONE in Section 1, 11-16 cm, is mottled, compact dolomite with possible hydrocarbon stain and odor. DOLOSTONE in CC, 21-55 cm, is mottled, possibly moldic porosity or bioturbation.</p> <p>SMEAR SLIDE SUMMARY (%):</p> <p style="text-align: right;">1,10 D</p> <p>COMPOSITION:</p> <p>Dolomite 100 Gypsum Tr</p>							

SITE 627		HOLE B		CORE 57X		CORED INTERVAL 1549.7-1553.3 mbsl; 524.2-527.8 mbsf	
TIME-ROCK UNIT	BIOSTRAT. ZONE / FOSSIL CHARACTER	PALEOMAGNETICS	PHYSICAL PROPERTIES	SECTION	METERS	GRAPHIC LITHOLOGY	DRILLING DISTURB. / SED. STRUCTURES / SAMPLES
	FORAMINIFERS MAMMOFOSILS RADIOLARIANS DIATOMS LARGER BENTH. FORAM.						
	LATE ALBIAN BARREN F			1 CC	0.5 1.0		
<p>LITHOLOGIC DESCRIPTION</p> <p>GYPSUM and DOLOSTONE</p> <p>GYPSUM, very dark brown (10YR 2/2) to translucent, occurs in Section 1, 19-61 cm, and in the CC. Organic inclusions occur throughout, and traces of DOLOMITE are present between mosaics.</p> <p>DOLOSTONE, gray to light gray (10YR 5/1 to 10YR 7/1), with fossils, white (10YR 8/2), occurs in Section 1, 0-19 cm and 61-70 cm; is fine-grained, bioturbated with some moldic porosity. Organic stains occur in Section 1, 19 cm, and in the CC. The interval in Section 1, 61-70 cm, may be a partial dolomite.</p> <p>SMEAR SLIDE SUMMARY (%):</p> <p style="text-align: right;">1,25 D</p> <p>COMPOSITION</p> <p>Gypsum 100</p>							

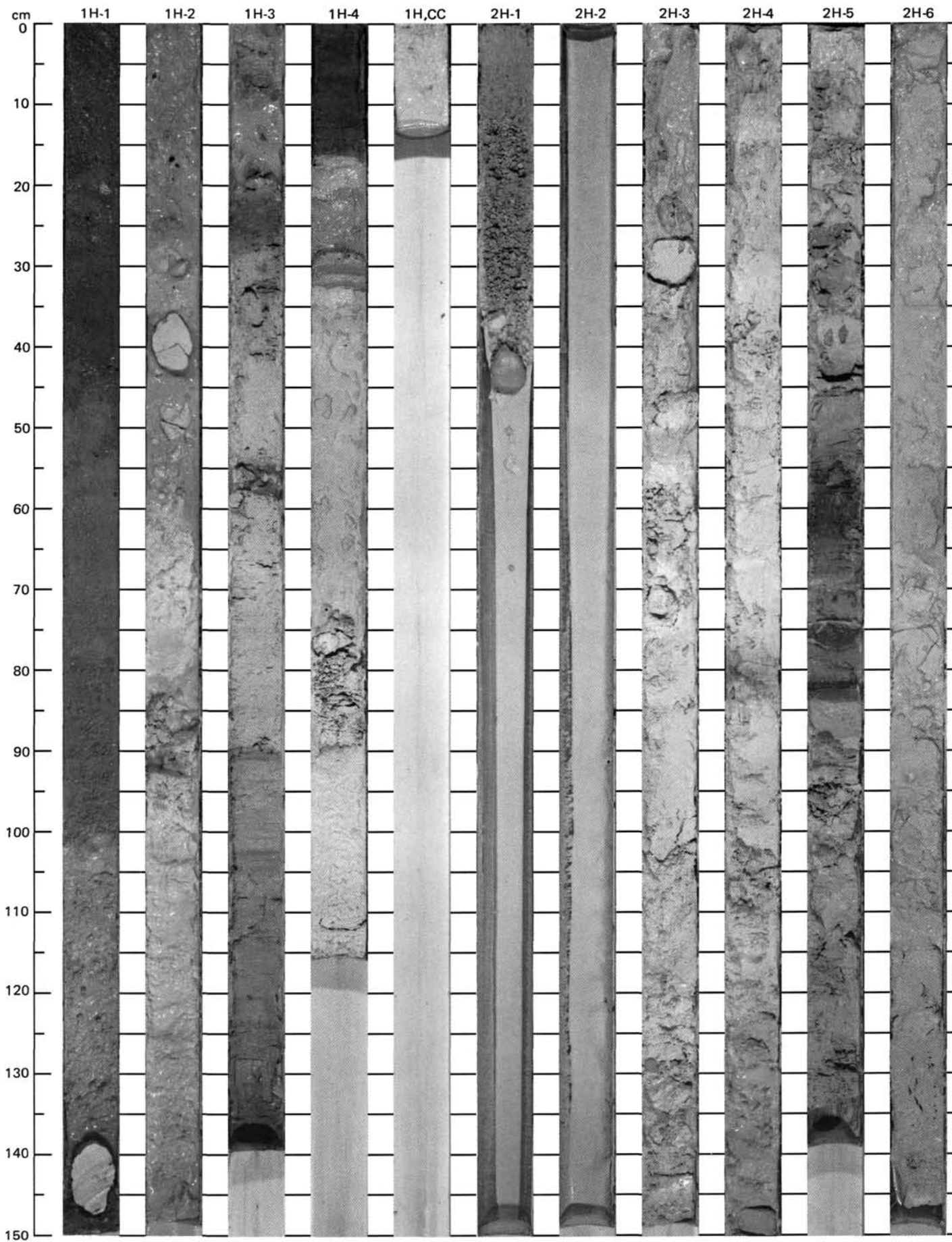
SITE 627		HOLE B		CORE 58X		CORED INTERVAL 1553.3-1556.1 mbsl; 527.8-530.6 mbsf	
TIME-ROCK UNIT	BIOSTRAT. ZONE / FOSSIL CHARACTER	PALEOMAGNETICS	PHYSICAL PROPERTIES	SECTION	METERS	GRAPHIC LITHOLOGY	DRILLING DISTURB. / SED. STRUCTURES / SAMPLES
	FORAMINIFERS MAMMOFOSILS RADIOLARIANS DIATOMS						
				CC			
<p>LITHOLOGIC DESCRIPTION</p> <p>GYPSUM and minor DOLOSTONE</p> <p>GYPSUM, gray to very dark gray (10YR 5/1 to 10YR 3/1), massive, crystalline, organic rich, with mosaic fabric, occurs as fragments in Section 1 and the CC. Strong hydrocarbon/hydrogen sulfide odors detected.</p> <p>DOLOSTONE, light brownish gray (2.5Y 6/2), present in the CC, 17-36 cm, as small piece fragments in drilling breccia.</p>							

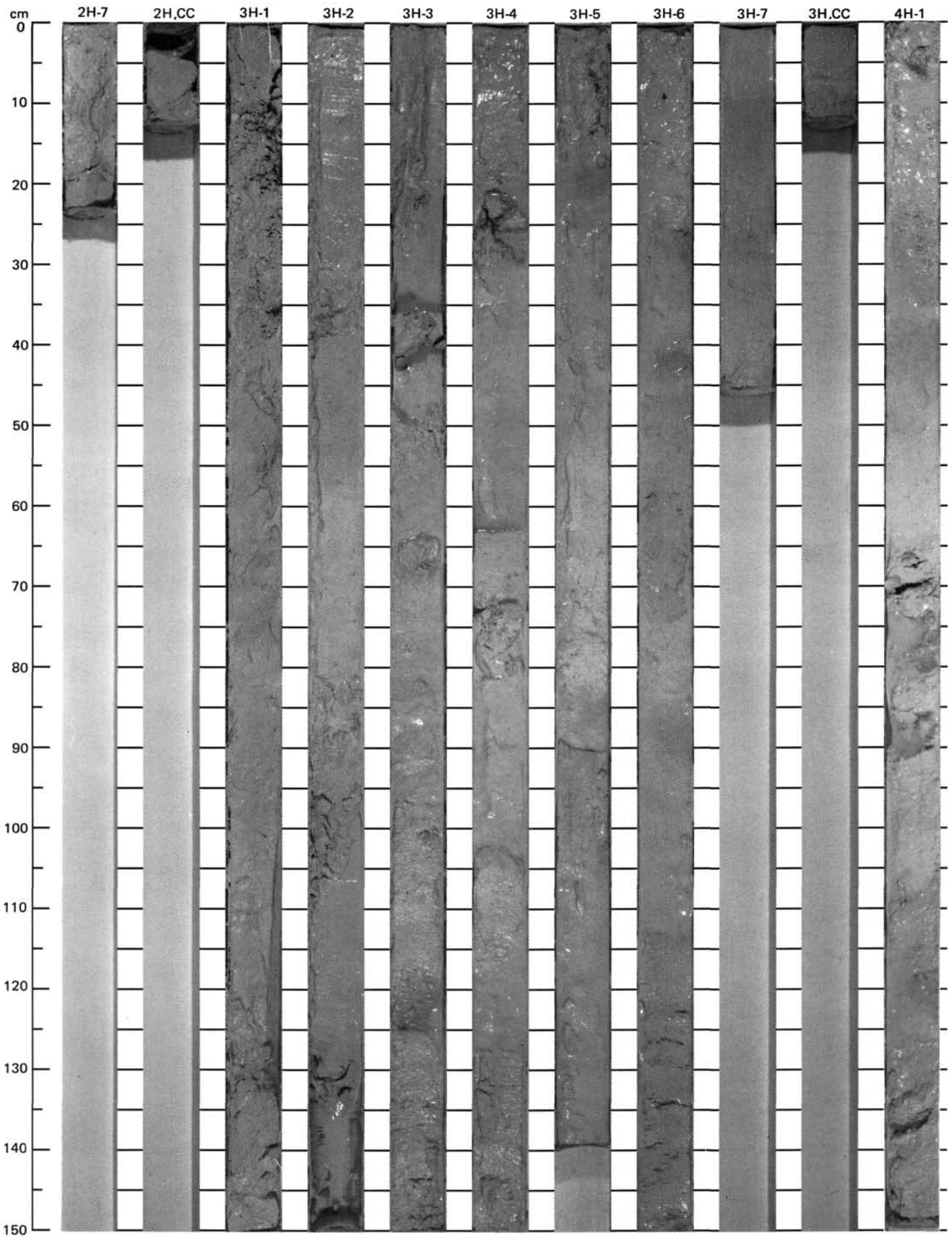
SITE 627		HOLE B		CORE 59X		CORED INTERVAL 1556.1-1559.3 mbsl; 530.6-533.8 mbsf	
TIME-ROCK UNIT	BIOSTRAT. ZONE / FOSSIL CHARACTER	PALEOMAGNETICS	PHYSICAL PROPERTIES	SECTION	METERS	GRAPHIC LITHOLOGY	DRILLING DISTURB. / SED. STRUCTURES / SAMPLES
	FORAMINIFERS MAMMOFOSILS RADIOLARIANS DIATOMS						
	BARREN		V-4850	1 CC	0.5		
<p>LITHOLOGIC DESCRIPTION</p> <p>GYPSUM and minor DOLOSTONE</p> <p>GYPSUM, dark grayish brown (2.5Y 4/2) to translucent, occurs both as massive GYPSUM and laminated with DOLOSTONE. Hydrocarbon odor detected.</p> <p>DOLOSTONE, brown (2.5Y 3/0), occurs in the CC as pieces of drilling breccia. Some moldic porosity present.</p>							

SITE 627		HOLE B		CORE 60X		CORED INTERVAL 1559.3-1561.3 mbsl; 533.8-535.8 mbsf	
TIME-ROCK UNIT	BIOSTRAT. ZONE / FOSSIL CHARACTER	PALEOMAGNETICS	PHYSICAL PROPERTIES	SECTION	METERS	GRAPHIC LITHOLOGY	DRILLING DISTURB. / SED. STRUCTURES / SAMPLES
	FORAMINIFERS MAMMOFOSILS RADIOLARIANS DIATOMS						
				1 CC			
<p>LITHOLOGIC DESCRIPTION</p> <p>GYPSUM and DOLOSTONE</p> <p>GYPSUM, light brownish gray (2.5Y 6/2), occurs in Section 1, 0-35 cm, and in the CC, 4-17 cm, with organic matter inclusions and stringers of DOLOMITE, in Section 1, 35-51 cm, clasts of DOLOMITE with inclusions of GYPSUM present; some shell molds occur. Material in the CC is brecciated, and gypsum pieces are white-coated due to drilling disturbance.</p>							

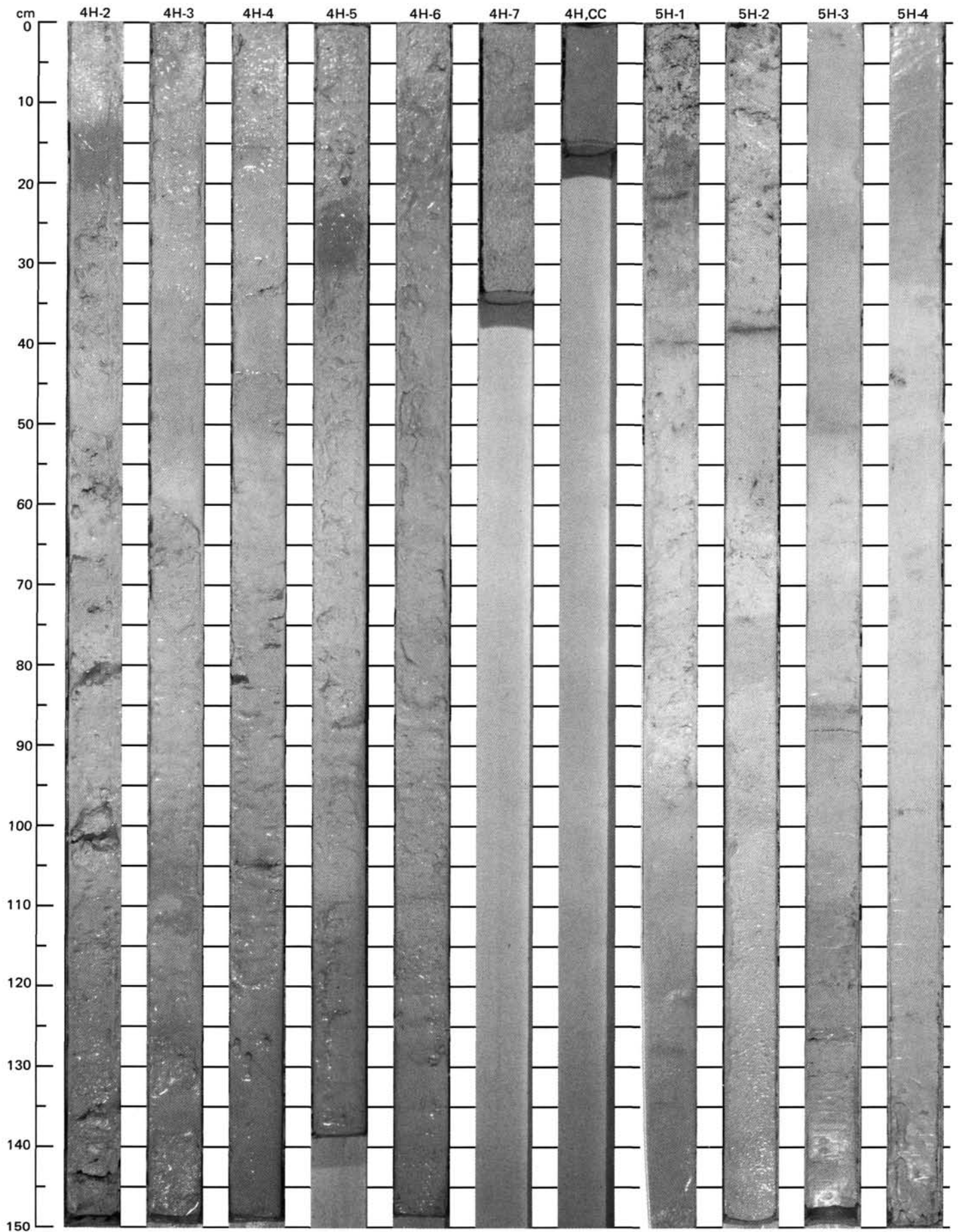


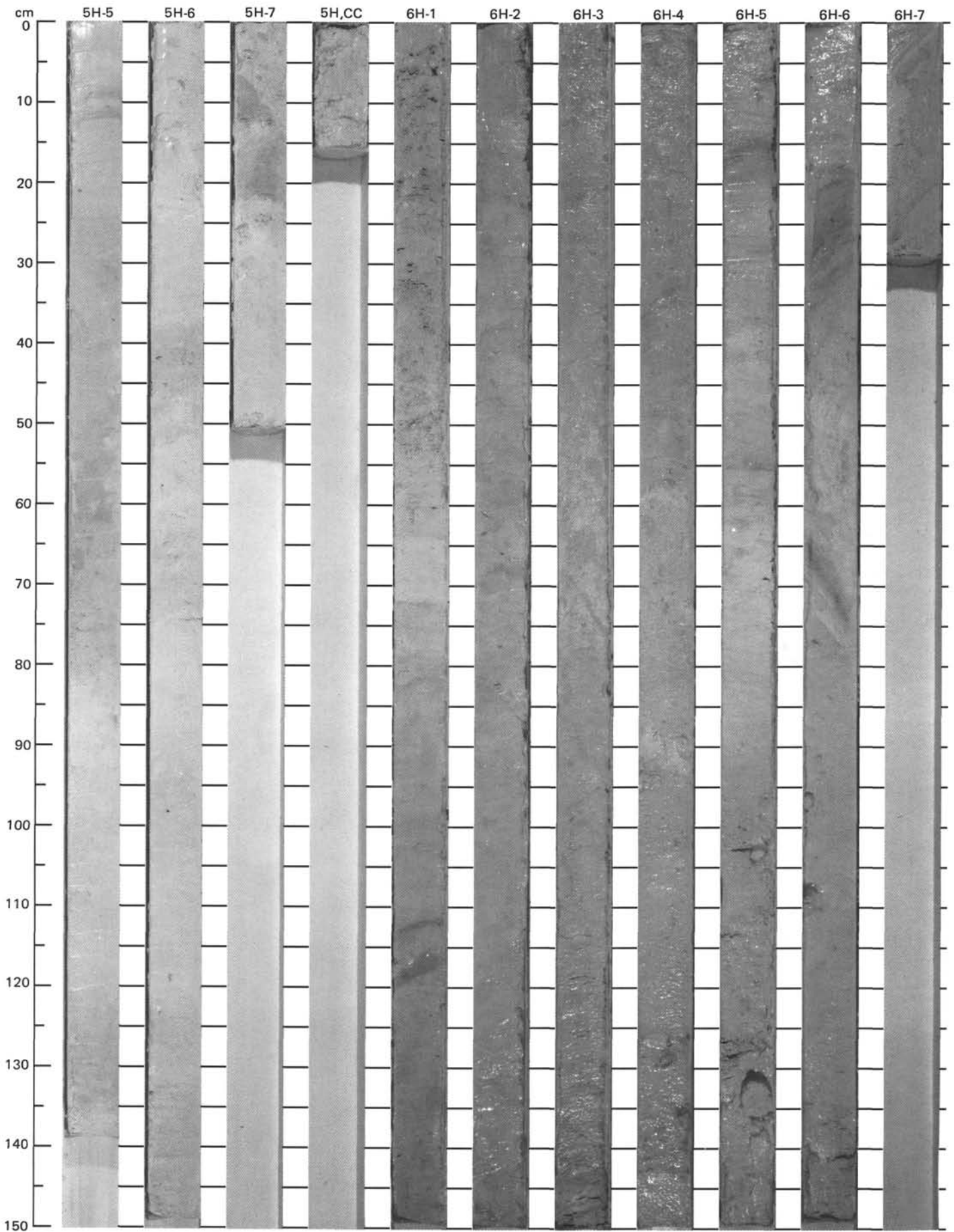
SITE 627 (HOLE B)



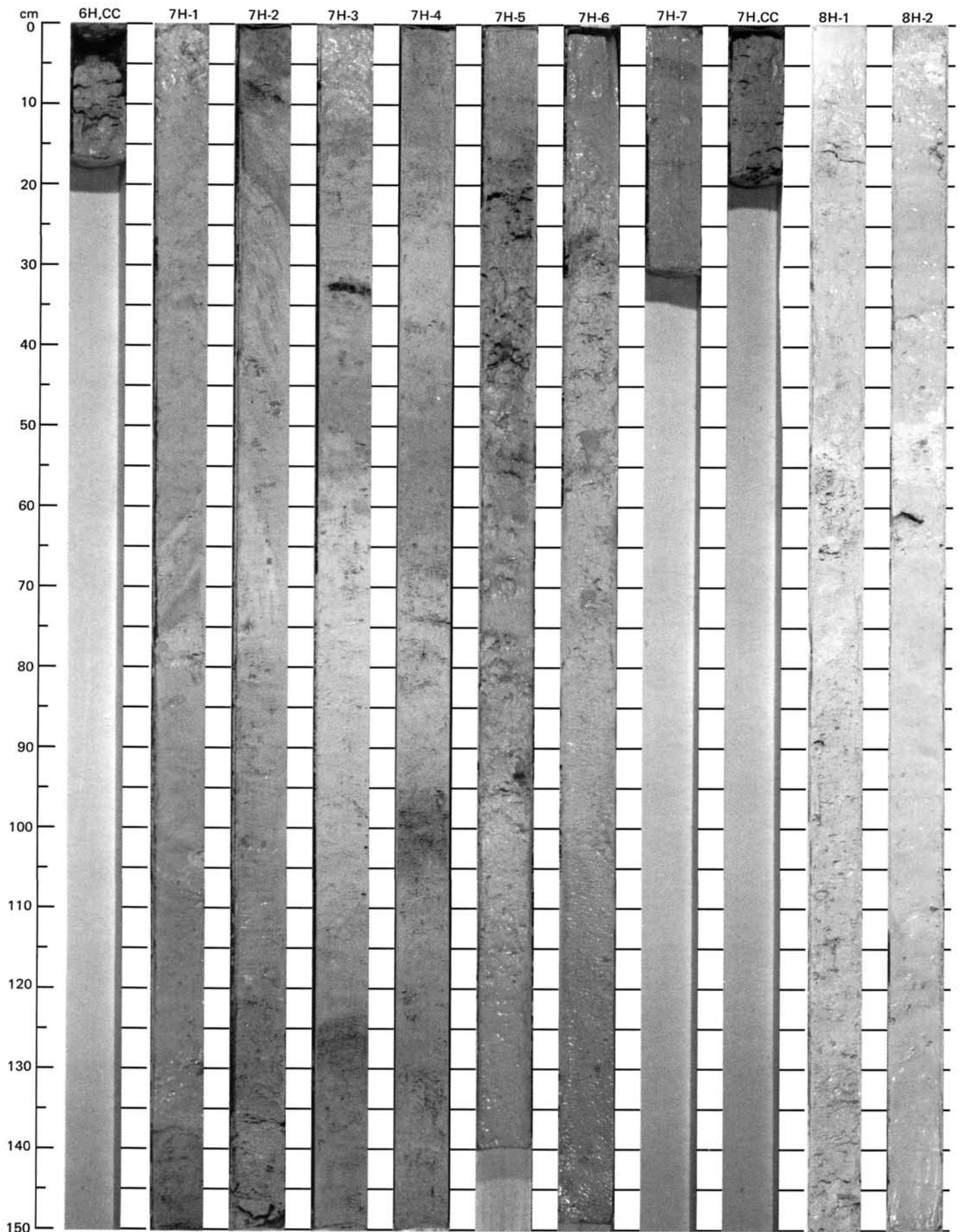


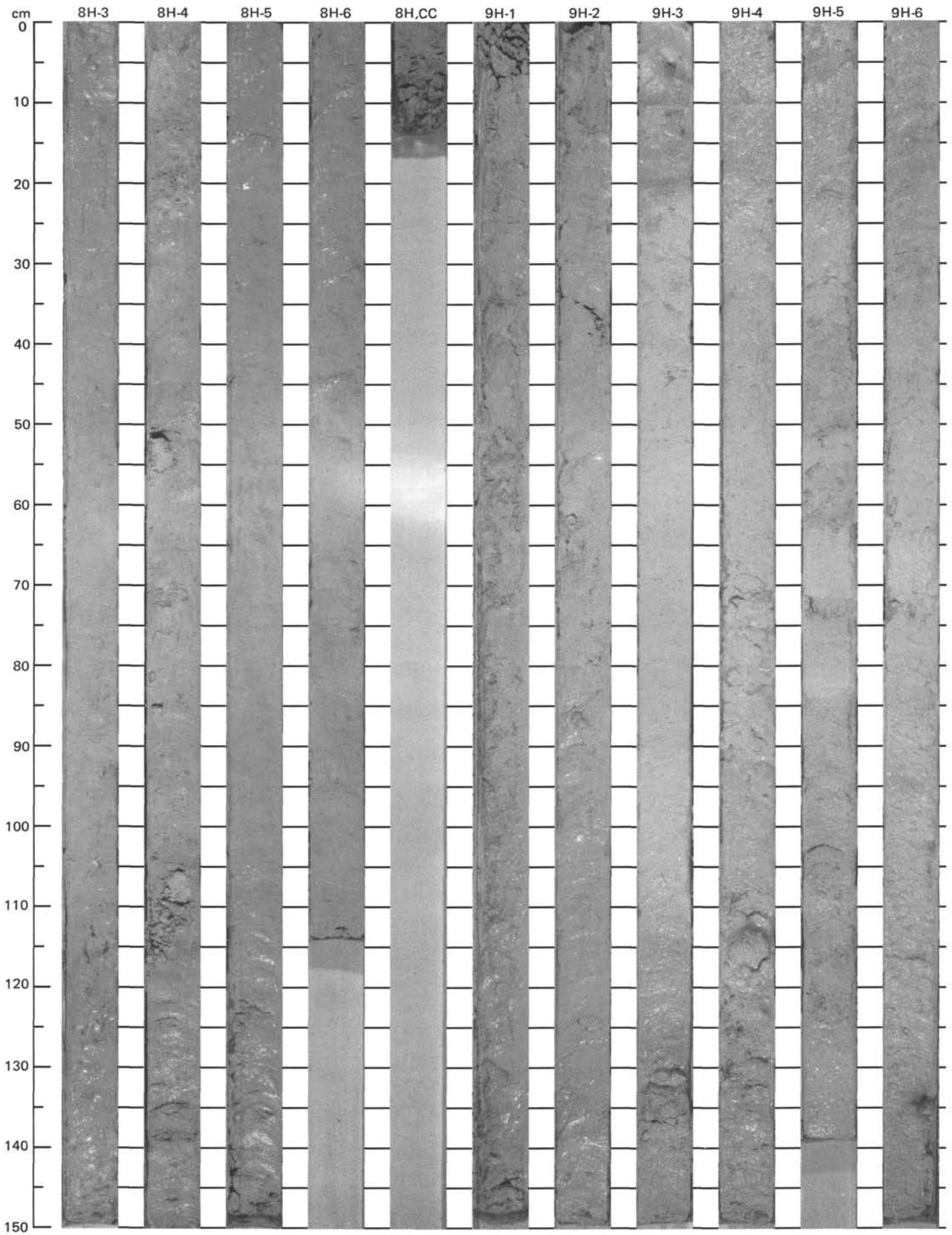
SITE 627 (HOLE B)



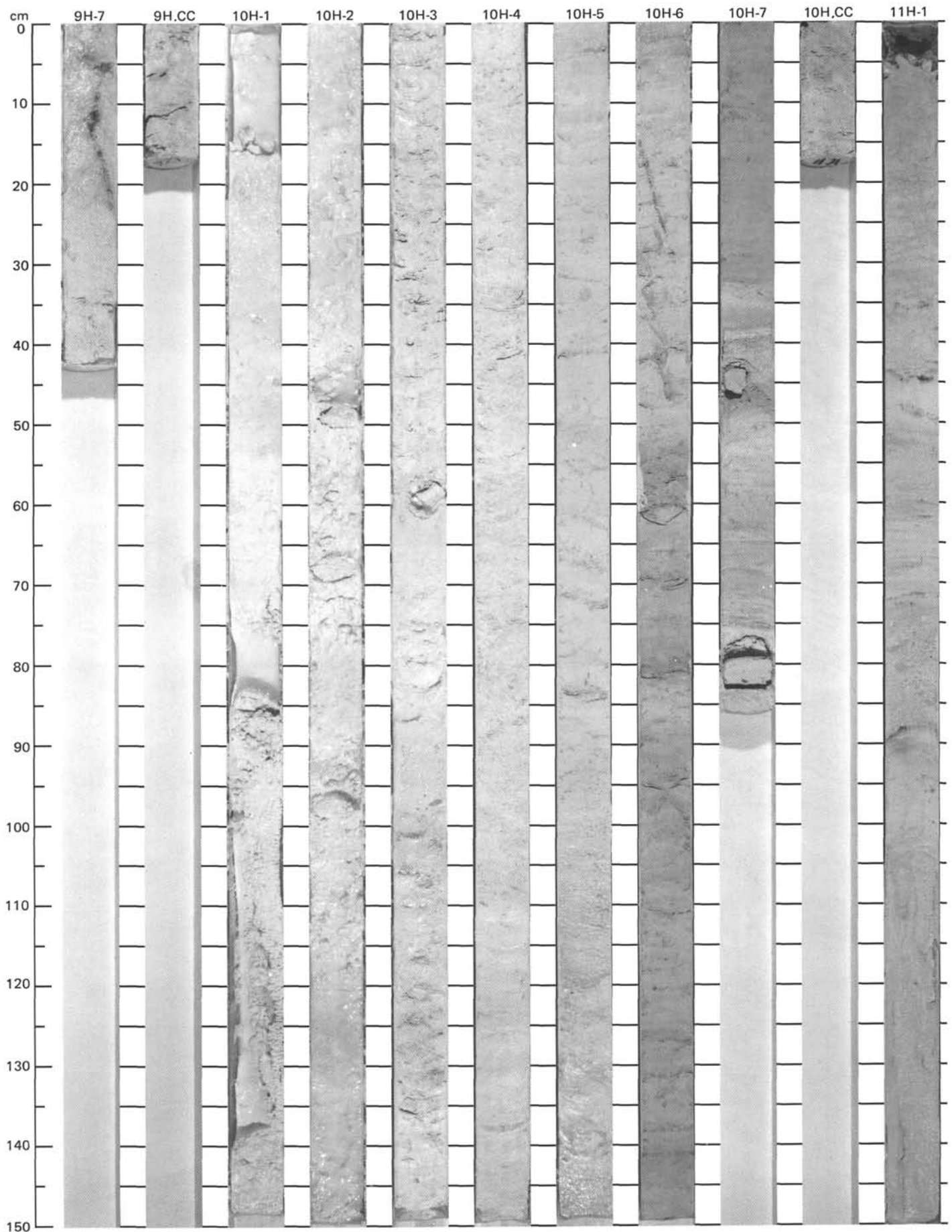


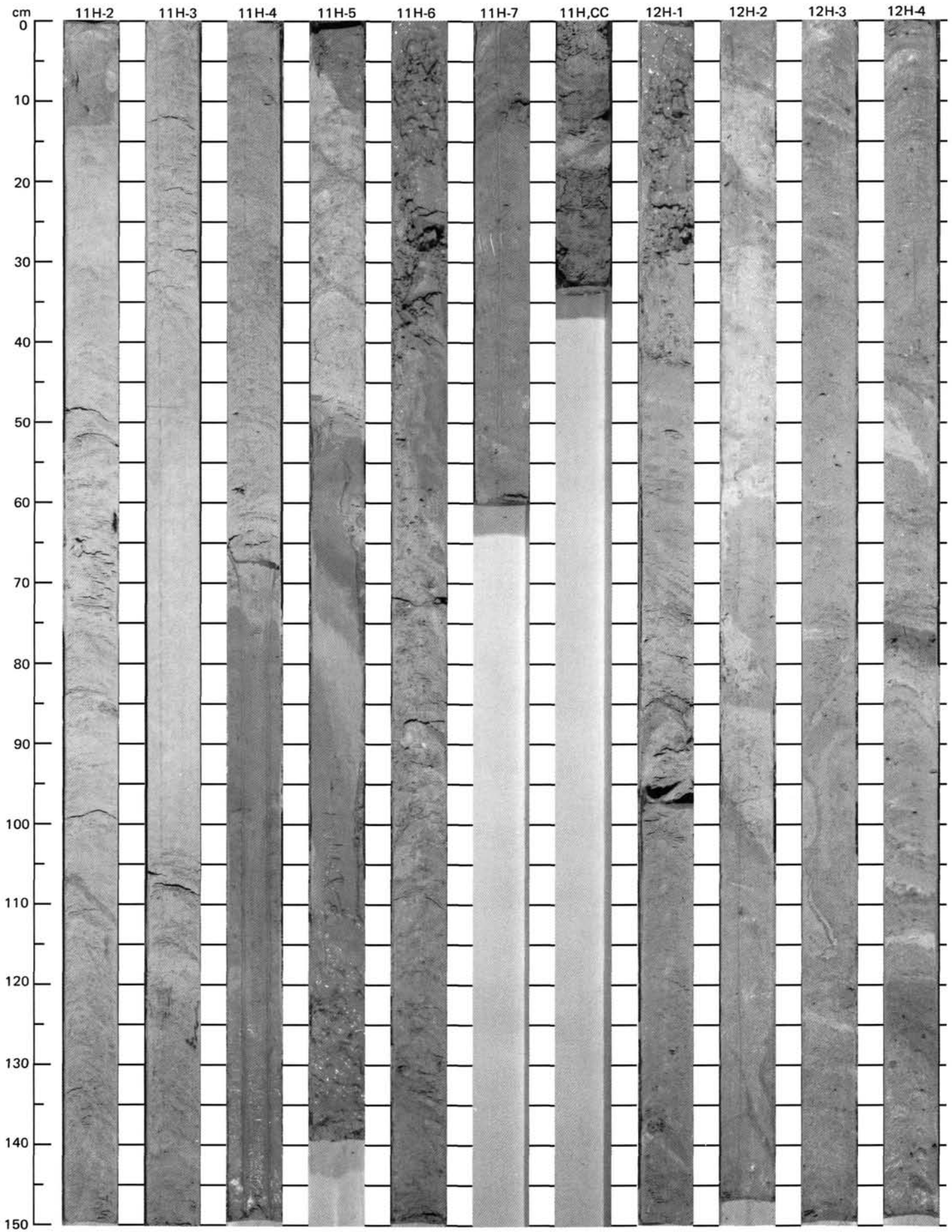
SITE 627 (HOLE B)



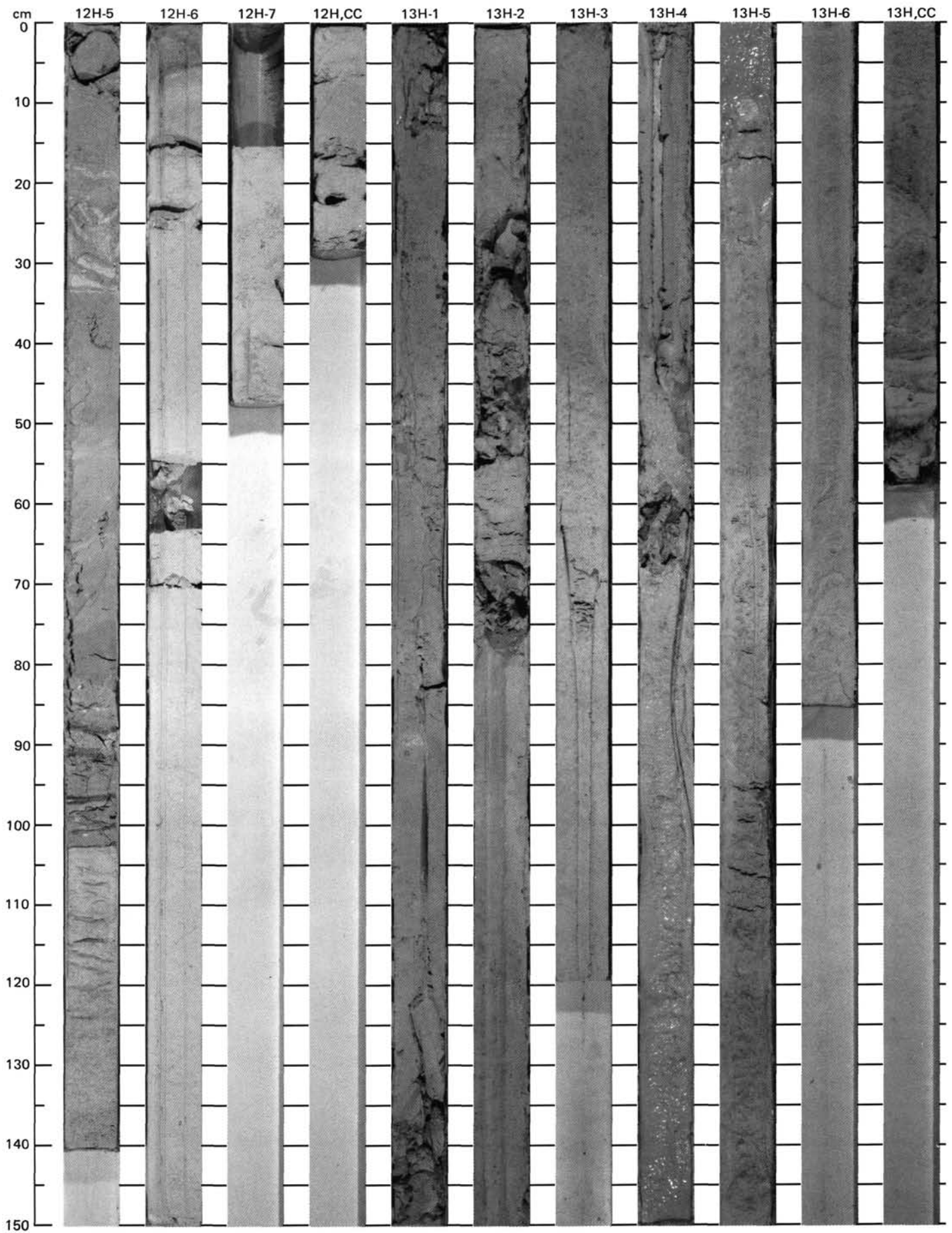


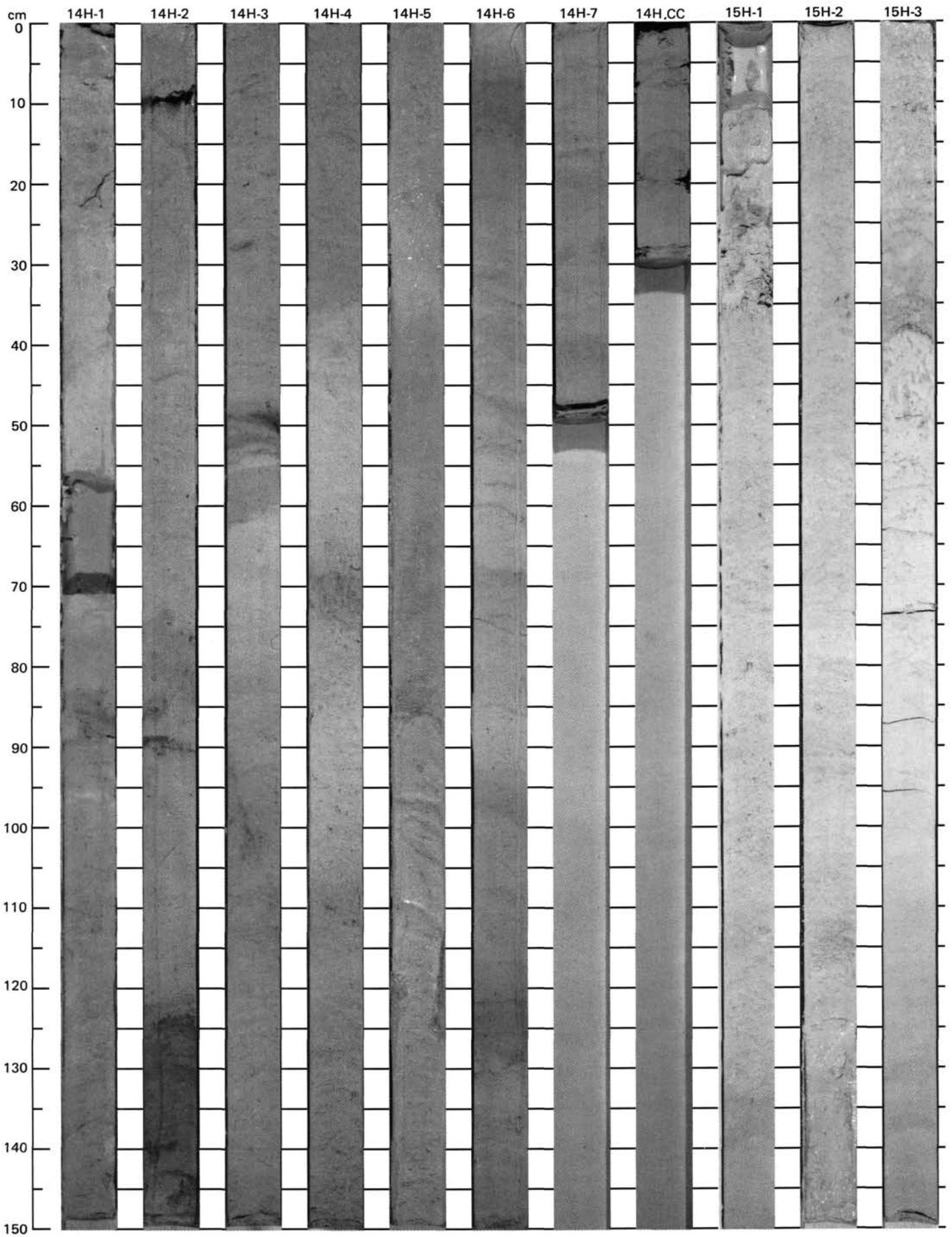
SITE 627 (HOLE B)



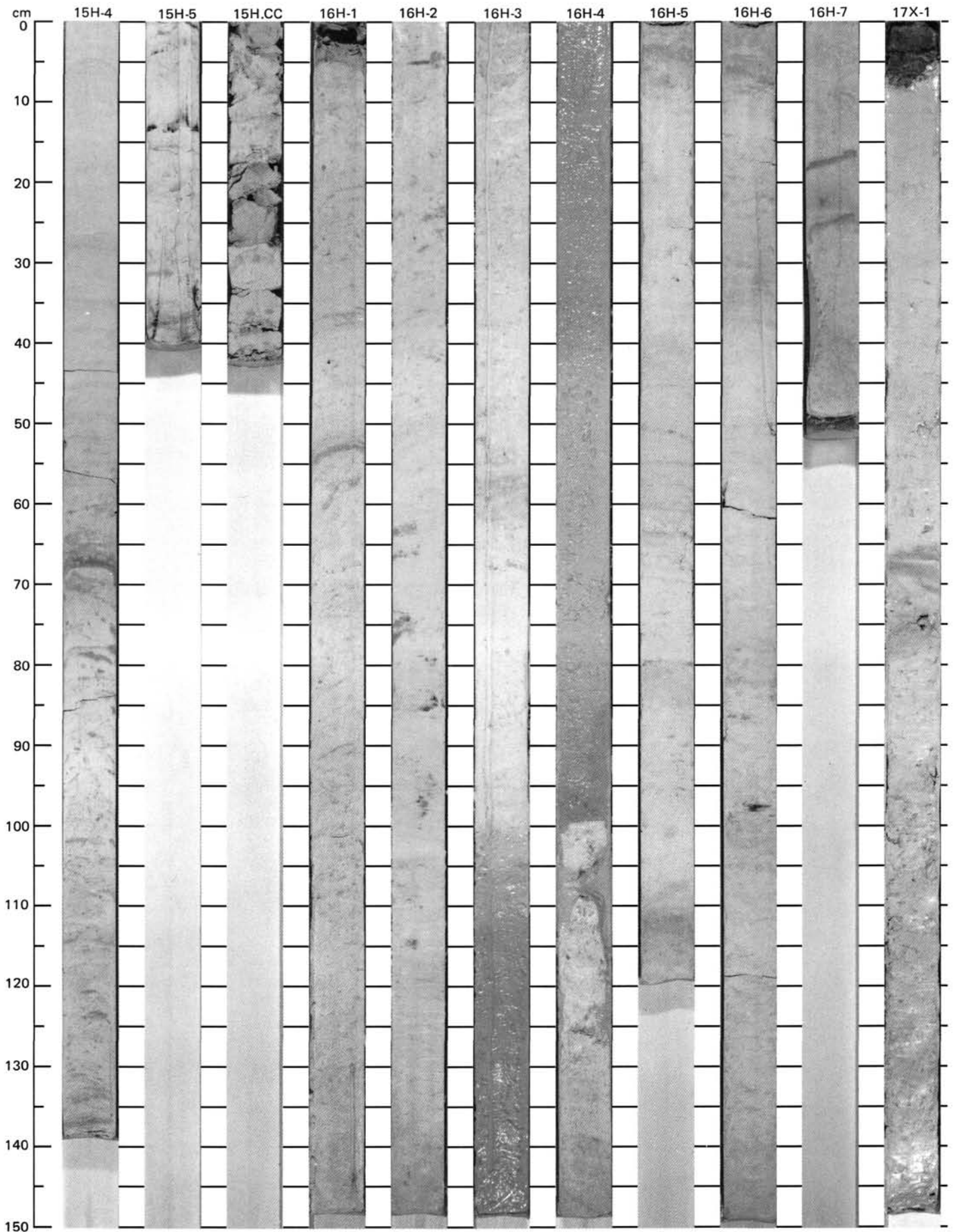


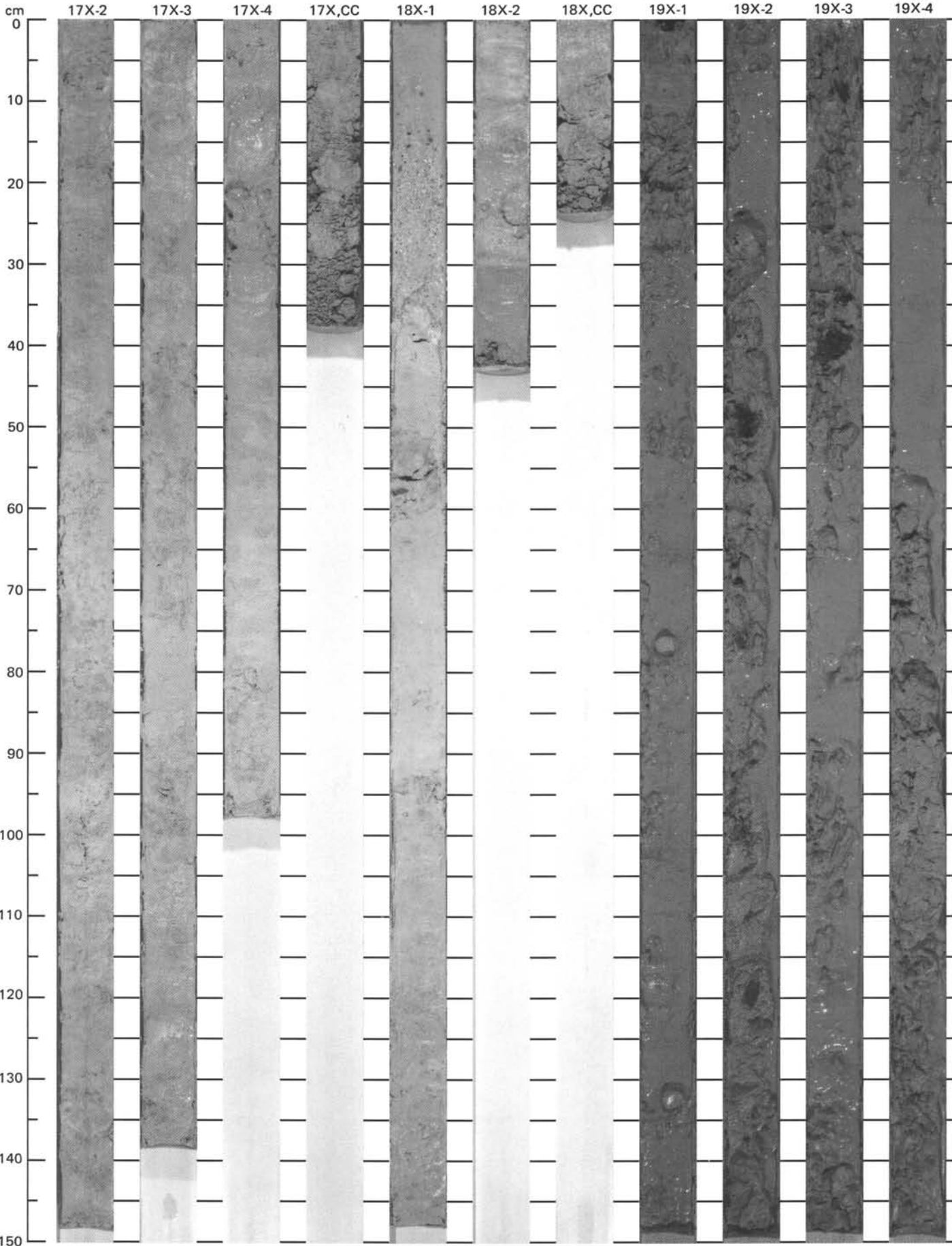
SITE 627 (HOLE B)



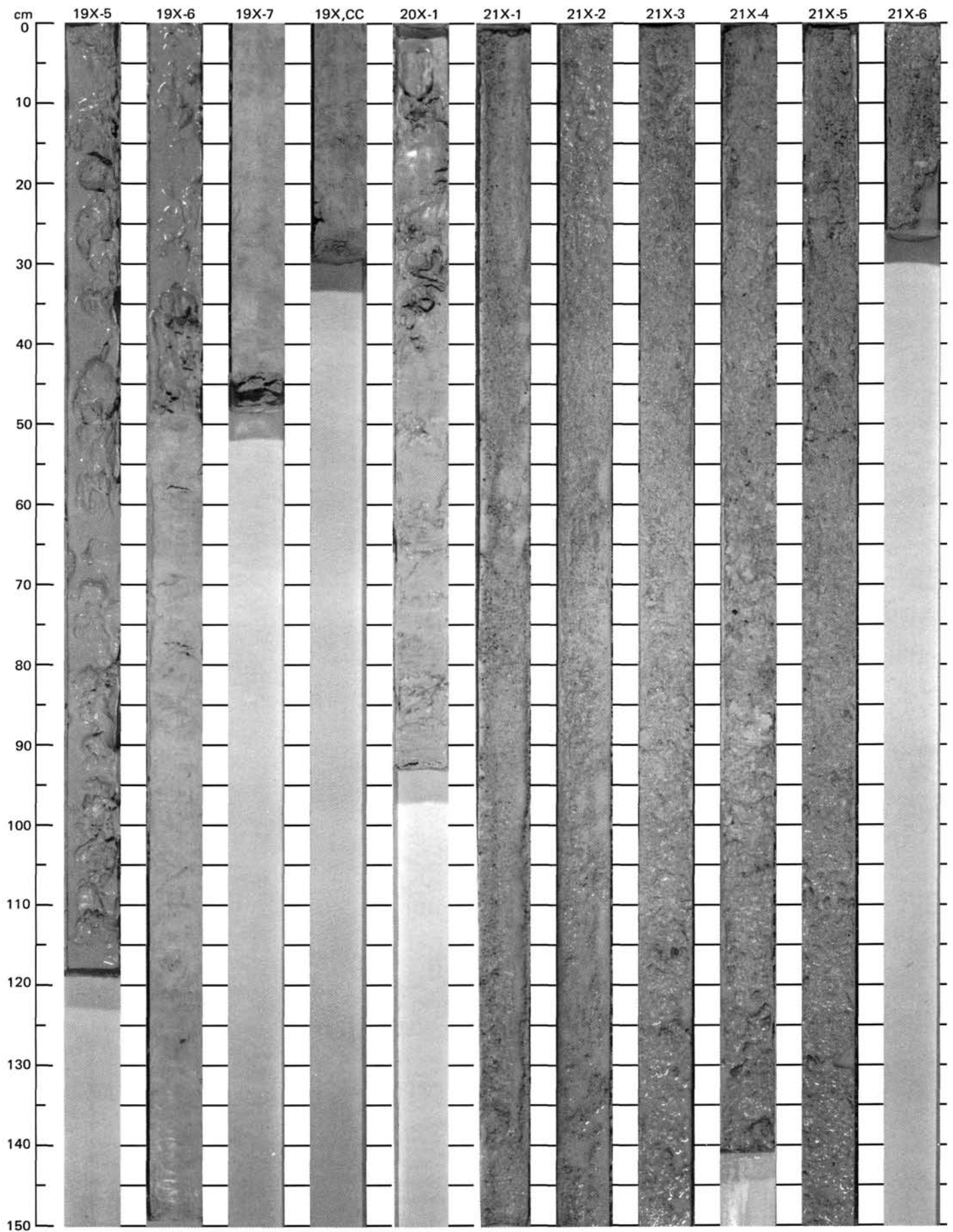


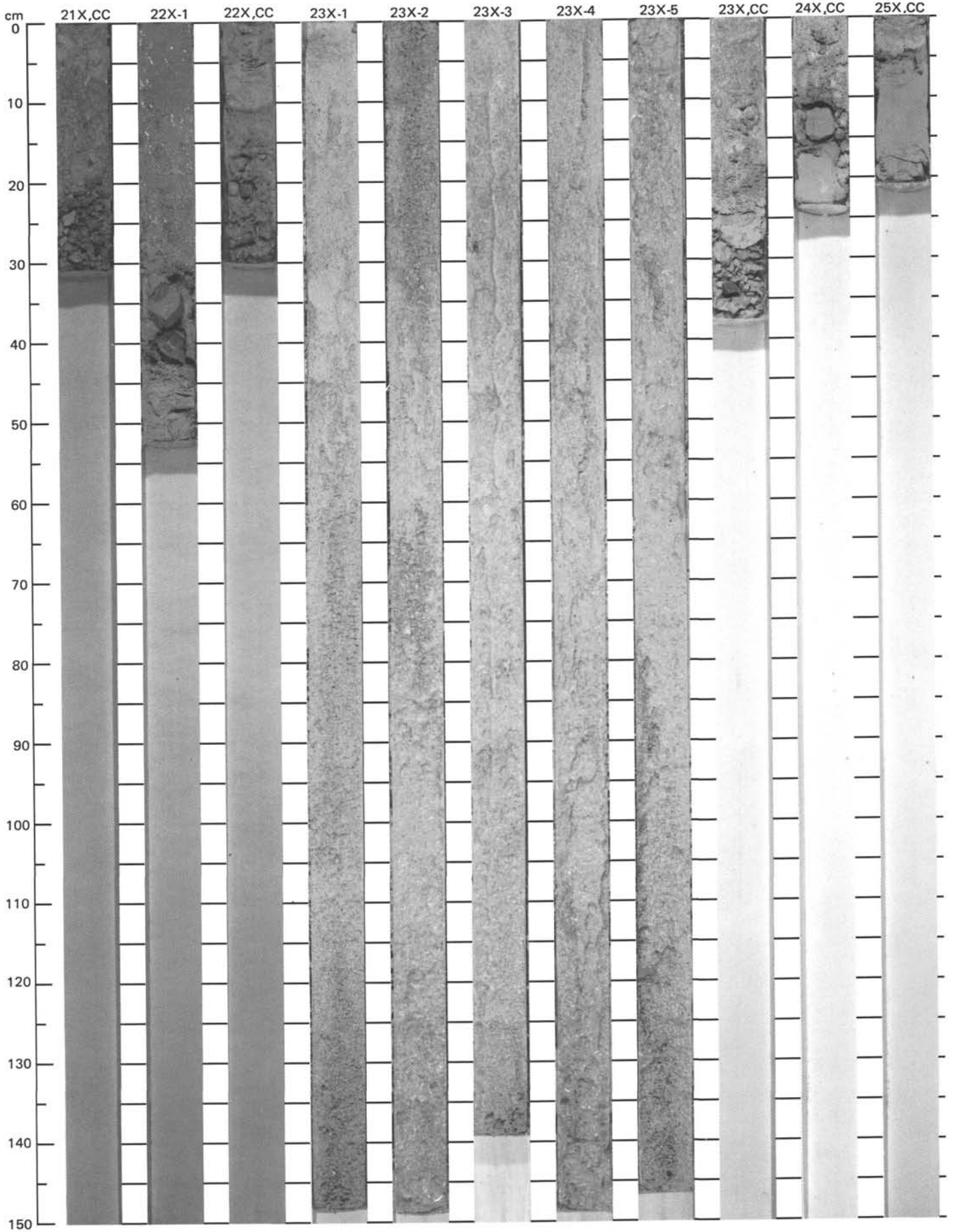
SITE 627 (HOLE B)



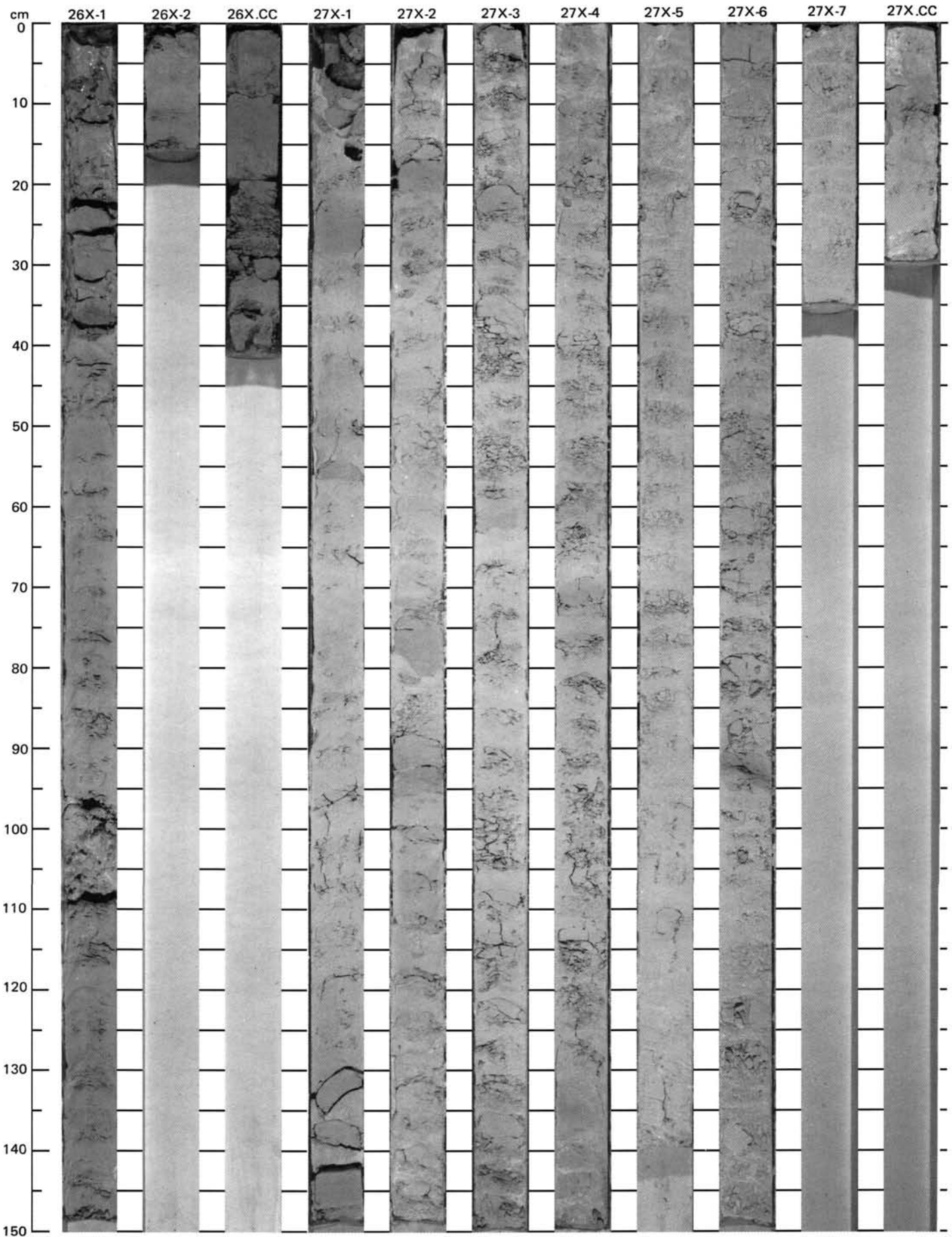


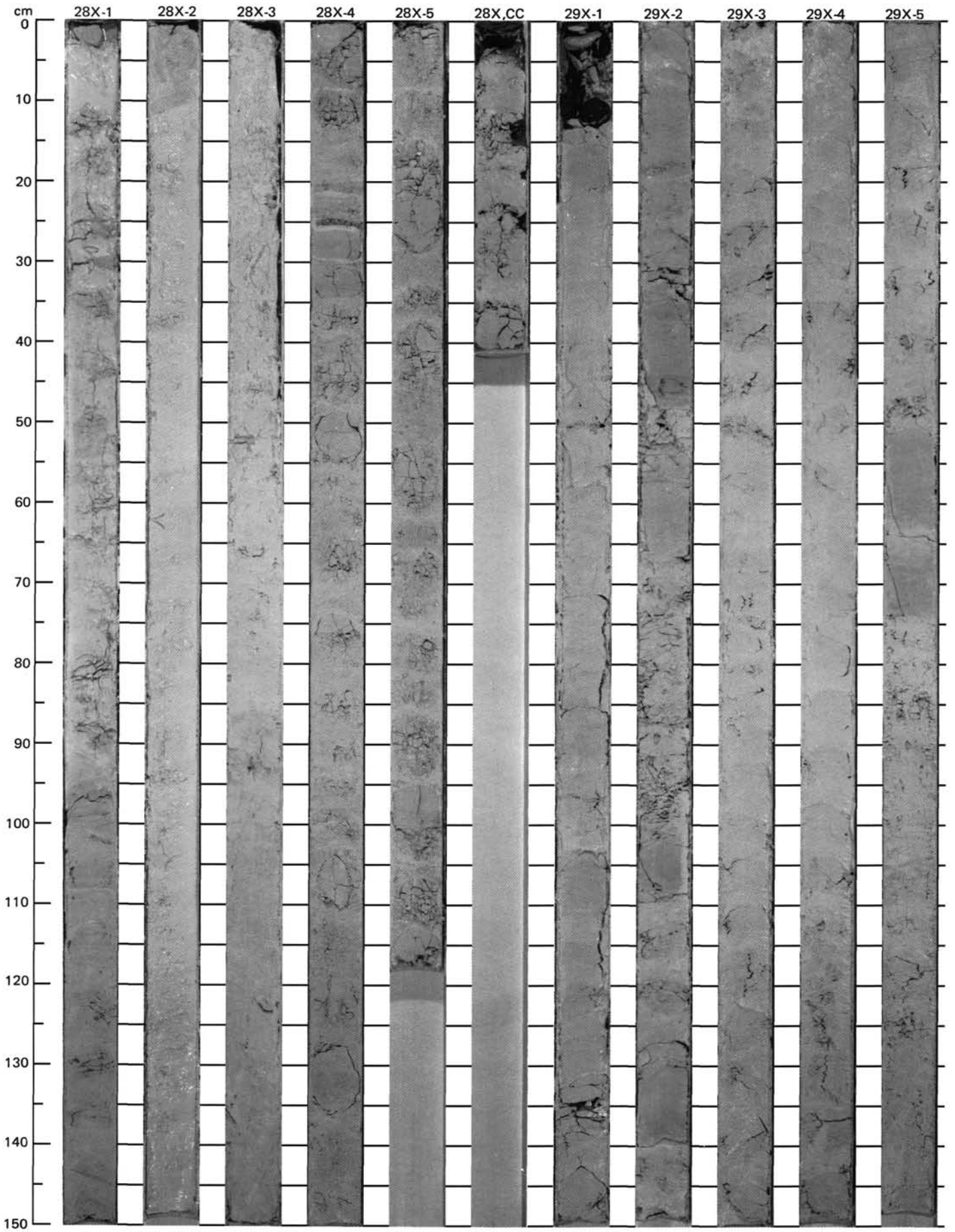
SITE 627 (HOLE B)



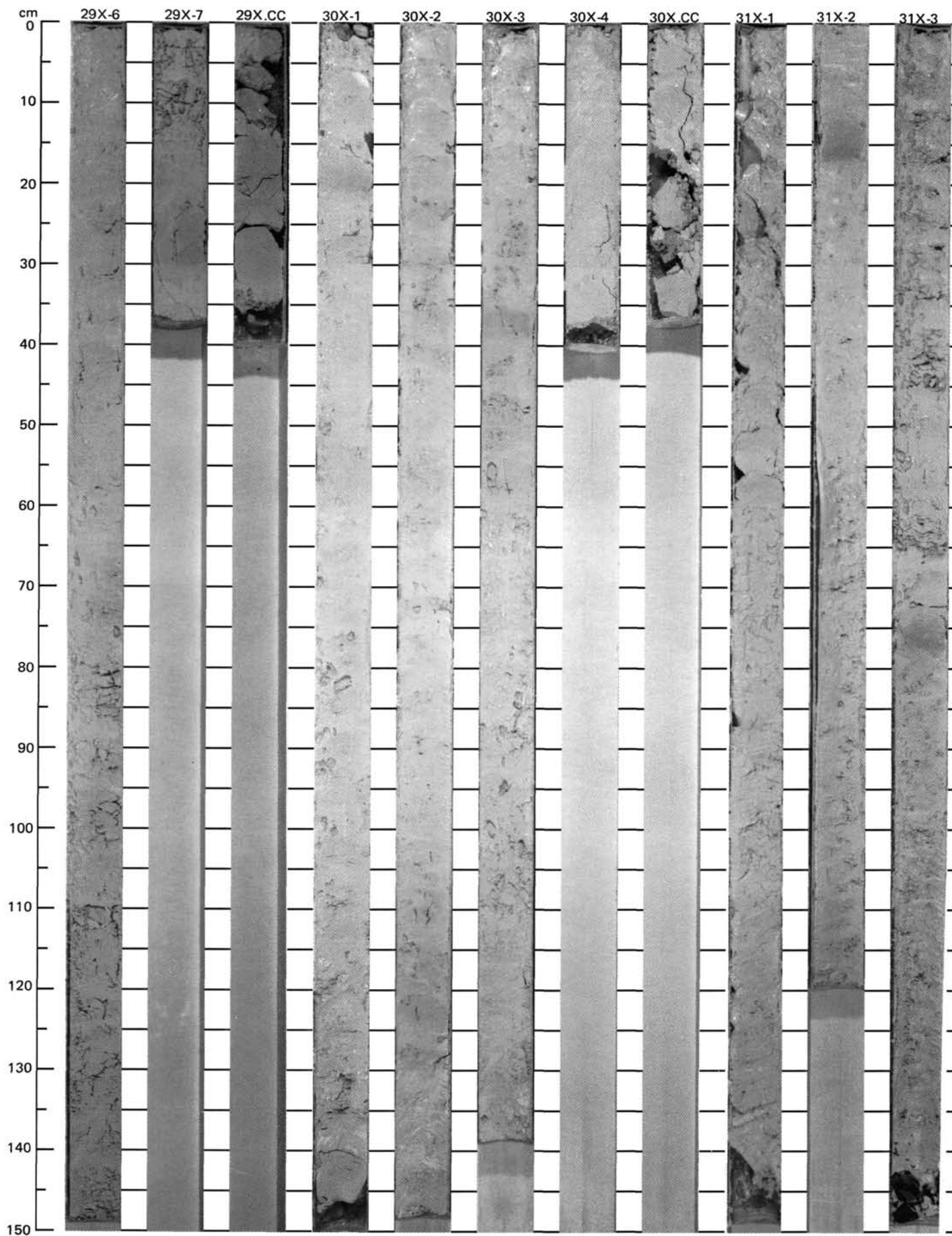


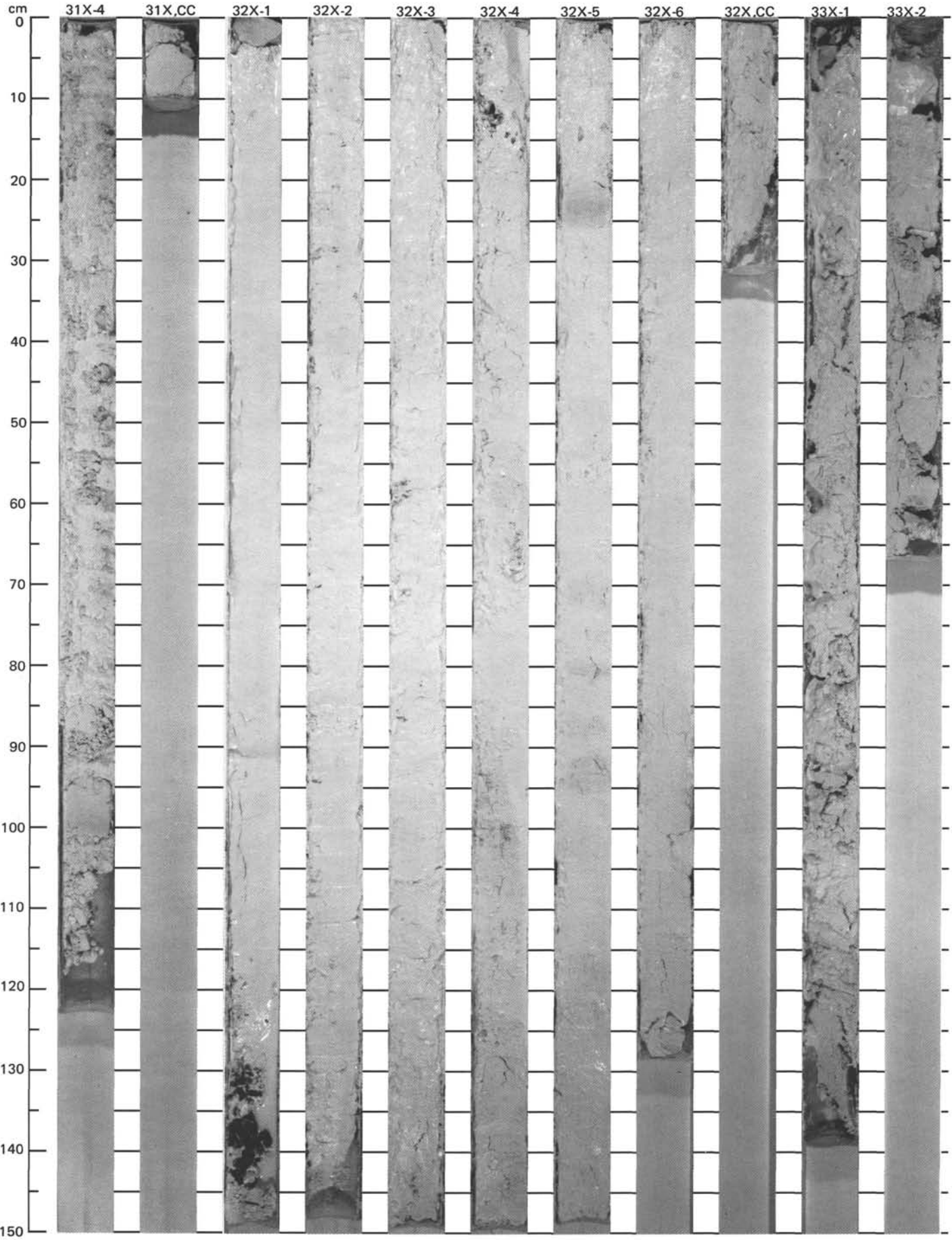
SITE 627 (HOLE B)



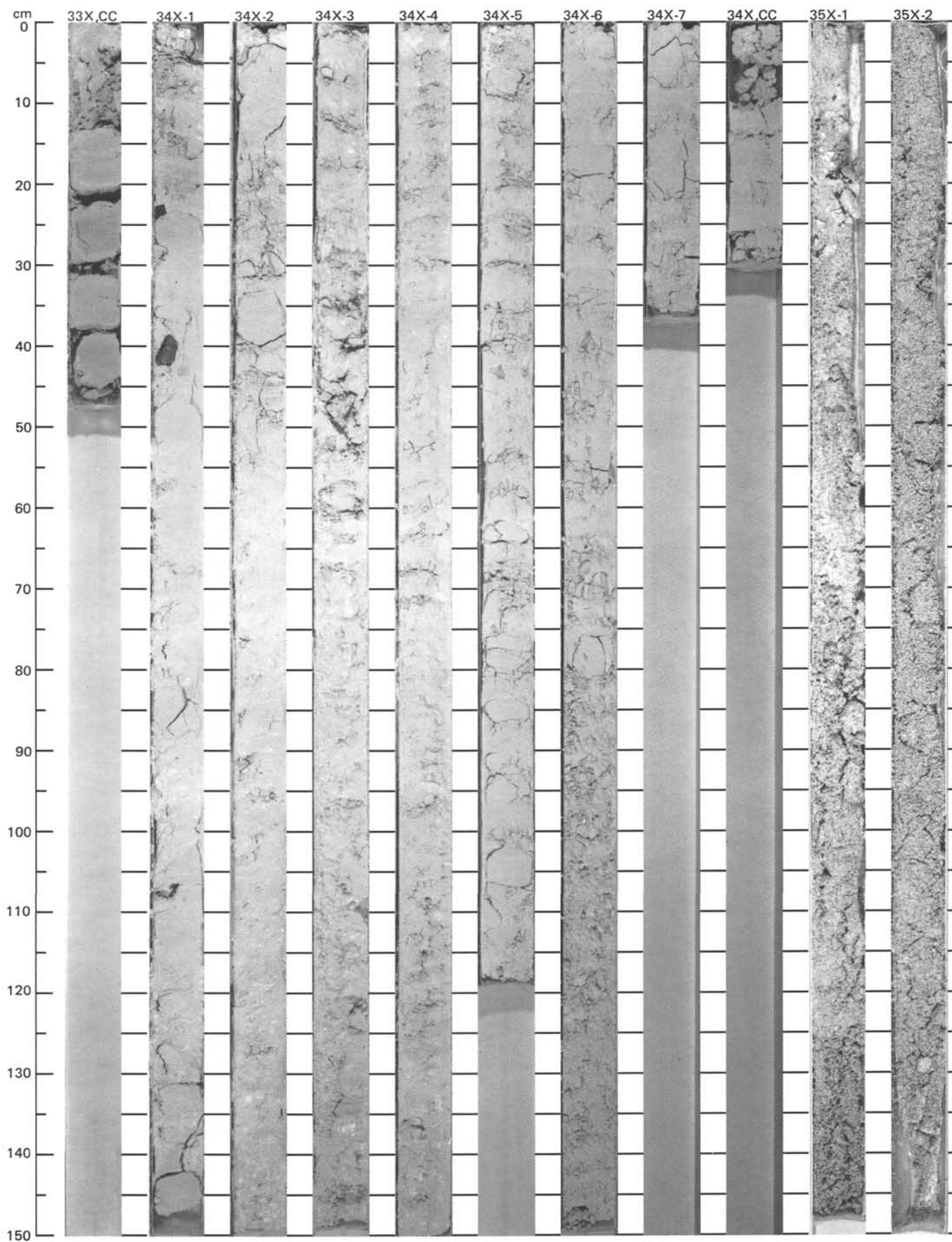


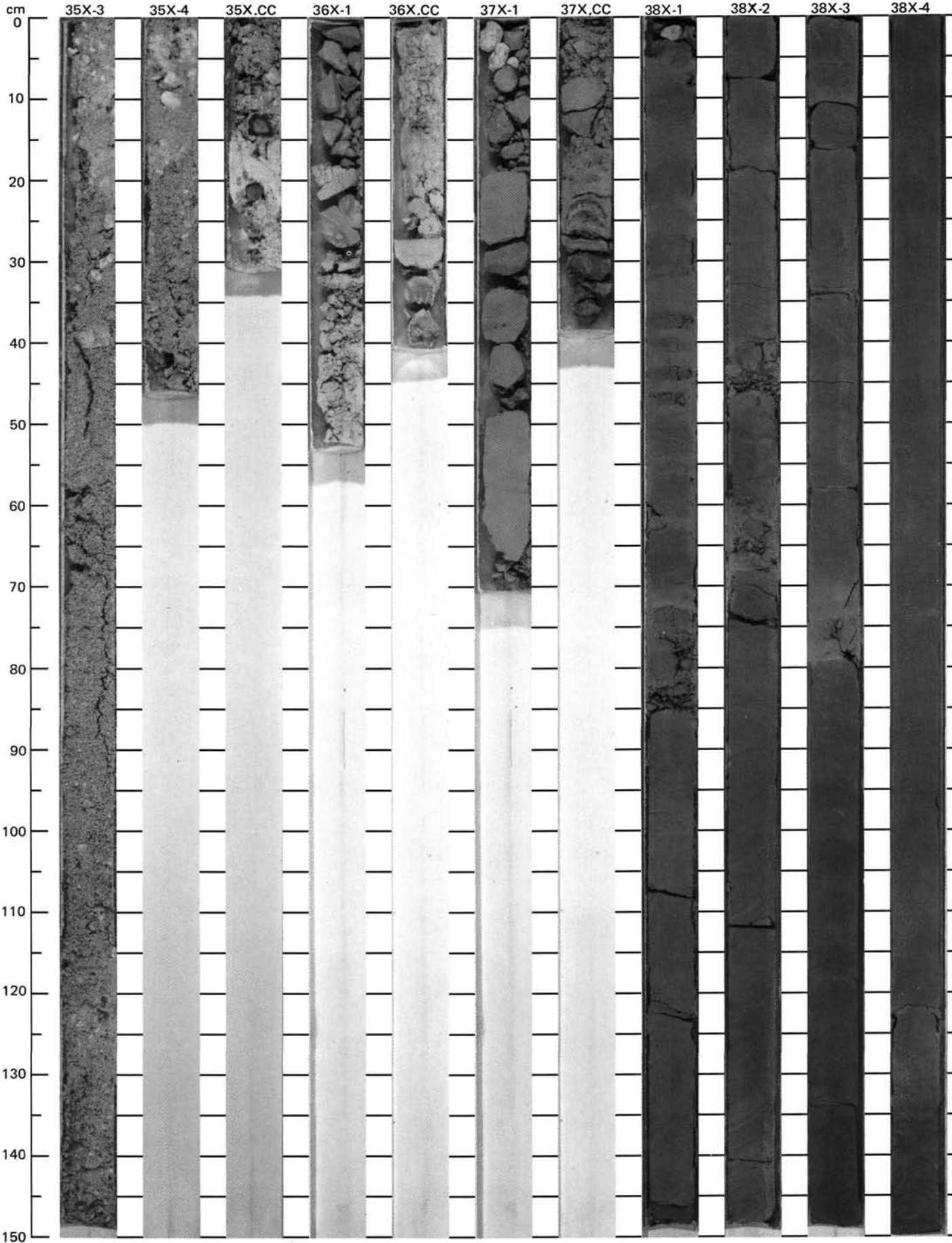
SITE 627 (HOLE B)



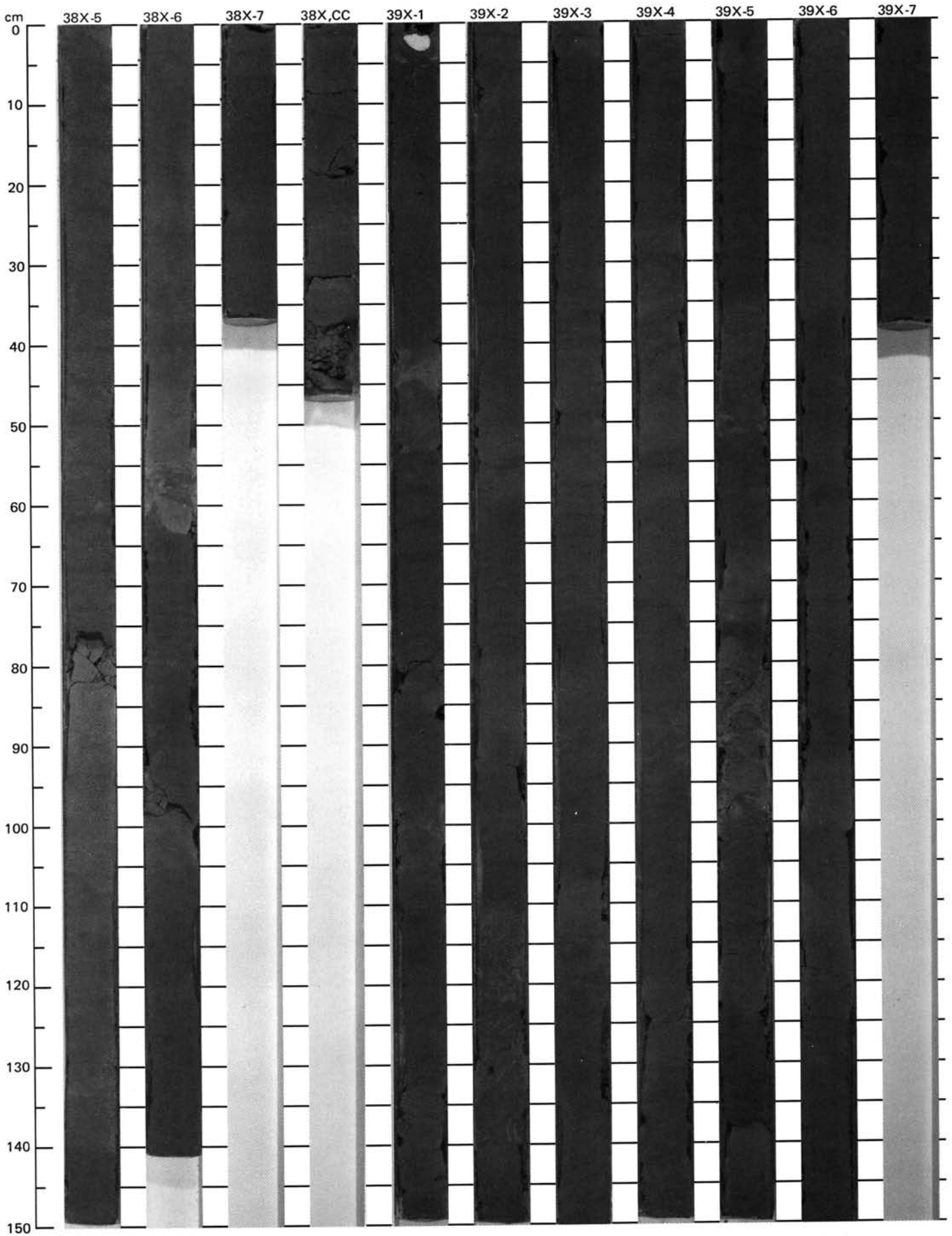


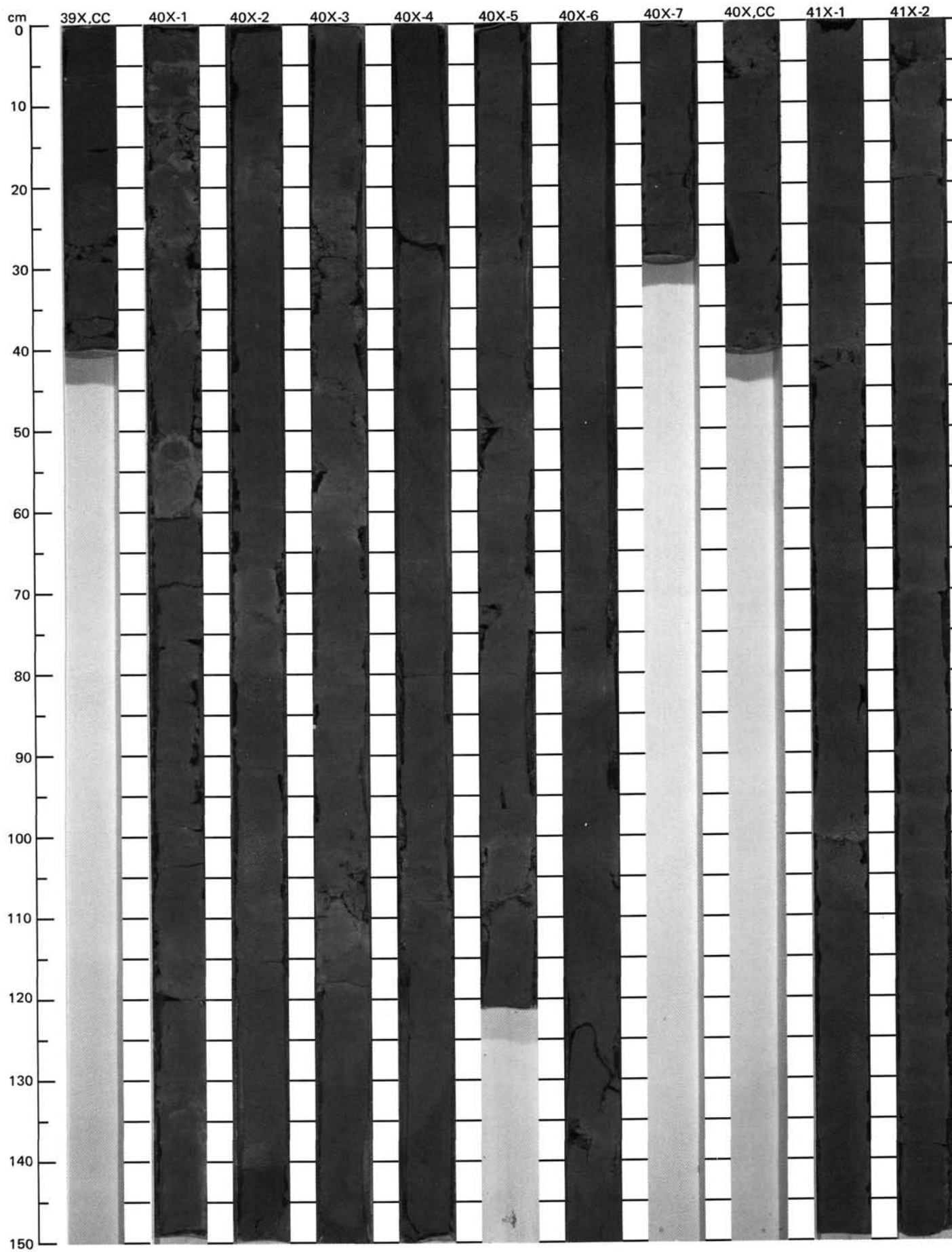
SITE 627 (HOLE B)



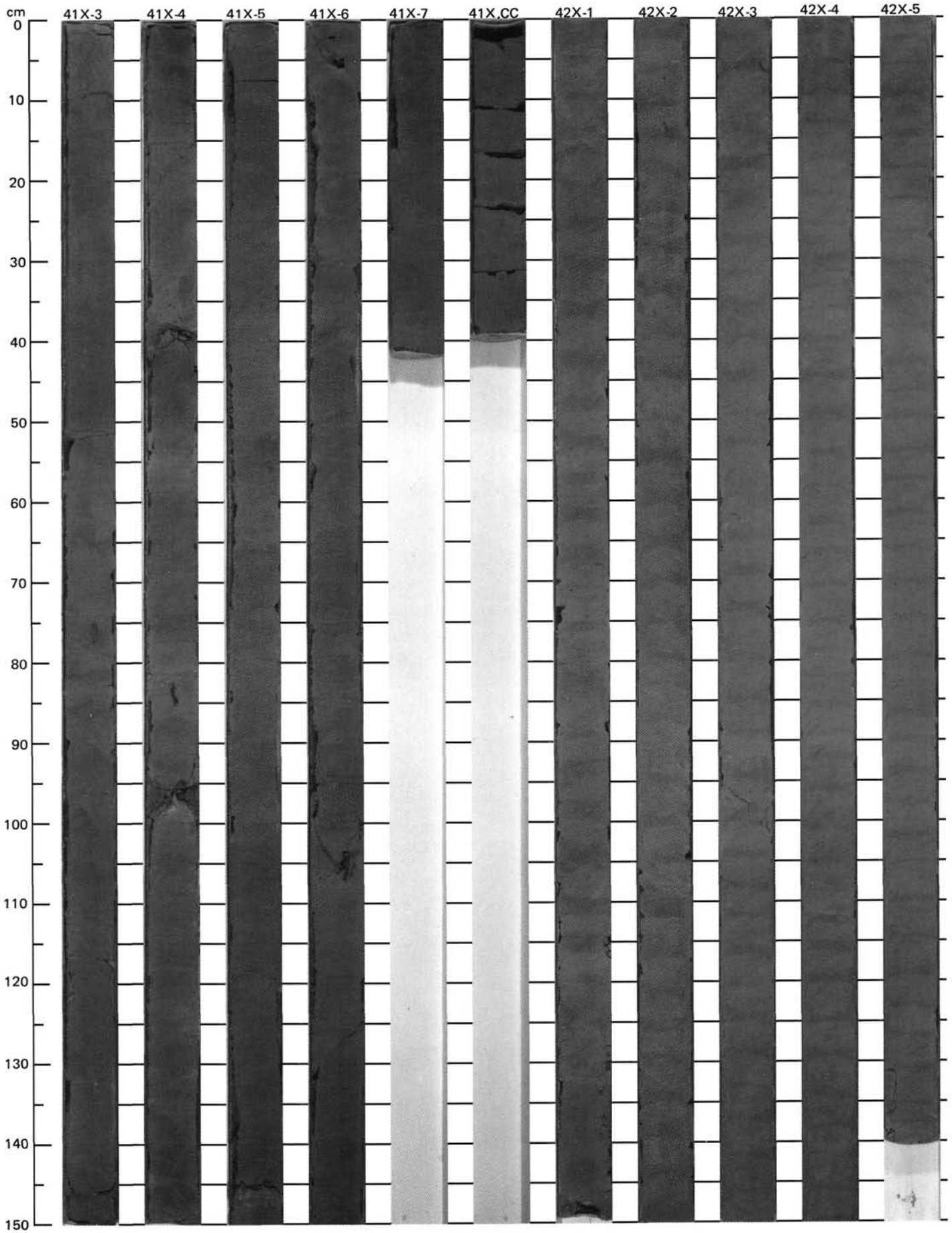


SITE 627 (HOLE B)

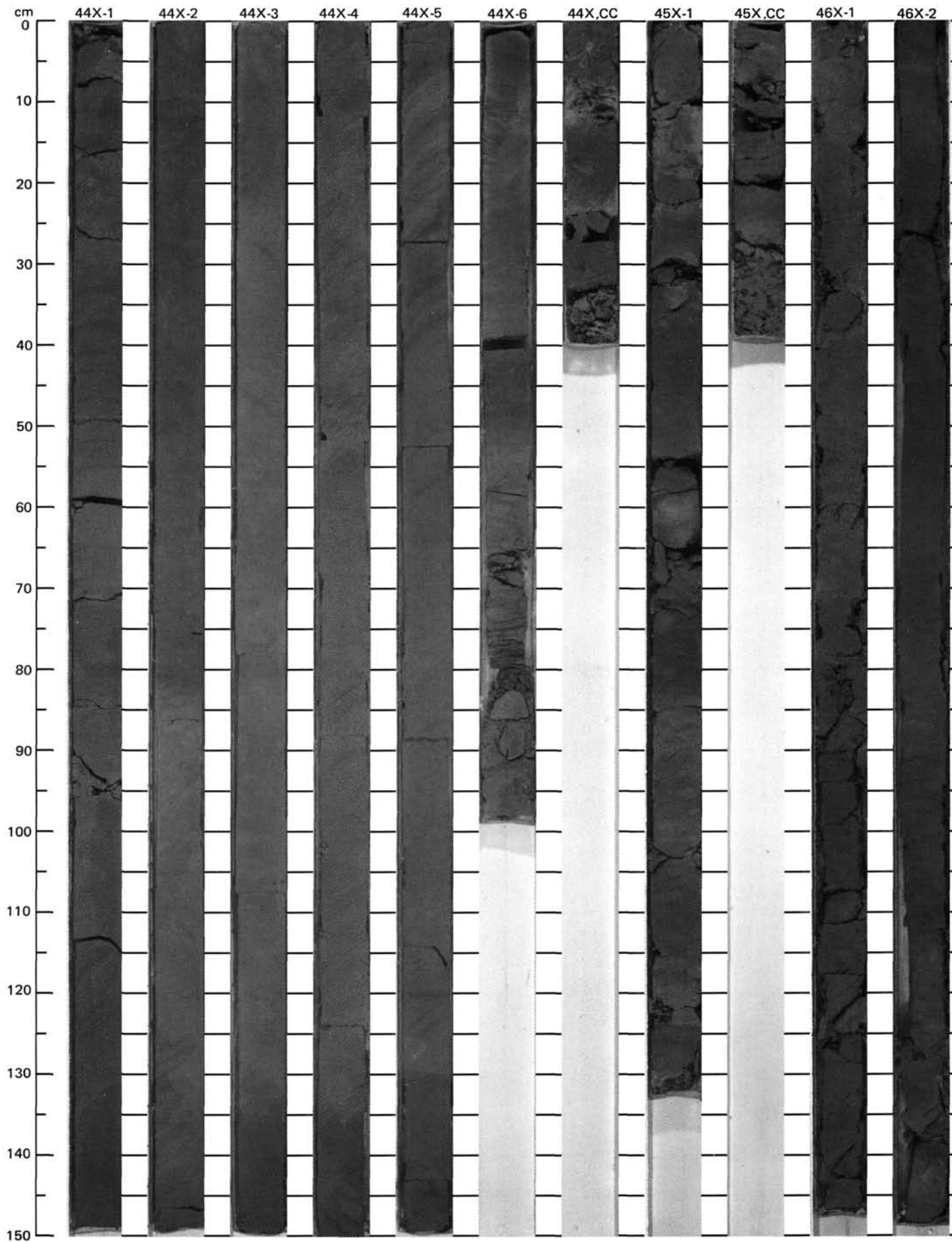


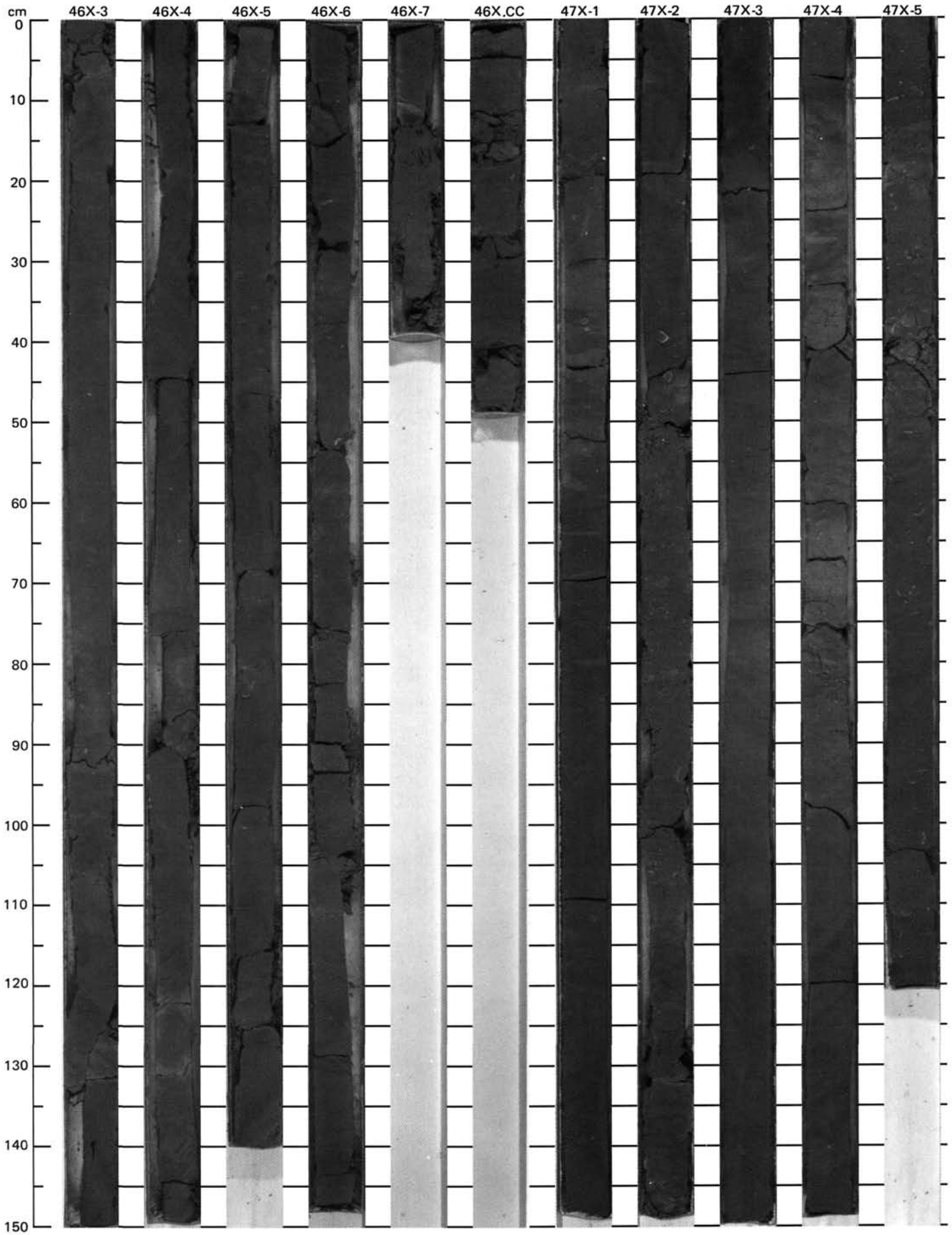


SITE 627 (HOLE B)

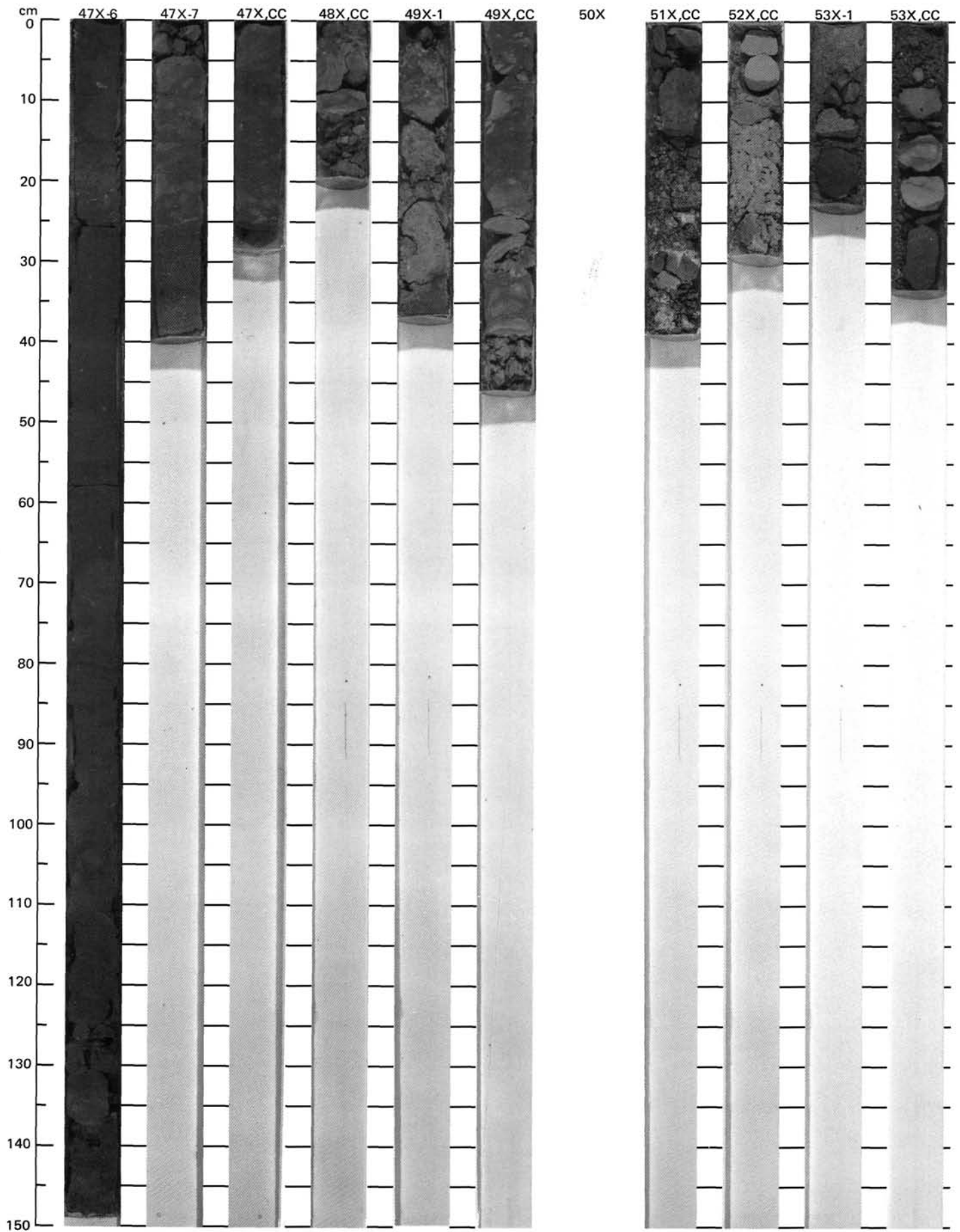


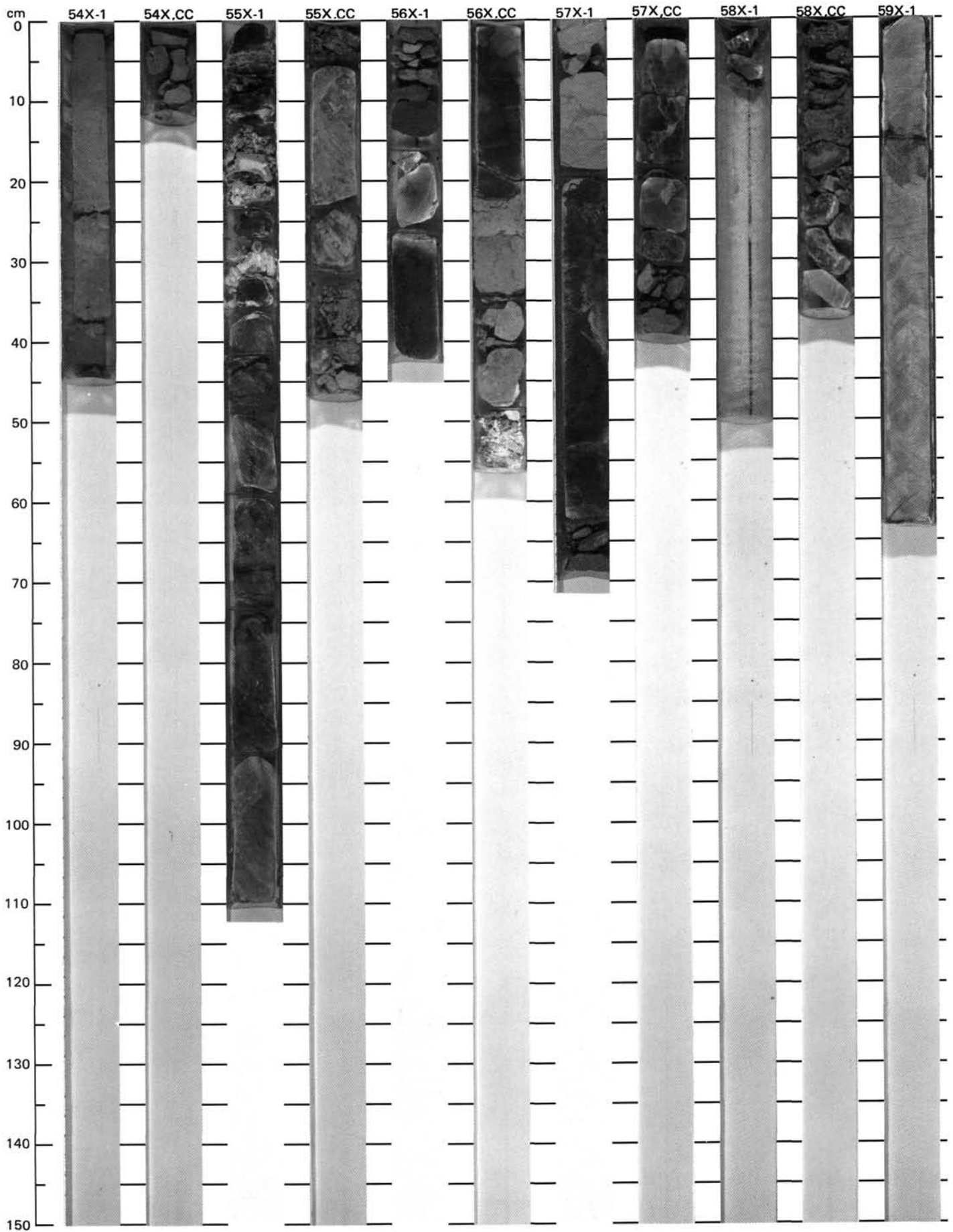
SITE 627 (HOLE B)





SITE 627 (HOLE B)





SITE 627 (HOLE B)

